

COSMOGENIC NUCLIDE QUANTIFICATION OF PALEO-FLUVIAL
SEDIMENTATION RATES IN RESPONSE TO CLIMATE CHANGE

by

Alan J. Hidy

Submitted in partial fulfilment of the requirements
for the degree of Doctor of Philosophy

at

Dalhousie University
Halifax, Nova Scotia
April 2013

© Copyright by Alan J. Hidy, 2013

DALHOUSIE UNIVERSITY
DEPARTMENT OF EARTH SCIENCES

The undersigned hereby certify that they have read and recommend to the Faculty of Graduate Studies for acceptance a thesis entitled “COSMOGENIC NUCLIDE QUANTIFICATION OF PALEO-FLUVIAL SEDIMENTATION RATES IN RESPONSE TO CLIMATE CHANGE” by Alan J. Hidy in partial fulfilment of the requirements for the degree of Doctor of Philosophy.

Dated: April 23, 2013

External Examiner: _____

Research Supervisor: _____

Examining Committee: _____

Departmental Representative: _____

DALHOUSIE UNIVERSITY

DATE: April 23, 2013

AUTHOR: Alan J. Hidy

TITLE: Cosmogenic Nuclide Quantification of Paleo-fluvial Sedimentation Rates
in Response to Climate Change

DEPARTMENT OR SCHOOL: Department of Earth Sciences

DEGREE: PhD CONVOCATION: October YEAR: 2013

Permission is herewith granted to Dalhousie University to circulate and to have copied for non-commercial purposes, at its discretion, the above title upon the request of individuals or institutions. I understand that my thesis will be electronically available to the public.

The author reserves other publication rights, and neither the thesis nor extensive extracts from it may be printed or otherwise reproduced without the author's written permission.

The author attests that permission has been obtained for the use of any copyrighted material appearing in the thesis (other than the brief excerpts requiring only proper acknowledgement in scholarly writing), and that all such use is clearly acknowledged.

Signature of Author

TABLE OF CONTENTS

LIST OF TABLES	viii
LIST OF FIGURES	ix
ABSTRACT	xi
LIST OF ABBREVIATIONS USED	xii
ACKNOWLEDGEMENTS	xiii
CHAPTER 1: Introduction	1
1.1. Overview of Thesis	1
1.2. Design of Thesis	4
CHAPTER 2: A geologically Constrained Monte Carlo Approach to Modeling Exposure Ages from Profiles of Cosmogenic Nuclides: An Example from Lees Ferry, Arizona.....	7
2.1. Abstract	7
2.2. Introduction	8
2.3. Background	9
2.3.1. Why Use a Depth Profile?	9
2.3.2. Lees Ferry Sample Site	12
2.4. Model Approach	17
2.4.1. Parameters and Uncertainty	17
2.4.2. Data Inputs	21
2.4.3. Profile Solutions.....	22
2.4.4. Model Constraints for Lees Ferry M4 Terrace	24
2.5. Results	30
2.5.1. Lees Ferry Sand Profile.....	30
2.5.2. Lees Ferry Pebble Profile.....	31
2.6. Discussion	37
2.6.1. Interpreting Results with this Program	37
2.6.2. Age of the Lees Ferry M4 Terrace.....	38
2.6.3. Implications for Sampling TCN Depth Profiles	39
2.7. Conclusions	40
2.8. Appendix	41
2.8.1. Lees Ferry, Specific Sampling Methods.....	41
2.8.2. Laboratory Methods	42

2.8.3. Model Run Time	43
2.9. Acknowledgments.....	44
2.10. Addendum	44
CHAPTER 3: Climatically-driven Variation in Sediment Flux from Interior Texas Established with Cosmogenic ¹⁰ Be and ²⁶ Al.....	46
3.1. Introduction	46
3.2. Study Area.....	48
3.2.1. Overview	48
3.2.2. Chronology and Stratigraphy of the Texas Coastal Plain.....	52
3.2.3. Sediment Flux from Major Texas Rivers.....	57
3.3. Methods.....	61
3.4. Results	62
3.4.1. New Lissie Chronology	62
3.4.2. Depositional ¹⁰ Be and ²⁶ Al.....	65
3.4.3. Catchment-wide Denudation and Sediment Flux	67
3.5. Discussion	68
3.5.1. Sediment Recycling on the Texas Coastal Plain.....	68
3.5.2. ¹⁰ Be Catchment-wide Sediment Fluxes	73
3.6. Conclusions.....	80
3.7. Acknowledgements.....	81
CHAPTER 4: A Latest Pliocene Age for the Earliest and Most Extensive Cordilleran Ice Sheet in Northwestern Canada	82
4.1. Abstract	82
4.2. Introduction	83
4.2.1. Klondike Area	85
4.2.2. Sample Site: Australia Hill	88
4.3. Methods.....	91
4.3.1. TCN Burial Dating.....	91
4.3.2. Sampling Strategy.....	92
4.3.3. Sample Preparation and Analysis	92
4.4. Results	94
4.5. Discussion	97
4.5.1. Interpretation of ²⁶ Al and ¹⁰ Be Data	97

4.5.2. Olduvai vs. Late Gauss Age.....	97
4.5.3. Muon Sensitivity Analysis.....	102
4.5.4. A 2.64 Ma Cordilleran Ice Sheet.....	102
4.6. Conclusions.....	106
4.7. Acknowledgements.....	106
CHAPTER 5: Discussion.....	107
5.1. Conclusions.....	107
5.1.1. Depth Profile Model.....	108
5.1.2. The First Cordilleran Ice Sheet.....	109
5.1.3. Denudation of Interior Texas.....	110
5.2. Implications and Future Work.....	112
5.2.1. The Regolith Hypothesis.....	112
5.2.2. Pliocene Denudation Rates.....	117
References.....	122
Appendices.....	143
A.1. Supplementary Information for Hidy et al. (2010): A Geologically Constrained Monte Carlo Approach to Modeling Exposure Ages from Profiles of Cosmogenic Nuclides: An Example from Lees Ferry, Arizona.....	143
A.1.1. Readme File for Profile Simulator.....	143
A.1.2. Chemical Worksheets for TCN Data.....	147
A.2. Supplemental Information for Hidy et al.: Climatically-driven Variation in Sediment Flux from Interior Texas Established with Cosmogenic ¹⁰ Be and ²⁶ Al.....	159
A.2.1. TCN Sample Collection and Preparation.....	159
A.2.2. ¹⁰ Be Catchment-wide Denudation Rates.....	162
A.2.3. ¹⁰ Be Depth Profiles.....	174
A.2.4. OSL Chronology.....	179
A.2.5. Matlab Codes for Computing Depositional Concentrations.....	180
A.2.6. Input and Output for Depositional Concentration Calculations.....	191
A.2.7. Matlab Codes for Calculating ¹⁰ Be Catchment-wide Production Rate.....	193
A.2.8. Chemical Worksheets for TCN Data.....	196
A.2.9. References for A.2.....	238
A.3. Supplemental Information for Hidy et al. (2013): A latest Pliocene Age for the Earliest and Most Extensive Cordilleran Ice Sheet in Northwestern Canada.....	244

A.3.1. Matlab Codes for Calculating Burial Ages	244
A.3.2. Chemical Worksheets for TCN Data	261
A.4. License Agreement for Manuscript ‘A Geologically Constrained Monte Carlo Approach to Modeling Exposure Ages from Profiles of Cosmogenic Nuclides: An Example from Lees Ferry. Arizona’, Published in Geochemistry, Geophysics, Geosystems	275
A.5. License Agreement for Manuscript ‘A Latest Pliocene Age for the Earliest and Most Extensive Cordilleran Ice Sheet in Northwestern Canada’, Published in Quaternary Science Reviews	276

LIST OF TABLES

Table 2.1 Summary of Sample Data from the Lees Ferry M4y Terrace	16
Table 2.2 Summary of User Options Available for Simulation.....	27
Table 2.3 Statistics for Simulation of the Sand and Pebble Profiles.....	36
Table 3.1 Summary of Chronology for the Units Targeted for Sampling	55
Table 3.2 Summary of Sediment Flux Measurements from Brazos, Colorado, and Trinity Rivers.....	60
Table 3.3 Calculated Results for Depositional TCN Concentrations	66
Table 4.1 Measured ^{10}Be and ^{26}Al Concentrations and Burial Ages	96
Table 5.1 ^{10}Be Denudation Rates Calculated from the Upper White Channel (UWC) Gravel at Australia Hill.....	121

LIST OF FIGURES

Figure 2.1 DEM of Sample Site at Lees Ferry, Arizona.....	14
Figure 2.2 Photograph of Excavated Pit in M4 Terrace at Lees Ferry, Arizona	15
Figure 2.3 Snapshot of the Graphical User Interface for the Matlab™ Version of this Program	26
Figure 2.4 Concentration vs. Depth Plots for 2σ Profile Solution Spaces and Best Fits ..	32
Figure 2.5 Results for the 2σ Age, Inheritance, and Erosion Rate Solution Spaces for the Six Sample Sand Profile in the Lees Ferry M4y Terrace	33
Figure 2.6 Age vs. Erosion Rate for a Sand Profile Simulation with no Erosion Constraint	34
Figure 2.7 Results for Age, Inheritance, and Erosion Rate Solution Spaces for the Four Sample Pebble Profile in the Lees Ferry M4y Terrace	35
Figure 3.1 Location of Study Area Showing General Geologic Map of Texas with Outlines of the Brazos, Colorado, and Trinity Catchments.....	51
Figure 3.2 General Stratigraphy with Glacial Context for Surfaces on the Texas Gulf Coast.....	54
Figure 3.3 Results for ¹⁰ Be Depth Profiles acquired from the Lissie Formation.....	64
Figure 3.4 Burial Plot Showing Depositional ¹⁰ Be and ²⁶ Al Data for the Colorado, Brazos, and Trinity Catchments	71
Figure 3.5 Measured ²⁶ Al/ ¹⁰ Be vs. Depositional Age for Brazos, Colorado, and Trinity Samples	72
Figure 3.6 Calculated Sediment Fluxes vs. Time	78
Figure 3.7 Calculated ¹⁰ Be Denudation Rate Plotted against Time-integrated δ ¹⁸ O	79
Figure 4.1 Map of Yukon Showing Extent of Major CIS Advancements.....	87
Figure 4.2 Stratigraphic Column with Magnetic Polarity (N,R = normal, reversed) at Australia Hill	90
Figure 4.3 Sensitivity of Interpreted Ages to Assumed Muon Production Rates.....	95
Figure 4.4 Burial Plot Showing Klondike Gravel Sample and UWC Gravel Samples at Australia Hill	100
Figure 4.5 Contour Plot of ²⁶ Al/ ¹⁰ Be Observed on a Surface as a Function of Exposure Time and Erosion Rate	101

Figure 4.6 Magnetic Susceptibility Record from Marine Core in the Gulf of Alaska
(ODP site 887; Rea et al., 1995)..... 105

Figure 5.1 Compiled $\delta^{18}\text{O}$ Record over the last 4 Ma (LR04 stack) Based on Benthic
Foraminifera from 57 Globally Distributed Sediment Cores 116

ABSTRACT

The magnitude of global sediment flux from streams to the oceans over the last 5 Ma is poorly quantified, yet important for predicting future fluxes and deciphering the relative control of tectonic uplift, climate change, vegetation, and related feedback mechanisms on landscape evolution. Despite numerous proxy studies on global sediment delivery to the oceans, it remains uncertain whether bulk sedimentation increased, decreased, or remained approximately constant across one of the most significant global climate changes: the Plio-Pleistocene transition.

New developments and strategies in the application of cosmic-ray-produced isotopes, in part developed by this thesis, provide records of pre-historic denudation of confined fluvial catchments in Texas and Yukon. Non-glaciated, tectonically passive regions were targeted in contrast to other studies on modern sedimentation rates in order to isolate the climate influence from glacial and tectonic controls. The results suggest that average catchment temperature, and surficial processes and other factors such as vegetation cover associated with temperature, are the primary controls on the variation in landscape denudation in regions lacking tectonics and direct glacial cover. Specifically, warmer temperatures yield higher denudation rates, both at the scale of glacial-interglacial climate change and over the Plio-Pleistocene transition. The implication is that stream sediment flux to the ocean from tropical and temperate regions was higher during the Pliocene than in the Quaternary. However, this may have been balanced by an increase in sediment flux from regions covered by warm-based glaciers during glacial periods, or by increased temporary continental storage during interglacial periods.

LIST OF ABBREVIATIONS USED

AMS	Accelerator Mass Spectrometry
CDF	Cumulative Density Function
CIS	Cordilleran Ice Sheet
DEM	Digital Elevation Model
GoM	Gulf of Mexico
ICP-MS	Inductively Coupled Plasma Mass Spectrometry
IRD	Ice Rafted Debris
LIS	Laurentide Ice Sheet
LWC	Lower White Channel
ODP	Ocean Drilling Project
OIS	Oxygen Isotope Stage
OSL	Optically Stimulated Luminescence
PDF	Probability Density Function
TCN	Terrestrial Cosmogenic Nuclide
TL	Thermoluminescence
UWC	Upper White Channel

ACKNOWLEDGEMENTS

I give special thanks to my supervisor, John Gosse, who sparked my interest in cosmogenic nuclide research and has been a dedicated mentor to me during my time at Dalhousie. John has always expressed a sustained interest in my future, providing excellent advice whenever requested, insisting and supporting my attendance of conferences, and including me in interesting projects outside the realm of my thesis. Perhaps most importantly John always seemed genuinely interested in my opinion, which led to numerous fruitful discussions from landscape evolution to experiment laboratory procedures, and everything in between. This not only provided depth to my graduate experience, but made me feel more like a colleague than a student.

My thesis committee who, in addition to my supervisor, consisted of Martin Gibling, Duane Froese and Mike Blum, provided an invaluable contribution to this work. I learned so much from each of these guys while in the field and during my committee meetings. They were invaluable to this thesis from design phase to writing phase. I immensely appreciate their time and input toward this work and toward cultivating me as a scientist, and feel very lucky to have had such an outstanding committee. Additionally, I'd like to thank Rebecca Jamieson, Markus Kienast, and Fred Phillips, who were part of my examination committee and provided very helpful comments on the final version of this manuscript.

This work wouldn't have been possible without the help of our laboratory supervisor Guang Yang. Guang spent countless hours with me in the lab making sure I didn't screw up, saved my butt by always keeping spare copies of my laboratory scribbles, somehow always knew exactly where I put those samples I was working on ages ago, and would routinely pop into my office with offerings of delicious homemade food. Thank you so much!

I had significant help from Matt Garvin during multiple field excursions in southeast Texas. I owe him many thanks for taking me out on the Trinity River, assisting me in collecting samples (in the middle of June with 105° F heat), and for teaching me much about the sedimentology and architecture of the Deweyville deposits that were targeted for study in *Chapter 3*. Also, thanks for spotting that water moccasin before I jumped out of the boat right on top of it!

I've met a number of amazing people at Dalhousie who have made my time here seem far too short. With the hope that I haven't omitted anyone, these people are: Joanna Gerlings, Sakalima Sikaneta, Jose-Luis Antinao, Anne Reuther, Sofie Gradmann, Neil Davies, Clare Warren, Paul Mattern, Mega Paul Mattern, Konstanze Stubner, Bob Farmer, Dawn Kellett, Oliva Gibb, John Fisher, Keir Colbo, Carl Guilmette, Holly Steenkamp, Louise Watremez, Matthias Delescluse, Julie Griffiths, T-Bone, Allesandro Ielpi, and Annina Margreth. Particularly, I thank Neil for never providing a dull moment, Joanna for breaking me in as a grad student and for being so sassy, Jose-Luis for many a late-night fiesta, Carl for consistently having a good argument to have just one more beer, Konstanze for always being enthusiastically up for anything and for intense matches of ping pong, Paul and Matthias for teaching me how to curse in German and French,

respectively, Annina for always retuning from Switzerland with a block of delicious cheese for me, and Bob for letting me crash, for far too long, in his apartment as I finished writing this thesis. You guys are awesome, and I hope to see you at the next Halifax reunion in Europe or wherever our paths may cross again.

Finally, I'd like to thank the Tassimo™ espresso machine conveniently located in the room adjacent to my office during the waning, yet taxing, moments of thesis writing. Whenever I was down, and tapping out a single word via keyboard felt like cruel medieval torture, you were there for me, pushing me to go on. Much of the text in this thesis, specifically in these acknowledgements, was fueled by your noble caffeinated offerings. Thank you!

CHAPTER 1: Introduction

1.1. Overview of Thesis

Global sediment flux from streams to the ocean is a significant component of the carbon cycle, directly impacts biogeochemical and element cycles in the ocean, and influences silicate weathering (Beaulieu et al., 2012)—a primary mechanism for the removal of CO₂ from the atmosphere. Furthermore, the delivery of continental materials to coastal regions controls the replenishing of beaches and sinking of deltas (Syvitski et al., 2009; Blum and Roberts, 2012), stresses some types of biota inhabiting these environments, and enhances risk of disaster to infrastructure during intense storms by depleting natural buffers in these typically densely populated areas. The relative importance of various mechanisms driving global sediment flux over the last 5 Ma, however, is hotly debated. The first order mechanisms are tectonic uplift (e.g. Raymo and Ruddiman, 1992) and global climate change (Molnar and England, 1990; Peizhen et al., 2001; Molnar, 2004), with secondary, related factors including threshold changes in vegetation (Bull, 1991; Hay et al., 2002; Antinao and McDonald, 2013), changes in the global proportions of fluvial and glacial erosion (Montgomery, 2002; Koppes and Montgomery, 2009), and the average gradients of continental surfaces (Willenbring et al., 2013). Unfortunately, global sediment flux estimates have remained elusive. The sediment flux from a single river cannot be measured with high accuracy, and the variation in sediment flux with time is even less tenable. Instead, proxy data such as mass reconstructions based on preserved basin-fills (Hay et al., 1989; Peizhen et al., 2001), isotopic signatures within oceanic sediment (Willenbring and Von Blanckenburg, 2010), and numerical models trained on modern rivers that implement space-for-time

substitutions (Milliman and Syvitski, 1992; Syvitski and Milliman, 2007) are utilized, but these proxies have produced conflicting results. This has led to uncertainty regarding whether global sediment flux to the oceans has increased (Peizhen et al., 2001; Molnar, 2004), decreased (Syvitski and Milliman, 2007), or remained the same (Willenbring and Von Blanckenburg, 2010) over one of the most significant global climate changes in the last ~50 Ma (the transition from the Pliocene to the Pleistocene), and an inability to assess the relative importance of the potential drivers of global sediment flux. The necessary pieces required to disentangle this problem, which has remained open for a century (Gilbert, 1900), are 1) robust estimates of paleo-sediment flux that can be traced to a specific land surface, and 2) obtaining these flux estimates from a region where a single driving factor can be isolated. Resolving these two pieces is the motivation for this thesis.

Since the foundational works in 1986 (Klein et al., 1986; Kurz, 1986a, b; Phillips et al., 1986), terrestrial cosmogenic nuclides (TCNs) have emerged as an important tool in geomorphology. This is because TCNs—produced within minerals during exposure to secondary cosmic ray flux—are uniquely capable of simultaneously deciphering ages and rates of surface processes. TCNs thus provide a means to decipher previously intractable hypotheses concerning landscape response to tectonics, glaciers, climate change, and anthropogenic forcing of landscapes. These terrestrial isotopes have also contributed significant multidisciplinary advancements by dating early *Homo sapiens* (e.g. Partridge et al., 2003), establishing the timing of important but otherwise dangling paleoclimate records (Rybczynski et al., 2013), helping develop molecular clocks in fish species (Ruzzante et al., 2008), and, in this thesis, have contributed to knowledge of physical and

chemical paleoceanography by quantifying the delivery of continental material to ocean basins.

Calibration of the first TCN production-rate scaling scheme by Lal (1991) provided the foundation for many modern geomorphic applications. Since then, an explosion of TCN-based strategies have been subsequently developed and refined. These include single-nuclide methods that obtain surface exposure ages from recently exhumed surfaces (Phillips et al., 1986) or within deposits (Anderson et al., 1996), and multiple-nuclide methods that reveal burial durations for material once exposed to the surface (Nishiizumi et al., 1991; Granger and Muzikar, 2001). At the same time, these dating techniques provide a direct avenue for calculating denudation rates, either at the location of sampling or integrated over a region sourcing the dated material (Brown et al., 1995; Bierman and Steig, 1996; Granger et al., 1996). The ability of TCNs to reveal regional rates of surface denudation from a single sample makes them highly valuable in fluvial settings, where catchment areas serve as natural laboratories that can be chosen to isolate and analyze the effects of various internal and external driving mechanisms on their landscapes.

The aim of this thesis is to investigate fluvial sediment transport and paleo-landscape evolution with TCNs. In particular, the main goals of this work are to isolate and study the landscape response to Pliocene and Quaternary climate changes, and to further develop and improve the TCN-based techniques necessary to achieve this. The studies described in the remaining chapters of this thesis utilize two radiogenic TCNs, ^{10}Be and ^{26}Al , since their half-lives are long enough (1.387 Ma and 0.705 Ma,

respectively) to glean insight into landscape evolution during the Pliocene and Quaternary.

1.2. Design of Thesis

In *Chapter 2*, a Monte Carlo-based Matlab™ program is developed to model depth profiles of TCNs such as ^{10}Be and ^{26}Al . The program is useful, in general, as a tool to calculate exposure age probability density functions (PDFs) from TCN depth profiles with the ability to incorporate a variety of user-defined geologic variables and their estimated uncertainties. Of pertinence to this thesis is the model's ability to simultaneously calculate PDFs for exposure age and depositional TCN concentration from a depth profile in fluvial sediment. This is because the calculation of ^{10}Be catchment-wide denudation rates from fluvial sediment requires knowledge of depositional age and ^{10}Be concentration.

A manuscript for *Chapter 2* has already been published in *Geochemistry, Geophysics, Geosystems* (September 2010) and the Matlab™ code in its entirety can be found online at the Dalhousie Geochronology Centre website (<http://geochronology.earthsciences.dal.ca/#>) under the 'Downloads>Models' directory.

In *Chapter 3*, a record of late Quaternary ^{10}Be catchment-wide denudation rates is acquired from two non-glaciated, passive-margin catchments in interior Texas. This record is established to explicitly examine how landscape erosion responds to climate at the resolution of glacial-interglacial changes and over the course of the Plio-Pleistocene transition. This work is significant in that it is the first to obtain ^{10}Be -derived paleo-denudation rates that 1) are measured over and characterize both glacial and interglacial cycles, and 2) apply to regions where denudation rates are not significantly influenced by

tectonics, glacial ice cover, or drainage reorganizations. This paleo-denudation record is unique in that its variation potentially characterizes the climate component of landscape denudation rates in temperate-tropical regions.

In addition to the paleo-denudation record, the work in *Chapter 3* provides insight into how sediment is stored and remobilized in coastal plain systems. This is done by using $^{26}\text{Al}/^{10}\text{Be}$ to quantify the relative abundance of material from deeply-buried storage in the stream's active bedload. The results from *Chapter 3* reveal that sea-level fluctuations and dam construction can have a profound impact on the evacuation of stored sediment from coastal plain settings and also on the calculation of ^{10}Be catchment-wide denudation rates. This chapter is currently being prepared for submission to *Earth and Planetary Science Letters*.

Chapter 4 utilizes $^{26}\text{Al}/^{10}\text{Be}$ burial dating to constrain the age of the oldest known Cordilleran Ice Sheet (CIS) in Northwestern Canada from gravel deposits in the Klondike Goldfields, Yukon. Because the first CIS is linked to the initiation of the extensive Northern Hemisphere glaciations that dominated the Quaternary, its age is important for examining interrelationships between terrestrial ice accumulation, changes in ocean dynamics, and orbital cycles that drive insolation. The timing of the first CIS also corresponds approximately to the Plio-Pleistocene boundary, where the most significant changes in the Earth's climate in the last ~50 Ma began. Previously, the timing of the first CIS had been constrained to two possible paleo-magnetically normal intervals. The goal of this chapter is to distinguish between these intervals with additional chronology. The manuscript for *Chapter 4* has already been published in *Quaternary Science Reviews* (February 2013).

Chapter 5 summarizes the key findings and implications of this thesis and outlines two future studies for which the previous chapters form a basis. Firstly, the burial dating analysis in *Chapter 4* provides a chronologic framework for a suite of thick gravel deposits in the Klondike Goldfields. Because the Klondike Goldfields is at the edge of the all-time limit of glaciation (non-glaciated), and is tectonically stable, it serves as a feasible location to examine the impact of climate change on Plio-Pleistocene denudation rates. Utilizing the methods presented in *Chapter 3*, preliminary catchment-wide denudation rates are calculated for two time periods within a package of gravels deposited during the Plio-Pleistocene transition. Secondly, a study aimed at investigating the “regolith hypothesis”, regarding glacial transport during the first large-scale glaciation, is described and explored using the results and methods from *Chapters 3* and *4*.

CHAPTER 2: A geologically Constrained Monte Carlo Approach to Modeling Exposure Ages from Profiles of Cosmogenic Nuclides: An Example from Lees Ferry, Arizona

Paper published in *Geochemistry Geophysics Geosystems*, doi:10.1029/2010GC003084

Alan J. Hidy¹(1), John C. Gosse (1), Joel L. Pederson (2), Jann Paul Mattern (3), and Robert C. Finkel (4)

(1)Department of Earth Sciences, Dalhousie University, Halifax, Nova Scotia B3H 4R2

(2)Department of Geology, Utah State University, Logan, UT, 84322-4505, USA

(3)Department of Mathematics and Statistics, Dalhousie University, Halifax, Nova Scotia B3H 3J5

(4)Earth and Planetary Science Department, University of California, Berkeley, 371 McCone Hall, Berkeley, CA 94720-4767, USA & CEREGE, BP 80 Europole Méditerranéen de l'Arbois, 13545 Aix en Provence Cedex 4

2.1. Abstract

We present a user-friendly and versatile Monte Carlo simulator for modeling profiles of in situ terrestrial cosmogenic nuclides (TCNs). Our program (available online at <http://geochronology.earthsciences.dal.ca/downloads-models.html>) permits the incorporation of site-specific geologic knowledge to calculate most probable values for exposure age, erosion rate, and inherited nuclide concentration while providing a rigorous treatment of their uncertainties. The simulator is demonstrated with ¹⁰Be data from a fluvial terrace at Lees Ferry, Arizona. Interpreted constraints on erosion, based on local soil properties and terrace morphology, yield a most probable exposure age and inheritance of $83.9^{+19.1}_{-14.1}$ ka, and $9.49^{+1.21}_{-2.52} \times 10^4$ atoms g⁻¹, respectively (2σ). Without the ability to apply some constraint to either erosion rate or age, shallow depth

¹Corresponding author.

Email addresses: alanhidy@dal.ca (A. J. Hidy), john.gosse@dal.ca (J. C. Gosse), joel.pederson@usu.edu (J. L. Pederson), paul.mattern@dal.ca (J. Mattern), rfinkel@berkeley.edu (R. C. Finkel).

profiles of any cosmogenic nuclide (except for nuclides produced via thermal and epithermal neutron capture, e.g., ^{36}Cl) cannot be optimized to resolve either parameter. Contrasting simulations of ^{10}Be data from both sand- and pebble-sized clasts within the same deposit indicate grain size can significantly affect the ability to model ages with TCN depth profiles and, when possible, sand—not pebbles—should be used for depth profile exposure dating.

2.2. Introduction

Analyses of the distribution with depth of concentrations of TCNs in amalgamated sediment samples—“depth profiles”—are useful for simultaneously determining exposure ages, rates of erosion or aggradation, and inherited TCN concentrations in a variety of geomorphic settings (Anderson et al., 1996). Recently, it has been demonstrated that depth profiles of ^{10}Be where TCN concentrations are not yet in equilibrium with the landscape will converge to a unique solution of exposure age, erosion rate, and inheritance when accounting for both nucleogenic and muogenic production pathways (Braucher et al., 2009). Previous depth profile approaches used χ^2 minimization or Monte Carlo methods (e.g. Anderson et al., 1996; Phillips et al., 1998; Stone et al., 1998; Brocard et al., 2003; Matsushi et al., 2006; Riihimaki et al., 2006; Braucher et al., 2009), but provided limited integration of age-inheritance-erosion rate solutions and an explicit treatment of error.

Driven by recent rejuvenation in active tectonics and surface processes research, there is an increasing need for a TCN depth-profile analysis tool that provides solutions of erosion rate, inheritance and TCN inventories of catchments, and surface exposure ages in unconsolidated sediment with physical estimates of uncertainties in these

variables. Here, we introduce a versatile, user-friendly, and widely applicable depth-profile simulator designed both in MathCad™ and Matlab™ for modeling profiles of cosmogenic nuclides that: 1) incorporates geologic knowledge about the study area and soils, 2) explicitly and dynamically propagates error from all pertinent internal sources, 3) yields not just optimized values for exposure age, rate of erosion, and inheritance, but most probable values for each parameter from parameter space distributions that fully incorporate user-defined and inferred error, 4) is easy to use and time efficient so that profile data can be rapidly analyzed without specialist consultation, and 5) is freely available for download. The model is currently available for ^{10}Be and ^{26}Al , but is also appropriate for ^{14}C , and ^{21}Ne . A different model will soon be available for thermal and epithermal neutron produced TCN. We demonstrate the utility of the geologically-constrained Monte Carlo approach using cosmogenic ^{10}Be depth profiles to determine the age (and explicit uncertainty of that age) of the deposition of an alluvial terrace deposit at Lees Ferry, Arizona.

2.3. Background

2.3.1. Why Use a Depth Profile?

To exposure date Late Cenozoic sediments within landforms—such as alluvial fans, fluvial and marine terraces, marine and lacustrine beaches, and raised deltas—one must consider the possible effects of erosion and aggradation, as well as a number of other controls on TCN concentration (Gosse and Phillips, 2001). For example, the sediment may have been previously exposed, or mixed by bioturbation, cryoturbation, or pedogenesis, or the bulk density of the sediment may have varied with time due to pedogenesis or changes in water content. For sediments that have not been vertically

mixed, a depth profile can be utilized to account for a change in TCN production rate as secondary cosmic ray flux attenuates through the material. For nuclides that are produced only from high energy nuclear and muogenic reactions (e.g. ^{10}Be , ^{14}C , ^{26}Al , and ^{21}Ne), the concentration C (atoms g^{-1}) for a specific nuclide m as a function of depth z (cm), exposure time t (a), and erosion rate ε (cm a^{-1}) can be written as

$$C_m(z, \varepsilon, t) = \sum_i \frac{P(0)_{m,i}}{\left(\frac{\varepsilon \rho_z}{A_i} + \lambda_m\right)} \cdot \exp\left(-\frac{z \rho_z}{A_i}\right) \cdot \left[1 - \exp\left(-t \left(\frac{\varepsilon \rho_z}{A_i} + \lambda_m\right)\right)\right] + C_{inh,m} \cdot \exp(-\lambda_m t) \quad (1)$$

where i represents the various production pathways for nuclide m (neutron spallation, fast muon spallation, and negative muon capture), $P(0)_{m,i}$ is the site-specific surface production rate for nuclide m via production pathway i (atoms $\text{g}^{-1} \text{a}^{-1}$), λ_m is the decay constant for radionuclide m (a^{-1}), ρ_z is the cumulative bulk density at depth z (g cm^{-3}), A_i is the attenuation length of production pathway i (g cm^{-2}), and $C_{inh,m}$ is the inherited (depositional) concentration of nuclide m (atoms $\text{g}^{-1} \text{a}^{-1}$). Although theoretical production from muons does not behave as a simple exponential function with depth as described by equation (1) (Heisinger et al., 2002a; 2002b), it has been shown that reasonable approximations to muon production can be made with multiple exponential terms for muon production pathways (e.g. Granger and Smith, 2000; Schaller et al., 2002). In this depth profile simulator, five exponential terms in accordance with equation (1) are used to approximate the total muon production with depth—two terms for fast muon spallation, and three terms for negative muon capture.

Curves generated from equation (1) decrease with depth as the sum of exponentials to an asymptote that identifies the inheritance of the profile. Inheritance is the TCN concentration that existed in the sample prior to final deposition, i.e., it is the

concentration accumulated during exposure on a hillslope, during temporary sediment storage, or during transport. In the case of a radionuclide, the inherited concentration will decrease with time due to decay. Inheritance concentrations will have less influence on exposure dating of very old landforms where $C \gg C_{inh}$, or in catchments with low TCN surface inventories due to very rapid erosion and transport rates, or for radionuclides with short mean lifetimes (e.g. ^{14}C). However, in landscapes where erosion is slow in terms of TCN production rate ($\bar{\varepsilon} \leq \bar{P}(0) \bar{\Lambda} / \rho t P(0)$, where the “bar” terms represent catchment-wide averages), in catchments with high relief where TCN production rates are in places much greater than that of the alluvium in question, or for young landforms, inheritance can have a significant control on the exposure age of the landform, and can exceed the in situ-produced concentration.

The shape of a depth-profile curve is characteristic of a given exposure age and time-integrated production rate, erosion history (or aggradation history), inheritance, mixing, and bulk-density variation (and for thermal and epithermal neutron produced ^{36}Cl , volumetric water content and chemical composition). A depth profile of a single nuclide can provide the information needed to interpret the sediment age, surface erosion rate, and inheritance if the other parameters can be estimated or assumed negligible and if the sampled depth of the profile is sufficient to characterize both nucleogenic and muogenic production.

A requirement for this depth-profile technique is that inheritance must be considered constant over the depth range of the samples (Anderson et al., 1996). That is, the deposit being analyzed must have been mixed well enough such that, at $t=0$, a statistically large sample contains the same TCN concentration at every depth in the

profile. However, variability in inheritance with depth is likely where deposition is incremental over significant time, where depositional processes vary in the profile, and where catchment-wide erosion rates vary significantly during the span of deposition.

2.3.2. Lees Ferry Sample Site

To demonstrate the utility of this program, we use ^{10}Be data from an alluvial terrace at Lees Ferry, Arizona, which lies at the terminus of Glen Canyon and the head of Marble Canyon, leading to Grand Canyon (Fig. 2.1). The relatively broad valley landscape here is developed where weak rocks are encountered at the confluence of the Colorado and Paria Rivers; this has allowed the preservation of a sequence of fill terraces. The sampled terrace lies atop the dominant Pleistocene alluvial fill at this location and is mapped as the M4 (mainstem) Colorado River fill deposit (Cragun, 2008). An advantage here is that the chronostratigraphy of this terrace sequence, and especially the M4 deposit, is established from several optically stimulated luminescence (OSL) dates (Cragun, 2008). Specifically, bracketing OSL depositional ages indicate the sampled terrace was abandoned between 98 ± 10 and 77 ± 8 ka (2σ errors; Pederson unpublished data). Thus, our model can be well tested with this example. It is not the purpose of this paper to discuss the relevance of this work for Grand Canyon geology as these matters have been dealt with elsewhere (e.g. Pederson et al., 2002; Pederson et al., 2006; Polyak et al., 2008).

To collect samples for this depth profile, a 2.5 m pit was hand-excavated in the center of the M4 terrace at 36.853° N, -111.606° W and 985 m above sea level. The pit was situated where the terrace surface is smooth and level, with no original bar-and-swale topography preserved. The sampled deposit is medium-bedded, clast-supported, pebble-

to-boulder gravel which in places is imbricated (Fig. 2.2). Moderately strong desert soil development in the deposit is marked by rubification, clast weathering, and stage II calcic-horizon development in two Bk horizons. A Byk horizon with gypsum translocation extends to the bottom of the excavated soil pit. In addition, there is a moderately-well developed desert pavement with interlocking angular pebbles of varnished chert, sandstone, felsic volcanics, and orthoquartzite overlying a 1-2 cm thick Av horizon. There is no evidence of buried or exhumed soil horizons. Based on these surface and subsurface soil features, and the lack of evidence for surface erosion within 15 m of the sample site, the surface is interpreted as very stable over at least Holocene time. However, the original depositional morphology is absent on the surface, some degree of bioturbation is evident, and development of an Av horizon under the pavement suggest the landform has experienced at least some modification, and probably net denudation, over late Quaternary time. We sampled approximately 2 kg of sediment for both pebble and sand in the same depth profile to a depth of 220 cm below the M4 surface (Table 2.1). Details of sampling and processing are given in the Appendix.

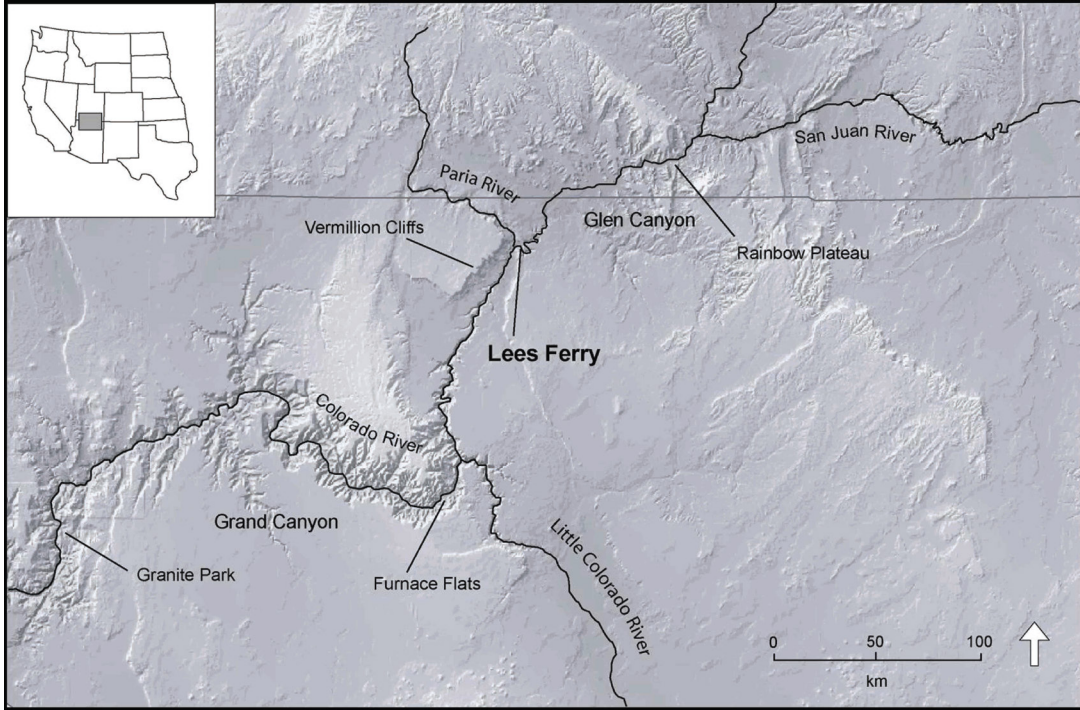


Figure 2.1 DEM of sample site at Lees Ferry, Arizona (modified after Cragun, 2008).

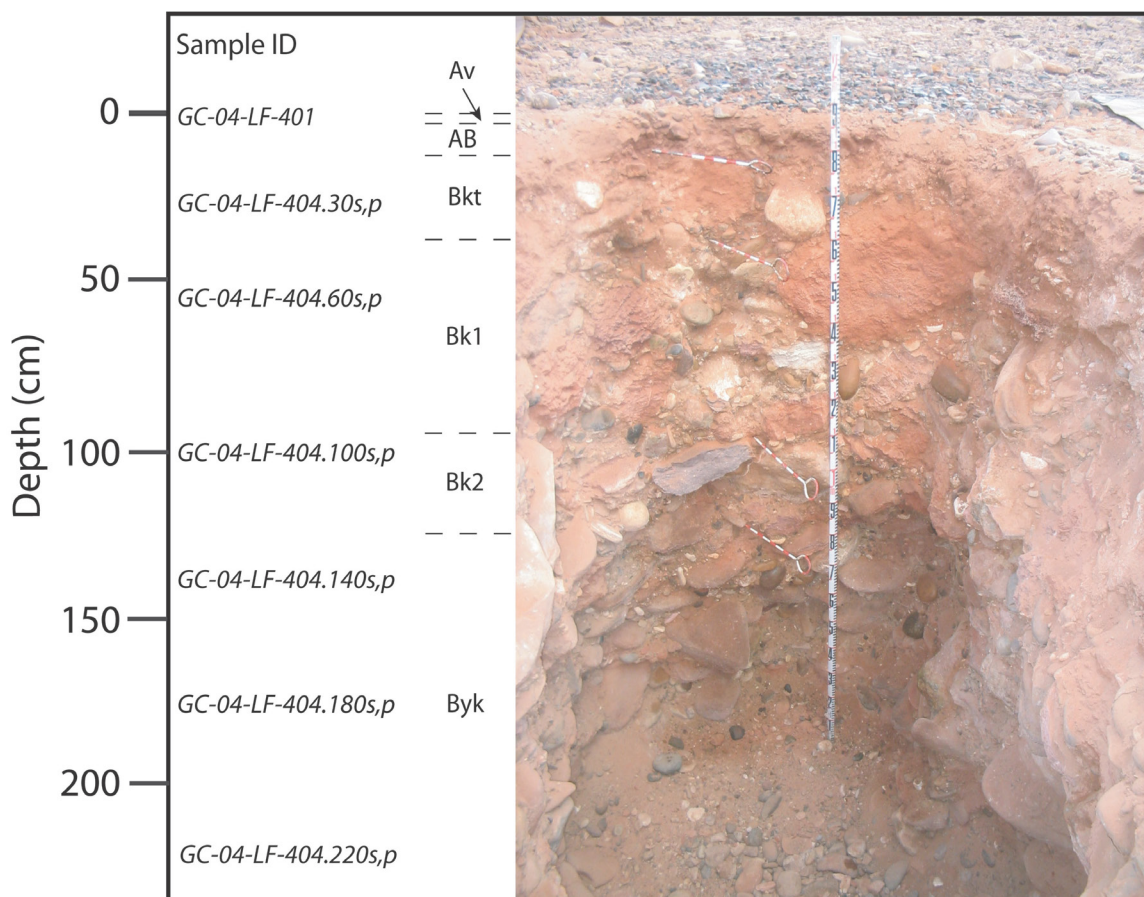


Figure 2.2 Photograph of excavated pit in M4 terrace at Lees Ferry, Arizona with identified soil horizons and TCN sample depths labeled (s, p = sand and pebble sample).

Sample ID	Depth (cm)	Thickness (cm)	Grain Size Range (μm)	Dissolved Mass (g)	Carrier Mass (g)	$^{10}\text{Be}/^9\text{Be}$ ($\times 10^{-13}$)	$[\text{}^{10}\text{Be}]$ (atoms/g)	1 σ AMS error (%)	1 σ total meas. err (%)
GC-04-LF-401	0	1 - 3	10000 - 30000	40.3970	0.2982	17.8	858320	2.30	3.05
GC-04-LF-404.30s	27.5	5	295 - 500	45.2566	0.3080	12.8	568744	2.31	3.05
GC-04-LF-404.60s	57.5	5	355 - 500	45.9469	0.3000	9.52	406713	1.99	2.82
GC-04-LF-404.100s	97.5	5	295 - 710	50.1042	0.3123	7.16	292243	2.33	3.07
GC-04-LF-404.140s	137.5	5	295 - 710	51.1421	0.3034	5.23	203072	2.33	3.07
GC-04-LF-404.180s	177.5	5	295 - 710	55.3693	0.3085	4.31	157209	2.40	3.13
GC-04-LF-404.220s	217.5	5	355 - 710	55.1112	0.2974	3.80	134198	2.10	2.90
GC-04-LF-404.30p	27.5	5	10000 - 30000	20.4567	0.2820	8.33	751848	2.35	3.08
GC-04-LF-404.60p	57.5	5	10000 - 30000	27.0228	0.2784	7.13	480425	2.14	2.93
GC-04-LF-404.100p	97.5	5	10000 - 30000	22.2058	0.2703	3.23	257602	2.55	3.24
GC-04-LF-404.140p	137.5	5	10000 - 30000	30.5314	0.2764	3.48	206250	2.55	3.24
GC-04-LF-404.180p	177.5	5	10000 - 30000	27.3406	0.2725	4.78	311548	3.35	3.90
GC-04-LF-404.220p	217.5	5	10000 - 30000	23.0414	0.2705	10.3	789506	2.37	3.10

Table 2.1 Summary of sample data from the Lees Ferry M4y terrace. Concentrations and errors were measured at the AMS facility at Lawrence Livermore National Laboratory; the total measurement error includes the AMS error added in quadrature with an estimated 2% 1 σ error in sample preparation and analysis (see Gosse and Phillips, 2001). All samples as well as a process blank were normalized with AMS standard KNSTD3110 and $^{10}\text{Be}/^9\text{Be}$ ratios were calculated using a ^{10}Be half-life of 1.387 Ma. ^{10}Be contribution from blank: 1.9 $\times 10^5$ atoms (sand samples), 5.4 $\times 10^5$ atoms (pebble samples).

2.4. Model Approach

The depth profile simulator generates solutions to equation (1) using a constrained Monte Carlo approach designed to let the user input as much inferred or assumed information as necessary about the dataset being analyzed. Probability distributions for pertinent parameters can be chosen depending on what is already known, assumed to be known, or believed about the sampled site. Additionally, constraints can be placed on coupled parameters to remove unrealistic scenarios from the parameter solution spaces. Afterward, remaining unknowns are simulated within the framework designated by the selected options (confidence limit, reduced chi-squared cut-off). The following sections describe all the parameters the user can define, and how their entered distributions are handled. See readme.txt available at

<http://geochronology.earthsciences.dal.ca/downloads-models.html>

for general instructions and system requirements. The program is available for use in both Mathcad™ and Matlab™ environments and is easily modified to the user's choice of options and parameter distributions.

2.4.1. Parameters and Uncertainty

2.4.1.1. Surface Production Rate, $P(0)$

A value of 4.76 atoms $\text{g}^{-1} \text{a}^{-1}$ (Stone (2000) recalibrated according to Nishiizumi (2007)) is set as the default ^{10}Be reference production rate at sea level and high latitude, which is scaled to the sample site using the Lal (1991) modified by Stone (2000) scaling scheme—a scheme based solely on measured latitude and atmospheric pressure (calculated from site altitude). Alternatively, the user can enter a spallogenic production

rate determined using an independent method. There are several published scaling schemes, including more complicated ones that account for longitudinal or temporal variations in production due to geomagnetic field effects (e.g. Dunai, 2000; Lifton et al., 2008). Additionally, the user can specify the reference production rate used for the built in scaling scheme.

The muogenic component of the surface production rate is calculated using the theoretical production equations of Heisinger (2002a; 2002b) We adopt the approach of Balco et al. (2008) to calculate muon production at a particular altitude and subsurface depth (in terms of mass-depth, g cm^{-2}). This approach assumes a negligible latitudinal effect on muon flux.

The user is prompted to adjust the site production rate for topographic shielding, surface geometry, and any assumed periodic cover of, for example, snow, ash, or loess. If already known, these effects can be quantified by manually entering them as scaling factors (see Gosse and Phillips (2001) for details on calculating scaling factors). For topographic shielding and geometry, a combined scaling factor is calculated within the program by importing angular measurements of the horizon at specified azimuths as well as the strike and dip of the sampled surface. The angular distribution of cosmic flux is then integrated over the entire sky less the horizon to generate a combined scaling factor.

The uncertainty of the surface production rate is relatively high. Balco et al. (2008) estimate that the 1σ error generated from empirical scaling schemes may be as high as 10%. Furthermore, by comparing production rate estimates using a variety of different scaling methods it is possible to quantify an additional uncertainty related to time-integrated geomagnetic field effects. Although this program allows the user to

propagate a production rate error through to the solution spaces of all calculated parameters, it is often not useful to do so since i) it is straightforward and explicit to propagate this error through to parameter solution spaces classically, after the simulation is performed, ii) incorporating the large, systematic error in production rate can obscure the potentially useful Monte Carlo calculated probability distributions, iii) it is commonplace for authors not to incorporate the systematic production rate error in published results, so comparisons of error for published TCN measurements may not be useful, and iv) unnecessary imputed error distributions increase model run time—a potentially significant effect for larger simulations. Thus, the uncertainty in the production rate at the surface of the landform being analyzed can be ignored and added in quadrature to the Monte Carlo generated uncertainty after computation.

2.4.1.2. Cumulative Bulk Density, ρ_z

Cumulative bulk density above each sample in a subsurface profile can be entered into the simulation in a variety of ways. For simple, homogeneous fills where cumulative bulk density may be presumed constant over the sampled depth range, high and low end members can be imputed with a random distribution, or with a normal distribution defined in terms of a mean value and standard error if bulk density is known. For surfaces with a complicated relationship between cumulative bulk density and depth (e.g. older sediment with a well-developed soil, or variations in sorting with depth), incremental measurements of bulk density within different horizons can be entered, each with their own user-defined normally distributed uncertainties. In circumstances where bulk density of a horizon may have changed significantly over time (e.g., eolian dust adding mass to an Av horizon (see Reheis et al. (1995)), or development of a petrocalcic horizon), an

estimate for time-integrated bulk density and uncertainty should be employed. The imputed measurements and errors are used to create a depth-dependent normally distributed solution for cumulative bulk density, which is then integrated over the thickness of each sample in the profile to generate mean cumulative bulk density values with normally distributed errors at the depth range of each sample.

2.4.1.3. Erosion Rate, ϵ

The shape of the upper few meters of a TCN depth profile is very sensitive to the age and erosion rate parameters and less so to inheritance. It is often necessary to provide constraint on erosion rate when modeling for an exposure age (or vice versa). Therefore, samples used for age and erosion estimates should be shallow whereas if precise estimates of inheritance are needed, samples should span over a deeper profile. The degree and depth of mixing will control how shallow samples can be collected, although attempts to interpret TCN profiles in the mixed zone have also been made (Perg et al., 2001). The program is designed to allow simultaneous constraint of both net erosion and erosion rate. In the field it is often difficult to deduce reasonable erosion rates, although estimates for other parameters, such as net erosion, may be more easily interpreted from field observations—particularly sediments with developed soils. For each depth profile solution generated, the erosion rate and age parameters are multiplied to yield a net erosion value, which must reside within the user-defined net erosion constraint to be stored as a possible solution. The values for erosion rate can be sampled randomly between end members, or normally about a mean value.

Constraining aggradation at the top of a profile surface, or negative values for erosion rate and net erosion, is also permitted by this program so long as the profile

samples are below the accumulation zone (otherwise the shallowest samples would not have been part of the profile since deposition). Changes in profile mass due to pedogenic processes (e.g. accretion of Bk or By horizons) are better treated separately, by assigning a time-averaged estimate of bulk density for those horizons (cf. previous section).

2.4.1.4. Other Parameters

The options available for constraining age, inheritance, and the neutron attenuation length are similar. Each parameter can vary randomly between two end members, or normally about a mean value. Unless the user has a priori knowledge of the age or inheritance, constraints for these parameters should be random and over conservative end members. For fast-nucleon attenuation length, a normally-distributed mean is suggested by the program based on the latitude of the sample site (Gosse and Phillips, 2001).

All production coefficients for the five-term exponential approximation of the muogenic component are determined internally and represent a best fit to the theoretical muon production calculated by Balco et al. (2008) after Heisinger (2002a; 2002b) at the site altitude and over a user-defined subsurface depth range. The default depth range is for 20 m of rock ($\sim 5400 \text{ g cm}^{-2}$), but can be extended to greater depths for deep profiles. The mean relative error of the fit is imposed as an error for the attenuation length coefficients; a normally distributed mean error in the total muogenic surface production rate can also be imposed by the user.

2.4.2. Data Inputs

There are four measured data required by the program for each sample: TCN concentration, total measurement error in TCN concentration, sample depth, and sample

thickness. This program does not reduce or standardize mass spectrometry or chemical data. Bulk density and topographic shielding may be measured or estimated as previously described. The total measurement error in TCN concentration should include the 1σ AMS uncertainty measurement as well as additional 1σ error associated with sample preparation and analysis (see Gosse and Phillips (2001) for an estimate). Although uncertainty for these measurements is entered with 1σ confidence, the program allows the user to select higher confidence limits for the output. The uncertainties in measurement for the sample's depth and thickness need not be included since random errors affecting changes in sample spacing and thickness are very small when compared to the depth range of the measured profile, and any systematic error from an uncertainty in measuring the distance to the surface boundary of the profile (potentially significant for vegetated or irregular surfaces) can be included in a conservative estimate for the uncertainty in cumulative bulk density.

2.4.3. Profile Solutions

After all parameter constraints are defined, parameter values are sampled from the assigned probability distributions to produce a solution to equation (1). The reduced chi-squared statistic is then generated from each simulated profile solution. The reduced chi-squared statistic is calculated as

$$\chi^2 = \frac{1}{d} \sum_{y=1}^x \frac{\left(\int_{T_y} C_m(z_y, \varepsilon, t) dz - N_{m,y} \right)^2}{(\sigma_{m,y} \cdot N_{m,y})^2} \quad (2)$$

where x is the number of samples in the profile, T_y is the thickness of indexed sample y (cm), $N_{m,y}$ is the measured concentration of nuclide m for sample y (atoms g^{-1}), $\sigma_{m,y}$ is the fractional standard error for $N_{m,y}$ (including all measurement errors), and d is the degrees of freedom in the dataset—a value equal to the number of samples in the profile less the number of calculated parameters (to obtain statistically robust results, it is imperative that the number of samples analyzed in a depth profile be greater than the number of calculated parameters, thus a minimum of four samples is recommended to resolve solutions for age, erosion rate, and inheritance). A cut-off value is then determined from the chi-squared probability distribution function

$$P(\chi_0) = \frac{2}{2^{d/2} \Gamma(d/2)} \int_{\chi_0}^{\infty} x^{d-1} \exp(-x^2/2) dx \quad (3)$$

where $P(\chi_0)$ is the probability of finding a chi-squared value greater than or equal to χ_0 (Taylor, 1997). Profiles yielding a reduced chi-squared statistic less than or equal to the cut-off value $P(\chi^2 \leq \chi_0)$ are accepted, and their parameters are stored as possible solutions to the profile within a user-defined confidence window (e.g. 1σ , 2σ). The simulation continues until a specified number of generated profiles are found with reduced chi-squared values lower than the cut-off. Although the cut-off is defined by the degrees of freedom permitted from the number of samples collected in the profile, the user is provided with the opportunity to define the chi-squared value to, for instance, permit cursory interpretation of TCN depth data that cannot be fit due to excessive scatter or insufficient number of samples.

2.4.4. Model Constraints for Lees Ferry M4 Terrace

A local spallogenic surface production rate of $9.51 \text{ atoms } ^{10}\text{Be} (\text{g SiO}_2)^{-1} \text{ a}^{-1}$ was calculated for the Lees Ferry site using the Stone (2000) after Lal (1991) scaling scheme (reference production rate of $4.76 \text{ atoms g}^{-1} \text{ a}^{-1}$), and accounting for topographic shielding (2.1% effect). The local total muogenic surface production rate was calculated to be $0.26 \text{ atoms } ^{10}\text{Be} (\text{g SiO}_2)^{-1} \text{ a}^{-1}$ after Heisinger (2002a; 2002b). The parameters for age, inheritance, and erosion rate were allowed to vary between conservative high and low values in order to avoid constraining by these parameters in the initial simulation. Net erosion of the M4 terrace surface was considered minimal and constrained between 0 and 30 cm. The fitted depth range for muon production was reduced to 5 m since this value is greater than the sum of our maximum allowed erosion and depth of deepest sample (a smaller depth range produces a better fit to the Heisinger (2002a; 2002b) muon production equations). Since measurements of bulk density in the excavated soil pit returned values of $2.5 \pm 0.2 \text{ g cm}^{-3}$ at each measured depth (30, 60 and 205 cm) (a flimsy plastic bag was inserted into hole and filled with a measured quantity of water to determine the volume of excavated mass at each depth), cumulative bulk density was modeled as constant over the sampled interval. However, the authors believe these measured bulk density values should be considered a maximum since excavation of the very coarse boulder-gravel fill may have led to a systematic error in determining the volume of sediment excavated; a density approaching that of solid granite (2.7 g cm^{-3}) is unreasonable for a fluvial deposit. Thus, cumulative bulk density was treated as constant with depth, but allowed to vary randomly between 2.2 and 2.5 g cm^{-3} . A normally distributed mean value of 160 g cm^{-2} with a 3% standard error was used for the neutron

attenuation length. See Table 2.2 for a summary of the Lees Ferry model constraints and Fig. 2.3 for a snapshot of the data entered into the MatlabTM graphical user interface. Each simulation continued until 100,000 profile solutions were obtained.

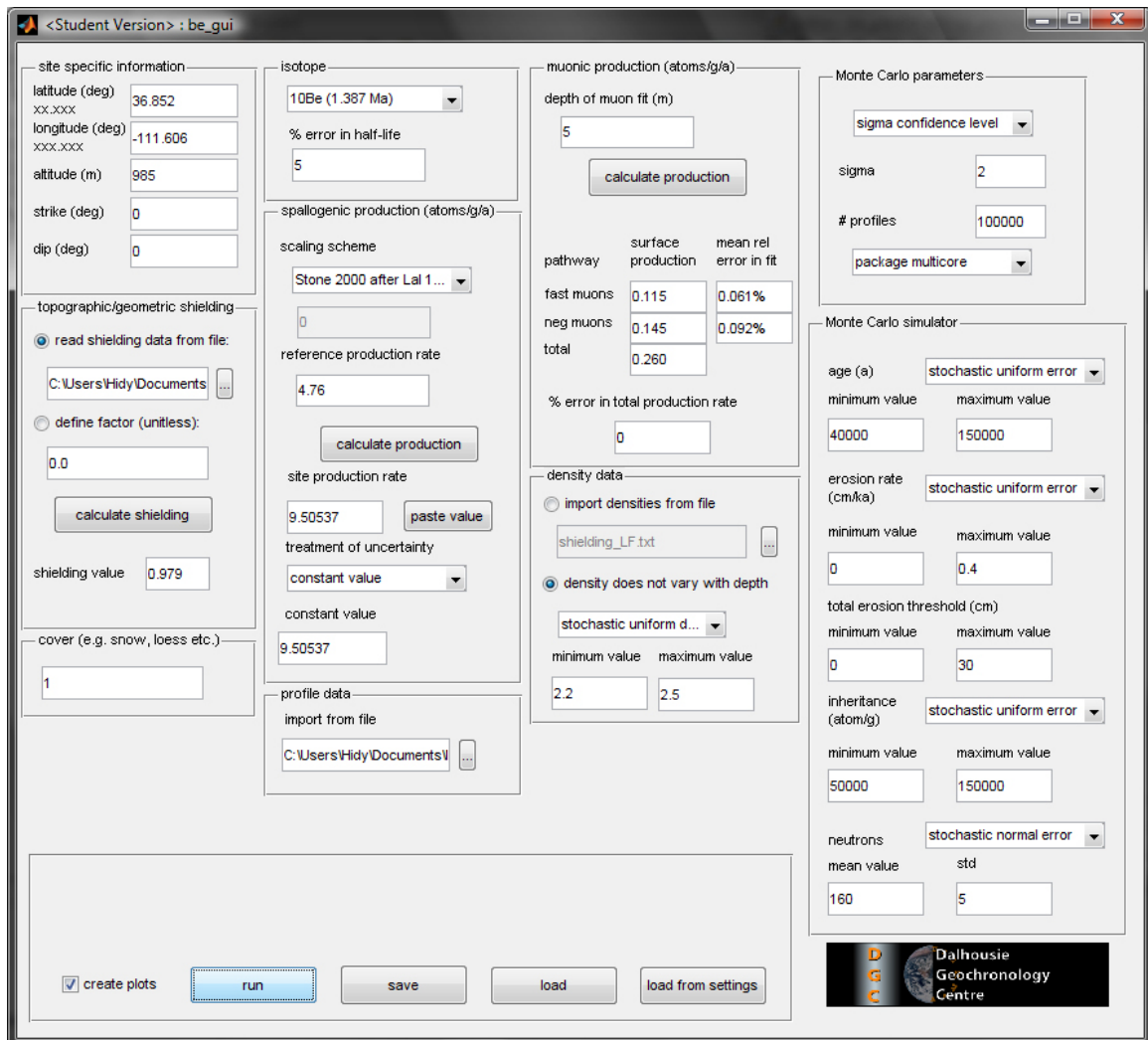


Figure 2.3 Snapshot of the graphical user interface for the Matlab™ version of this program

Parameter	Value	Unit	Description
<i>Location data</i>			
latitude	36.852	deg	latitude of profile site in decimal degrees
longitude	-111.606	deg	longitude of profile site in decimal degrees
altitude	985	m	site altitude
strike	0	deg	strike of surface (0 - 360 deg)
dip	0	deg	dip of surface (0 - 90 deg; right hand rule)
<i>Shielding data</i>			
azimuths	0 ^a	deg	data are imported from ASCII text file; first column with azimuth measurements, second column
angles	15 ^a	deg	with corresponding angle to horizon
<i>Sample data</i>			
depths	27.5 ^a	cm	
thickness	5 ^a	cm	data are imported from ASCII text file with four columns of data in the following order: depths (to
isotope concentration	568744 ^a	atoms g ⁻¹	(depth to top of each sample), thicknesses (sample thickness), sample concentrations, error in
measurement error	0.0305 ^a	NA (fraction)	measurement. See Table 2.1 for suite of data used for simulation
<i>Density data</i>			
depth dependent			
depths	NA ^a	cm	data are imported from ASCII text file with three columns of data in the following order: depths (to
densities	NA ^a	g cm ⁻³	top of each horizon--always starts with 0), horizon densities, and estimated uncertainty in density
individual uncertainties	NA ^a	g cm ⁻³	measurement
depth constant			
option 1 constant value	NA	g cm ⁻³	density is constant with depth, and it's value is fixed
option 2 mean value	NA	g cm ⁻³	density is constant with depth, but value varies with a normal distribution about a mean value
option 3 std	NA	g cm ⁻³	
option 3 max value	2.2	g cm ⁻³	density is constant with depth, but varies randomly between two end member values
option 3 min value	2.2	g cm ⁻³	

^aNot entered as a single value, but as a column matrix of data from an ASCII text file; value shown is one example

^bValue is a boundary condition and a conservative estimate for the particular end member; efficient end members are determined iteratively (see Appendix).

Table 2.2 Summary of user options available for simulation. Data and simulation parameters shown are those entered for the Lees Ferry sand profile.

Parameter	Value	Unit	Description
<i>Spall. production</i>			
<i>option 1</i>	manual entry	atoms g ⁻¹ a ⁻¹	enter a production rate calculated from some other source
<i>option 2</i>	internally calculated	atoms g ⁻¹ a ⁻¹	production rate calculated from Stone (2000) after Lal (1991)
	reference production rate	atoms g ⁻¹ a ⁻¹	from Stone (2000) recalibrated after Nishiizumi (2007); user can edit
uncertainty			
<i>option 1</i>	constant value	atoms g ⁻¹ a ⁻¹	surface production rate is constant
<i>option 2</i>	mean value	atoms g ⁻¹ a ⁻¹	surface production rate varies with a normal distribution about a mean value
	std	atoms g ⁻¹ a ⁻¹	
<i>option 3</i>	max value	atoms g ⁻¹ a ⁻¹	surface production rate varies randomly between two end member values
	min value	atoms g ⁻¹ a ⁻¹	
<i>Neutron atten.</i>			
<i>option 1</i>	constant value	g cm ⁻²	neutron attenuation length is constant
<i>option 2</i>	mean value	g cm ⁻²	neutron attenuation length varies with a normal distribution about a mean value
	std	g cm ⁻²	
<i>option 3</i>	max value	g cm ⁻²	neutron attenuation length varies randomly between two end member values
	min value	g cm ⁻²	
<i>Muon production</i>			
	depth of production fit	5 m	depth of curve fit to muon production of Balco et al. (2008) after Heisinger (2002a,2002b); total
	total uncertainty	0 NA (%)	uncertainty for fast and negative muons
<i>Isotope half-life</i>			
	uncertainty in half life	5 NA (%)	estimated uncertainty in half life
<i>Age</i>			
<i>option 1</i>	constant value	NA	age is treated as constant during simulation (useful for sensitivity analyses)
<i>option 2</i>	mean value	NA	age varies with a normal distribution about a mean value (independent age measurement)
	std	NA	
<i>option 3</i>	max value	40,000 ^b	age varies randomly between two end member values (end members should be conservative enough to
	min value	150,000 ^b	not constrain simulation)

^aNot entered as a single value, but as a column matrix of data from an ASCII text file; value shown is one example

^bValue is a boundary condition and a conservative estimate for the particular end member; efficient end members are determined iteratively (see Appendix).

Table 2.2 (continued) Summary of user options available for simulation. Data and simulation parameters shown are those entered for the Lees Ferry sand profile.

Parameter	Value	Unit	Description
<i>Erosion</i>			
net erosion			
max value	30	cm	maximum erosion estimated from site (use large value if unknown)
min value	0	cm	minimum erosion estimated from site (can be negative for aggradation)
erosion rate			
constant value	NA	cm ka ⁻¹	erosion rate is treated as constant during simulation (useful for sensitivity analyses)
mean value	NA	cm ka ⁻¹	erosion rate varies with a normal distribution about a mean value (independent erosion rate measurement)
std	NA	cm ka ⁻¹	
option 1	0.4 ^b	cm ka ⁻¹	erosion rate varies randomly between two end member values (end members should be conservative enough to not constrain simulation; must not contradict net erosion cut-offs)
option 2	0	cm ka ⁻¹	
option 3			
Inheritance			
option 1	NA	atoms g ⁻¹	inheritance is treated as constant during simulation (useful for sensitivity analyses)
option 2	NA	atoms g ⁻¹	inheritance varies with a normal distribution about a mean value (independent inheritance measurement)
option 3	50,000 ^b	atoms g ⁻¹	inheritance varies randomly between two end member values (non-negative values only; conservative end members can usually be estimated from deepest sample)
	150,000 ^b	atoms g ⁻¹	
MC settings			
option 1	NA	unit less	only accepts profile solutions with a lower reduced chi-squared value
option 2	2	unit less	only accepts profile solutions within specified sigma confidence
	Y	NA	allows parallel utilization of multiple core and processor machines (see readme.txt)
	100,000	unit less	number of acceptable solutions to generate before simulation ends
^a Not entered as a single value, but as a column matrix of data from an ASCII text file; value shown is one example			
^b Value is a boundary condition and a conservative estimate for the particular end member; efficient end members are determined iteratively (see Appendix).			

Table 2.2 (continued) Summary of user options available for simulation. Data and simulation parameters shown are those entered for the Lees Ferry sand profile.

2.5. Results

2.5.1. Lees Ferry Sand Profile

The ^{10}Be data for the six sand samples (see Table 2.1) were modeled using the constraints shown in Table 2.2. These data permitted solutions that exceeded the chi-squared cut-off for the 95% (2σ) confidence window and exhibited a well-behaved exponential decrease in ^{10}Be concentration with depth (Fig. 2.4a); only solutions at or below this value were retained for analysis in order to appropriately propagate error through to the calculated parameters. Because of our imposed constraint on net erosion, the erosion-rate solution space is truncated, and thus is not useful for estimating an erosion rate (Fig. 2.5). The six sample simulation yields modal values of $83.9^{+19.1}_{-14.1}$ ka, and $9.49^{+1.21}_{-2.52} \times 10^4$ atoms g^{-1} for age and inheritance, respectively (Table 2.3a, Fig. 2.5).

Although a minimum chi-squared value is returned for the set of curves generated by the simulation, comparison of the solution space for age and associated chi-squared values (Fig. 2.5) demonstrates that, for this profile, optimization will not converge to a single solution. These results show a wide range of ages with chi-squared values essentially identical to the minimum chi-squared value. That is, as the chi-squared value decreases to the minimum value allowed by this dataset, the resulting age does not approach a unique value. This is in contrast to the inheritance solution space (Fig. 2.5) which does converge to a unique solution as chi-squared value decreases. Examination of the resulting age and erosion rate pairs in an unconstrained simulation further demonstrates no relationship between minimized chi-squared and age; Fig. 2.6 shows that any age greater than ~ 70 ka is equally likely to be obtained from an optimization

algorithm. Therefore, for this dataset, without some constraint on either net erosion or erosion rate only a minimum age can be resolved.

2.5.2. Lees Ferry Pebble Profile

The measured TCN concentrations for the sand profile produce a theoretical exponential distribution with depth in concordance with equation (1); the pebble profile, however, does not demonstrate an exponential decrease in TCN concentration with depth (Fig. 2.4b). In particular, the ^{10}Be concentrations of the deepest two samples in the pebble profile deviate significantly from the theoretical profile shape that the upper four follow. Because of such an extreme deviation ($\sim 75\%$ and $\sim 500\%$ from the expected concentrations based on the trend of the upper four), these two deepest pebble samples could not be included in the model, as it is apparent that no solution would satisfy all six samples.

The ^{10}Be data for the four uppermost pebble samples (see Table 2.1) were modeled using the same model constraints as those imposed on the sand samples since they were collected in the same pit. For these samples, no solution existed at or below the chi-squared cut-off for the 95% (2σ) confidence window. Thus, to obtain some result, the chi-squared cut-off was manually increased to look at the distributions for each parameter's solution space based on the collection of best possible fits to the data. Although this cripples our ability to quantify error in the calculated parameters using equation (3), it still allows the determination of most probable (modal) values based on the data. The simulation yields modal values of 117 ka, and 4.60×10^4 atoms g^{-1} for age and inheritance, respectively (Table 2.3b, Fig. 2.7).

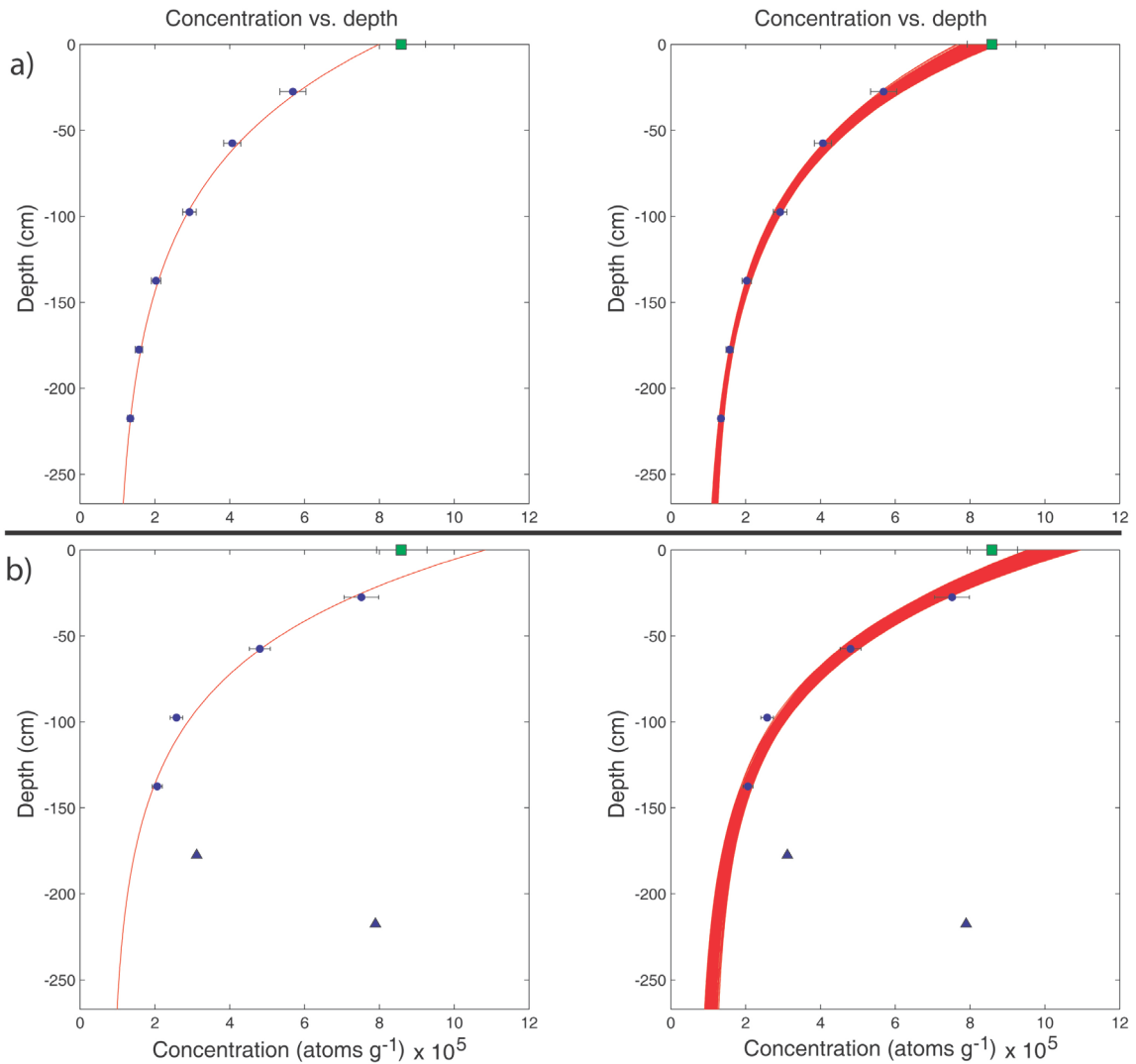


Figure 2.4 Concentration versus depth plots illustrating the (right) 2σ profile solution spaces and (left) best fits to equation (1) for (a) the sand profile and (b) the pebble profile. Error bars represent 2σ total measurement error (see Table 2.1). The lower two samples in the pebble profile (blue triangles) were not part of the simulation due to extreme discordance with the theoretical change in nuclide concentration with depth. The green square represents an amalgamated desert pavement sample; this sample was not included in any simulation since erosion or aggradation may have changed its position with respect the other samples in the profile.

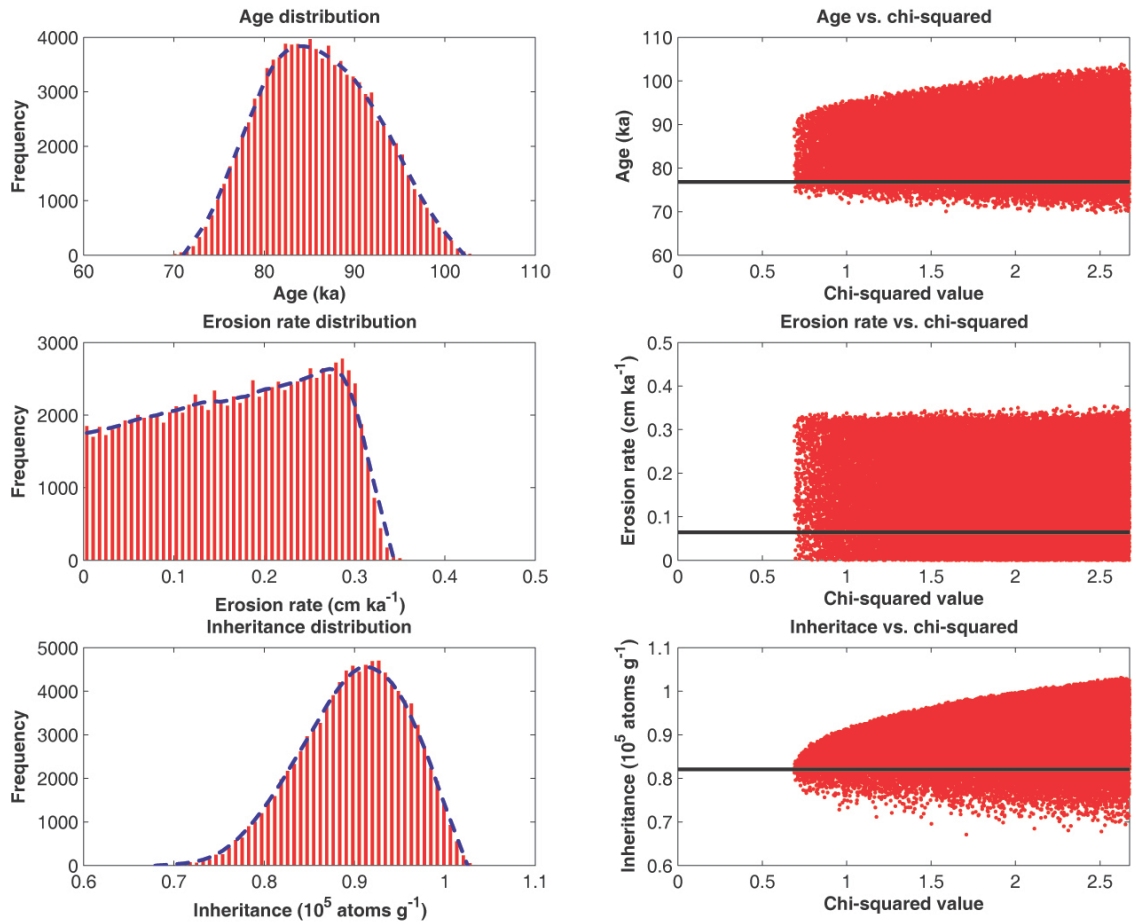


Figure 2.5 Results for the 2σ age, inheritance, and erosion rate solution spaces for the six sample sand profile in the Lees Ferry M4y terrace. Solid black lines indicate the lowest chi-squared value. The chi-squared cut-off was obtained from equation (4). Statistics for this simulation are shown in Table 2.3.

Age vs. erosion rate

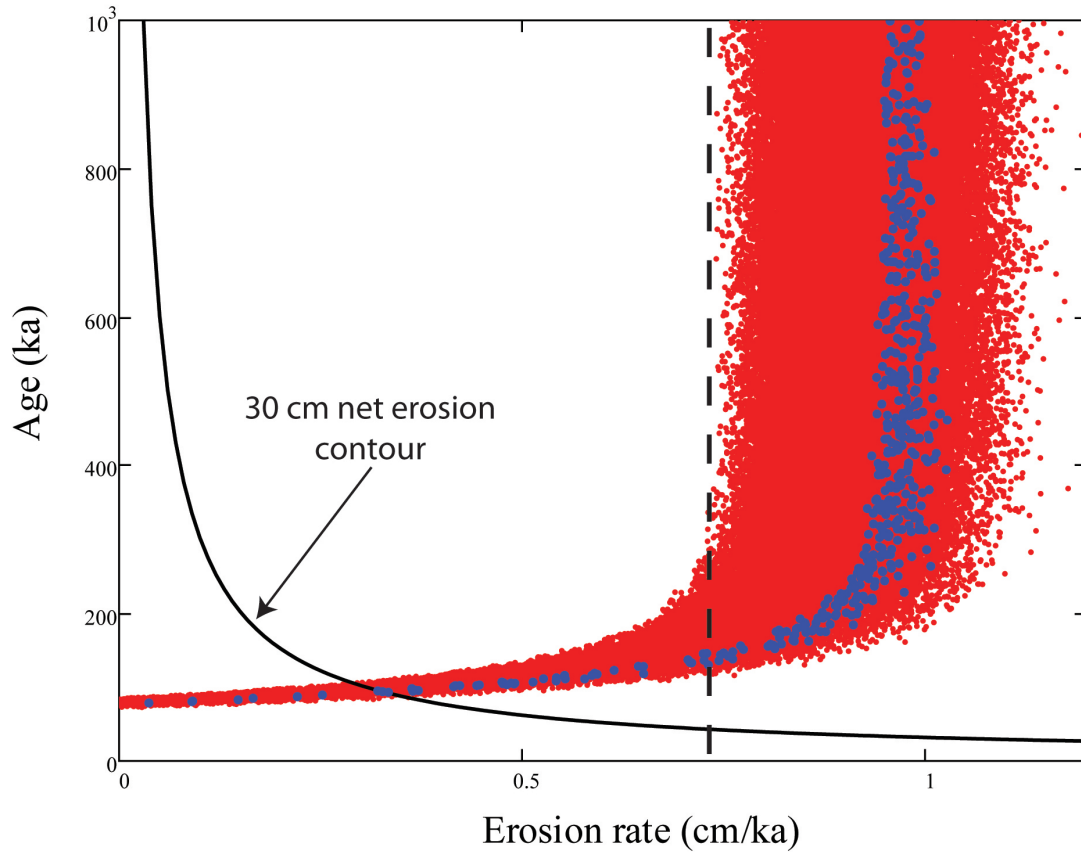


Figure 2.6 Age versus erosion rate for a sand profile simulation with no erosion constraint. Small red dots define the solution space; large blue dots mark the 500 best (lowest chi-squared) solution pairs (out of 100,000). The solid black curve marks the 30 cm net erosion cut-off for our sample site. The dashed black line marks the erosion rate cut-off that would be needed to resolve a finite age. Notice 1) that the lowest chi-squared solutions are broadly scattered with respect to age, and 2) that without a constraint on erosion (or erosion rate), only a lower age limit can be determined for this data set.

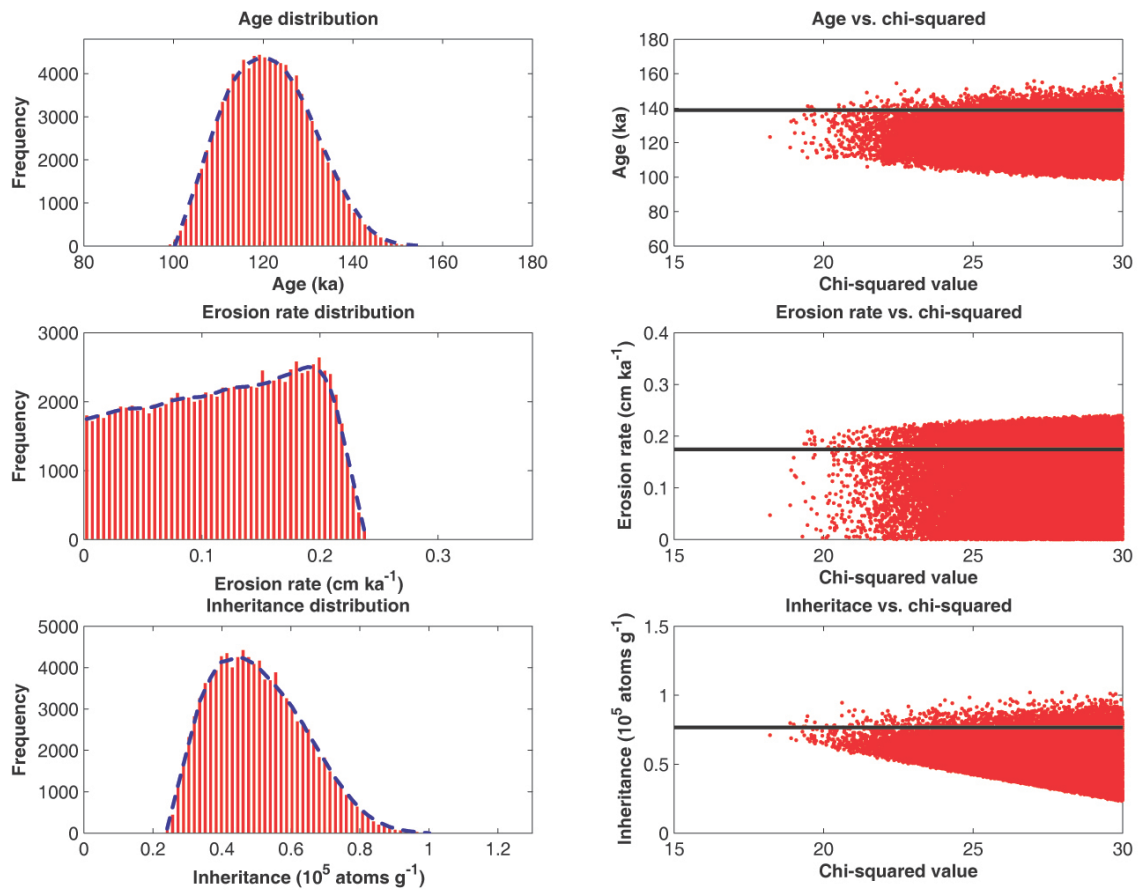


Figure 2.7 Results for age, inheritance, and erosion rate solution spaces for the four sample pebble profile in the Lees Ferry M4y terrace. Solid black lines indicate the lowest chi-squared value. A chi-squared cut-off of 30 was artificially imposed to generate these distributions. The statistics for this simulation are shown in Table 2.4.

Table 2.3 Statistics for simulation of the a) six sample sand profile, and b) four sample pebble profile. Maximum and minimum values represent the 95% (2σ) confidence window for each parameter for the sand data; for the pebble data a cut-off of $\chi^2 \leq 30$ was imposed and therefore no reasonable uncertainty can be obtained from the simulation. Statistics are shown for erosion rate; however, since constraint was placed on net erosion they cannot be used to report a value for erosion rate.

Statistic	Age (ka)	Inheritance (10^4 atoms g^{-1})	Erosion rate ($cm\ ka^{-1}$)
<i>a) sand profile (6 samples)</i>			
<i>mean</i>	86.0	9.35	0.17
<i>median</i>	85.7	9.40	0.18
<i>mode</i>	83.9	9.49	0.28
<i>lowest χ^2</i>	76.8	8.21	0.06
<i>maximum</i>	104	10.7	0.35
<i>minimum</i>	69.8	6.97	0.00
<i>b) pebble profile (4 samples)</i>			
<i>mean</i>	121	5.24	0.12
<i>median</i>	121	5.09	0.12
<i>mode</i>	117	4.78	0.20
<i>lowest χ^2</i>	139	7.67	0.17
<i>maximum</i>	157	10.6	0.24
<i>minimum</i>	98.6	2.43	0.00

2.6. Discussion

2.6.1. Interpreting Results with this Program

Depending on the quality of the dataset being analyzed, this profile simulator can be used in different ways. For data where equation (1) provides sufficient solutions within the desired confidence window, it is straightforward to enter appropriate parameter constraints, run the simulation, obtain desired statistics on the parameter solution spaces, and report an age. Maximum and minimum values would represent the upper and lower 2σ error in age. However, in some sediment TCN concentrations may vary sporadically with depth or perhaps the profile contains fewer samples than the four needed to use equation (3) to calculate a chi-squared cut-off. In those circumstances a rigorous treatment of error is not possible with this program; however, the model can still be used to generate modal values for the calculated constraints. For the case of data that are broadly scattered with depth, the chi-squared cut-off can be manually increased until a desired number of profile solutions can be generated (as was done for the Lees Ferry pebble profile). This allows the user to view and collect the best possible fits to the data and ascertain if the calculated parameters converge to a solution. We stress, however, that any solutions obtained via this approach cannot be quoted with an uncertainty as such data violate the model's assumption that inheritance is constant with depth. For sparse data ($d < 1$) that is not broadly scattered with depth, we recommend setting the chi-squared cut-off to the number of samples in the profile. This results in parameter solution spaces defined by curves with a lower chi-squared value than that of pseudo-data existing at the maximum error for each measured sample; this approach should yield a conservative estimate of error in the calculated parameters.

2.6.2. Age of the Lees Ferry M4 Terrace

The most probable exposure age for the abandonment of the M4 terrace is $83.9^{+19.1}_{-14.1}$ ka based on the six-sample sand profile. The maximum and minimum simulated values of 103 ka and 69.8 ka represent our 2σ confidence limits for this age (+23% and -17%, respectively). This incorporates all relevant sources of error except the poorly known systematic errors in spallogenic and muogenic production rates. This result agrees with independent OSL-derived depositional ages that bracket the exposure age between 98 ± 10 and 77 ± 8 ka (2σ errors). We reject the results of the pebble profile data, which yield a modal age of 117 ka, for several reasons: i) the lowest two samples in the profile do not agree with the theoretical relationship between ^{10}Be concentration and depth (which was demonstrated by the sand profile, indicating that there is no mixing of sediment) (Fig. 2.5b), ii) the remaining four samples that appeared to agree with this theoretical relationship did not pass the chi-squared test at the 95% confidence window—implying less than a 5% probability that these data are governed by the expected distribution of equation (1), iii) the number of individual clasts acquired for the amalgamated pebble samples (150 – 200) was much less than that acquired for the sand samples ($\sim 10^7$); thus, the pebble samples produce statistically weaker results along with an increased potential for ^{10}Be within a single clast to dominate the amalgamated concentration, and iv) the pebble age result is significantly older than the independent geochronologic constraints at the site.

Interestingly, the ^{10}Be concentration of the desert pavement sample at the surface is in complete agreement with the modeled surface concentrations from the sand profile (Fig. 2.4); this supports the field interpretation that the terrace surface has been relatively

stable over the duration of exposure, with negligible denudation over time, and may have implications for the longevity of desert pavement stability.

2.6.3. Implications for Sampling TCN Depth Profiles

The Monte Carlo-constrained program can help devise sampling strategies for TCN depth profiles and assist the interpretation of their data. For example, the model can be run in a forward style to test the sensitivity of parameters, calculate optimal sample depths, and test the feasibility of exposure dating a particular site.

The deviation between the Lees Ferry sand and pebble data is an important result that should guide future profile sampling. Since the pebble and sand samples acquired from the excavated soil pit were collected from the same horizons, the post-depositional production of ^{10}Be in both the sand and pebble samples should be the same. The results, however, are widely different—especially for the two lowest samples. Since the sand data yield a tight concentration vs. depth relationship, we exclude the possibility of post-depositional mixing. Instead, either our lower pebble samples are not representative of the average inherited TCN concentration, or the assumption that the TCN inventory is constant with depth is invalid. We cannot preclude unrecognized error in chemistry or AMS measurement, but we believe this is unlikely considering the precision of the measurements and process blank. Although Repka et al. (1997) suggested that an amalgamated pebble sample of 30 or more clasts is sufficient to provide a representative average TCN concentration, this may not be true for all alluvial deposits, particularly those in arid environments. Firstly, a much higher variability of clast-specific inheritance concentrations is to be expected in sediment sourced by catchments with overall low rates of denudation. Secondly, mixing of gravel clasts is likely to be less complete than mixing

of sand. We recommend always sampling sand if available and emphasize caution when sampling pebbles for TCN depth profiles because the probability of a constant inherited TCN concentration with depth likely decreases with increasing grain size.

For ^{36}Cl depth profiles, procedures outlined by Kirby et al. (2006) provide a thorough means of considering the effect of soil moisture. However, the added complication of a depth variation in thermal neutron flux due to chemical variations in the soil profile must also be considered when sampling. If the thermal neutron component is unavoidable, or if it is sought due to the extra sensitivity of the cumulative thermal neutron profile to surface erosion, then collecting swaths of sediment between each sample and above the uppermost sample should be considered in order to provide a more thorough means of establishing elemental abundances of thermal neutron absorbers and producers throughout the profile. A version of the MathCad™ profile code for interpreting ^{36}Cl depth profiles is available online; a Matlab™ version is currently being coded.

2.7. Conclusions

This program allows the performance of rapid, simple, comprehensive Monte Carlo simulations of TCN depth profiles which can be constrained from knowledge of the geology at the collection site. Additionally, it permits an explicit propagation of all error sources to calculated values for age, inheritance, and erosion rate.

Results generated from simulating a sand profile from the Lees Ferry M4 terrace are robust, and agree with independent OSL chronology. However, a simulation performed on the Lees Ferry sand profile without constraint on erosion yields a non-unique and non-finite age (Fig. 2.6). This indicates that without constraint on erosion rate

or age, neither parameter can be resolved with a shallow depth profile (specific to TCNs without production from thermal and epithermal neutrons).

Concentrations from a pebble profile (derived from the same pit as a sand profile) indicate that grain size can significantly influence age models due to the higher probability of poor mixing and higher contributions of inheritance from individual larger clasts during deposition.

Because many different profile curves (reflecting uncertainty in variation of density and inheritance with depth) can explain TCN concentrations measured in the subsurface, the total uncertainty in ages estimated from depth profile studies is higher than normally reported using a minimum chi-squared optimization approach or a simpler curve fitting method. This intrinsic error analysis better reflects the true uncertainty of TCN dating with depth profiles.

2.8. Appendix

2.8.1. Lees Ferry, Specific Sampling Methods

A 250 cm pit was hand-excavated in the M4y terrace and six ~1 kg samples of both sand and pebbles were collected at regular depth intervals of 30 – 40 cm (Fig. 2.2). Depth contours were marked by a level line nailed into the pit walls, and the samples were collected from a ± 2.5 cm swath along each contour. Sand samples were sieved in the field to remove the coarse (>2 mm) grains, then later sieved to the desired size range (Table 2.1); pebble samples (~1 – 3 cm) with high quartz content were collected indiscriminately, but consisted primarily of chert and quartzite. Each pebble sample consisted of ~150 – 200 individual clasts. Additionally, one surface sample of the desert pavement was collected in a fashion identical to that of the pebble samples. The physical

and chemical sample preparation procedures used for all samples at Dalhousie Geochronology Centre are provided in Appendix B. From 20 - 60 g of pure quartz per sample, the thirteen ^{10}Be targets (plus two process blanks) were mixed 1:1 with niobium powder, packed in stainless steel target holders, and analyzed at the Center for Accelerator Mass Spectrometry at Lawrence Livermore National Laboratory.

2.8.2. Laboratory Methods

Sand samples were sieved to extract the 355 – 500 μm range; the desert pavement and other pebble samples were crushed, and then sieved to extract this same size range in order to accelerate digestion. Ranges were expanded to 295 – 710 μm for samples that did not contain enough mass in the 355 – 500 μm bin. All samples were processed at the Dalhousie Geochronology Centre, AMS measurements were completed at CAMS-LLNL, and the resulting ^{10}Be concentrations are reported in Table 2.1.

Each sample was subjected to the following laboratory procedures outlined in the DGC-CNEF laboratory manual (<http://cnef.earthsciences.dal.ca>): aqua regia (3:1 of $\text{HCl}:\text{HNO}_3$), HF etching, ultrasonic quartz separation, magnetic separation, sand abrasion, and hand picking. These procedures purified the samples to ~99% quartz, dissolved aggregate grains and weak silicates, and removed any atmospheric ^{10}Be adsorbed to the grain surfaces. Approximate 0.2 mg of Be carrier was added to each sample to facilitate AMS by isotope dilution. The carrier was produced by J. Klein from a shielded beryl crystal extracted from the Homestake Gold Mine and has a long term average $^{10}\text{Be}/^9\text{Be}$ of 4×10^{-15} at LLNL. Additionally, two process blanks were analyzed and used to subtract any background concentration, which in all instances was <10% the adjusted value. The samples were digested in a $\text{HF}-\text{HClO}_4$ mixture and the Be^{+2} cation

extracted via ion chromatography. After precipitating the Be^{+2} cation at pH 9.2 with ultrapure ammonia gas, the samples were baked in a furnace at 850°C for one hour to produce a small amount of beryllium oxide powder—which was mixed 1:1 with niobium and sent to Lawrence Livermore National Laboratory for AMS analysis.

2.8.3. Model Run Time

It is difficult to categorically state the time it will take for this simulator to adequately model a given dataset as the duration will depend on the quality of the dataset, how tightly the various pertinent parameters can be constrained, the desired confidence window of the calculated results, and also, of course, the computer used to run the program. However, once the user has set all parameters and constraints, an estimate can be made by performing a quick test run with a low number of desired profiles (we suggest ~ 1000). This allows the user to extrapolate the duration for a much larger simulation, as processing speed is linear, and, more importantly, get a better sense of how well the constraints imposed on the calculated parameters agree with the data. For example, say the exposure age of a given surface is unknown and that the user can only say confidently that it is somewhere between 5 – 500 ka. After a quick test run with this age range, however, it is seen that no solutions exist outside of an age range of 50 – 100 ka. The user should then feel comfortable further constraining the age window, keeping in mind that a distribution generated from a low number of simulated profiles will only yield a rough estimate for the age window boundaries. Constraining the simulated age window to, say, 20 – 150 ka would probably now be justified and would also speed up the run time for the larger simulation. On the contrary, if any test simulation (or full simulation) yields solutions at either boundary of a calculated parameter window, then

that parameter window should be expanded accordingly unless the user has some reason to constrain it.

2.9. Acknowledgments

Thanks to G. Yang for support in the Dalhousie Geochronology Centre cosmogenic nuclide lab. We appreciate the support of the staff of the LLNL-CAMS during the AMS runs, J.L. Antinao for early discussions on the model, and E. McDonald for insights into soils geomorphology. J. Stone and G. Balco, and F. Phillips provided Matlab- and Excel-based codes for ^{10}Be and ^{36}Cl , respectively. Thanks to F. Phillips, S. Marrero, and B. Borchers for evaluating the Beta version of the ^{36}Cl depth profile code and providing extremely helpful feedback. We benefited from comments by two anonymous and thorough reviews on a previous version of the manuscript (and code). The MatlabTM Central database provided several code packages used by our simulator (datatablepackage, horrorbar, and multicore). The authors acknowledge funding from the following sources: JCG: AIF-100-1052, CFI, NSERC Discovery Grant, NSF-EAR9903126. JP: NSF-EAR 0346054.

2.10. Addendum

Following publication of the depth profile calculator described in this chapter, an updated version was created that uses an importance sampling of the Monte Carlo simulation results to construct Bayesian probability density functions (PDFs) and estimates of most probable values. The Bayesian solutions are a more complete representation of the most probable values for age, erosion rate, and inheritance solutions as statistics are kept for both the accepted and rejected profile. This was done to obtain continuous probability curves within the constraints set by the user (thanks to B. Borchers

for suggesting this via pers. comm. 2010). The PDFs are constructed by weighting each parameter result by its resulting chi-squared value using the chi-squared likelihood function—converting chi-squared values into probabilistic values. These probabilistic values are summed and then averaged into evenly spaced bins that divide each parameter solution space (the number of bins is arbitrarily large and depends on the size of the simulation). The mean probability at each binned parameter value is then smoothed and normalized such that the area under the resulting PDF is equal to 1. The most probable solution for each parameter is then obtained as the maximum value of the PDF; 2σ upper and lower uncertainties are determined by first constructing a cumulative distribution function from the PDF and obtaining the parameter values at 97.7% and 2.3%.

CHAPTER 3: Climatically-driven Variation in Sediment Flux from Interior Texas Established with Cosmogenic ^{10}Be and ^{26}Al

(manuscript in preparation for submission to Earth and Planetary Science Letters)

Alan J. Hidy (1)², John C. Gosse (1), Mike D. Blum (2), and Martin R. Gibling (1)

(1)Department of Earth Sciences, Dalhousie University, Halifax, Nova Scotia B3H 4R2

(2)Exxonmobil Upstream Research Company, Houston, Texas 77252

3.1. Introduction

High-amplitude and high-frequency oscillations in climate are suggested mechanics to explain an apparent mid-latitude increase in sediment accumulation since the late Pliocene (Davies et al., 1977; Peizhen et al., 2001; Molnar, 2004). This view implies that long-term rates of landscape erosion, as well as feedbacks associated with isostatic uplift in response to erosion, were influenced by these climate changes. A variation on this hypothesis postulates that a global increase in late Cenozoic orogenic activity (i.e. the uplift of the Himalaya, Rocky Mountains, and Andes) enhanced regional elevation, causing an increase in sediment supplied to the oceans and a climate destabilization since the late Pliocene (Raymo and Ruddiman, 1992). In contrast, sediment flux from major global rivers is greatest in tropical regions, and weathering and sediment-availability models trained with modern data from the world's largest rivers (Syvitski and Milliman, 2007; Kettner and Syvitski, 2008) suggest the opposite—that global erosion would have been greater in the warmer Pliocene relative to the colder

²Corresponding author.

Email addresses: alanhidy@dal.ca (A. J. Hidy), john.gosse@dal.ca (J. C. Gosse), mike.blum@exxonmobile.com (M. D. Blum), martin.gibling@dal.ca (M. R. Gibling)

Pleistocene. Recent analyses of $^{10}\text{Be}/^9\text{Be}$ measurements in ocean sediments spanning the last 12 Ma indicate a third possibility, that global silicate erosion rates were relatively constant over this timespan (Willenbring and Von Blanckenburg, 2010), and that the Plio-Pleistocene climate transition has had a negligible impact on global erosion rates. These opposing interpretations reflect the difficulty of using macro-scale proxies to discern the relative impact of climate change on surface processes; these proxies also incorporate locally variable and potentially overwhelming effects of tectonics, spatial and temporal changes in sediment routing, and glacial erosion.

To circumvent these issues, we raise a currently untested question: in catchments that are non-glaciated and in tectonically stable regions, what is the impact of climate change on long-term erosion rates? We attempt to address this question by estimating past and present catchment-wide average denudation rates during glacial and interglacial periods within catchments that i) have been eroding continuously over the past ~ 5 Ma, ii) have never been glaciated, and iii) drain a passive-margin setting that has been minimally influenced by tectonics over the duration of interest. The goal is to determine how denudation rates in these regions respond to glacial-interglacial climates, and also to the climate change that occurred during the Plio-Pleistocene transition.

We obtain our catchment-wide denudation rates using in situ-produced ^{10}Be in fluvial sediment (Brown et al., 1995; Bierman and Steig, 1996; Granger et al., 1996). This approach can be used to determine modern and past denudation rates (e.g. Schaller et al., 2002). Here, we apply this technique to Quaternary fluvial deposits within three river systems that drain the Texas interior and enter the Gulf of Mexico (GoM). For these rivers, we obtained denudation rates integrated over ~ 20 -40 ka, a sufficiently short period

to capture potential changes in rates due to the eccentricity-driven 100 ka climate cycle and long enough to buffer recent anthropogenic forcing. We show that, where tectonic activity is minimized, and glaciers are absent, long-term variations in denudation rate in these temperate catchments correlate broadly with mean catchment temperature, agreeing with the model predictions of Syvitski and Milliman (2007) and Kettner and Syvitski (2008). We suggest that, during the warmer interval of the Pliocene, the climatic component of tropical-temperate denudation rates was higher than during later, generally colder periods, despite the ^{10}Be marine record that suggests a negligible change in global net erosion (Willenbring and Von Blanckenburg, 2010). This disparity with the global record may be resolved if polar-temperate regions responded to the Plio-Pleistocene transition in the opposite direction. That is, erosion in polar-temperate zones increased during colder periods (Montgomery, 2002), possibly due to threshold changes in warm-based ice-cover or enhanced freeze-thaw cycling. Alternatively, this disagreement could be resolved by an increase in stored sediment removal during colder periods. However, our data suggest that enhanced sediment storage removal during cold periods is not adequate to balance the observed increase in hinterland erosion during warm periods.

3.2. Study Area

3.2.1. Overview

The Colorado, Brazos, and Trinity Rivers (Fig. 3.1) drain the majority of inland Texas ($\sim 110,000 \text{ km}^2$, $\sim 115,000 \text{ km}^2$, and $\sim 45,000 \text{ km}^2$, respectively) and supply most of the sediment to its coast. The coastal plain represents the most recent of a succession of amalgamated alluvial-deltaic deposits that prograded during the Cenozoic and extends $\sim 200 \text{ km}$ from the GoM (DuBar et al., 1991; Galloway et al., 2000). The Cenozoic

succession of shoreline-parallel deposits constitutes nearly half the area of Texas. Tectonic activity in the region drained by these rivers has been minimal since the Pliocene. Although diapirs and syndepositional faulting are ubiquitous on the outer coastal plain and shelf margin (Ewing, 1991; Diegel et al., 1995), their effect on up-catchment erosion is assumed to have been negligible and relatively shallow incision implies a small contribution to the total sediment supply. However, the drainage basins probably experienced isostatic adjustment to sediment excavation and may have been marginally affected by broad-wavelength epeirogenic uplift associated with the Rocky Mountains (McMillan et al., 2002; McMillan et al., 2006). Neither of these effects, however, control millennial-scale changes in sedimentation rates, and post-depositional tilt measurements of the Miocene Ogallala Group bordering the Rocky Mountains indicates a minimal change in post-depositional slope >200 km from the foothills, where the headwaters for the catchments in this study reside (McMillan et al., 2002). Long-term regional tectonic stability, a virtually continuous record of sedimentation, and pre-existing geochronological information make the Texas coastal plain an ideal setting for studying source-to-sink responses of fluvial systems to changes in climate.

The three drainage basins have low relief and are dominated by flat-lying siliciclastic rocks. Some exceptions to this are Paleozoic carbonates that outcrop in north and central Texas (Edwards Plateau), and Precambrian granites exposed near Austin, TX. Most surficial deposits in these catchments were originally sourced from the Rocky Mountains (Galloway et al., 2011). During the Pliocene to Early Pleistocene, these rivers were severed from the Rockies by the northward migration of the Pecos River and their catchments have maintained roughly the same configuration since then (Reeves, 1976;

Winker, 1979; Galloway et al., 2011). The modern rivers erode sediment primarily from recycled Plio-Pleistocene and older fluvial deposits that were laid down prior to regional stream reorganization; such recycling probably produced the mature, clean, and quartz-rich sand ubiquitous on the Texas Gulf Coast. The ubiquitous quartz, low relief, and long term stability of their catchments make the Colorado, Brazos, and Trinity rivers suitable for the application of ^{10}Be basin-wide denudation rates.

The Texas coastal plain can be divided into zones of net erosion and net aggradation, with the transition between these zones referred to as the hinge zone. Upstream of the hinge zone these fluvial systems are transport-limited and drain mixed bedrock-alluvial valleys (Blum and Aslan, 2006). Downstream, deposition follows classic lateral-accretion architecture, and the river paths become highly sinuous. Lateral channel migration permits the rivers to sweep across their confining valleys, emplacing continuous 5 – 10 m thick channel-belt deposits. These deposits consist of cross-bedded to horizontally-bedded point-bar sand beneath sandy and muddy floodplain facies capped by paleosols (Blum and Price, 1998). At a larger scale and as a consequence of avulsion, these channel belts form part of regional morphostratigraphic units that make up the coastal plain. Over time, these avulsions distribute sediment from hinterland streams, coalescing to create composite units with nearly seamless topographic surfaces. Avulsion on the Texas Gulf Coast is largely a response to changes in climate and sea level, which strongly influence valley incision and filling in this passive-margin setting (Blum and Törnqvist, 2000; Blum and Hattier-Womack, 2009).

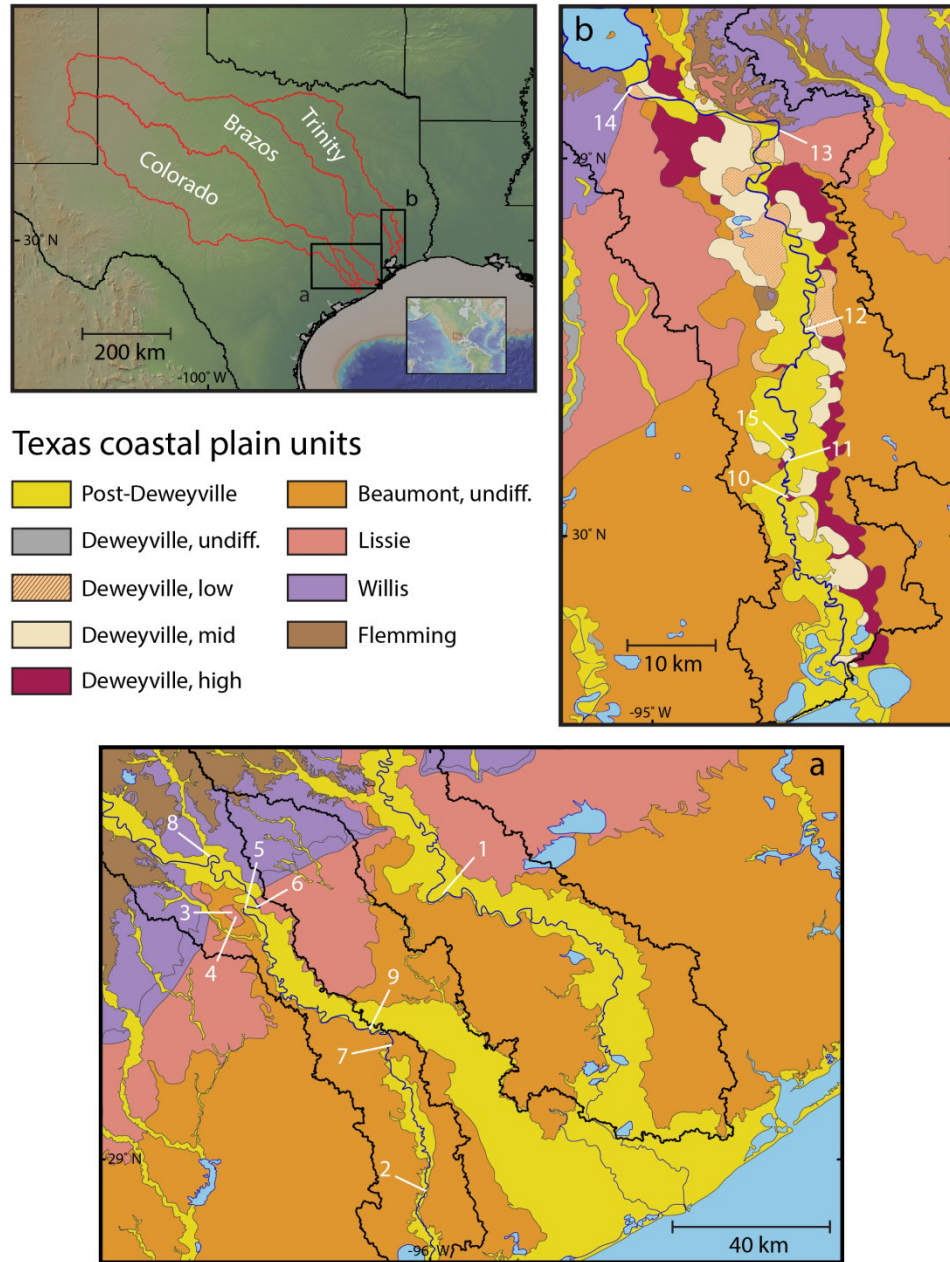


Figure 3.1: Location of study area showing general geologic map of Texas with outlines of the Brazos, Colorado, and Trinity catchments. Inset maps detail mapped major morphostratigraphic surfaces within the Colorado (a) and Trinity (b) catchments. Additional detail for Deweyville deposits in the Trinity catchment provided by Garvin (2008). Sample locations are shown on inset graphs and referenced in Table 3.1.

3.2.2. Chronology and Stratigraphy of the Texas Coastal Plain

Fluvial deposits within outer coastal plain valleys that formed during the Pleistocene are of primary interest to this study because 1) the present major drainage networks were most likely established prior to this time, after deposition of the Mio-Pliocene Ogallala Group ceased and the rivers were cut off from their Rocky Mountain source (Reeves, 1976; Winker, 1979; Galloway et al., 2011), 2) the sediment record of this time span is well-preserved since vertical erosion on the outer coastal plain has been minimal, 3) many Late Pleistocene and Holocene units have been mapped and put into a dated stratigraphic framework (e.g. Blum and Valastro, 1994; Blum and Price, 1998; Garvin, 2008), and 4) glacial vs. interglacial context is already known for targeted Beaumont and post-Beaumont sediments based on mapping of genetic sequence boundaries from cores, outcrops along cut banks, soil development, topographic projection of surfaces, and supporting chronologies (see Blum and Aslan (2006) and references therein).

The major shoreline-parallel deposits of the Plio-Pleistocene are divided into three morphostratigraphic units, in chronologic order: the Willis, Lissie, and Beaumont Formations (Doering, 1935). The Beaumont is characterized by thick dark clayey soils and relatively planar topography, the Lissie by silty and sandy red soils and relatively planar topography, and the Willis by its heavily dissected topography and coarser sediment. Post-Beaumont stratigraphy includes a Holocene floodplain and three other distinct terraces with elevations above the floodplain but below the Beaumont surface. These intermediate terraces are termed “Deweyville” and represent the latest Pleistocene regression (Blum et al., 1995) (Fig. 3.2). Due to the composite nature of the coastal-plain

units, regional depositional ages cannot be inferred from an age obtained elsewhere within a mapped unit. Thus, all sampling sites used for paleo-denudation rate measurements require chronological analysis (see Table 3.1).

Period	Epoch	Age (ka)	OIS	Unit name	
Quaternary	Holocene	11	1	modern	
	Pleistocene	upper	126	2	Deweyville L M H
				3	
				4	
				5	
	Pleistocene	middle	781	6 - 9/10?	Beaumont
				9/10? - ?	
	Pleistocene	lower	2,588	?	Lissie
				?	
	Neogene	Pliocene			Willis

Figure 3.2: General stratigraphy with glacial context for surfaces on the Texas Gulf Coast (Blum and Aslan, 2006; Garvin, 2008).

Surface	Site #	Estimated age ¹ (ka)	Method of chronology	Source
Brazos				
modern post-dam	1	0.0	Inferred; active point bar	this work
Colorado				
modern post-dam	6	0.0	Inferred; active point bar	this work
modern pre-dam	8	0.1 ± 0.1	Inferred; modern scroll bar with moderately developed vegetation	this work
Holocene (CBA-1)	5	8.5 ± 3.5	¹⁴ C; organic detritus in fluvial sediment	Blum and Valastro (1994)
Dew eyville	9	35 ± 2	TL; quartz	Durbin et al. (1997)
Beaumont (U)	7	119 ± 9.5	TL; quartz	Blum and Price (1998)
Beaumont (L)	2	155 ± 15	TL; quartz	Blum and Price (1998)
Lissie	3	560 ^{+190/-130}	TCN depth profile; fluvial sand	this work
Lissie	4	560 ^{+190/-130}	TCN single shielded sample; fluvial sand	this work
Trinity				
modern pre-dam	12	0.1 ± 0.1	Inferred; modern scroll bar with moderately developed vegetation	this work
L. Dew eyville	14	20 ± 1	OSL; single-grain aliquot on quartz	Garvin (2008)
L. Dew eyville	15	20 ± 1	OSL; single-grain aliquot on quartz	Garvin (2008)
M. Dew eyville (U)	11	25 ± 5	OSL; single-grain aliquot on quartz	Garvin (2008)
M. Dew eyville (L)	11	29 ± 5	OSL; single-grain aliquot on quartz	Garvin (2008)
H. Dew eyville	10	33 ± 2	OSL; single-grain aliquot on quartz	Garvin (2008)
Lissie	13	>520 ± 150	OSL; single-grain aliquot on quartz	this work
		590 ^{+110/-310}	TCN depth profile; fluvial sand	this work

Table 3.1: Summary of chronology for the units targeted for sampling for this study. Location of sites is indicated on Figure 3.1. OSL = optically stimulated luminescence; TCN = terrestrial cosmogenic nuclide; TL = thermoluminescence

3.2.2.1. Willis and Lissie Formations

Precise age control for the Willis and Lissie formations has not yet been obtained. Kukla and Opdyke (1972) measured normal magnetic polarity for Willis sediments and reverse magnetic polarity for younger Lissie within “floodloams and silty interlayers” and suggested that the Willis and Lissie were, in part, deposited during the Gauss (2.5 – 3.4 Ma) and Matuyama (0.79 – 2.5 Ma) polarity chrons, respectively. This would place at least some of the Willis in the late Pliocene, although deposition may have spanned the Plio-Pleistocene boundary. The slope of the Lissie surface has been projected down-dip to offshore seismic reflectors in the relatively well-constrained marine record of the GoM (Winker, 1979; DuBar et al., 1991). The foraminifer *Trimosina denticulata* first appears just above the projected Lissie surface, placing the end of Lissie deposition at approximately 600 ka (Armentrout and Clement, 1990). In the Colorado River catchment, the Lava Creek “B” (~640 ka; Lanphere et al., 2002) was observed in a dissected terrace (Mandel and Caran, 1992) and projected to an elevation between the Lissie and Beaumont surfaces (Blum and Valastro, 1994). Considering an observed reverse polarity, the Lissie Formation spans at least 200 ka, and possibly represents the bulk of sedimentation during the early and middle Pleistocene.

3.2.2.2. Beaumont Formation and post-Beaumont Deposits

More precise chronostratigraphy exists for the Beaumont and post-Beaumont strata. Blum and Price (1998) used thermoluminescence (TL) methods to date three distinct valley fills at 115 – 323 ka within the Beaumont along the Colorado and Navidad Rivers. Also in the Colorado River, Blum and Valastro (1994) reported minimum ¹⁴C ages of 16 – 23 ka for the lower Deweyville. From the Nueces River, Durbin et al. (1997)

recorded thermoluminescence (TL) ages of 31 – 53 ka for a suite of Deweyville deposits and 72 - 92 ka for the earliest Beaumont fill. In the Trinity River, Garvin (2008) obtained optically stimulated luminescence (OSL) ages of 20 – 33 ka for a sequence of Deweyville terraces that represent falling stage to low-stand of sea level during the last glacial period. In a climatic context, these ages suggest that the Beaumont encompasses deposits from OIS 5-9, and the Deweyville represents OIS 2-4. The post-Deweyville fill in the Colorado River has been radiocarbon dated to 1 – 14 ka (Blum and Valastro, 1994).

3.2.3. Sediment Flux from Major Texas Rivers

Mass-balance and volumetric measurements of large-scale sediment delivery to the Gulf of Mexico suggest that net sedimentation has substantially increased since the Late Pliocene (e.g. Davies et al., 1977; Hay et al., 1989; Galloway et al., 2000; Galloway et al., 2011). Unfortunately, because of poor constraint on the timing of the most recent drainage reconfiguration (Galloway et al., 2011) it is difficult to determine if the observed increase in sediment accumulation is a result of a net increase in terrestrial erosion rates or changes in basin geometry. Furthermore, a major source of GoM sediment comes from terrain affected by Quaternary glaciations (Mississippi catchment), making it difficult to preclude an ice-driven source for some of the shelf sediment. Thus, the observation of increased sediment flux to the GoM since the Late Pliocene does not necessarily imply increased erosion in stable, non-glaciated catchments.

Over the last century the major rivers draining Texas have been dammed, significantly reducing sediment delivery and controlling water discharge to the coastal plain. Estimates of modern sediment fluxes are thus restricted to pre-dam settings or derived from numerical models (see Table 3.2). Prior to and during the construction of

major dams (ca. 1940s) on the Brazos, Colorado, and Trinity Rivers, suspended sediment measurements obtained by Bloodgood and Meador (1941) and Bloodgood (1955) from main-stem sampling stations on the outer coastal plain yielded time-averaged mass fluxes of 31 Mt a⁻¹, 8.1 Mt a⁻¹, and 5.5 Mt a⁻¹, respectively. In the Colorado system, Kanen (1970) obtained a mean rate of 13 Mt a⁻¹ by recompiling these data and including estimates of flux during years absent from the main-stem record. These fluxes accompanied mean stream discharges of ~200 m³ s⁻¹, ~120 m³ s⁻¹, and ~220 m³ s⁻¹ for the Brazos, Colorado, and Trinity Rivers, respectively, over the same time-averaged interval. The measurements represent the best known estimates of sediment fluxes and stream discharges from the unobstructed rivers. However, because of extensive agricultural development, particularly in the Southern High Plains areas of the Colorado and Brazos catchments, these modern rates likely involve significant anthropogenic forcing. More recently, modern sediment flux estimates of 27 Mt a⁻¹ (Brazos) and 13.3 Mt a⁻¹ (Colorado), and 5.5 Mt a⁻¹ (Trinity) have been obtained by Blum and Hattier-Womack (2009), and Garvin (2008), respectively, by adapting the BQART sediment-flux model of Syvitski and Milliman (2007):

$$Q_s = 0.0006 BQ^{0.31}A^{0.5}RT \quad \text{for } T \geq 2^\circ\text{C, and} \quad (1)$$

$$Q = 0.075A^{0.8}, \quad (2)$$

where Q_s is sediment flux (Mt a⁻¹), B is a geologic factor determined by catchment lithology, human influence, glacial coverage, and trapping efficiency of lakes and reservoirs, Q is the mean annual water discharge (km³ s⁻¹), A is the area of the catchment (km²), R is the relief of the catchment (km), and T is the average catchment-wide

temperature (°C). This widely-used empirical sediment-flux model has been trained with a global database of 488 rivers that explains 96% of the variance between modern suspended sediment yields. It predicts paleo-sediment flux values to be proportional to catchment-averaged temperatures in the absence of significant changes in relief, area, and the geologic and human factors that contribute to B , and suggests that stream can be approximated from catchment area. Using this formulation, sediment delivered to the GoM by the Brazos, Colorado, and Trinity rivers during the last glacial maximum has been predicted to be ~25-30% less than modern values (Garvin, 2008; Blum and Hattier-Womack, 2009). Although this predicted relative change in sediment flux between cold and warm periods can be tested with ^{10}Be sediment flux estimates, the magnitudes of the ^{10}Be and BQART sediment flux estimates are likely not comparable. This is because 1) the decadal resolution of the data available to train the BQART model is likely too noisy to extrapolate to the millennial-scale ^{10}Be sediment flux rates, and 2) the BQART model is derived from suspended sediment yields, whereas ^{10}Be sediment flux rates are estimated from medium- to coarse-grained sand (mostly bedload material).

Source	Sediment flux (Mt a ⁻¹)	Recorded dates	Total integrated time	Method of measurement	Location	Type
Brazos						
Bloodgood (1955)	37.1	1923 - 1941	17.3 a	suspended sediment	Richmond, station 1	pre-dam
	22.3	1941 - 1954	13.0 a	suspended sediment	Richmond, station 1	post-dam
	30.8	1923 - 1954	30.3 a	suspended sediment	Richmond, station 1	mixed
Blum and Hattier-Womack (2009) after Syvitski and Milliman (2007)	26.5	NA	NA	modified BQART model	w hole catchment	pre-dam
This work	7.67	NA	30 ka	TCN catchment-wide erosion rate	w hole catchment	post-dam
Colorado						
Bloodgood and Meador (1941)	9.82	1929 - 1933	3.2 a	suspended sediment	Columbus, station 18	pre-dam
	6.08	1937 - 1940	2.7 a	suspended sediment	Columbus, station 18	post-dam
	8.09	1929 - 1940	5.9 a	suspended sediment	Columbus, station 18	mixed
Kanes (1970) after Bloodgood and Meador (1941)	17.7	1931 - 1935	5 a	suspended sediment w ith interpolation	Columbus, station 18	pre-dam
	10.7	1936 - 1945	10 a	suspended sediment w ith interpolation	Columbus, station 18	post-dam
	12.7	1931 - 1945	15 a	suspended sediment w ith interpolation	Columbus, station 18	mixed
Blum and Hattier-Womack (2009) after Syvitski and Milliman (2007)	13.3	NA	NA	modified BQART model	w hole catchment	pre-dam
This work	6.49	NA	29 ka	TCN catchment-wide erosion rate	w hole catchment	pre-dam
	6.59	NA	28 ka	TCN catchment-wide erosion rate	w hole catchment	pre-dam
	6.07	NA	33 ka	TCN catchment-wide erosion rate	w hole catchment	post-dam
Trinity						
Bloodgood (1955)	6.97	1935 - 1948	12.1 a	suspended sediment	Romayor, station 48	pre-dam
	2.58	1948 - 1954	6.00 a	suspended sediment	Romayor, station 48	post-dam
	5.52	1935 - 1954	18.1 a	suspended sediment	Romayor, station 48	mixed
Garvin (2008) after Syvitski and Milliman (2007)	5.50	NA	NA	modified BQART model	w hole catchment	pre-dam
This work	4.53	NA	17 ka	TCN catchment-wide erosion rate	w hole catchment	pre-dam
	4.75	NA	17 ka	TCN catchment-wide erosion rate	w hole catchment	pre-dam

Table 3.2: Summary of sediment flux measurements from the Brazos, Colorado, and Trinity Rivers acquired from suspended sediment measurements, BQART model estimates, and ¹⁰Be estimates from this work.

3.3. Methods

Estimating ^{10}Be catchment-wide denudation rates from pre-modern fluvial sediment requires: 1) an averaged ^{10}Be production rate for the contemporaneous catchment, and 2) the depositional ^{10}Be concentration in sediment evacuated from the catchment, which includes correcting for production and decay of ^{10}Be since the time of deposition. Catchment-wide ^{10}Be production rates can be calculated from catchment hypsometry and from the distribution of the sampled mineral (quartz) in the catchment (see A.2.2.). For modern rates, the concentration is inversely proportional to the catchment's average denudation rate (Brown et al., 1995; Bierman and Steig, 1996; Granger et al., 1996). In older deposits, post-depositional ^{10}Be production becomes increasingly significant with time and must be subtracted from the measured concentration (Schaller et al., 2002). Because ^{10}Be production rates are depth-sensitive, modeling post-depositional ^{10}Be production requires knowledge of depositional age and surface erosion or aggradation rate of the target deposit, as well as the depositional ages and erosion or aggradation history of all overlying deposits. Furthermore, an adjustment for ^{10}Be lost to decay since deposition is necessary. Thus, each paleo-catchment-wide estimate of average denudation rate requires a sample-specific model constrained by absolute chronology and stratigraphic measurements. In this study, pre-existing chronology can be reasonably utilized for the majority of the sampled sites; for other sites, ^{10}Be depth profiles were modeled to obtain new chronology (Anderson et al., 1996; Hidy et al., 2010). Details regarding sample preparation (A.2.1.), the calculation of ^{10}Be denudation rates (A.2.2.), and model parameters for the depth profiles (A.2.3.) are given in the supplemental material.

Recent work looking at spatial changes in ^{10}Be concentration in river sediment on a coastal plain suggests that sediment stored in floodplains of large drainage basins and then reintroduced into the active stream through bank erosion has a negligible effect on basin-wide denudation rates as measured with long-lived TCN such as ^{10}Be and ^{26}Al (Wittmann and Von Blanckenburg, 2009; Wittmann et al., 2009). This is because the amount of sediment derived from hillslopes tends to be overwhelmingly larger than sediment derived from bank erosion, bedload transport timescales are shorter than those of hillslope erosion processes (Whipple and Tucker, 1999), and because much of the material eroded from a coastal plain is finer than the medium- to coarse-grained material targeted for ^{10}Be measurements. However, measuring both ^{26}Al and ^{10}Be within a deposit can provide a check on whether a portion of the sediment has experienced significant burial between its exposure on hillslope surfaces and its present deposition (Granger and Muzikar, 2001). Additionally, if the source of the stored sediment can be constrained and its average $^{26}\text{Al}/^{10}\text{Be}$ can be assumed, then sediment contributions from buried sediment storage and from surficial hinterland erosion may be estimated using a binary mixing algorithm (Wittmann et al., 2011b). Thus, ^{26}Al measurements were acquired in conjunction with ^{10}Be for chronologically distinct depositional intervals in order to quantify this effect, adjust our calculated denudation rates, and determine the relative abundance of up-catchment and buried sediment in the stream sediment yield.

3.4. Results

3.4.1. New Lissie Chronology

We obtained new chronology from two ^{10}Be depth profiles within the Lissie Formation, one each from the Colorado and Trinity catchments (Fig. 3.3); additionally,

an optically stimulated luminescence (OSL) sample was acquired in conjunction with the depth profile in the Trinity catchment and represents a minimum age (see A.2.3.). For both ^{10}Be profiles the χ^2 statistic converged to a unique solution, therefore we report this minimized χ^2 value as the interpreted age; 1σ error ranges for these ages are determined from Bayesian cumulative distribution functions (see Hidy et al., 2010; Mercader et al., 2012).

The ^{10}Be depth profiles and OSL sample acquired from within the Colorado and Trinity catchments represent the first independent age estimates for the Lissie Formation. An age of 560^{+190}_{-130} ka (1σ ; ^{10}Be profile) at site 4, and ages of 590^{+110}_{-310} ka (1σ ; ^{10}Be profile) and 520 ± 150 ka (1σ ; minimum OSL age) at site 13 are consistent with each other. They are also consistent with ages inferred from seismic records and dating of ash, as described in section 3.2.2.1.

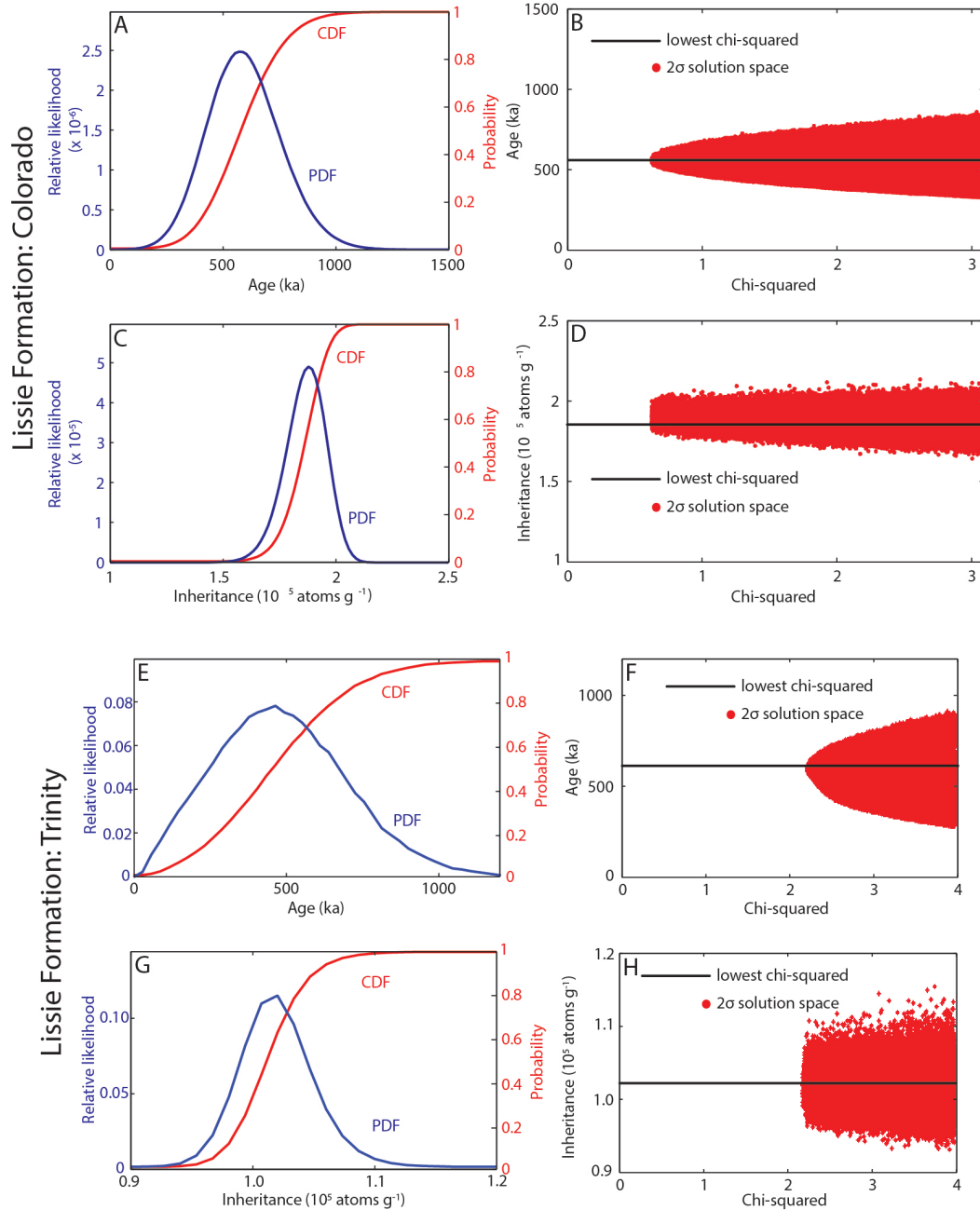


Figure 3.3: Results for ^{10}Be depth profiles acquired from the Lissie Formation in the Colorado (A-D) and Trinity (E-H) catchments. Probability density functions (PDFs) and cumulative distribution functions (CDFs) for depositional age and ^{10}Be concentration are calculated after Hidy et al. (2010) from a 100,000 curve Monte Carlo simulation. For ages, χ^2 values converged to a minimum value and therefore are interpreted as the most probable value; for depositional concentrations, the most probable value was acquired from the PDF since χ^2 minimization did not approach a unique age. 1σ uncertainties are taken from the CDF and are asymmetric. See A.2.3. for details on model parameters and output.

3.4.2. Depositional ^{10}Be and ^{26}Al

Calculated values for depositional ^{26}Al and ^{10}Be concentrations are shown in Table 3.3. Depositional ^{10}Be concentrations range from $1.3\text{-}2.9 \times 10^5$ atoms g^{-1} in the Colorado catchment and $0.7\text{-}1.0 \times 10^5$ atoms g^{-1} in the Trinity catchment. A single modern measurement in the Brazos catchment yielded a value of 2.1×10^5 atoms g^{-1} . For duplicate measurements acquired from samples with different grain size ($n = 4$), the coarser sample returned a lower ^{10}Be or ^{26}Al concentration in all cases, consistent with the results of previous studies where hillslope processes were a first-order erosion mechanism in the source regions (Matmon et al., 2003; Belmont et al., 2007; Wittmann et al., 2011a; Codilean et al., 2012). A pair of measurements ($n = 2$) from the Low Deweyville separated spatially by 105 km (sites 14 and 15) returned statistically identical depositional ^{10}Be and ^{26}Al concentrations (Table 3). This is consistent with recent work that suggests minimal influence of the outer coastal plain on depositional TCN concentrations (Wittmann and Von Blanckenburg, 2009; Wittmann et al., 2009).

Table 3.3: Calculated results for depositional TCN concentrations, up-catchment denudation rates, up-catchment sediment flux, and sediment from storage. Int. time refers to the integration time of the denudation rates; f_b refers to the fraction buried material in the sample. Total 1σ errors in concentrations include AMS errors, an estimated 2% uncertainty for sample preparation and, for ^{26}Al samples, a 5% uncertainty from ICP-MS native Al measurements. For samples in the two ^{10}Be depth profiles, the depositional ^{10}Be and uncertainty were acquired directly from the Hidy et al. (2010) model output; for all other ^{10}Be samples, and for all ^{26}Al samples, depositional concentrations were calculated as described in section 3.2.2. Errors in the post-depositional production were obtained by propagating upper and lower 1σ errors for relevant unit ages through the calculations. Calculated concentrations do not include the unknown error in post-depositional (primarily muon) production rates or errors in decay constants (assumed negligible for late Pleistocene and younger deposits).

Surface	Grain size (μm)	Dep. [^{10}Be] (10^9 atoms g^{-1})		Dep. [^{26}Al] (10^9 atoms g^{-1})		Dep. $^{26}\text{Al}/^{10}\text{Be}$		f_b	^{10}Be denudation rate (cm ka^{-1})			Int. time (ka)	^{10}Be sediment flux (Mt a^{-1})			
		[^{10}Be]	$\pm 1\sigma$	[^{26}Al]	$\pm 1\sigma$	$^{26}\text{Al}/^{10}\text{Be}$	$\pm 1\sigma$		raw	corr	$\pm 1\sigma$		raw	corr	$\pm 1\sigma$	storage
Brazos																
modern post-dam	355-500	2.14	0.06	11.66	0.70	5.44	0.36	0.19	2.02	1.73	0.06	35	6.18	5.29	0.18	1.49
Colorado																
modern post-dam	355-500	2.52	0.08	14.89	1.00	5.90	0.44	0.13	1.85	1.67	0.06	36	5.31	4.80	0.17	0.76
modern pre-dam	355-500	2.23	0.06	13.88	0.84	6.22	0.41	0.08	2.10	1.98	0.06	30	5.98	5.65	0.16	0.51
modern pre-dam	355-500	2.20	0.07					0.08	2.13	2.01	0.06	30	6.07	5.73	0.18	0.52
CBA-1	355-500	2.58	0.09	12.72	0.76	4.94	0.34	0.27	1.81	1.41	0.06	43	5.20	4.07	0.18	1.91
Deweyville	355-500	2.19	0.05	11.69	0.71	5.33	0.35	0.21	2.12	1.79	0.05	34	6.14	5.18	0.15	1.63
Beaumont (U)	250-355	2.94	0.04	16.18	0.72	5.50	0.26	0.18	1.57	1.33	0.02	45	4.56	3.87	0.06	1.03
Beaumont (U)	355-500	2.26	0.06	13.26	0.94	5.87	0.45	0.13	2.06	1.86	0.06	33	5.96	5.38	0.17	0.89
Beaumont (L)	355-500	2.62	0.09						1.76	NA	0.06	34	5.15	NA	0.17	NA
Lissie	355-500	1.74	$^{+0.23}_{-0.18}$					0.17	2.69	2.38	$^{+0.31}_{-0.32}$	25	7.75	6.85	$^{+0.90}_{-0.92}$	1.62
Lissie	355-500	1.88	$^{+0.07}_{-0.11}$					0.17	2.49	2.19	$^{+0.16}_{-0.09}$	28	7.16	6.30	$^{+0.45}_{-0.26}$	1.50
Lissie	500-850	1.33	$^{+0.24}_{-0.18}$	7.40	$^{+2.40}_{-1.96}$	5.58	$^{+2.07}_{-1.66}$	0.17	3.54	3.20	$^{+0.56}_{-0.55}$	19	10.19	9.20	$^{+1.61}_{-1.57}$	2.13
Trinity																
modern pre-dam	250-355	0.84	0.03	5.13	0.40	6.12	0.51	0.09	3.47	3.23	0.11	19	4.11	3.83	0.13	0.42
modern pre-dam	250-355	0.80	0.02					0.09	3.64	3.40	0.10	18	4.31	4.03	0.12	0.44
L. Deweyville	355-500	0.95	0.03	4.77	0.30	5.03	0.35	0.26	3.08	2.46	0.09	25	3.50	2.80	0.11	1.20
L. Deweyville	355-500	0.99	0.03	5.00	0.34	5.07	0.38	0.25	2.94	2.35	0.09	26	3.53	2.82	0.10	1.16
M. Deweyville (U)	150-250	0.73	0.04						3.99	NA	0.22	15	4.79	NA	0.26	NA
M. Deweyville (U)	250-355	0.70	0.05						4.13	NA	0.27	15	4.96	NA	0.32	NA
M. Deweyville (L)	150-250	0.83	0.04	4.43	0.28	5.31	0.42	0.21	3.48	2.95	0.17	20	4.17	3.54	0.20	1.13
M. Deweyville (L)	150-250	0.88	0.03					0.21	3.29	2.77	0.11	22	3.96	3.32	0.13	1.07
H. Deweyville	250-355	0.98	0.05	7.25	0.46	7.40	0.60		2.96	2.96	0.15	20	3.55	3.55	0.18	0.00
H. Deweyville	250-355	0.94	0.04						3.08	3.08	0.13	20	3.70	3.70	0.16	0.00
Lissie	250-500	1.02	$^{+0.02}_{-0.04}$	5.77	$^{+1.10}_{-3.50}$	5.66	$^{+1.08}_{-3.44}$	0.16	2.85	1.75	$^{+0.12}_{-0.06}$	34	3.32	2.04	$^{+0.14}_{-0.06}$	0.64

3.4.3. Catchment-wide Denudation and Sediment Flux

Depositional ^{10}Be and ^{26}Al concentrations and errors were used (see A.2.2) to calculate catchment denudation rates and sediment fluxes, sediment fluxes from buried storage, total sediment flux, and the time spans over which the catchment rates and fluxes are integrated (Table 3.3). In the Brazos catchment, only a single modern (post-dam) sample was measured, yielding an average denudation rate of $1.73 \pm 0.06 \text{ cm ka}^{-1}$, and corresponding to a sediment flux of $5.29 \pm 0.18 \text{ Mt a}^{-1}$ averaged over the last 35 ka. A suite of modern and late Pleistocene samples was measured from the Colorado and Trinity rivers. In the Colorado catchment, denudation rates and sediment fluxes were calculated at $1.33 - 3.20 \text{ cm ka}^{-1}$ and $3.87 - 9.20 \text{ Mt a}^{-1}$, with average integration times of 19 - 45 ka. Measurements from the Trinity catchment yielded denudation rates and sediment fluxes of $1.75 - 3.40 \text{ cm ka}^{-1}$ and $2.04 - 4.03 \text{ Mt a}^{-1}$, with average integration times of 18 - 34 ka. The errors listed in Table 3.3 for these values do not include the large uncertainty in the scaling scheme used to calculate site production rates, which may be up to $\sim 10\%$ (1σ) due to uncertainty in the paleomagnetic field and reference production rate (Balco et al., 2008). However, due to the long integration time of the denudation rates (15 - 45 ka) it is assumed here that time-varying TCN production due to changes in Earth's magnetic field is negligible and not significantly different among samples. Thus, the production-rate uncertainty is considered systematic for samples within the same catchment and would only affect the magnitude of the calculated rates, not their relative values.

3.5. Discussion

3.5.1. Sediment Recycling on the Texas Coastal Plain

The catchment-wide denudation rates calculated for the Brazos, Colorado, and Trinity rivers are high enough to suggest that the depositional $^{26}\text{Al}/^{10}\text{Be}$ should approximately equal the spallogenic production ratio (6.75). However, with a sole exception of the High Deweyville, all measured $^{26}\text{Al}/^{10}\text{Be}$ from these rivers have significant and variably depressed ratios (Fig. 3.4). This indicates that remobilization of buried stored sediment contributes significantly to the total sediment flux passing through the Texas coastal plain, and its relative contribution varies temporally throughout the late Pleistocene. In both the Colorado and Trinity rivers, depositional $^{26}\text{Al}/^{10}\text{Be}$ was highest for units deposited during periods of relatively higher sea level and lowest for units deposited during periods of relatively lower sea level. A comparison of our $^{26}\text{Al}/^{10}\text{Be}$ data with a relative sea level time series shows a consistent correlation between sea level and depositional $^{26}\text{Al}/^{10}\text{Be}$ (Fig. 3.5). This relationship implies that a lower sea level enhances erosion of buried sediment in long-term ($\sim 10^5$ years) storage. Possible sources of the stored component reflected in these data are limited and likely exclude the outer coastal plain for several reasons. Firstly, the depositional $^{26}\text{Al}/^{10}\text{Be}$ measured in the Low Deweyville near the hinge zone, and ~ 100 km downstream, are similar agreeing with previous studies suggesting a negligible influence of coastal flood plain erosion on ^{10}Be denudation measurements (Wittmann and Von Blanckenburg, 2009; Wittmann et al., 2009). If the outer coastal plain was the source of lowered $^{26}\text{Al}/^{10}\text{Be}$, then a systematic downstream decrease in depositional $^{26}\text{Al}/^{10}\text{Be}$ should have been observed. Secondly, the minimum burial time (neglecting post-depositional production) needed to depress

$^{26}\text{Al}/^{10}\text{Be}$ from the production ratio to the observed low-stand ratios (~ 5) is >600 ka. The bulk of the outer coastal plain, however, consists of Beaumont and post-Beaumont sediments (<350 ka). Thus, the majority of outer coastal plain sediments are too young to produce the observed ratios from post-depositional storage, although they may have inherited the low ratios if the sediment was stored farther upstream prior to deposition. Furthermore, the $^{26}\text{Al}/^{10}\text{Be}$ in the recycled material must be significantly lower than the observed ratios, unless the up-catchment component of sediment flux is negligible. Thirdly, the depositional $^{26}\text{Al}/^{10}\text{Be}$ within high-stand deposits is relatively high, so merely cannibalizing a previous high-stand sediment prism during a low stage is insufficient to depress the $^{26}\text{Al}/^{10}\text{Be}$. Finally, much of the outer coastal plain is dominated by material that is finer than the grain sizes used for this study (150 - 850 μm). Thus, calculated volumes of sediment known to have been removed during coastal-plain incision (e.g. Garvin, 2008) probably do not factor significantly into our TCN measurements, as further evidenced by spatially consistent TCN concentrations and ratios in the Low Deweyville.

The most likely source for the remobilized sediment signal is thus from the inner coastal plain above the hinge zone, which is dominated by the Lissie and Willis formations. These Plio-Pleistocene formations: 1) are of the right depositional age such that their depositional $^{26}\text{Al}/^{10}\text{Be}$ has decayed significantly, but not completely, 2) host a significant fraction of the medium to coarse sand grain-sizes targeted for sampling, particularly in the Willis (Doering, 1935; Heinrich and McCulloh, 2000), and 3) dip more steeply than outer coastal plain deposits, with parts of the Willis forming heavily dissected cuestas grading into the hinge zone (Winker, 1979).

The important implication of this recycling is that, during times of lower sea-level, up-catchment sediment flux may be significantly overestimated (~10-30%). Since ^{10}Be in buried Plio-Pleistocene sediment has decayed substantially since deposition, its concentration relative to that in the up-catchment flux should be much lower. Because denudation rates are inversely proportional to ^{10}Be concentration, measurements that significantly integrate long-term stored sediment represent maximum estimates of sediment flux, and the effect cannot be compensated without knowing the precise burial ages and proportions of the different sediment sources. An exception to this reasoning would be if the inner coastal plain Plio-Pleistocene sediments were laid down during times when catchment-wide denudation rates were several orders of magnitude lower (i.e., TCN concentrations were higher) so that, even after substantial decay, their ^{10}Be concentrations are greater than in the up-catchment flux. However, this is unlikely since 1) depositional concentrations calculated from the Lissie Formation are similar, or less than, those from younger deposits, and 2) ^{10}Be measurements from undated sediment stratigraphically below the Lissie profile acquired at site 13 (sample IDs 2257 and 2258 in A.2.1.) are an order of magnitude *less* than all other depositional concentrations calculated for this study.

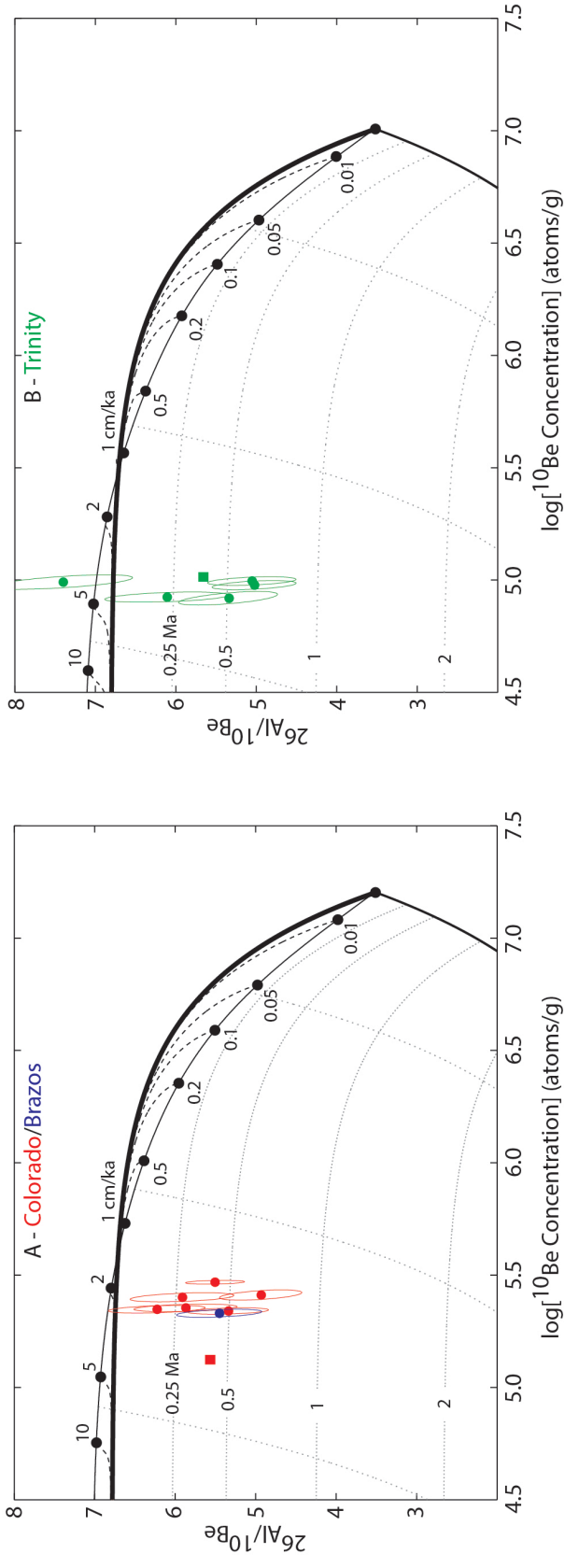


Figure 3.4: Burial plot showing depositional ^{10}Be and ^{26}Al data for the (A) Colorado (red) and Brazos (blue), and (B) Trinity (green) catchments. Material derived solely from vertical erosion of catchment surfaces should plot within the “erosion banana” defined by solid black lines. Samples plotting below these curves indicate mixing with material that has experienced burial (dotted contours). Because up-catchment material for the denudation rates in these rivers should have an $^{26}\text{Al}/^{10}\text{Be}$ of ~ 6.75 , the observation of a depressed ratio in the measured sample implies that the buried material incorporated into the sample has an even lower ratio. Thus, the burial contours indicate a minimum age of burial for the stored sediment. Pre-Lissie concentrations are indicated by dots and are displayed with error ellipses that represent 1σ values; most probable values for Lissie concentrations are indicated by squares.

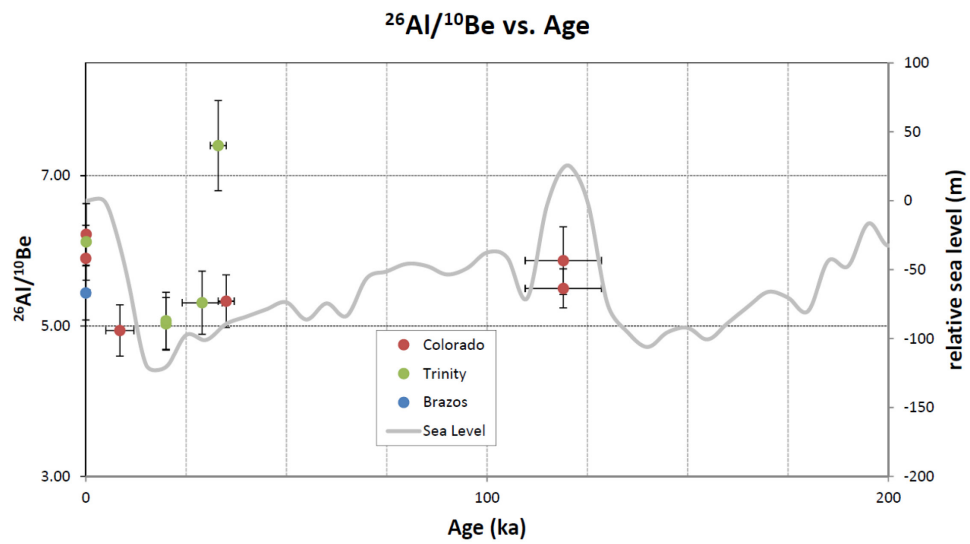


Figure 3.5: Measured $^{26}\text{Al}/^{10}\text{Be}$ vs. depositional age for Brazos, Colorado, and Trinity samples. Grey curve indicates relative sea level over the last 200 ka (Miller et al., 2005). Ratios should plot at ~ 6.75 if samples contain no burial signal. Lower ratios indicate an increasing significance of buried stored sediment contribution to the samples.

3.5.2. ¹⁰Be Catchment-wide Sediment Fluxes

3.5.2.1. *Modern Rates*

Our sediment flux estimates from modern pre-dam sediments are reproducible and are consistent with modern pre-dam observations of sediment flux in the three river systems. That is, the sediment flux magnitudes from these streams based on pre-dam estimates from sediment traps (LeBlanc and Hodgson, 1959; Kanes, 1970) are in the same relative order as the ¹⁰Be-derived measurements. The magnitude of the modern ¹⁰Be-determined sediment flux values, however, are all lower than the pre-dam estimates of Kanes (1970) and LeBlanc and Hodgson (1959). Furthermore, although the rates measured in the Trinity catchment compare favorably with previous data (see Table 3.2), those obtained in the Colorado and Brazos catchments are an order of magnitude lower. This is likely the result of a combination of two factors: 1) the ¹⁰Be rates integrate tens of thousands of years while the rates determined from the sediment traps were acquired over decades, and 2) the sediment-trap data, although acquired prior to the construction of high dams on these rivers, were measured after the catchment landscapes were significantly altered by irrigation infrastructure and agriculture, and thus were artificially more prone to sediment evacuation. Since the Colorado and Brazos catchments have a proportionally larger area developed for agriculture than those in the Trinity catchment, our data suggest that those suspended sediment analyses included a significant positive anthropogenic component. This anthropogenic effect is buffered for the time-averaged ¹⁰Be rates since the integration timescale implied by modern erosion rate calculations ($\sim 10^4$ a) is much larger than the time since the landscape became heavily modified by agriculture ($\sim 10^2$ a) (Brown et al., 1998).

Although most modern samples analyzed here were acquired from deposits laid down prior to dam construction in order to avoid the effects of sediment trapping, we also obtained a single sample from an active point-bar in the Colorado River to test the sensitivity of the up-catchment ^{10}Be -derived sediment flux rates to dam construction and sediment trapping. The post-dam sediment flux was found to be ~15% lower than that of the pre-dam setting (Table 3.2), suggesting that the ~70 year existence of these dams has had a significant effect on the downstream ^{10}Be concentrations. Since these dams effectively shut down the up-catchment medium- to coarse-grained sediment supply (bed load material, and target for this study), this increase in ^{10}Be concentration is likely the result of an increase in the active bed load of remobilized storage downstream from the dam. Because the ^{10}Be concentration in the post-dam sediment was greater than in pre-dam sediment, but had a similar $^{26}\text{Al}/^{10}\text{Be}$ value, we presume that the construction of the dam caused increased scouring of downstream coastal-plain sediments

3.5.2.2. Paleo-denudation Rates and Climate Change

Our ^{10}Be -derived denudation rates and sediment fluxes from the Colorado and Trinity Rivers (Table 3.3) indicate a positive correlation with the global marine $\delta^{18}\text{O}$ record, suggesting that glacial-interglacial conditions induce a landscape erosion response in these rivers (Fig. 3.6). For both rivers, up-catchment sediment flux significantly increases (~30-35%) from glacial to interglacial times, which is consistent with the magnitude of variation calculated by Blum and Hattier-Womack (2009) and Garvin (2008) using the temperature-dependent BQART model of Syvitski and Milliman (2007). In the Colorado River record, this increase is observed even prior to correcting our denudation rates using the $^{26}\text{Al}/^{10}\text{Be}$ ratio. The Trinity River record, however, indicates

that sediment recycling is relatively more important during sea-level fluctuations as the observed variation in the corrected fluxes is obscured in the raw values. This likely reflects lower sediment yields from the Trinity catchment, which would be more responsive to varied input from storage, the relative contribution of which varies from ~10-30% in both rivers. Such obscuring of the catchment sediment flux record emphasizes the importance of correcting ^{10}Be denudation rate estimates for sediment recycling. We also obtained sediment fluxes from the Lissie Formation in both catchments, but because of a large age uncertainty, did not assign them a climatic context based on chronology, considering them only as Mid-Pleistocene rates. These fluxes, however, are significantly different from those measured over the last few glacial-interglacial cycles. In the Colorado catchment, Mid-Pleistocene sediment fluxes are ~20% larger than any of our estimates over the last ~200 ka; conversely, in the Trinity catchment we obtained a flux ~40% lower than the lowest flux measured over the last ~50 ka. Uncertainties in chronology aside, this could be the result of integrating rates over OIS 15 and OIS 16 in the Colorado and Trinity Rivers, respectively. This interpretation is consistent with the relative chronology at the two Lissie sites from this work, and also with global temperature records that indicate these isotope stages represent exceptionally extended cold and warm periods (e.g. Lüthi et al., 2008). Furthermore, in the Trinity catchment, analysis of buried TCN concentrations from channel-belt sand underlying the Lissie profile (potentially Willis or an earlier stage of Lissie) indicate, along with field observations of an erosive basal contact (i.e. no preserved paleosol), that significant vertical incision occurred contemporaneously with Lissie deposition this site. This magnitude of removal, which is greater than the overlying

~7 m package of Lissie Formation, indicates a time of significant valley incision that may be a response to base level change, i.e., a relative cold period. This suggests that the low sediment flux estimated from the Lissie profile in the Trinity River represents a glacial period, with OIS 16 being the most probable based on the chronology.

Our paleo-denudation rate estimates assume that the response time of the ^{10}Be signal on the landscape is short compared to the driving frequency of glacial-interglacial change. However, it is important to ascertain whether or not climatically-induced fluctuations in erosion rate would produce a measureable change in ^{10}Be denudation rate. An examination of the response time of TCN denudation rates to step functions of episodic landscape denudation by Bierman and Steig (1996) demonstrated that for rapid denudation rates (5-15 cm ka^{-1}), TCN concentrations responded within 10-20 ka. The modeled response time is inversely proportional to the denudation rate, and leads to an overestimate and underestimate of applied low and high denudation rates, respectively. Because the landscape denudation rates reported from the rivers in this study are on the order of 1-4 cm ka^{-1} , the response time is slightly higher (~25 ka). However, this response time should be rapid enough to discern glacial and interglacial denudation rates that, in the Late Pleistocene, are driven primarily by a ~100 ka orbital cycle. An apparent phase shift in the response due to time integration of the ^{10}Be denudation rates will also occur; thus, a comparison of the ^{10}Be denudation rates should be compared to an appropriately integrated relative temperature. This integrated comparison reveals a positive correlation of ^{10}Be denudation rate to temperature (Fig. 3.7).

Minimal tectonic activity, lack of ice cover, stability of interior Texas catchments during the Quaternary, and a minimized anthropogenic signature due to long (~ 10^4 a)

temporal integration indicate that our calculated paleo-denudation rates represent a robust response of landscapes to climate change in a tropical-temperate region. Because the climate of central Texas was significantly wetter during cold intervals over the last ~71 ka (Musgrove et al., 2001), we assume that the observed increase in sediment discharge during warm intervals cannot be explained by higher net stream discharge. Instead, other temperature-dependent processes such as chemical weathering, precipitation intensity and frequency (e.g. Molnar, 2001), changes in vegetation cover (e.g. Hay et al., 2002), or changes in soil thickness may have dominated the variation in sediment discharge from these systems. If we extrapolate this trend to Pliocene times, our observed temperature-denudation relationship implies that, for these catchments, landscape erosion rates would have been significantly higher than in the Pleistocene. We recognize that this trend may have been interrupted by threshold changes in landscape erosion during the Plio-Pleistocene transition. However, if our inference is confirmed, the prospect of tropical-temperate and tectonically inactive regions eroding more rapidly during warm periods has implications for global sediment budgets. Supposing a constant global flux of terrestrial material to the ocean over the last ~12 Ma, as argued by Willenbring and Von Blanckenburg (2010), an increase in flux from tropical-temperate regions would require an opposing response from temperate-polar regions. This could explain the observed apparent global increase in Quaternary sediment flux to the oceans (Peizhen et al., 2001; Métiévier et al., 2002; Molnar, 2004) since the sources for the records in those studies are almost exclusively glaciated and/or tectonically active landscapes, and not necessarily representative of a global average.

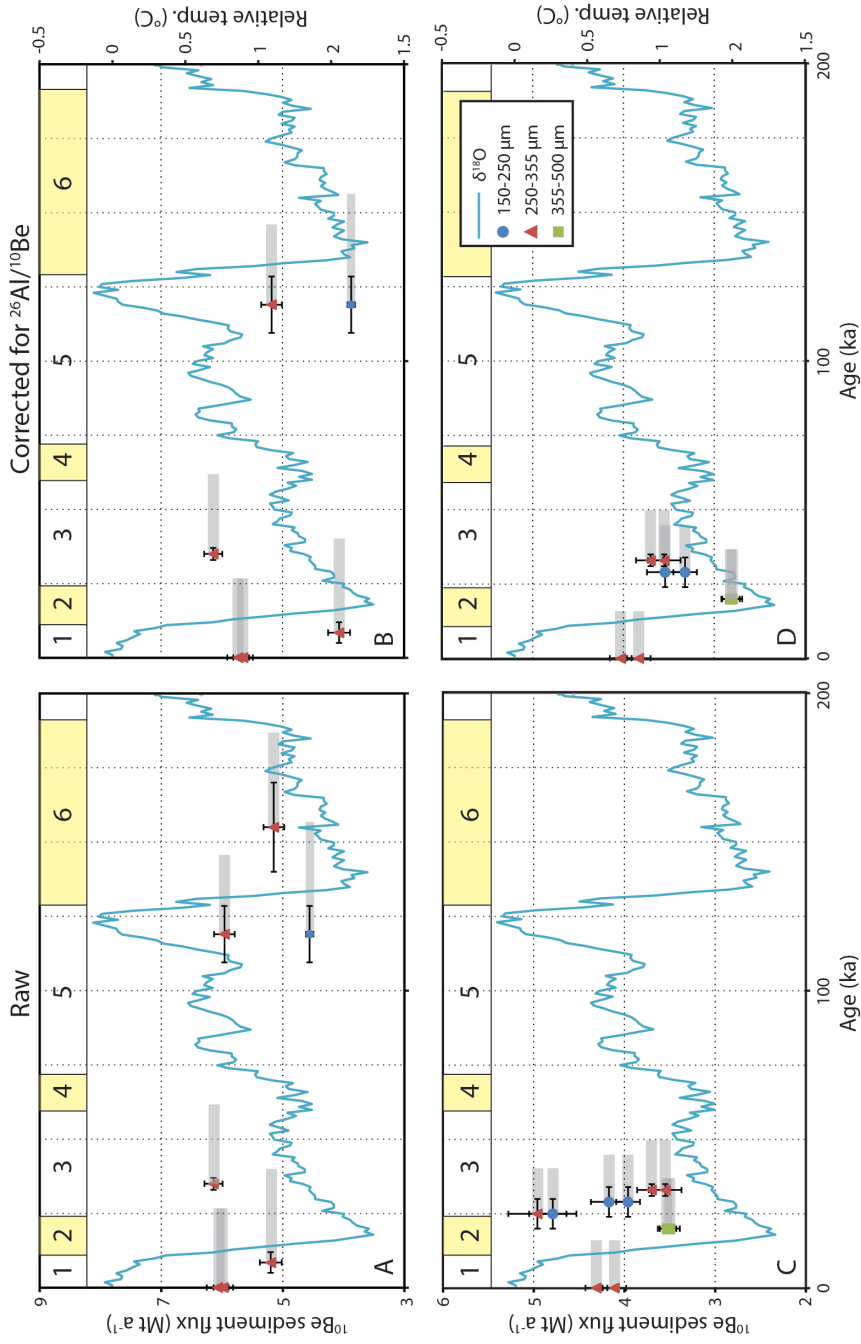


Figure 3.6: Calculated sediment fluxes vs. time from (A) raw depositional ^{10}Be concentrations from the Colorado catchment, (B) ^{10}Be concentrations from the Colorado catchment corrected using $^{26}\text{Al}/^{10}\text{Be}$, (C) raw depositional ^{10}Be concentrations from the Trinity catchment, and (D) ^{10}Be concentrations from the Trinity catchment corrected using $^{26}\text{Al}/^{10}\text{Be}$ (see A.2.2.). Even oxygen isotope stages indicated by yellow shaded rectangles; global relative temperature curve, based on the Lisiecki and Raymo (2005) LR04 benthic stack, is indicated by solid blue line. Shaded gray rectangles denote integration intervals of associated sediment flux measurement.

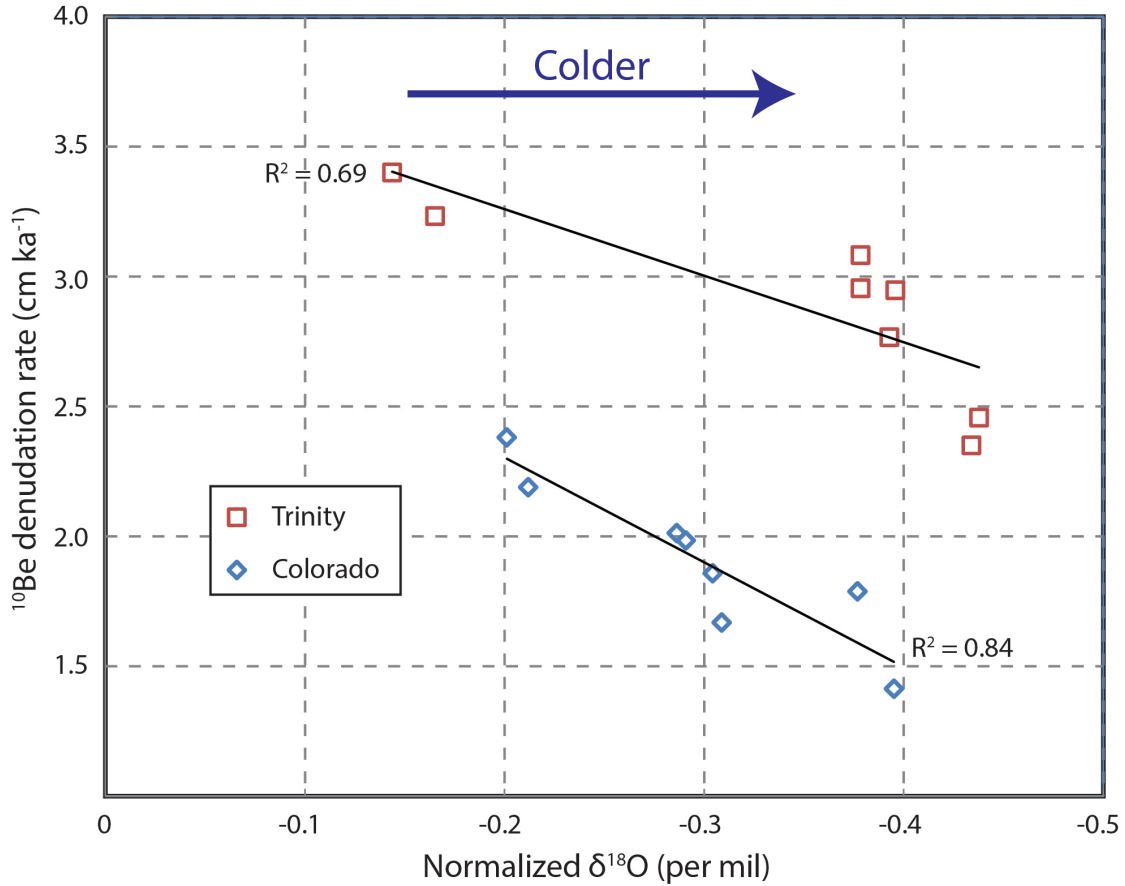


Figure 3.7: Calculated ^{10}Be denudation rate plotted against time-integrated $\delta^{18}\text{O}$, after the LR04 benthic stack of Lisiecki and Raymo (2005). $\delta^{18}\text{O}$ data are normalized to the modern value, and negative values correspond to times of greater average global ice mass. Linear regression curves (R^2 values shown on plot) for paleo-denudation rates from Colorado and Trinity catchments show a trend of decreased denudation rate with general decrease in average temperature. Plot shows all $^{26}\text{Al}/^{10}\text{Be}$ -corrected denudation rates except for those acquired from Lissie sediments; these were excluded since their poor temporal resolution precluded a reasonable calculation of time-integrated $\delta^{18}\text{O}$.

3.6. Conclusions

1) Measurements of denudation rates from catchments draining a tectonically inactive and non-glaciated landscape in Texas indicate a 30-35% increase in up-catchment flux from glacial to interglacial intervals during the Late Pleistocene, consistent with predictions of temperature-driven models of paleo-sediment flux estimates. These results suggest that tropical-temperate, passive-margin landscapes erode more rapidly during times of elevated temperature. Furthermore, recent data suggesting constant global erosion rates from the Pliocene onwards may not be at odds with mass-balance calculations indicating a significant increase in global erosion rates entering the Quaternary if the landscape response to climate is reversed in tropical-temperate vs. temperate-polar zones.

2) During times of low sea-level, we observe an increase in both the relative abundance and magnitude of stored sediment in sediment flux from the Colorado and Trinity rivers. For these systems, about 10-30% of the total medium- to coarse-grained sediment flux is from buried storage. Our data imply the source of the evacuated storage is from Plio-Pleistocene deposits that reside above the stream hinge zones in the outer coastal plain. This enhanced erosion of stored sediment is contemporaneous with decreased up-catchment denudation—dampening the variation in glacial vs. interglacial sediment delivery to the GoM.

3) The damming of sediment appears to have a significant effect on measurements of ^{10}Be catchment-wide denudation rates acquired from post-dam sediment. This indicates that, if possible, pre-dam deposits should always be targeted for this technique to avoid potential anthropogenic effects. However, this rapid response

provides an opportunity for the application of cosmogenic ^{10}Be and ^{26}Al to measuring bed load transport times.

4) We obtain the first absolute ages within the Lissie Formation from a pair of ^{10}Be depth profiles and an OSL sample. The results (~520-590 ka) support existing stratigraphic frameworks and provide a means to improve GoM sediment models that rely on the onshore-offshore correlations and rates of long-term shelf migration.

3.7. Acknowledgements

We thank M. Garvin for field assistance during multiple sample trips, and for thoughtful discussions of coastal plain sedimentology; G. Yang for support at the Dalhousie Geochronology Centre cosmogenic nuclide lab; T. Rittenour and J. Pederson at the Utah State University Luminescence Lab for assistance with interpreting our OSL data; and R. Farmer for providing logistical services during the culmination of this manuscript. JG acknowledges support from the 2004 Petro-Canada Young Investigators Award, NSERC Discovery Grant, and NSERC Major Resources Support Grant for field travel, chemical preparation, AMS measurements, and OSL date for the Lissie Formation; AJH appreciates research funds from the Geological Society of America (GSA), American Geophysical Union (AGU), and Gulf Coast Association of Geological Societies (GCAGS) for travel and accommodation during field work.

CHAPTER 4: A Latest Pliocene Age for the Earliest and Most Extensive Cordilleran Ice Sheet in Northwestern Canada

Paper submitted for publication in Quaternary Science Reviews (July 2012)

Alan J. Hidy³(1), John C. Gosse (1), Duane G. Froese (2), Jeffery D. Bond (3), and Dylan H. Rood (4,5)

(1)Department of Earth Sciences, Dalhousie University, Halifax, Nova Scotia B3H 4R2

(2)Department of Earth and Atmospheric Sciences, University of Alberta, Edmonton, Alberta T6G 2E3

(3)Yukon Geological Survey, P.O. Box 2703, Whitehorse, Yukon, Canada Y1A 2C6

(4)Scottish Universities Environmental Research Centre (SUERC), East Kilbride G75 0QF, UK

(5)Earth Research Institute, University of California, Santa Barbara, CA 93106, USA

4.1. Abstract

The Klondike gravel is a widespread glaciofluvial gravel marking the earliest and most-extensive Cordilleran Ice Sheet (CIS) in NW North America. New terrestrial cosmogenic nuclide (TCN) burial ages indicate this gravel was emplaced $2.64^{+0.20}_{-0.18}$ Ma (1σ). Coupled with previously interpreted paleomagnetic stratigraphy, this numerical age constrains the timing the earliest CIS to the late Gauss Chron and provides a minimum age for the Upper White Channel gravel, a significant placer gold source in the Yukon. This implies the first CIS glacial maximum pre-dates the maximum extent of the Laurentide Ice Sheet, indicating that during the initial stages of northern hemisphere glaciation, the most extensive glaciers were present in the relatively cold and high

³Corresponding author.

Email addresses: alanhidy@dal.ca (A. J. Hidy), john.gosse@dal.ca (J. C. Gosse), duane.froese@ualberta.ca (D. G. Froese), Jeff.Bond@gov.yk.ca (J. D. Bond), drood@eri.ucsb.edu (D. H. Rood).

elevation northern Cordillera. Our results verify the CIS as a likely source of persistent coeval ice-rafted debris in the northern Pacific, and suggest that the first CIS formed as a response to the establishment of the northern Pacific halocline and emergence of the 41 ka obliquity cycle during the Plio-Pliocene transition.

4.2. Introduction

The onset of extensive northern hemisphere glaciation interrupted a gradual lowering of global atmospheric CO₂ and a slow cooling trend through the Pliocene (e.g. Pagani et al., 2009). The widespread occurrence of ice-rafted debris in late Pliocene and early Pleistocene marine sediments provides an indirect record of the growth of northern hemisphere glaciers with implications for the potential mechanisms that led to extensive continental glaciation (e.g. Maslin et al., 1998; Haug et al., 2005). Differences in the timing and magnitude of ice-rafted sediments in these records suggest regional differences in the distribution of glaciers that contributed to the marine record, but provide little indication of their former extent or distribution. Unfortunately, dating the sparse terrestrial record of early glaciation is difficult since subsequent glaciations tend to obscure the depositional record of earlier advances, and few numerical dating methods are applicable.

Beyond the limit of the last Cordilleran Ice Sheet (CIS) in northwestern Canada are multiple drift deposits that record the earliest glaciations in North America (Froese et al., 2000; Barendregt et al., 2010; Duk-Rodkin et al., 2010). The oldest CIS advance, which is associated with the most extensive glaciation to affect the northern Cordillera, is recorded in extensive drift—including the normally-magnetized Klondike glaciofluvial gravel—that marks the first presence of extrabasinal clasts in the region (Hughes et al.,

1972; Froese et al., 2000). The advance was proposed to be of Pliocene age (late Gauss Chron) on the basis of normal magnetic polarity of basal tills in sedimentary sequences and associated outwash (Froese et al., 2000; Barendregt et al., 2010; Duk-Rodkin et al., 2010; Barendregt and Duk-Rodkin, 2011). Independent constraints on the late Gauss age interpretation are that this normally-magnetized outwash gravel (Klondike gravel) has an inset terrace with a loess mantle having multiple polarities that record the Brunhes, Jaramillo and late Matuyama chrons (Froese et al., 2000). A Gauss interpretation is further supported by glass fission-track ages on tephra of 1.37 ± 0.13 Ma from loess cover below the Jaramillo-aged sediments, 1.03 ± 0.17 Ma within the Jaramillo-aged material, and 2.82 ± 0.24 Ma within gravel stratigraphically below the Klondike gravel (Westgate et al., 2003; Preece et al., 2011). However, because no close limiting ages from tephra beds overlying the outwash are known, it is possible that the normal magnetozone is either a subchron of the early Matuyama (i.e. Olduvai or Reunion) or late Gauss (Froese et al., 2000). The late Gauss interpretation is preferred because previous studies propose that pre-Olduvai periglacial and glacial conditions existed elsewhere in the northern Cordillera (Westgate et al., 1990; Barendregt et al., 1996; Duk-Rodkin et al., 1996; Froese et al., 2000), and since North Pacific marine cores indicate significant ice rafting in the late Pliocene (Krissek, 1995; Rea et al., 1995; Mudelsee and Raymo, 2005; Polyak et al., 2010). An Olduvai interpretation, however, is also possible as Olduvai deposition correlates with the onset of significant glacial events that define the former Pleistocene boundary. Here, we report new TCN burial ages for the Klondike gravel that support the late Gauss interpretation for the earliest CIS.

4.2.1. Klondike Area

The lower Klondike valley is located southeast of Dawson City, Yukon, near the confluence of the Yukon and Klondike rivers. The region is at the all-time limit of glaciation, marking the boundary of former Cordilleran ice and the non-glaciated portion of the Klondike Plateau (Fig. 4.1). Here, strata of gravel from small, non-glaciated catchments draining King Solomon Dome (White Channel gravel) and from glaciofluvial outwash (Klondike gravel) are interfingering where their drainages meet in the Klondike valley—indicating contemporaneous deposition of uppermost White Channel and basal Klondike gravel (Hughes et al., 1972; Froese et al., 2000).

The Klondike gravel forms the highest terrace in the lower Klondike valley, and can be traced westward into central Alaska (Duk-Rodkin et al., 2004) and eastward to the Flat Creek beds where a till is sandwiched between outwash gravel. The terrace surface descends from the Flat Creek beds toward the Klondike valley with paleoflow directions to the west (Froese et al., 2000). Outwash from this early Cordilleran glaciation also breached the divide from the Stewart River and spilled into the Indian River (Jackson et al., 2009). Paleoflow measurements and deposition of equivalent normally magnetized outwash in the Indian River valley preclude a local montane ice source from the Ogilvie Mountains to the north; collectively this evidence indicates a CIS source for the Klondike and equivalent gravel, marking the most extensive CIS glaciation of the northern Cordillera (Froese et al., 2000; Duk-Rodkin et al., 2010). Pollen from overbank deposits within the Klondike gravel indicates shrub-tundra vegetation, marking the first appearance of vegetation typical of Pleistocene cold stages and the last occurrence of

taxonomically-richer boreal forest associated with the Miocene and early Pliocene pre-glacial boreal forest (Schweger et al., 2011).

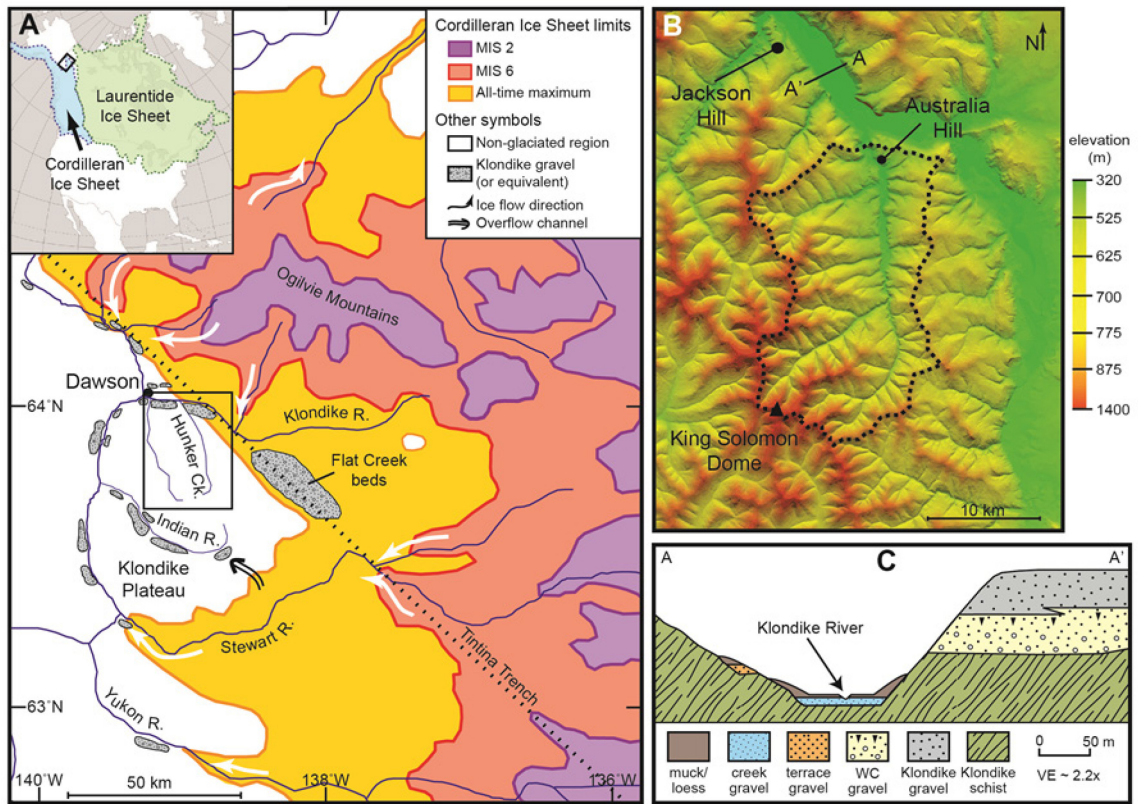


Figure 4.1 Map of Klondike area showing extent of major CIS advancements after Duk-Rodkin et al. (2004) (A) with inset DEM of Hunker Creek (B), and cross-section of the Klondike River valley through the high terrace gravels (D).

4.2.2. Sample Site: Australia Hill

Modern mining in the Klondike Goldfields has exposed multiple 60-80 m thick sequences of Klondike and White Channel gravel. The exposure near the mouth of Hunker Creek (Australia Hill) was chosen for this study because here: 1) the contact between the Klondike and White Channel gravel is visible and laterally extensive for hundreds of meters; 2) the Upper White Channel (UWC) gravel interfingers with the Klondike gravel and is distinguishable from the Lower White Channel (LWC) gravel; and 3) paleomagnetic data indicate a normal magnetization in both the UWC and Klondike gravel (Froese et al., 2000) (Fig. 4.2). The LWC gravel is interpreted as proximal braided and gravity flow deposits sourced from Hunker Creek (Froese et al., 2000). White Channel gravel lithologies are mainly quartz (~80%), and derived primarily from the Paleozoic Klondike Schist, which comprises much of the King Solomon Dome area. Local igneous and metamorphic lithologies are strongly weathered, with much of the LWC showing pronounced clay enrichment due to groundwater flow in the deposit (Lowey et al., 2001). At Australia Hill the UWC gravel unconformably overlies the LWC gravel, and can be mapped up-valley to adjacent exposures. The deposit is entirely derived from local lithologies and has a lower percentage of quartz clasts (ca. 40-50%). Locally the unit contains ice-wedge casts and other periglacial structures (Hughes et al., 1972; Froese et al., 2000; Schweger et al., 2011). At Australia Hill and other sites along the Klondike valley, the Klondike gravel overlies and interfingers with the UWC gravel. The unit consists of planar gravel with thin planar-tabular crossbeds interpreted to have been deposited in a medial to distal braided river environment (Froese et al., 2000). Lithologies consist largely of black chert, quartzite, and other sedimentary rocks sourced

from the Cordillera. All but the lower ~8 m of the Klondike gravel at Australia Hill was removed by recent mining, but immediately upslope and adjacent to the site, the well preserved nearly flat terrace surface is present, with its distinctive Wounded Moose paleosol (Smith et al., 1986). The Klondike gravel terrace extends nearly continuously from the Flat Creek area through the lower Klondike valley, including the neighboring Jackson Hill site (Fig. 4.1). Projections indicate that the original thickness of the Klondike gravel at Australia Hill was ~35 m.

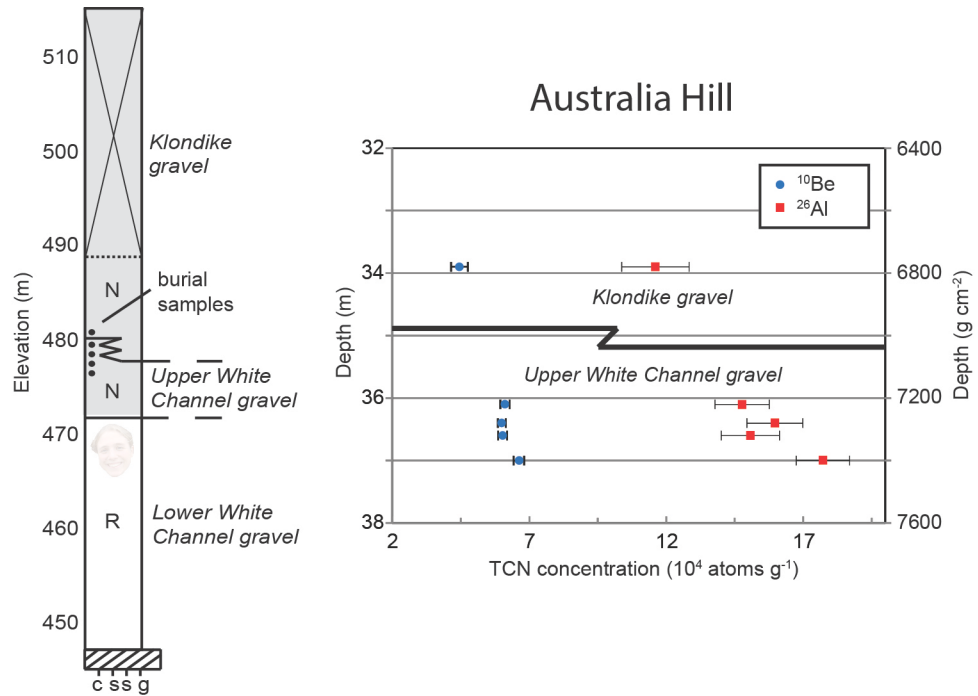


Figure 4.2 Stratigraphic column with magnetic polarity (N,R = normal, reversed) at Australia Hill (after Froese et al., 2000) and location of TCN burial samples. TCN concentrations do not systematically decrease with depth below the contact between the Klondike and Upper White Channel gravels—bolstering our assumption of a negligible exposure time between their depositions.

4.3. Methods

4.3.1. TCN Burial Dating

TCN burial dating techniques use a pair of in situ-produced radionuclides with different half-lives (in our case, ^{26}Al , $t_{1/2} = 0.705 \text{ Ma}$ and ^{10}Be , $t_{1/2} = 1.387 \text{ Ma}$; Nishiizumi (2004), Chmeleff et al. (2010), Korschinek et al.(2010)). The simplest case of burial dating applies to material that is first exposed to cosmic rays at or near the Earth's surface and then instantaneously buried to a depth shielding it from significant cosmic ray bombardment (Granger and Muzikar, 2001). The production rates of ^{26}Al and ^{10}Be in exposed surface material have a constant ratio; if this material is then buried deeply and rapidly so that production ceases, the $^{26}\text{Al}/^{10}\text{Be}$ decreases in a predictable way over time as the two isotopes decay. The difference between the measured ratio and the production ratio can be used to infer a burial age assuming that: 1) the $^{26}\text{Al}/^{10}\text{Be}$ at the time of deposition is approximately equal to the production ratio (~ 6.75), and 2) the post-depositional production via deeply penetrating muons is negligible or can be quantified. The first assumption is invalid for material that has experienced significant burial ($>200 \text{ ka}$), or prolonged surface stability ($>1 \text{ Ma}$) prior to deposition (see section 4.5.2). Because our samples are deeply buried ($\sim 35 \text{ m}$, or $\sim 7000 \text{ g cm}^{-2}$), the post-depositional TCN production rates are extremely low. However, over million-year durations there may be sufficient production by muons to affect the measured ratio, so it must be considered. We adopt deep muon production rates of half the theoretical values of Heisinger et al. (2002a; 2002b). A significant overestimation of the widely used Heisinger et al. rates has been previously suggested (Braucher et al., 2003; Balco et al., 2005; Braucher et al., 2011), and this value is supported by preliminary ^{10}Be and ^{26}Al results from the $>25 \text{ m}$

deep Beacon Heights bedrock core in Antarctica which, for deep samples ($>2000 \text{ g cm}^{-2}$), indicate that Heisinger et al. (2002a; 2002b) systematically overestimated muon production by a factor of ~ 2 (pers. comm. J. Stone). For comparison, we also performed a sensitivity analysis using an incremental muon production rate from zero to that of Heisinger et al. (2002a; 2002b).

4.3.2. Sampling Strategy

Since the UWC gravel interfingers with the base of the Klondike gravel, these units should share approximately the same burial age at this general level. We thus collected: 1) a single sample at the base of the Klondike gravel, and 2) a four-sample depth profile at the top of the UWC gravel. If measured TCN concentrations in the UWC gravel profile are constant with depth, this supports our assumption of a negligible hiatus between the two units. Alternatively, if these concentrations exhibit an exponential decrease with depth, an interval of exposure is indicated prior to Klondike gravel deposition and an isochron approach could be used to infer a burial age independent of the assumptions required for burial dating (Balco and Rovey, 2008); this, however, was not observed (Fig. 4.2). If the measured $^{26}\text{Al}/^{10}\text{Be}$ in the two units is similar, their depositional ratios must also have been similar since they share the same burial history. Samples from both units can then be used to interpret a simple burial age for the Klondike gravel.

4.3.3. Sample Preparation and Analysis

Amalgamated samples were collected (June 2009) and sieved in the field to remove the coarse ($>2 \text{ mm}$) grains, then later sieved to extract the 150-850 μm grain-size fraction. Chemical preparation of the samples was performed at the Dalhousie

Geochronology Centre cosmogenic geochemistry lab. The laboratory manual is available online at <http://cnf.earthsciences.dal.ca>. Quartz purification included multiple cycles of treatment with aqua regia (3:1 of HCl:HNO₃), HF etching, ultrasonication, and magnetic separation. These procedures purified the samples to ~99% quartz, dissolved aggregate grains and weak silicates, and removed any atmospheric ¹⁰Be adsorbed to grain surfaces (Kohl and Nishiizumi, 1992). Between 70-180 g pure quartz was dissolved for each sample. To each sample, approximately 200 µg ⁹Be and 1000 µg ²⁷Al were added to facilitate AMS sample preparation by isotope dilution. The samples were digested in a HF-HClO₄ mixture and the Be⁺² and Al⁺² cations extracted via ion chromatography. After quartz digestion, samples were brought to 100 ml in 2% HCl. Two 5 ml aliquots were extracted from this solution, one before addition of the Al carrier and one after. These aliquots were then dried, brought up in a solution of 2% HNO₃, and diluted for ICP-MS total Al measurement. Results from both dilutions were used to calculate native Al concentrations and obtain uncertainties (1-4%) which are incorporated in total measurement uncertainties for each ²⁶Al measurement. Following geochemistry, which included centrifugation, anion chromatography, controlled precipitation, cation chromatography, and precipitation with ammonia gas, the samples were oxidized with a Bunsen burner at a temperature of >1000°C for one minute to produce BeO and Al₂O₃ powders. Be and Al oxides were mixed 1:1 with niobium and silver (by volume), respectively, and sent to the Center for Accelerator Mass Spectrometry at Lawrence Livermore National Laboratory (CAMS-LLNL) for AMS analysis. Standards at CAMS-LLNL used for Be and Al measurements were 07KNSTD3110 with a ratio of 2850 x 10⁻¹⁵ (Nishiizumi et al., 2007), and KNSTD10650 with a ratio of 10650 x 10⁻¹⁵ (Nishiizumi,

2004), respectively. Separate process blanks for Be and Al were analyzed and used to subtract any background concentration, which in all instances was between 1-3% of the adjusted ^{10}Be value (148950 atoms) and $\sim 1\%$ of the adjusted ^{26}Al value (183923 atoms).

4.4. Results

We obtained an error-weighted mean ($n=4$) burial age of $2.61^{+0.20}_{-0.19}$ Ma for the four UWC gravel samples and an age of $3.06^{+0.98}_{-0.72}$ Ma from the single Klondike gravel sample yielding an error-weighted grand mean ($n=5$) of $2.64^{+0.20}_{-0.18}$ Ma (1σ ; Table 4.1). All asymmetric error-weighted means were computed using the linear variance method of Barlow (2004). Varying muon production rates from naught to that of Heisinger et al. (2002a; 2002b) resulted in error-weighted grand mean burial ages between $2.07^{+0.13}_{-0.12}$ Ma ($n=5$) and $3.92^{+0.49}_{-0.39}$ Ma ($n=4$), respectively (1σ ; Fig. 4.3). The single sample from the Klondike gravel unit is excluded from the age calculated with the Heisinger et al. rates since the modeled post-depositional muon production component of ^{26}Al exceeded the concentration measured in the sample by $\sim 35\%$. All ^{26}Al and ^{10}Be measurement and decay constant errors are included in these estimates (see Gosse and Phillips, 2001; Korschinek et al., 2010). Error estimates do not include the unknown systematic error in the assumed pre-depositional $^{26}\text{Al}/^{10}\text{Be}$ (see section 4.5.2). Additionally, gradual erosion of the Klondike gravel surface was ignored due to its negligible effect on deep production rates.

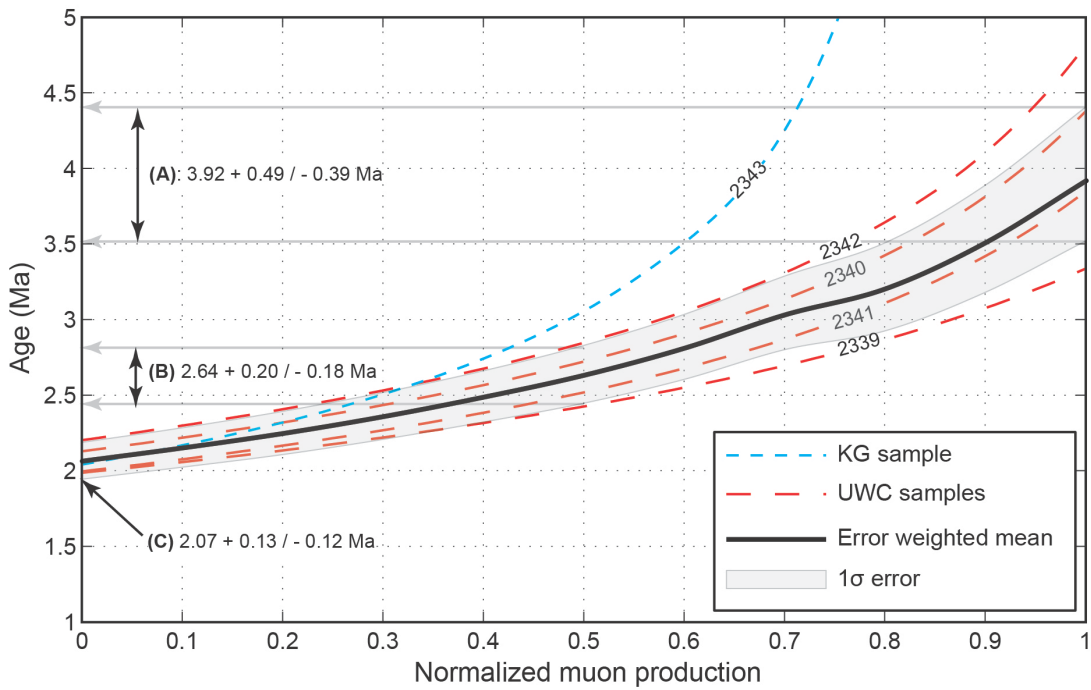


Figure 4.3 Sensitivity of interpreted individual burial ages to assumed muon production rates. Rates are normalized to Heisinger et al. (2002a; 2002b). Error-weighted mean of all burial ages with 1σ errors shown for: (A) full Heisinger et al. rates, (B) half Heisinger et al. rates (assumed for this work), and (C) zero muon production. Numbers on curves indicate sample IDs (see Table 4.1). KG = Klondike gravel; UWC = Upper White Channel gravel. At ~ 0.75 normalized muon production, the interpreted age of the Klondike gravel sample approaches infinity. This implies a muon correction greater than the measured TCN concentrations for this sample—indicating the muon production rates cannot be greater than ~ 0.75 of the full Heisinger et al. rates. The calculated error-weighted mean curve excludes the Klondike gravel sample for muon production rates greater than 0.75.

^a Unit	Sample ID	Depth (m)	[¹⁰ Be] (atoms g ⁻¹)	^b Unc. (atoms g ⁻¹)	[²⁶ Al] (atoms g ⁻¹)	^b Unc. (atoms g ⁻¹)	²⁶ Al/ ¹⁰ Be	Age (Ma)	^b Unc. +/- (Ma)
KG	2343	33.9	44504	3041	116065	12282	2.61	3.06	0.98/0.74
UWC	2342	36.1	61140	1674	147686	9838	2.42	2.85	0.46/0.40
UWC	2341	36.4	59992	1447	159669	10227	2.66	2.52	0.43/0.34
UWC	2340	36.6	60276	1653	150692	10641	2.50	2.72	0.47/0.40
UWC	2339	37.0	66336	1814	177198	9757	2.67	2.42	0.35/0.31
UWC error weighted mean:								2.61	0.20/0.19
Total error weighted mean:								2.64	0.20/0.18

Note: Latitude, longitude, and elevation of site are 64.023 N, -139.147 W, and 520 m, respectively.

^aKG = Klondike gravel; UWC = Upper White Channel gravel.

^bAll uncertainties are 1σ and include AMS measurement errors (CAMS-LLNL) and an estimated 2% uncertainty for sample preparation errors. For ²⁶Al only, an additional 1-4% random error from ICP-MS native Al measurements is included. Error-weighted means calculated after Barlow (2004).

Table 4.1 Measured ¹⁰Be and ²⁶Al concentrations and burial ages

4.5. Discussion

4.5.1. Interpretation of ^{26}Al and ^{10}Be Data

Measurements of ^{26}Al and ^{10}Be obtained at the top of the UWC gravel are approximately constant with depth, which is consistent with our assumption that Klondike gravel deposition coincided with, or immediately followed, that of the upper UWC gravel (i.e. no prolonged period of exposure occurred between their deposition). Furthermore, the muon-corrected $^{26}\text{Al}/^{10}\text{Be}$ from both gravel units agree within error. This implies that the depositional $^{26}\text{Al}/^{10}\text{Be}$ for both units were similar and either both were equal to the production ratio or both deviated indistinguishably from the production ratio. This agreement suggests an insensitivity of the depositional ratios to the widely different sediment sources, glacial histories, and transport mechanisms responsible for the two deposits, and supports our assumption of a simple burial history. However, the observed agreement in depositional $^{26}\text{Al}/^{10}\text{Be}$ may be because the dated sediment originated from the very first CIS. Prior to CIS advance, the regional source for the Klondike gravel would not have been shielded significantly by ice, and conditions in the well constrained source area for the UWC gravel may also have applied to areas sourcing the Klondike gravel. Thus, it is possible that TCN burial dating with simple assumptions can be applied to glacial materials from the earliest large-scale glaciations.

4.5.2. Olduvai vs. Late Gauss Age

Interpreting our data assuming a simple 1-stage burial model yields a late Gauss age of 2.64 Ma for Klondike gravel deposition and is consistent with the established paleomagnetic and tephrochronological framework. However, our goal to distinguish between the two likely paleomagnetic ages for Klondike gravel deposition (Olduvai or

late Gauss) requires precluding effects of additional possibilities that could have lowered the depositional $^{26}\text{Al}/^{10}\text{Be}$ in our amalgamated samples and caused a systematic overestimate of age (Fig. 4.4). We restrict the following arguments to the UWC gravel because its erosional, glacial, and transport history is well constrained.

Let us consider a depositional $^{26}\text{Al}/^{10}\text{Be}$ of 5.1 (Fig. 4.4, region O)—the maximum value for the UWC gravel data to support an Olduvai age. Scenario (1) invokes multiple stages of burial between hillslope source and final deposition. By this mechanism, the average UWC gravel clast would have needed to experience ~ 0.6 Ma of cumulative deep burial prior to deposition. We consider this improbable since: 1) prolonged temporary sediment storage prior to rapid emplacement of the UWC gravel in a small (~ 200 km²) catchment like Hunker Creek is unlikely; 2) there is no evidence for significant transient burial by ice or loess; and 3) there is no evidence for older terrace remnants or significant landslide deposits in the upper reaches of the catchment.

Scenario (2), a reduction in the ratio due to extremely long exposure prior to stripping, requires: 1) a Hunker Creek catchment where hillslopes were stable long enough for ^{26}Al and ^{10}Be production to begin equilibrating with decay, followed by 2) rapid and deep stripping of up-catchment surfaces. Inferred boundary conditions for this scenario rule out an Olduvai age. These conditions require the average up-catchment surface source of the UWC gravel to have experienced: 1) zero physical or chemical erosion for a minimum of 1.5 Ma, or 2) a maximum erosion rate of 50 cm Ma⁻¹ for longer exposures (Fig. 4.5). We reject this possibility since the 2.82 Ma tephra (Westgate et al., 2003; Preece et al., 2011) found within the UWC gravel indicates that significant aggradation in the basin occurred at this time. Since this deposition would have at least

partially reset the up-catchment TCN exposure clock via erosion and stripping of hillslope surfaces, there would not have been sufficient time of stability (>1.5 Ma) for the $^{26}\text{Al}/^{10}\text{Be}$ to decay to 5.1, as needed to be consistent with Olduvai deposition. Furthermore, even for zero surface erosion, the deep, in situ (chemical) weathering that concentrated the quartz comprising the White Channel gravel prior to deposition would have had the same effect as surface erosion. This is due to a reduction in mass-depth for material in the zone of high TCN production (upper 2-3 m) as regolith weathers. Chemical weathering would have been significant in these catchments since regolith development was likely deep and quartz purification extensive. Thus, the up-catchment conditions required to explain our data with an Olduvai depositional age are implausible.

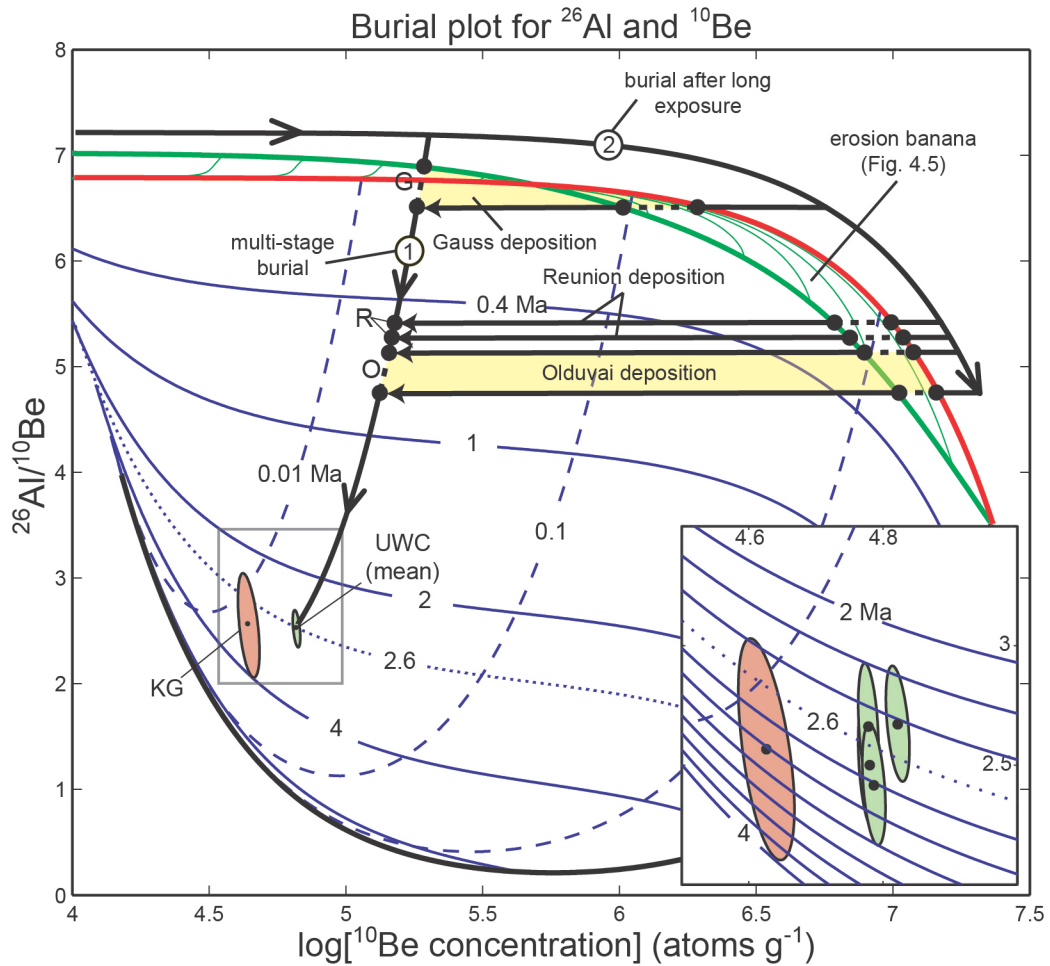


Figure 4.4 Burial plot showing Klondike gravel sample (red) and UWC gravel samples (green; 4-sample mean, individual samples shown on inset) at Australia Hill. Solid red line represents the continuous exposure curve with no surface erosion; solid green lines represent contours of the continuous exposure curve at successively increasing surface erosion rates (collectively known as the erosion banana). Samples will plot somewhere in the erosion banana prior to burial. Once buried, samples follow a path parallel to the dashed blue lines (pre-burial exposure duration), with burial durations indicated by solid blue lines. The measured ratios could represent a simple burial event, multiple events (scenario 1), or a single event after long exposure (scenario 2). Scenario (2) is possible because a stripping event may have occurred that instantaneously mixed surface material at high TCN concentrations with deeper material at exponentially lower TCN concentrations. This mixed material would have approximately the same $^{26}\text{Al}/^{10}\text{Be}$ as expected from the surface, but would be significantly lower in ^{10}Be concentration. Thus, the path of scenario (2) moves horizontally to the left from an erosion banana defined by surface concentrations. Points (R) and dotted line segments (O) and (G) indicate where samples must have plotted at deposition to support a Reunion, Olduvai, and Gauss age, respectively. Error ellipses represent 1σ values. Burial contours adjusted for continuous muon production at 7000 g cm^{-2} depth. Burial contours and erosion banana both use half the Heisinger et al. (2002a; 2002b) muon production rates.

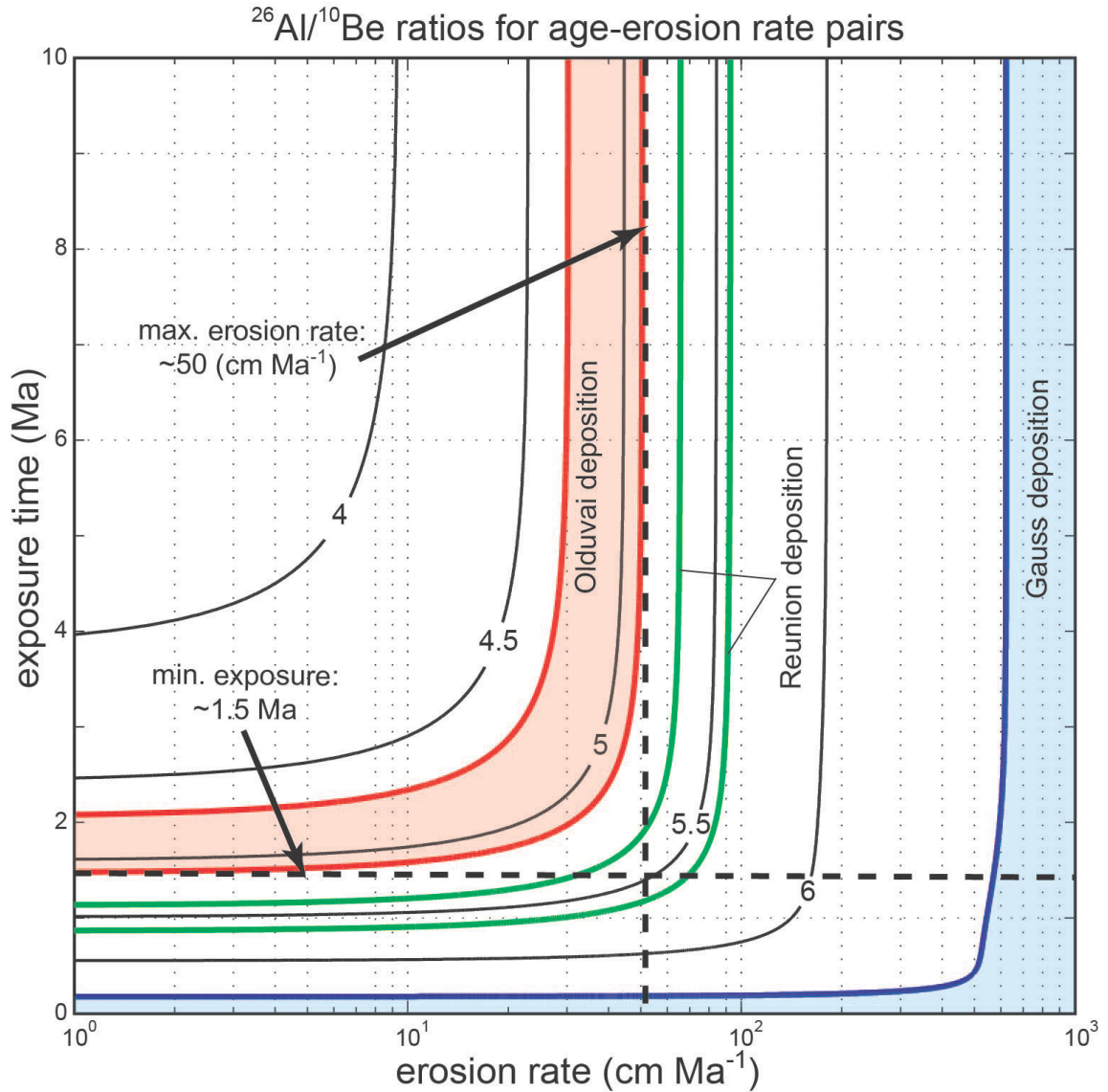


Figure 4.5 Contour plot of $^{26}\text{Al}/^{10}\text{Be}$ observed on a surface as a function of exposure time and erosion rate (mean conditions of catchment surfaces sourcing the UWC gravel). Colored regions indicate allowable regions for an Olduvai (red) or Gauss (blue) interpretation (Fig. 4.4; scenario 2). Reunion subchrons are shown as green lines. Dashed black lines indicate the maximum average erosion rate and minimum average exposure time of the catchment surfaces sourcing the Upper White Channel gravel that are necessary for an Olduvai interpretation of the burial ages presented in this work.

4.5.3. Muon Sensitivity Analysis

Using the full Heisinger et al. (2002a; 2002b) rates places the burial ages from the UWC gravel samples (Fig. 4.3) significantly outside the pre-existing chronologic framework (1.46 - 2.82 Ma from bracketing constraints by normal polarity and glass fission-track ages on tephras). The full rates are also discordant with the TCN measurements obtained for the Klondike gravel sample as the muonic correction is larger than the measured TCN concentrations. The lower rates indicated by the Beacon Heights core data and assumed for this work, however, are consistent with already established chronologies. Our data suggest that the Heisinger et al. (2002a; 2002b) rates significantly overestimate muon production at these depths and provide further support for the adopted lower values. Although results from the Beacon Heights calibration site are not yet finalized or published, even if the preliminary rates are off by ~20% in either direction, our error-weighted mean age would still support a late Gauss interpretation of the Klondike gravel (Fig. 4.3).

4.5.4. A 2.64 Ma Cordilleran Ice Sheet

From the extensive marine record, a gradual amplification of prolonged Northern Hemisphere cooling, and a significant and sustained source of moisture to the northern Canadian Cordillera occurred during the Plio-Pleistocene transition. The initiation of regional ice sheets is thought to be a threshold response to these conditions (Haug et al., 2005), and is generally thought to be an exclusively Quaternary phenomenon. Our 2.64 Ma age for the earliest CIS places the time of this response in the latest Pliocene, supporting the preferred interpretation of the composite paleomagnetic stratigraphy in the Klondike area (Froese et al., 2000; Barendregt et al., 2010; Duk-Rodkin et al., 2010). The

terrestrial and coeval marine glacial evidence (IRD observed throughout the northern Pacific (Krissek, 1995; Rea et al., 1995)) of early expansion of the CIS to its greatest extent coincides with the emergence of the 41 ka orbital cycle (obliquity). This correlation supports the hypothesis that an increased amplitude of this cycle was the dominant driver of global ice volume during the Plio-Pliocene transition (Berger and Loutre, 1991) (Fig. 4.6). At this time, the sub-arctic Pacific halocline was already established (Haug et al., 2005). Our data are consistent with the inference that this halocline, which produced warmer sea surface temperatures in the north Pacific, served as the moisture source for the early CIS (sensu Prentice and Matthews, 1991). This moisture source may have accounted for the asynchronous advance of Cordilleran over Laurentide ice, as northern Pacific-sourced moisture fueled ice expansion initially in the high elevations of the proximal northern Cordillera. As atmospheric CO₂ concentrations and equilibrium line altitudes continued to lower due to prolonged cooling leading up to the Quaternary, conditions were ripe for expansion of ice beyond mountain fronts, initiating more extensive ice sheets in the continental interior beginning at ~2.4 Ma (Balco and Rovey, 2010). Although the initiation of ice in North America likely began as early as 3.6 Ma based on globally distributed marine $\delta^{18}\text{O}$ records (Mudelsee and Raymo, 2005), our ages, and those of Balco and Rovey (2010), reflect the time of the maximum extent of this ice.

Significant regional drainage reorganization, including a change in the paleo-Yukon River flow that diverted it from the Gulf of Alaska to the Bering Sea, has been interpreted as a consequence of the first CIS advance in the North American Cordillera (Duk-Rodkin et al., 2001). This diversion would have increased discharge of fresh water

into the Bering Sea and locally enhanced siliciclastic sediment flux at a crucial circulation bottleneck that links the northern Pacific to the Arctic and Atlantic Oceans. Now that the age of the Klondike gravel is established, further stratigraphic evidence that connects the Klondike gravel to this drainage reorganization may come to light.

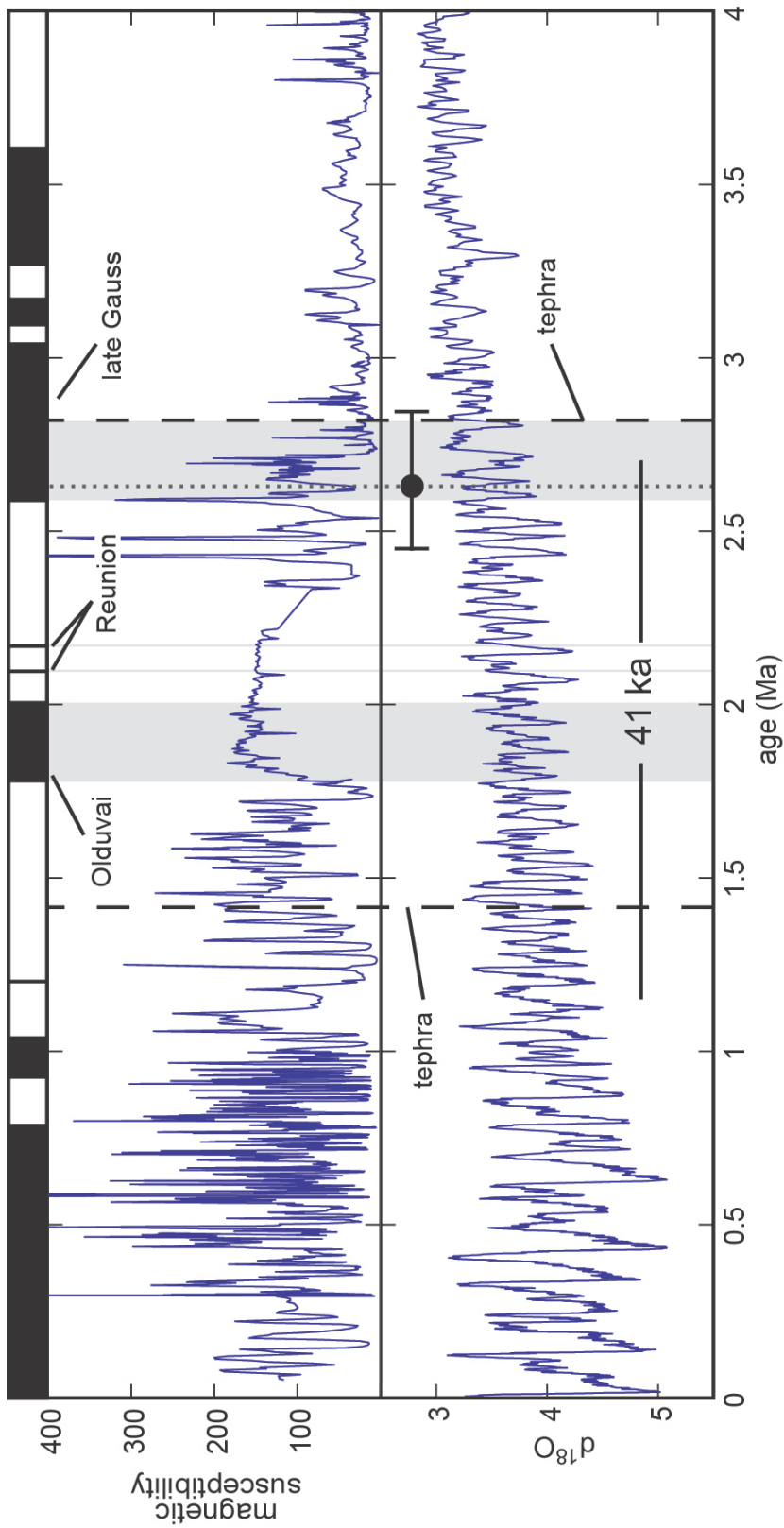


Figure 4.6 Top: magnetic susceptibility record from marine core in the Gulf of Alaska (ODP site 887; Rea et al., 1995). Bottom: compiled $\delta^{18}O$ record of Listeki and Raymo (2005) based on benthic foraminifera from 57 globally distributed sediment cores (LR04) shown with the geomagnetic polarity time scale. Previous constraints on Klondike gravel is defined by gray shaded regions that combines magnetic polarity measurements with ages on tephra within sediments that stratigraphically bracket the Klondike gravel. Mean TCN burial age with 1σ error (this work) indicated by black dotted line.

4.6. Conclusions

TCN burial ages confirm a latest Pliocene ($2.64^{+0.20}/_{-0.18}$ Ma, 1σ) age for deposition of the Klondike gravel and place the earliest Cordilleran Ice Sheet in the late Gauss chron. The geological conditions that created the White Channel gravel of the Klondike Goldfields afford an opportunity for obtaining robust simple TCN burial ages. Although it is tempting to interpret the agreement of our burial ages obtained in the (fluvial) Upper White Channel and (glaciofluvial) Klondike gravel as evidence of the technique's applicability to glacial sediment elsewhere, we stress the need to consider the source-to-sink history of sediments targeted for burial dating. Our results confirm the age of the large ice sheet previously proposed by others to explain the extensive late Pliocene ice-rafted debris in the north Pacific, and provide evidence to support obliquity-dominated forcing for models of a two-staged (Cordilleran, then Laurentide) North American ice-sheet evolution.

4.7. Acknowledgements

We thank J. Stone for providing us with unpublished muon calibration data from the Beacon Heights core; B. Jensen and R. Gibson for field assistance; and G. Yang for support in the Dalhousie Geochronology Centre cosmogenic nuclide lab. This manuscript was greatly improved by spirited (and slightly intoxicated) discussions with K. Stubner, C. Guilmette, and N. Davies, and by reviews from J. Clague and B. Goehring. Funding from the Yukon Geological Survey (YGS contribution #012), SINED, NSERC Discovery Grants, and NSERC Northern Supplements supported this research.

CHAPTER 5: Discussion

5.1. Conclusions

The following sections summarize the key findings of this thesis as they relate to the general theme of using in situ-produced ^{10}Be and ^{26}Al to quantify paleo-erosion rates and sediment recycling from non-glaciated fluvial systems. The major results of this thesis are as follows. 1) A new Monte Carlo-based calculator was created that provides the cosmogenic nuclide dating community with a means to not only date alluvial deposits, but also to establish depositional (inherited) concentrations in the sediment, thereby enabling the calculation of paleo-denudation rates. The calculator also provides the community with a more robust means of establishing uncertainty in these calculated values. 2) The age of the oldest and most extensive Cordilleran Ice Sheet in northwestern Canada was obtained, which confirms a previous hypothesis based on magnetic polarity measurements and tephrochronology (Froese et al., 2000), and has direct implications for the timing of a dramatic change in course of the Yukon River. 3) The prediction of the Syvitski and Milliman (2007) model has been supported. A correlation between catchment denudation rate and temperature has been demonstrated for streams draining interior Texas. The exact impact of the temperature controls on sediment fluxes is uncertain, and undoubtedly complex. They involve the amount and intensity of precipitation, type and density of vegetation, weathering rates and pedogenesis, and various related thresholds (Bull, 1991). This research significantly contributes to the climate-landscape response debate by demonstrating the temperature-denudation rate relationship and hypothesizing that global sediment flux to the ocean can

be balanced with different processes operating in different climate regimes at different times.

5.1.1. Depth Profile Model

The calculator developed in *Chapter 2* provides probability density functions (PDFs) of modeled exposure ages, depositional concentrations, and surface erosion rates from profiles of ^{10}Be and ^{26}Al . These PDFs are derived from a Bayesian-Monte Carlo simulation that uses user-inferred, or measured, constraints on a variety of parameters controlled by site-specific geology. They represent a significant improvement over optimization techniques in estimating realistic probability spaces. Furthermore, this calculator provides a useful tool for running a variety of sensitivity analyses and for evaluating the feasibility of potential sampling sites and strategies.

Using a case study from a ^{10}Be depth profile at Lees Ferry, AZ, two important contributions to the depth profile technique are demonstrated in *Chapter 2*. 1) Shallow depth profiles (<2.5 m), which represent the majority of this technique's use, require constraints on either the surface erosion rate or exposure age in order to resolve a unique optimum solution for the other parameter. This work stresses the importance of using net surface erosion (often easier to quantify or justify than an erosion rate) as a constraint which circumvents this problem for determining exposure age. 2) Use of pebble-sized samples, which was common practice, should be avoided in lieu of coarse sand since an insufficient number of pebble clasts is more likely to yield results that violate a fundamental assumption of the depth profile technique—that every sample contains the same mean inherited concentration. These concepts were used to obtain the first independent age estimates for Mid-Pleistocene (Lissie Formation) sediments (*Chapter 3*).

5.1.2. The First Cordilleran Ice Sheet

In *Chapter 4*, chronology was obtained for the earliest and most extensive Cordilleran Ice Sheet (CIS) in northwestern Canada that marked the onset of widespread Northern Hemisphere glaciation during the Plio-Pleistocene transition. The 2.6 Ma burial age obtained in this work from the terrestrial record (glacial outwash) correlates with the observation of increased and sustained ice-rafted debris in the North Pacific marine record. This date is within error of, but slightly post-dates, the establishment of the North Pacific halocline (2.7 Ma; Haug et al. (2005)) and shortly precedes the first Laurentide Ice sheet (2.4 Ma; Balco and Rovey (2010)), which is consistent with a “snow gun” hypothesis for the onset of Northern Hemisphere glaciation (Prentice and Matthews, 1991; Haug et al., 2005). That is, a change in ocean circulation increased sea-surface temperatures in the North Pacific during late summer and early autumn, providing a moisture source (snow gun) for extensive ice-sheet development. Because the Canadian Cordillera is proximal to this North Pacific moisture source, and was at a higher elevation than the continental interior, progressive cooling into the Quaternary led to asynchronous (Cordilleran then Laurentide) ice-sheet evolution.

A significant hurdle to obtaining the robust chronology for glacial outwash associated with the first CIS was justifying assumptions in the simple two-isotope burial dating approach of Granger and Muzikar (2001). This involved a source-to-sink evaluation of the target sediment considering durations of temporary burial during storage or ice cover, sediment transport time and mechanism, and paleo-landscape erosion rates and styles. Indeed, the assumptions for the chronology in *Chapter 4* would have been unjustified if not for the observation that deposition of the glacial outwash was

contemporaneous with deposition from small, non-glaciated catchments in the Klondike Goldfields. It was sediment from these catchments that was targeted, and from which sound constraints on pre-depositional history could be inferred on the basis of catchment geomorphology and pre-existing magnetic- and tephro-chronostratigraphy (Froese et al., 2000). Thus, the glacial outwash was dated by association. With respect to two-isotope burial techniques, this study stressed the importance of considering the source-to-sink history of sediment before making a chronologic interpretation. In *Chapter 3*, this idea was further developed and applied to dated sediments in order to infer the erosional history of the source area.

5.1.3. Denudation of Interior Texas

Over the past century, applied and basic science has sought a measure of sediment flux to the oceans to answer questions such as: How fast are mountains eroding? What controls the flux of sediment delivered by streams? How should sediment flux variability be accounted for in order to predict petroleum maturity models? In *Chapter 3*, a Late Quaternary record of catchment-wide average denudation rates was acquired from a non-glaciated and tectonically passive region (interior Texas) in order to isolate and quantify the effects of climate change on landscape erosion. Erosion rates from interglacial periods were found to be ~30-35% greater than rates from the same catchments during glacial periods. This relative increase agrees with estimates obtained from previous studies that applied the BQART sediment flux model (Garvin, 2008; Blum and Hattier-Womack, 2009). That model was calibrated using modern suspended sediment data from a collection of the world's largest rivers and finds a directly proportional relationship between a catchment's sediment flux and some factor (i.e., vegetation, soil cover,

precipitation style) that is linked to its average temperature (Syvitski and Milliman, 2007). The implication is that, for tropical-temperate regions with minimal tectonic activity, average temperature is possibly the most important control on the variation in landscape erosion rates. Extrapolating this relationship to the Pliocene, when global average temperatures were warmer, implies that sediment yields from tropical-temperate regions were greater during this time than in the Quaternary. Recent data suggest that globally averaged erosion rates have been constant since the Pliocene (Willenbring and Von Blanckenburg, 2010). This is in contrast to numerous sediment yield data indicating an apparent increase in primarily glacially influenced and tectonically active regions since the Pliocene (e.g. Peizhen et al., 2001). This apparent dilemma can be resolved with a spatially inverse response of global sediment flux to Quaternary cooling. That is, sediment flux may have decreased in tropical-temperate regions and at the same time increased in temperate-polar regions, thus maintaining an approximately constant global average.

Obtaining a paleo-denudation record, which used fluvial deposits on the Texas coastal plain, required distinguishing the component of sediment newly derived from up-catchment surfaces from sediment recycled from long-term storage sites, such as floodplains, valley terraces, and channel fills. This distinction was accomplished using a two-isotope burial analysis, and led to the observation that evacuation of long-term sediment storage increased during times of lowered sea level. The source of the stored sediment was narrowed to a band of Plio-Pleistocene sediments located within the alluvial bedrock valleys of the inner coastal plain. Conversely, no stored sediment was detected from the outer coastal plain. This observation suggests that rates of valley

incision in the outer coastal plain during sea level fall were relatively insignificant, supporting the conveyor-belt model for coastal plain systems (Blum and Törnqvist, 2000).

Comparison of pre-dam and post-dam measurements suggests that the construction of dams has a profound and immediate effect on calculations of catchment-wide average denudation rates. This is due to the nearly complete retention behind the dam of bed load material, which represents the majority of the grain-size spectrum used for cosmogenic nuclide-based denudation rates.

5.2. Implications and Future Work

5.2.1. The Regolith Hypothesis

In the waning years of the Pliocene, with the initiation of major Northern Hemisphere glaciation, successions of dated till suggest that Laurentide and Cordilleran ice was at its greatest spatial extent (Duk-Rodkin et al., 2004; Balco and Rovey, 2010). In contrast, marine $\delta^{18}\text{O}$ records demonstrate that global ice volume became significantly greater during later Quaternary glaciations (Fig. 5.1). Clark and Pollard (1998) reconciled this apparent paradox by suggesting that earlier ice sheets benefit from landscapes conditioned with thick regolith that deformed readily when overrun by ice. This low-shear strength regolith would have served as a lubricating substrate that became less available as the regolith was scoured away by subsequent glaciations. A reduction in regolith thickness would explain the apparent extent-volume paradox by supposing that late Pliocene to early Pleistocene ice sheets were thinner, but more erosive, than those that developed after the Middle Pleistocene. This hypothesis was supported by modeling of substrate erosion and by geochemical analyses of preserved Laurentide tills, which

indicated that deposits from earlier ice sheets are relatively enriched in minerals and isotopes (e.g. kaolinite, iron oxides, and meteoric ^{10}Be) associated with weathered regolith (Roy et al., 2004; Refsnider and Miller, 2010).

A prediction of this hypothesis is that the oldest significant ice advance in North America is represented by the oldest preserved terrestrial record of ice sheet advance (i.e. the Klondike gravel), since subsequent ice sheets are inferred to have been less extensive. However, records of the most extensive ice cover will always appear to be the oldest, since advancing ice tends to obliterate records of less-extensive glaciations (Gibbons et al., 1984). This presents a quandary for obtaining definitive physical evidence in support of the regolith hypothesis for the oldest directly observed ice sheets, since no previous terrestrial ice-sheet records exist for comparison. Furthermore, offshore records of coupled $\delta^{18}\text{O}$ and sediment thicknesses can gauge global ice volume, but not ice sheet geometry at times of high sedimentation rates.

One potential approach to testing the regolith hypothesis for the first North American ice sheet, and circumventing the need for an intact terrestrial record, evolves from *Chapter 4*. In the non-glaciated Klondike Goldfields region, ^{26}Al and ^{10}Be concentrations from the Upper White Channel (UWC) gravel, which underlies glacial outwash from the earliest known CIS (Klondike gravel), indicate a simple one-stage exposure-burial history. That is, UWC material was transported from a hillslope source to its present location without significant time spent buried in temporary storage. This simple exposure-burial history allowed the calculation of a robust age for burial of the UWC gravel by the Klondike gravel at ~ 2.6 Ma, and dated the oldest known ice sheet in the Canadian Cordillera. Intriguingly, ^{26}Al and ^{10}Be measurements at the base of the

Klondike gravel and from the same outcrop produced a statistically identical age result. The implication is that the material in the Klondike gravel has experienced the same net burial history as the UWC material, implying that both deposits share a similar lack of transitional burial between hillslope source and deposition.

The lack of a pre-depositional burial signature supports the regolith hypothesis for the first CIS. Consider the following argument. Suppose that a less extensive ice sheet, or several ice sheets, existed prior to the oldest known CIS. These warm-based temperate ice sheets would have mobilized sediment and created deposits of outwash and till. Presumably, if these ice sheets were significantly extensive and erosive, their deposits would be thick enough (>5 m) for the decay of ^{26}Al and ^{10}Be to cause the $^{26}\text{Al}/^{10}\text{Be}$ to decrease during burial. Sometime later, when ice from the 2.6 Ma CIS remobilized these deposits, they would be integrated into the Klondike gravel. If this partially shielded recycled sediment was a significant component of the Klondike gravel, and if the cumulative burial duration for the earlier ice sheets was great enough to be within the measureable limit of the burial-dating technique (>200 ka), then burial ages from the Klondike gravel should be systematically older than those obtained from the non-glaciated UWC gravel. Thus, a test of the regolith hypothesis for the first CIS could be made by checking whether the simple burial age of Klondike gravel material is 2.6 Ma. If it is, this implies that deep sediment storage in the Canadian Cordillera was insignificant prior to the 2.6 Ma CIS, which is consistent with the regolith hypothesis. If it is older, this implies that the Cordilleran landscape either 1) contained a significant amount of buried sediment storage prior to 2.6 Ma, or 2) experienced low average erosion rates ($< 1 \text{ cm ka}^{-1}$

¹) for a long duration (> 1 Ma) so that ²⁶Al/¹⁰Be approached its secular equilibrium minima.

Although the burial age obtained from the single Klondike gravel in *Chapter 4* was statistically identical to 2.6 Ma, its most probable age was significantly greater (3.06^{+0.98}/_{-0.74} Ma, 1σ). The large age uncertainty from this sample does not permit a reasonable test of the regolith hypothesis. A more definitive test in a future study would require several burial ages from duplicate samples and from multiple locales in the Klondike gravel.

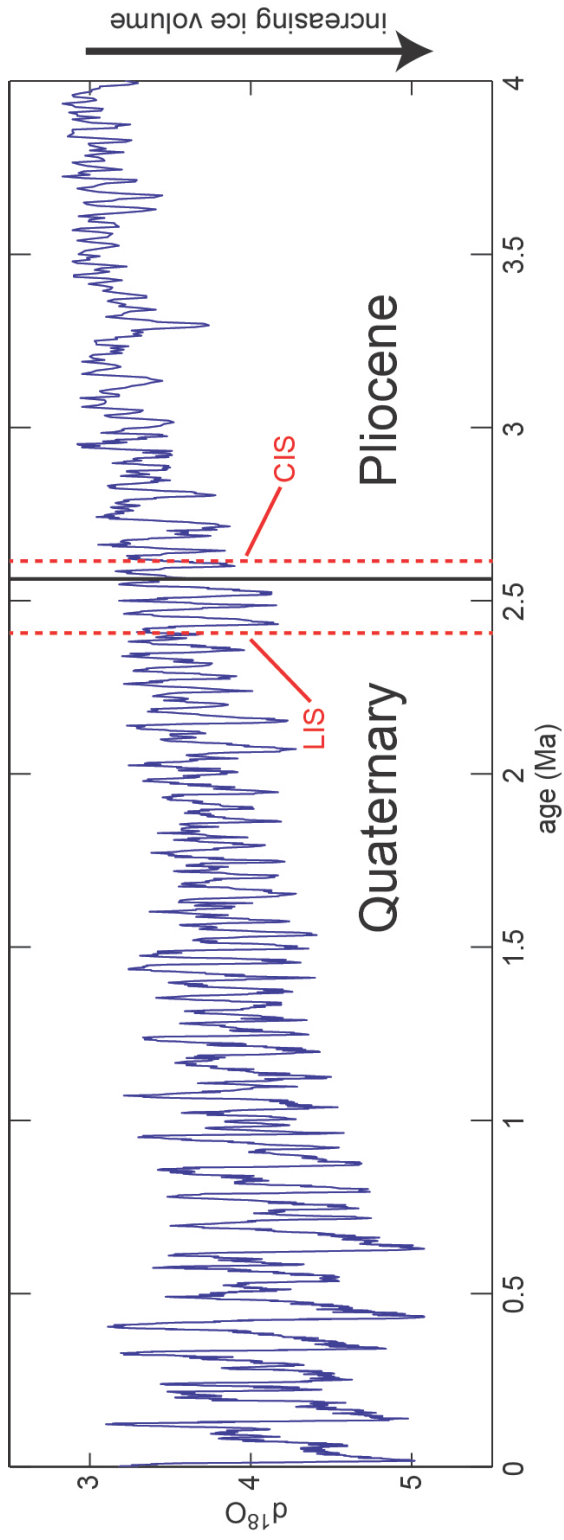


Figure 5.1: Compiled $\delta^{18}\text{O}$ record over the last 4 Ma (LR04 stack) based on benthic foraminifera from 57 globally distributed sediment cores (Lisiecki and Raymo, 2005). This record is a proxy for global ice volume, which greatly increases for glacial periods during the Quaternary. Ages for oldest known Cordilleran (see Chapter 3) and Laurentide (after Balco and Rovey, 2010) ice sheets are indicated by red dotted lines and labeled CIS and LIS, respectively.

5.2.2. Pliocene Denudation Rates

Ultimately, extrapolating the Quaternary denudation rates obtained from the Texas catchments in *Chapter 3* to the Pliocene by assuming a similar temperature dependence is insufficient to test how such non-glaciated, passive landscapes may have responded to climate destabilization during the Plio-Pleistocene transition. Ideally, a Pliocene denudation record should be obtained for comparison within the same catchments. However, the following hurdles need to be overcome before such a record can be obtained from the Texas river systems investigated in this thesis. 1) Timing of the Plio-Pleistocene drainage reorganization of these systems needs to be better constrained. This event would have drastically changed the area and average relief of these catchments, and likely would have had a significant impact on the magnitude of sediment routed through them. ^{10}Be denudation rates calculated from sediment prior to the reorganization could not be compared with the Quaternary rates measured in *Chapter 3* because they may represent different spatial averaging that could lead to underestimating the catchment-wide production rate by a factor of ~ 3 . 2) Pliocene samples would likely have to be acquired from onshore sediment cores. This is in part due to the limited exposure of Pliocene-aged sediment along active cut banks, but primarily because preserving the depositional ^{10}Be signature for durations of >2 Ma requires long-term burial at great depths (>40 m) in order to minimize post-depositional ^{10}Be production by muons. 3) Pliocene sediment on the Texas coastal plain lacks absolute chronology. Furthermore, burial dating these sediments, as described in *Chapter 4*, would likely only yield a maximum age since the low depositional $^{26}\text{Al}/^{10}\text{Be}$ observed in sediments of the outer coastal plain (see *Chapter 3*) precludes a one-stage burial age model for these

sediments. Thus, the prospect of obtaining robust Pliocene catchment-wide denudation rates from the Texas river systems is fairly unlikely, and would require considerable work before becoming feasible.

Alternatively, in the Klondike Goldfields of the Yukon, conditions appear to be ideal for obtaining a Pliocene record of ^{10}Be catchment-wide denudation rates. A robust Pliocene chronostratigraphic framework already exists for the White Channel gravels from tephrochronology and magnetic polarity data (Froese et al., 2000) and from TCN burial dating undertaken in *Chapter 4*. Furthermore, the results of that burial dating analysis reveal that depositional $^{26}\text{Al}/^{10}\text{Be}$ in the UWC gravel was equivalent to the surface production ratio. This eliminates the difficulty of correcting ^{10}Be concentrations with a binary mixing algorithm, as was required for the denudation rates obtained in Texas, since there is no discernible input of material buried during long-term sediment storage. Finally, because the catchments are small and drainage patterns entrained, it is unlikely that a significant drainage capture or change in catchment geometry has occurred during or since UWC gravel deposition.

Because of this simplification, and because the depositional age of the UWC gravel is known, the measured ^{10}Be concentrations can be converted to depositional ^{10}Be concentrations and catchment-wide denudation rates using the methods outlined in *Chapter 3*. Here, catchment-wide denudation rates are calculated for the samples in the profile acquired at the top of the UWC and for an individual sample at the bottom of the UWC, yielding a mean value ($n=4$) of $3.71^{+0.80}/_{-0.54} \text{ cm ka}^{-1}$ and $8.48^{+3.84}/_{-1.20} \text{ cm ka}^{-1}$ (1σ errors) for the top and bottom of the UWC gravel, respectively (see Table 5.1). The basal denudation rate calculated for the UWC gravel assumes that the entire ~ 15 m sediment

package was deposited instantaneously. If the aggradation time of the UWC gravel was significant (>200 ka), then the calculated depositional ^{10}Be concentration would be overestimated due to insufficient correction for post-depositional ^{10}Be produced by muons. Importantly, this means that any deficiency in the assumption of instantaneous UWC gravel deposition would cause an *underestimate* of the denudation rate for the bottom of the UWC gravel, and so this calculated denudation rate is considered a *minimum* value. However, considering that the entire section of UWC gravel falls within a single magnetic interval (Froese 2000), and because we observed no palaeosols or other evidence of a hiatus between the lower and upper samples, we believe that the duration of deposition of the UWC gravel may be less than ~200 ka and that the apparent decrease in catchment erosion rate with deposition time is not a function of some complexity in cosmogenic nuclide production.

As described in *Chapter 4*, the source region for the White Channel gravel is similar to that of interior Texas in that it has never been glaciated and is minimally affected by tectonics. However, Plio-Pleistocene uplift of the St. Elias mountains, ~400 km south of the Klondike area, was intense (Enkelmann et al., 2009), and perhaps significantly influenced the climate of the Klondike by creating a rain shadow that kept the region largely ice-free during subsequent Quaternary glaciations. Furthermore, this proximal uplift may have also intensified the influence of Plio-Pleistocene climate change on the erosion of King Solomon Dome. Unlike in Texas, however, the source catchments for the White Channel gravel have maintained an approximately constant geometry since the Pliocene. Thus, it is likely that Pliocene denudation rate variation in the Klondike Goldfield region can be attributed to changes in climate. The presence of ice-wedge casts

at the top of the UWC, and their absence at the bottom, suggests that this deposit represents a gradual cooling interval that culminated at the very end of the Pliocene, i.e., consistent with a record of denudation at what is essentially the Plio-Pleistocene transition. During this transition, a more than two-fold decrease in ^{10}Be catchment-wide denudation rates is observed, consistent with the temperature-dependent denudation rates measured in *Chapter 3*. Together, the denudation rate records of interior Texas and the Klondike Goldfields provide a strong argument that, without significant tectonic forcing or the presence of glaciers, landscape erosion rates in the Pliocene were higher than those in the Quaternary and seem to support the inference of Syvitski and Milliman (2007)

Unit	Sample ID	Depth (m)	Measured			Deposited			Denudation rate			
			[¹⁰ Be] (10 ⁵ atoms g ⁻¹)	Unc. +/- (10 ⁵ atoms g ⁻¹)	Age (Ma)	Unc. +/- (Ma)	[¹⁰ Be] (10 ⁵ atoms g ⁻¹)	Unc. +/- (10 ⁵ atoms g ⁻¹)	P(0) (atoms g ⁻¹)	ε (cm ka ⁻¹)	Unc. +/- (cm ka ⁻¹)	integration time (ka)
UWC	2342	36.1	0.61	0.02	2.85	0.46/0.40	2.10	0.46/0.49	11.8	3.36	1.04/0.61	18
UWC	2341	36.4	0.60	0.01	2.52	0.43/0.34	1.77	0.37/0.35	11.8	4.00	0.99/0.68	15
UWC	2340	36.6	0.60	0.02	2.72	0.47/0.40	1.95	0.43/0.46	11.8	3.62	1.12/0.66	17
UWC	2339	37.0	0.66	0.02	2.42	0.35/0.31	1.91	0.32/0.34	11.8	3.70	0.80/0.54	16
Mean value for UWC profile												
UWC	2338	48.9	0.30	0.01	2.61	0.20/0.19	0.84	0.14/0.26	11.8	8.48	3.84/1.20	7.1

Note : Latitude, longitude, and elevation of site are 64.023 N, -139.147 W, and 520 m, respectively.

^aKG = Klondike gravel; UWC = Upper White Channel gravel.

^bAll uncertainties are 1σ and include AMS measurement errors (CAMS-LLNL) and an estimated 2% uncertainty for sample preparation errors. For ²⁶Al only, an additional 1-4% random error from ICP-MS native Al measurements is included. Error-weighted means calculated after Barlow (2004).

Table 5.1: ¹⁰Be denudation rates calculated from the Upper White Channel (UWC) gravel at Australia Hill. All uncertainties are 1σ and include AMS measurement precision (CAMS-LLNL) and an estimated 2% uncertainty for chemistry errors. Error-weighted mean values are calculated using the linear variance method of Barlow (2004). Samples 2339-2342 are from the top of the UWC; sample 2338 is from the bottom of the UWC.

References

- Aguilar, G., Carretier, S., Regard, V., Vassallo, R., Riquelme, R., and Martinod, J., 2013, Grain size-dependent ^{10}Be concentrations in alluvial stream sediment of the Huasco Valley, a semi-arid Andes region: *Quaternary Geochronology*.
- Anderson, R. S., Repka, J. L., and Dick, G. S., 1996, Explicit treatment of inheritance in dating depositional surfaces using in situ ^{10}Be and ^{26}Al : *Geology*, v. 24, no. 1, p. 47.
- Antinao, J. L., and McDonald, E., 2013, A reduced relevance of vegetation change for alluvial aggradation in arid zones: *Geology*, v. 41, no. 1, p. 11-14.
- Armentrout, J., and Clement, J., Biostratigraphic calibration of depositional cycles: a case study in High Island-Galveston-East Breaks areas, offshore Texas, *in* Proceedings Sequence Stratigraphy as an Exploration Tool: Concepts and Practices in the Gulf Coast: Gulf Coast Section of the Society of Economic Paleontologists and Mineralogists Foundation, Proceedings of the 11th Annual Research Conference 1990, p. 21-51.
- Balco, G., and Rovey, C., 2008, An isochron method for cosmogenic-nuclide dating of buried soils and sediments: *American Journal of Science*, v. 308, no. 10, p. 1083.
- , 2010, Absolute chronology for major Pleistocene advances of the Laurentide Ice Sheet: *Geology*, v. 38, no. 9, p. 795.
- Balco, G., Stone, J. O., Lifton, N. A., and Dunai, T. J., 2008, A complete and easily accessible means of calculating surface exposure ages or erosion rates from ^{10}Be and ^{26}Al measurements: *Quaternary Geochronology*, v. 3, no. 3, p. 174-195.

- Balco, G., Stone, J. O. H., and Mason, J. A., 2005, Numerical ages for Plio-Pleistocene glacial sediment sequences by $^{26}\text{Al}/^{10}\text{Be}$ dating of quartz in buried paleosols: *Earth and Planetary Science Letters*, v. 232, no. 1, p. 179-191.
- Barendregt, R., Enkin, R., Baker, J., and Duk-Rodkin, A., 1996, Paleomagnetic evidence for late Cenozoic glaciations in the Mackenzie Mountains of the Northwest Territories, Canada: *Canadian Journal of Earth Sciences*, v. 33, no. 6, p. 896-903.
- Barendregt, R., Enkin, R., Duk-Rodkin, A., and Baker, J., 2010, Paleomagnetic evidence for multiple late Cenozoic glaciations in the Tintina Trench, west-central Yukon, Canada: *Canadian Journal of Earth Sciences*, v. 47, no. 7, p. 987-1002.
- Barendregt, R. W., and Duk-Rodkin, A., 2011, Chronology and Extent of Late Cenozoic Ice Sheets in North America: A Magnetostratigraphical Assessment: *Developments in Quaternary Science*, v. 15, p. 419-426.
- Barlow, R., 2004, Asymmetric errors: [arXiv:physics/0401042](https://arxiv.org/abs/physics/0401042).
- Beaulieu, E., Godd ris, Y., Donnadieu, Y., Labat, D., and Roelandt, C., 2012, High sensitivity of the continental-weathering carbon dioxide sink to future climate change: *Nature Climate Change*, v. 2, no. 5, p. 346-349.
- Belmont, P., Pazzaglia, F., and Gosse, J., 2007, Cosmogenic ^{10}Be as a tracer for hillslope and channel sediment dynamics in the Clearwater River, western Washington State: *Earth and Planetary Science Letters*, v. 264, no. 1, p. 123-135.
- Berger, A., and Loutre, M. F., 1991, Insolation values for the climate of the last 10 million years: *Quaternary Science Reviews*, v. 10, no. 4, p. 297-317.

- Bierman, P., and Steig, E. J., 1996, Estimating rates of denudation using cosmogenic isotope abundances in sediment: *Earth Surface Processes and Landforms*, v. 21, no. 2, p. 125-139.
- Bloodgood, D. W., 1955, Sixteenth annual report of silt load of Texas streams for water year 1953-54: Texas Water Development Board.
- Bloodgood, D. W., and Meador, A. A., 1941, The silt load of Texas streams--part II.
- Blum, M. D., and Aslan, A., 2006, Signatures of climate vs. sea-level change within incised valley-fill successions: Quaternary examples from the Texas Gulf Coast: *Sedimentary Geology*, v. 190, no. 1-4, p. 177-211.
- Blum, M. D., and Hattier-Womack, J., 2009, Climate change, sea-level change, and fluvial sediment supply to deepwater depositional systems: SEPM Special Publication, Tulsa, Oklahoma, USA, p. 15-39.
- Blum, M. D., Morton, R. A., and Durbin, J. M., 1995, Deweyville" terraces and deposits of the Texas Gulf coastal plain: *Gulf Coast Association of Geological Societies Transactions*, v. 45, p. 53-60.
- Blum, M. D., and Price, D. M., 1998, Quaternary alluvial plain construction in response to glacio-eustatic and climatic controls, Texas Gulf coastal plain: SEPM Special Publication, v. 59, p. 31-48.
- Blum, M. D., and Roberts, H. H., 2012, The Mississippi Delta Region: Past, Present, and Future: *Annual Review of Earth and Planetary Sciences*, v. 40, p. 655-683.
- Blum, M. D., and Törnqvist, T. E., 2000, Fluvial responses to climate and sea-level change: a review and look forward: *Sedimentology*, v. 47, p. 2-48.

- Blum, M. D., and Valastro, S. J., 1994, Late Quaternary sedimentation, lower Colorado River, Gulf Coastal Plain of Texas: Geological Society of America Bulletin, v. 106, no. 8, p. 1002-1016.
- Braucher, R., Brown, E., Bourles, D., and Colin, F., 2003, In situ produced ^{10}Be measurements at great depths: implications for production rates by fast muons: Earth and Planetary Science Letters, v. 211, no. 3, p. 251-258.
- Braucher, R., Del Castillo, P., Siame, L., Hidy, A., and Bourlès, D., 2009, Determination of both exposure time and denudation rate from an in situ-produced ^{10}Be depth profile: A mathematical proof of uniqueness. Model sensitivity and applications to natural cases: Quaternary Geochronology, v. 4, no. 1, p. 56-67.
- Braucher, R., Merchel, S., Borgomano, J., and Bourlès, D., 2011, Production of cosmogenic radionuclides at great depth: A multi element approach: Earth and Planetary Science Letters, v. 309, no. 1-2, p. 1-9.
- Brocard, G., Van der Beek, P., Bourlès, D., Siame, L., and Mugnier, J. L., 2003, Long-term fluvial incision rates and postglacial river relaxation time in the French Western Alps from ^{10}Be dating of alluvial terraces with assessment of inheritance, soil development and wind ablation effects: Earth and Planetary Science Letters, v. 209, no. 1-2, p. 197-214.
- Brown, E. T., Stallard, R. F., Larsen, M. C., Bourlès, D. L., Raisbeck, G. M., and Yiou, F., 1998, Determination of predevelopment denudation rates of an agricultural watershed (Cayaguás River, Puerto Rico) using in-situ-produced ^{10}Be in river-borne quartz: Earth and Planetary Science Letters, v. 160, no. 3, p. 723-728.

- Brown, E. T., Stallard, R. F., Larsen, M. C., Raisbeck, G. M., and Yiou, F., 1995, Denudation rates determined from the accumulation of in situ-produced ^{10}Be in the Luquillo Experimental Forest, Puerto Rico: *Earth and Planetary Science Letters*, v. 129, no. 1-4, p. 193-202.
- Bull, W. B., 1991, *Geomorphic responses to climatic change*, Oxford, UK, Oxford University Press, 326 p.:
- Chmeleff, J., von Blanckenburg, F., Kossert, K., and Jakob, D., 2010, Determination of the ^{10}Be half-life by multicollector ICP-MS and liquid scintillation counting: *Nuclear Instruments and Methods in Physics Research Section B: Beam Interactions with Materials and Atoms*, v. 268, no. 2, p. 192-199.
- Clark, P. U., and Pollard, D., 1998, Origin of the middle Pleistocene transition by ice sheet erosion of regolith: *Paleoceanography*, v. 13, no. 1, p. 1-9.
- Codilean, A. T., Fenton, C. R., Fabel, D., Bishop, P., and Xu, S., 2012, Discordance between cosmogenic nuclide concentrations in amalgamated sands and individual fluvial pebbles in an arid zone catchment: *Quaternary Geochronology*.
- Cragun, W. S., 2008, *Quaternary evolution of the Colorado River at Lees Ferry, Arizona*: Utah State University.
- Davies, T. A., Hay, W. W., Southam, J. R., and Worsley, T. R., 1977, Estimates of Cenozoic oceanic sedimentation rates: *Science*, v. 197, no. 4298, p. 53.

- Diegel, F., Karlo, J., Schuster, D., Shoup, R., and Tauvers, P., 1995, Cenozoic structural evolution and tectono-stratigraphic framework of the northern Gulf Coast continental margin, *in* M. P. A. Jackson, D. G. R., and S. Snelson, ed., Salt tectonics: a global perspective, Volume 65, Amer Assn of Petroleum Geologists, p. 109-151.
- Doering, J., 1935, Post-Fleming surface formations of coastal southeast Texas and south Louisiana: Assoc. Petroleum Geologists Bull, v. 19, no. 5, p. 651-688.
- DuBar, J., Ewing, T., Lundelius Jr, E., Otvos, E., and Winker, C., 1991, Quaternary geology of the Gulf of Mexico coastal plain: Quaternary Non-Glacial Geology of the Conterminous United States: Boulder, Colorado, The Geological Society of America, The Geology of North America, v. 2, p. 583-610.
- Duk-Rodkin, A., Barendregt, R., Tarnocai, C., and Phillips, F., 1996, Late Tertiary to late Quaternary record in the Mackenzie Mountains, Northwest Territories, Canada: stratigraphy, paleosols, paleomagnetism, and chlorine-36: Canadian Journal of Earth Sciences, v. 33, no. 6, p. 875-895.
- Duk-Rodkin, A., Barendregt, R., White, J., and Singhroy, V., 2001, Geologic evolution of the Yukon River: implications for placer gold: Quaternary International, v. 82, no. 1, p. 5-31.
- Duk-Rodkin, A., Barendregt, R. W., Froese, D. G., Weber, F., Enkin, R., Rod Smith, I., Zazula, G. D., Waters, P., and Klassen, R., 2004, Timing and extent of Plio-Pleistocene glaciations in north-western Canada and east-central Alaska: Developments in Quaternary Science, v. 2, p. 313-345.

- Duk-Rodkin, A., Barendregt, R. W., and White, J. M., 2010, An extensive Late Cenozoic terrestrial record of multiple glaciations preserved in the Tintina Trench of west-central Yukon: Stratigraphy, paleomagnetism, paleosols, and pollen: *Canadian Journal of Earth Sciences*, v. 47, no. 7, p. 1003-1028.
- Dunai, T. J., 2000, Scaling factors for production rates of in situ produced cosmogenic nuclides: a critical reevaluation: *Earth and Planetary Science Letters*, v. 176, no. 1, p. 157-169.
- Durbin, J. M., Blum, M. D., and Price, D. M., 1997, Late Pleistocene stratigraphy of the lower Nueces River, Corpus Christi, Texas: glacio-eustatic influences on valley-fill architecture: *Gulf Coast Association of Geological Societies: Transactions*, v. 47, p. 119-129.
- Enkelmann, E., Zeitler, P., Pavlis, T., Garver, J., and Ridgway, K., 2009, Intense localized rock uplift and erosion in the St Elias orogen of Alaska: *Nature Geoscience*, v. 2, no. 5, p. 360-363.
- Ewing, T. E., 1991, Structural framework: The Gulf of Mexico Basin: *Geological Society of America, The Geology of North America*, v. J, p. 31-52.
- Froese, D., Barendregt, R., Enkin, R., and Baker, J., 2000, Paleomagnetic evidence for multiple late Pliocene-early Pleistocene glaciations in the Klondike area, Yukon Territory: *Canadian Journal of Earth Sciences*, v. 37, no. 6, p. 863-877.
- Galloway, W. E., Ganey-Curry, P. E., Li, X., and Buffler, R. T., 2000, Cenozoic depositional history of the Gulf of Mexico basin: *AAPG bulletin*, v. 84, no. 11, p. 1743.

- Galloway, W. E., Whiteaker, T. L., and Ganey-Curry, P., 2011, History of Cenozoic North American drainage basin evolution, sediment yield, and accumulation in the Gulf of Mexico basin: *Geosphere*, v. 7, no. 4, p. 938.
- Garvin, M. G., 2008, Late Quaternary Geochronologic, Stratigraphic, and Sedimentologic Framework of the Trinity River Incised Valley: East Texas Coast [Masters: Louisiana State University].
- Gibbons, A. B., Megeath, J. D., and Pierce, K. L., 1984, Probability of moraine survival in a succession of glacial advances: *Geology*, v. 12, no. 6, p. 327-330.
- Gilbert, G. K., 1900, Rhythms and geologic time: *Science*, v. 11, p. 1001-1012.
- Gosse, J. C., and Phillips, F. M., 2001, Terrestrial in situ cosmogenic nuclides: theory and application: *Quaternary Science Reviews*, v. 20, no. 14, p. 1475-1560.
- Granger, D., and Muzikar, P., 2001, Dating sediment burial with in situ-produced cosmogenic nuclides: theory, techniques, and limitations: *Earth and Planetary Science Letters*, v. 188, no. 1-2, p. 269-281.
- Granger, D. E., Kirchner, J. W., and Finkel, R., 1996, Spatially averaged long-term erosion rates measured from in situ-produced cosmogenic nuclides in alluvial sediment: *Journal of Geology*, v. 104, no. 3, p. 249-257.
- Granger, D. E., and Smith, A. L., 2000, Dating buried sediments using radioactive decay and muogenic production of Al-26 and Be-10: *Nuclear Instruments & Methods in Physics Research Section B-Beam Interactions with Materials and Atoms*, v. 172, p. 822-826.

- Haug, G. H., Ganopolski, A., Sigman, D. M., Rosell-Mele, A., Swann, G. E. A., Tiedemann, R., Jaccard, S. L., Bollmann, J., Maslin, M. A., and Leng, M. J., 2005, North Pacific seasonality and the glaciation of North America 2.7 million years ago: *Nature*, v. 433, no. 7028, p. 821-825.
- Hay, W. W., Shaw, C. A., and Wold, C. N., 1989, Mass-balanced paleogeographic reconstructions: *Geologische Rundschau*, v. 78, no. 1, p. 207-242.
- Hay, W. W., Soeding, E., DeConto, R. M., and Wold, C. N., 2002, The Late Cenozoic uplift-climate change paradox: *International Journal of Earth Sciences*, v. 91, no. 5, p. 746-774.
- Heinrich, P. V., and McCulloh, R. P., 2000, Pliocene Surface Stratigraphy in the Fort Polk Region: Implications for Louisiana Surface Geology: (Louisiana Geological Survey) *Basin Research Institute Bulletin*, v. 9, p. 51-74.
- Heisinger, B., Lal, D., Jull, A., Kubik, P., Ivy-Ochs, S., Knie, K., and Nolte, E., 2002a, Production of selected cosmogenic radionuclides by muons: 2. Capture of negative muons: *Earth and Planetary Science Letters*, v. 200, no. 3-4, p. 357-369.
- Heisinger, B., Lal, D., Jull, A., Kubik, P., Ivy-Ochs, S., Neumaier, S., Knie, K., Lazarev, V., and Nolte, E., 2002b, Production of selected cosmogenic radionuclides by muons: 1. Fast muons: *Earth and Planetary Science Letters*, v. 200, no. 3-4, p. 345-355.
- Hidy, A. J., Gosse, J. C., Froese, D. G., Bond, J. D., and Rood, D. H., 2013, A latest Pliocene age for the earliest and most extensive Cordilleran Ice Sheet in northwestern Canada: *Quaternary Science Reviews*, v. 61, p. 77-84.

- Hidy, A. J., Gosse, J. C., Pederson, J. L., Mattern, J. P., and Finkel, R. C., 2010, A geologically constrained Monte Carlo approach to modeling exposure ages from profiles of cosmogenic nuclides: An example from Lees Ferry, Arizona: *Geochem. Geophys. Geosyst.*, v. 11, p. Q0AA10.
- Hughes, O. L., Rampton, V., and Rutter, N. W., Quaternary geology and geomorphology, southern and central Yukon (northern Canada) 1972, 24th International Geological Congress.
- Jackson, L., Froese, D., Huscroft, C., Nelson, F., Westgate, J., Telka, A., Shimamura, K., and Rotheisler, P., 2009, Surficial geology and late Cenozoic history of the Stewart River and northern Stevenson Ridge map areas, west-central Yukon Territory: Geological Survey of Canada, Open File, v. 6059, p. 414.
- Kanes, W. H., 1970, Facies and development of the Colorado River delta in Texas: *Deltaic Sedimentation: Modern and Ancient*. Society of Economic Paleontologists and Mineralogists, Special Publication, v. 15, p. 78-106.
- Kettner, A. J., and Syvitski, J. P. M., 2008, HydroTrend v. 3.0: A climate-driven hydrological transport model that simulates discharge and sediment load leaving a river system: *Computers & Geosciences*, v. 34, no. 10, p. 1170-1183.
- Kirby, E., Burbank, D. W., Reheis, M., and Phillips, F., 2006, Temporal variations in slip rate of the White Mountain fault zone, eastern California: *Earth and Planetary Science Letters*, v. 248, no. 1-2, p. 168-185.
- Klein, J., Giegengack, R., Middleton, R., Sharma, P., Underwood, J., and Weeks, R., 1986, Revealing histories of exposure using in situ produced ²⁶Al and ¹⁰Be in Libyan desert glass: *Radiocarbon*, v. 28, no. 2A, p. 547-555.

- Kohl, C., and Nishiizumi, K., 1992, Chemical isolation of quartz for measurement of in-situ-produced cosmogenic nuclides: *Geochimica Et Cosmochimica Acta*, v. 56, no. 9, p. 3583-3587.
- Koppes, M. N., and Montgomery, D. R., 2009, The relative efficacy of fluvial and glacial erosion over modern to orogenic timescales: *Nature Geoscience*, v. 2, no. 9, p. 644-647.
- Korschinek, G., Bergmaier, A., Faestermann, T., Gerstmann, U., Knie, K., Rugel, G., Wallner, A., Dillmann, I., Dollinger, G., and Von Gostomski, C. L., 2010, A new value for the half-life of ^{10}Be by Heavy-Ion Elastic Recoil Detection and liquid scintillation counting: *Nuclear Instruments and Methods in Physics Research Section B: Beam Interactions with Materials and Atoms*, v. 268, no. 2, p. 187-191.
- Krissek, L., 1995, Late Cenozoic ice-rafting records from Leg 145 sites in the North Pacific: late Miocene onset, late Pliocene intensification, and Pliocene-Pleistocene events, Volume 145, Ocean Drilling Program, p. 179-194.
- Kukla, G., and Opdyke, N., 1972, American glacial stages in paleomagnetic time scale: *Geol: Soc. America, Abs. with Programs (Ann. Mtg.)*, v. 4, p. 569-570.
- Kurz, M. D., 1986a, Cosmogenic helium in a terrestrial igneous rock: *Nature*, v. 320, p. 435-439.
- , 1986b, *In situ* production of terrestrial cosmogenic helium and some applications to geochronology: *Geochimica Et Cosmochimica Acta*, v. 50, no. 12, p. 2855-2862.
- Lal, D., 1991, Cosmic ray labeling of erosion surfaces: in situ nuclide production rates and erosion models: *Earth and Planetary Science Letters*, v. 104, no. 2-4, p. 424-439.

- Lanphere, M. A., Champion, D. E., Christiansen, R. L., Izett, G. A., and Obradovich, J. D., 2002, Revised ages for tuffs of the Yellowstone Plateau volcanic field: Assignment of the Huckleberry Ridge Tuff to a new geomagnetic polarity event: Geological Society of America Bulletin, v. 114, no. 5, p. 559-568.
- LeBlanc, R. J., and Hodgson, W., 1959, Origin and development of the Texas shoreline: Gulf Coast Association of Geological Societies Transactions IX, p. 197-220.
- Lifton, N., Smart, D., and Shea, M., 2008, Scaling time-integrated in situ cosmogenic nuclide production rates using a continuous geomagnetic model: Earth and Planetary Science Letters, v. 268, no. 1-2, p. 190-201.
- Lisiecki, L. E., and Raymo, M. E., 2005, A Plio-Pleistocene stack of 57 globally distributed benthic ^{18}O records: Paleoceanography, v. 20, p. 522–533.
- Lowey, G. W., Emond, D., Weston, L., and Lewis, L., 2001, White Channel Gravel alteration revisited: Yukon exploration and geology, p. 147-162.
- Lüthi, D., Le Floch, M., Bereiter, B., Blunier, T., Barnola, J.-M., Siegenthaler, U., Raynaud, D., Jouzel, J., Fischer, H., and Kawamura, K., 2008, High-resolution carbon dioxide concentration record 650,000–800,000 years before present: Nature, v. 453, no. 7193, p. 379-382.
- Mandel, R. D., and Caran, S. C., 1992, Late Cenozoic Alluvial Stratigraphy and Prehistory of the Inner Gulf Coastal Plain, South-central Texas, Draft guidebook to the 10th annual meeting of the South-Central Friends of the Pleistocene: Lubbock, Texas, Lubbock Lake Quaternary Research Center Series 4.

- Maslin, M., Li, X., Loutre, M. F., and Berger, A., 1998, The contribution of orbital forcing to the progressive intensification of Northern Hemisphere glaciation: *Quaternary Science Reviews*, v. 17, no. 4-5, p. 411-426.
- Matmon, A., Bierman, P., Larsen, J., Southworth, S., Pavich, M., Finkel, R., and Caffee, M., 2003, Erosion of an ancient mountain range, the Great Smoky Mountains, North Carolina and Tennessee: *American Journal of Science*, v. 303, no. 9, p. 817-855.
- Matsushi, Y., Wakasa, S., Matsuzaki, H., and Matsukura, Y., 2006, Long-term denudation rates of actively uplifting hillcrests in the Boso Peninsula, Japan, estimated from depth profiling of in situ-produced cosmogenic ^{10}Be and ^{26}Al : *Geomorphology*, v. 82, no. 3-4, p. 283-294.
- McMillan, M. E., Angevine, C. L., and Heller, P. L., 2002, Postdepositional tilt of the Miocene-Pliocene Ogallala Group on the western Great Plains: Evidence of late Cenozoic uplift of the Rocky Mountains: *Geology*, v. 30, no. 1, p. 63.
- McMillan, M. E., Heller, P. L., and Wing, S. L., 2006, History and causes of post-Laramide relief in the Rocky Mountain orogenic plateau: *Geological Society of America Bulletin*, v. 118, no. 3-4, p. 393-405.
- Mercader, J., Gosse, J. C., Bennett, T., Hidy, A. J., and Rood, D. H., 2012, Cosmogenic nuclide age constraints on Middle Stone Age lithics from Niassa, Mozambique: *Quaternary Science Reviews*, v. 47, p. 116-130.
- Métivier, F., Gaudemer, Y., Tapponnier, P., and Klein, M., 2002, Mass accumulation rates in Asia during the Cenozoic: *Geophysical Journal International*, v. 137, no. 2, p. 280-318.

- Miller, K. G., Kominz, M. A., Browning, J. V., Wright, J. D., Mountain, G. S., Katz, M. E., Sugarman, P. J., Cramer, B. S., Christie-Blick, N., and Pekar, S. F., 2005, The Phanerozoic record of global sea-level change: *Science*, v. 310, no. 5752, p. 1293-1298.
- Milliman, J. D., and Syvitski, J. P., 1992, Geomorphic/tectonic control of sediment discharge to the ocean: the importance of small mountainous rivers: *The Journal of Geology*, v. 100, no. 5, p. 525-544.
- Molnar, P., 2001, Climate change, flooding in arid environments, and erosion rates: *Geology*, v. 29, no. 12, p. 1071-1074.
- Molnar, P., 2004, Late Cenozoic Increase in Accumulation Rates of Terrestrial Sediment: How Might Climate Change Have Affected Erosion Rates?: *Annu. Rev. Earth Planet. Sci.*, v. 32, p. 67-89.
- Molnar, P., and England, P., 1990, Late Cenozoic uplift of mountain ranges and global climate change: chicken or egg?: *Nature*, v. 346, no. 6279, p. 29-34.
- Montgomery, D. R., 2002, Valley formation by fluvial and glacial erosion: *Geology*, v. 30, no. 11, p. 1047-1050.
- Mudelsee, M., and Raymo, M. E., 2005, Slow dynamics of the Northern Hemisphere glaciation: *Paleoceanography*, v. 20, no. 4, p. PA4022.
- Murray, A. S., and Wintle, A. G., 2000, Luminescence dating of quartz using an improved single-aliquot regenerative-dose protocol: *Radiation measurements*, v. 32, no. 1, p. 57-73.

- Musgrove, M., Banner, J. L., Mack, L. E., Combs, D. M., James, E. W., Cheng, H., and Edwards, R. L., 2001, Geochronology of late Pleistocene to Holocene speleothems from central Texas: Implications for regional paleoclimate: Geological Society of America Bulletin, v. 113, no. 12, p. 1532-1543.
- Nishiizumi, K., 2004, Preparation of ^{26}Al AMS standards: Nuclear Instruments and Methods in Physics Research Section B: Beam Interactions with Materials and Atoms, v. 223, p. 388-392.
- Nishiizumi, K., Imamura, M., Caffee, M. W., Southon, J. R., Finkel, R. C., and McAninch, J., 2007, Absolute calibration of ^{10}Be AMS standards: Nuclear Instruments and Methods in Physics Research Section B: Beam Interactions with Materials and Atoms, v. 258, no. 2, p. 403-413.
- Nishiizumi, K., Kohl, C., Arnold, J., Klein, J., Fink, D., and Middleton, R., 1991, Cosmic ray produced ^{10}Be and ^{26}Al in Antarctic rocks: exposure and erosion history: Earth and Planetary Science Letters, v. 104, no. 2, p. 440-454.
- Pagani, M., Liu, Z., LaRiviere, J., and Ravelo, A. C., 2009, High Earth-system climate sensitivity determined from Pliocene carbon dioxide concentrations: Nature Geoscience, v. 3, no. 1, p. 27-30.
- Partridge, T., Granger, D., Caffee, M., and Clarke, R., 2003, Lower Pliocene hominid remains from Sterkfontein: Science, v. 300, no. 5619, p. 607-612.
- Pederson, J., Karlstrom, K., Sharp, W., and McIntosh, W., 2002, Differential incision of the Grand Canyon related to Quaternary faulting—Constraints from U-series and Ar/Ar dating: Geology, v. 30, no. 8, p. 739.

- Pederson, J. L., Anders, M. D., Rittenhour, T. M., Sharp, W. D., Gosse, J. C., and Karlstrom, K. E., 2006, Using fill terraces to understand incision rates and evolution of the Colorado River in eastern Grand Canyon, Arizona: *Journal of Geophysical Research*, v. 111, no. F2, p. F02003.
- Peizhen, Z., Molnar, P., and Downs, W. R., 2001, Increased sedimentation rates and grain sizes 2–4 Myr ago due to the influence of climate change on erosion rates: *Nature*, v. 410, no. 6831, p. 891-897.
- Perg, L., Anderson, R., and Finkel, R., 2001, Use of a new ^{10}Be and ^{26}Al inventory method to date marine terraces, Santa Cruz, California, USA: *Geology*, v. 29, no. 10, p. 879.
- Phillips, F. M., Leavy, B. D., Jannik, N. O., Elmore, D., Kubik, P. W., Dorn, R., and Roddy, D., 1986, The accumulation of cosmogenic chlorine-36 in rocks: A method for surface exposure dating: *Science*, v. 231, no. 4733, p. 41-43.
- Phillips, W. M., McDonald, E. V., and Reneau, S. L., 1998, Dating soils and alluvium with cosmogenic ^{21}Ne depth profiles: case studies from the Pajarito Plateau, New Mexico, USA: *Earth and Planetary Science Letters*, v. 160, no. 1-2, p. 209-223.
- Polyak, L., Alley, R. B., Andrews, J. T., Brigham-Grette, J., Cronin, T. M., Darby, D. A., Dyke, A. S., Fitzpatrick, J. J., Funder, S., and Holland, M., 2010, History of sea ice in the Arctic: *Quaternary Science Reviews*, v. 29, no. 15, p. 1757-1778.
- Polyak, V., Hill, C., and Asmerom, Y., 2008, Age and evolution of the Grand Canyon revealed by U-Pb dating of water table-type speleothems: *Science*, v. 319, no. 5868, p. 1377.

- Preece, S., Westgate, J., Froese, D., Pearce, N., Perkins, W., and Fisher, T., 2011, A catalogue of late Cenozoic tephra beds in the Klondike goldfields and adjacent areas, Yukon Territory: *Canadian Journal of Earth Sciences*, v. 48, no. 10, p. 1386-1418.
- Prentice, M., and Matthews, R., 1991, Tertiary ice sheet dynamics: The snow gun hypothesis: *Journal of Geophysical Research*, v. 96, no. B4, p. 6811-6827.
- Prescott, J., and Hutton, J., 1994, Cosmic ray contributions to dose rates for luminescence and ESR dating: large depths and long-term time variations: *Radiation measurements*, v. 23, no. 2, p. 497-500.
- Proctor Jr, C., Brown, T., Waechter, N., Aronow, S., and Barnes, V., 1974, Seguin sheet: The University of Texas at Austin: Bureau of Economic Geology, *Geologic Atlas of Texas*, scale, v. 1, no. 250,000.
- Raymo, M., and Ruddiman, W. F., 1992, Tectonic forcing of late Cenozoic climate: *Nature*, v. 359, no. 6391, p. 117-122.
- Rea, D., Basov, I., and Krissek, L., 1995, the Leg 145 Scientific Party, 1995. Scientific results of drilling the North Pacific transect 1995, Volume 145, p. 577-596.
- Reeves, C., 1976, Quaternary stratigraphy and geologic history of southern High Plains, Texas and New Mexico: *Quaternary stratigraphy of North America*: Stroudsburg, Pa., Dowden, Hutchinson and Ross, p. 213-223.
- Refsnider, K. A., and Miller, G. H., 2010, Reorganization of ice sheet flow patterns in Arctic Canada and the mid-Pleistocene transition: *Geophysical Research Letters*, v. 37, no. 13, p. L13502.

- Reheis, M. C., Goodmacher, J. C., Harden, J. W., McFadden, L. D., Rockwell, T. K., Shroba, R. R., Sowers, J. M., and Taylor, E. M., 1995, Quaternary soils and dust deposition in southern Nevada and California: Geological Society of America Bulletin, v. 107, no. 9, p. 1003.
- Repka, J. L., Anderson, R. S., and Finkel, R. C., 1997, Cosmogenic dating of fluvial terraces, Fremont River, Utah: Earth and Planetary Science Letters, v. 152, no. 1-4, p. 59-73.
- Riihimaki, C. A., Anderson, R. S., Safran, E. B., Dethier, D. P., Finkel, R. C., and Bierman, P. R., 2006, Longevity and progressive abandonment of the Rocky Flats surface, Front Range, Colorado: Geomorphology, v. 78, no. 3-4, p. 265-278.
- Roy, M., Clark, P. U., Raisbeck, G. M., and Yiou, F., 2004, Geochemical constraints on the regolith hypothesis for the middle Pleistocene transition: Earth and Planetary Science Letters, v. 227, no. 3, p. 281-296.
- Ruzzante, D. E., Walde, S. J., Gosse, J. C., Cussac, V. E., Habit, E., Zemplak, T. S., and Adams, E. D., 2008, Climate control on ancestral population dynamics: insight from Patagonian fish phylogeography: Molecular Ecology, v. 17, no. 9, p. 2234-2244.
- Rybczynski, N., Gosse, J. C., Harington, C. R., Wogelius, R. A., Hidy, A. J., and Buckley, M., 2013, Mid-Pliocene warm-period deposits in the High Arctic yield insight into camel evolution: Nature Communications, v. 4, p. 1550.

- Schaller, M., Von Blanckenburg, F., Veldkamp, A., Tebbens, L., Hovius, N., and Kubik, P., 2002, A 30,000 yr record of erosion rates from cosmogenic ^{10}Be in Middle European river terraces: *Earth and Planetary Science Letters*, v. 204, no. 1-2, p. 307-320.
- Schweger, C., Froese, D., White, J. M., and Westgate, J. A., 2011, Pre-glacial and interglacial pollen records over the last 3 Ma from northwest Canada: Why do Holocene forests differ from those of previous interglaciations?: *Quaternary Science Reviews*, v. 30, no. 17-18, p. 2124-2133.
- Smith, C., Tarnocai, C., and Hughes, O., 1986, Pedological investigations of Pleistocene glacial drift surfaces in the central Yukon: *Géographie physique et Quaternaire*, v. 40, no. 1, p. 29-37.
- Stone, J., Evans, J., Fifield, L., Allan, G., and Cresswell, R., 1998, Cosmogenic chlorine-36 production in calcite by muons: *Geochimica Et Cosmochimica Acta*, v. 62, no. 3, p. 433-454.
- Stone, J. O., 2000, Air pressure and cosmogenic isotope production: *Journal of Geophysical Research*, v. 105, no. B10, p. 23753-23723,23759.
- Syvitski, J. P., Kettner, A. J., Overeem, I., Hutton, E. W., Hannon, M. T., Brakenridge, G. R., Day, J., Vörösmarty, C., Saito, Y., and Giosan, L., 2009, Sinking deltas due to human activities: *Nature Geoscience*, v. 2, no. 10, p. 681-686.
- Syvitski, J. P. M., and Milliman, J. D., 2007, Geology, geography, and humans battle for dominance over the delivery of fluvial sediment to the coastal ocean: *Journal of Geology*, v. 115, no. 1, p. 1-19.

- Taylor, J. R., 1997, An introduction to error analysis: the study of uncertainties in physical measurements, Univ Science Books.
- Von Blanckenburg, F., 2005, The control mechanisms of erosion and weathering at basin scale from cosmogenic nuclides in river sediment: Earth and Planetary Science Letters, v. 237, no. 3, p. 462-479.
- Westgate, J., Sandhu, A., Preece, S., and Froese, D., 2003, Age of the gold-bearing White Channel gravel, Klondike district, Yukon: In: Yukon Exploration and Geology 2002, D.S. Emond and L.L. Lewis (eds.), Exploration and Geological Services Division, Yukon Region, Indian and Northern Affairs Canada, p. 241-250.
- Westgate, J., Stemper, B., and Péwé, T., 1990, A 3 My record of Pliocene-Pleistocene loess in, interior Alaska: Geology, v. 18, no. 9, p. 858.
- Whipple, K. X., and Tucker, G. E., 1999, Dynamics of the stream-power river incision model: Implications for height limits of mountain ranges, landscape response timescales, and research needs: Journal of Geophysical Research, v. 104, no. B8, p. 17661-17617,17674.
- Willenbring, J. K., Codilean, a. T., and McElroy, B., 2013, Earth is (mostly) flat: Apportionment of the flux of continental sediment over millennial time scales: Geology, v. 41, no. 3, p. 343-346.
- Willenbring, J. K., and Von Blanckenburg, F., 2010, Long-term stability of global erosion rates and weathering during late-Cenozoic cooling: Nature, v. 465, no. 7295, p. 211-214.
- Winker, C. D., 1979, Late Pleistocene fluvial-deltaic deposition, Texas coastal plain and shelf.

- Wittmann, H., and Von Blanckenburg, F., 2009, Cosmogenic nuclide budgeting of floodplain sediment transfer: *Geomorphology*, v. 109, no. 3, p. 246-256.
- Wittmann, H., Von Blanckenburg, F., Guyot, J. L., Maurice, L., and Kubik, P., 2009, From source to sink: Preserving the cosmogenic ^{10}Be -derived denudation rate signal of the Bolivian Andes in sediment of the Beni and Mamoré foreland basins: *Earth and Planetary Science Letters*, v. 288, no. 3, p. 463-474.
- Wittmann, H., von Blanckenburg, F., Maurice, L., Guyot, J. L., Filizola, N., and Kubik, P. W., 2011a, Sediment production and delivery in the Amazon River basin quantified by in situ-produced cosmogenic nuclides and recent river loads: *Geological Society of America Bulletin*, v. 123, no. 5-6, p. 934-950.
- Wittmann, H., von Blanckenburg, F., Maurice, L., Guyot, J. L., and Kubik, P. W., 2011b, Recycling of Amazon floodplain sediment quantified by cosmogenic Al-26 and Be-10: *Geology*, v. 39, no. 5, p. 467-470.

Appendices

A.1. Supplementary Information for Hidy et al. (2010): A Geologically Constrained Monte Carlo Approach to Modeling Exposure Ages from Profiles of Cosmogenic Nuclides: An Example from Lees Ferry, Arizona

A.1.1. Readme File for Profile Simulator

Version history:

Updates will occasionally be made to fix any bugs or make improvements to the codes. Details for any changes made will be logged here.

Current versions:

Matlab - 1.2
MathCad - 1.0

Archived versions:

Matlab - 1.0
Matlab - 1.1

Description of version modifications:

1.2 - Implemented importance sampling of simulation to create Bayesian probability distribution curves and estimates of most probable values as well as errors. The Bayesian solutions are a more accurate representation of the most probable values for age, erosion rate, and inheritance solutions considering the entire 3D space. The importance sampling is performed not only on the accepted profile solutions, but on the rejected solutions as well. This yields a continuous probability solution within the constraints set by the user. Thanks to B. Borchers for suggesting this! The pdf plots also contain a smoothed curve showing the minimum chi-squared value for each age, erosion rate, and inheritance over the entire space. This was added to help check for statistical bias that can be generated from user constraints. For example, this is useful when the chi-squared statistic approaches a single value and can thus be minimized, but the Bayesian most-likely value (weighted over the total simulation space) is significantly different. This can happen due to the irregular and asymptotic way the solution space projects onto the various parameter axes (specifically, for age and erosion rate). The tendency is for the age probability to be weighted toward the minimum age and the erosion rate probability to be

weighted toward the maximum erosion rate since that is where the solution density is naturally greatest for those parameters.

The best 100 chi-squared values are now plotted on the Age-Erosion solution space plot.

A text file called 'simulation_results.txt' is now automatically exported to your working directory whenever a simulation is run. This file contains four columns of data:

- column (1) - chi squared value
- column (2) - age value (ka)
- column (3) - erosion rate (cm/ka)
- column (4) - inheritance (atoms/g)

Subsequent simulation runs will overwrite this file, so rename the file before running the next simulation if you wish to keep the contents of the first.

1.1 - Incorrect plotting of concentration vs. depth plots. These graphics displayed inheritance values that were not corrected for decay. Resulting solutions were drawn systematically to the right on plots. This bug did not affect analytical results, just the graphics.

System requirements:

Matlab version:

This program was created with Matlab & Simulink Student Version (R2009a). This program may not work on older versions of Matlab. In addition, this program utilizes built-in toolboxes (curve fitting, statistics, and image processing) that may or may not come standard with your version of Matlab. Please visit <http://www.mathworks.com> for information on the minimum system requirements to run Matlab on your computer.

MathCad version:

This program was created with MatchCad 14. This program does not work on older versions of MathCad. MathCad 14 requires a Windows Operating System (Windows 2000 or later). Please visit <http://www.ptc.com> for information on the minimum system requirements to run MathCad on your computer.

Known bugs and fixes/work-arounds:

Operation instructions for Matlab:

1. Unzip Matlab_version_1.0.zip. Open Matlab and copy the contents of 10Be_profile_simulator to your current directory.

2. This program uses data packages from the Matlab central file exchange, to utilize these packages enter the following into the Matlab command line:

```
addpath depth_profile_simulator_10Be [enter]
addpath datatablepackage [enter]
addpath herrorbar [enter]
addpath multicore [enter]
```

Alternatively, you may edit the file path in startup.m to you current working directory and then restart Matlab.

3. Type the following in the Matlab command line:

```
be_gui [enter]
```

This opens the program's GUI and allows the user to enter and save their profile data and simulation parameters

4. To load the Lees Ferry test settings, click the "load" button in the GUI and select 'Leesferrysand_settings'. Then, load the shielding data file (LF_shield.txt) and the profile data file (Leesferry_sand6.txt) from the "topographic/geometric shielding" window and "profile data" window, respectively.

5. Click the 'run' button in the GUI to begin the simulation.

Multicore feature (for advanced users):

1. In the GUI under the 'Monte Carlo parameters' window, select 'package multicore'.

2. Open n-1 additional Matlab environments, where n is the number of cores you wish to use in parallel. Make sure that the current directory of each of these new environments is set to your current working directory.

3. In each additional Matlab environment type the following into the command line:

```
addpath multicore [enter]
be_startmulticoreslave [enter]
```

4. Click the 'run' button in the GUI to begin the simulation. The simulation speed should be just under n times faster than a non-parallel simulation!

Operation instructions for MathCad worksheet:

1. Unzip MathCad_version_1.0, making sure to keep all the files in the same directory. Open 10Be_profile_simulator_v1.0.xmcd. Detailed instructions for use are embedded in the worksheet.

WS5_ICP Aliquot and AI spiking

This worksheet outlines the steps for collecting ICP aliquots and adding AI carrier.

Chemist: GY

Date: 01/13/05

- 1 Label one 10 ml volumetric flasks per sample (8)
- 2 Label one ICP vial with CNEF ID per sample (8)

	1	2	3	4	5	6	7	8	examples
CNEF ID	1590	1595	1596	1597	1598	1599	1600	1537	105
Sample ID	GC-04-LF-401	GC-04-LF-404.30s	GC-04-LF-404.60s	GC-04-LF-404.100s	GC-04-LF-404.140s	GC-04-LF-404.180s	GC-04-LF-404.220s	Blank	WY-96-001
AI carrier ID								AI Carrier4	ALI-carrier
Quant-EM est. AI in qtz								0	ppm
Volume carrier to add to smpl								1.0036	ml
Volume carrier to add to vol A									ml
Volume carrier to add to vol. B									ml
<small>Tare between mass measurements</small>									
Mass 100 ml volumetric	67.1812	67.7314	65.2040	67.7939	67.3565	69.2252	67.7446	68.8734	66.9239 g
100ml volumetric+sample+2%HCl	168.3528	169.1271	166.3273	169.2272	168.5285	170.2019	168.8337	169.8432	166.9875 g
Mass 5 ml smpl pipetted to vol A	10.0000	10.0129	10.0045	10.0140	10.0032	10.0066	10.0061	10.0101	5.0000 g
Final Mass of 100 ml vol and smpl	158.3384	159.1093	156.3130	159.2053	158.5155	160.1907	158.8202	159.8260	1.0100 g
Mass AI carrier to remaining (row 18)									1.0100 g
Unaccounted mass									0.0100 g

PRINT this form

- 3 Get digestion vessel and cover ready, Do not wipe now.
- 4 Transfer the 90 ml sample back into vessel
- 5 Bring contents of volumetrics A and B to 10 ml
- 6 Transfer contents volumetrics to ICP vials with same number

WS8_Cation Column Chemistry

This worksheet outlines the steps for the Cation Column Chemistry

Chemist: ^{GY/JG}

Date: ^{mm/dd/yy}

[Print this page](#)

- ₁ Dissolve in 5 ml conc. HCl and evaporate to dryness at 125°C
- ₂ Redissolve in 2.5 ml 1N HCl and 2.5 ml 0.5 N HCl
- ₃ Transfer to centrifuge tube, rinse with 1 ml 0.5N, and centrifuge

Column ID	1	2	3	4	5	6	7	8	examples
CNEF ID	1590	1595	1596	1597	1598	1599	1600	1537	105
Sample ID	GC-04-LF-401	GC-04-LF-404.30s	GC-04-LF-404.60s	GC-04-LF-404.100	GC-04-LF-404.140	GC-04-LF-404.180	GC-04-LF-404.220	Blank	WY-96-001

- ₄ Pipette all of the sample into designated conditioned cation column
- ₅ Discard the eluant. Add 220 ml 0.5 N HCL (bottle C6)
- ₆ Collect eluant as Cation Supernate, add 200 ml 0.5 N HCl (bottle C7)
- ₇ Collect eluant as Be-Sample into vessels.
- ₈ Add 30 ml 1N HCl (bottle8)
- ₉ Save this as Be-sample as well.
- ₁₀ Add 100 ml 4.5 N HCl, save as Al sample.
- ₁₁
- ₁₂
- ₁₃ **CONDITION CATION COLUMN**

- (bottle C1) 100 ml 9N HCl
- (bottle C2) 50 ml 4.5 N HCl
- (bottle C3) 50 ml 1 N HCl
- (bottle C4) 50 ml water
- (bottle C5) 100 ml 0.5 N HCl

WS9_Be Sample Chemistry

This worksheet outlines the steps to prepare the BeO sample

Chemist: ^{GY}

Date: ^{form: mm/dd/yy}

Print this page

- ₁ Evaporate Be Sample from column in wiped digestion vessels at 125°C
- ₂ Add 2-5 ml 20% perchloric and evaporate at 200°C
- ₃ Again, add 2-5 ml 20% perchloric and evaporate at 200°C
- ₄ Dissolve sample in 10 ml of 0.5 N HCl (optima grade)
- ₅ Transfer to 15 ml centrifuge tube
- ₆ Centrifuge and decant into clean centrifuge tube
- ₇ Heat centrifuge tubes in water bath at 60°C
- ₈ Precipitate Be(OH)₂ using Matheson ultimate grade ammonia gas
Gently bubble NH₃ with clean pipet tip on hose
for ca.15 bubbles, or ca. 8-12 sec until ppt forms
Optimum pH=9.2; 1N HCl may be added
- ₉ Centrifuge 15 min., decant (save and redo ₈ if pH of liquid is < 8)
- ₁₀ Wash with water, vortex, centrifuge for 10 min, and decant
- ₁₁ Record mass quartz vials, label, and place them in furnace holder

CNEF ID	1590	1595	1596	1597	1598	1599	1600	1537	
Sample ID	GC-04-LF-401	GC-04-LF-404.30s	GC-04-LF-404.60s	GC-04-LF-404.100s	GC-04-LF-404.140s	GC-04-LF-404.180s	GC-04-LF-404.220s	Blank	105 WY-96-001
Mass Qtz Vial	2.4625	2.5357	2.5349	2.509	2.428	2.5702	2.5599	2.5528	2.1400 g
Mass Vial+Spl	2.4629	2.5358	2.535	2.5091	2.4284	2.5711	2.5604	2.553	2.1410 g
Mass Spl	0.0004	0.0001	0.0001	0.0001	0.0004	0.0009	0.0005	0.0002	1 mg

- ₁₂ Add 1 small drop of water with micropipet, slurry precipitate
- ₁₃ Transfer sample into quartz vial, cover with alumina vial
- ₁₄ Heat in oven at 120°C for 2-3 hours
- ₁₅ Let cool and scrape sample down from walls of quartz tube
- ₁₈ Place in furnace. Convert to BeO in furnace at 850°C for minimum 1 hr
- ₁₉ Determine mass of vial + sample

This worksheet outlines the steps for collecting ICP aliquots and adding AI carrier.

Chemist: ^{GY}

Date: ^{form: 02/17/01}

1 Label one 10 ml volumetric flasks per sample (8)

2 Label one ICP vial with CNEF ID per sample (8)

	B9	B10	B11	B12	B13	B14	B15	B16	examples
CNEF ID	1601	1602	1603	1604	1605	1606	1589	1623	105
Sample ID	GC-04-LF-404.30p	GC-04-LF-404.60p	GC-04-LF-404.100p	GC-04-LF-404.140p	GC-04-LF-404.180p	GC-04-LF-404.220p	BPK-04-C2	Blank	WY-96-001
AI carrier ID									ALI-carrier
Quant-EM est. AI in qtz									ppm
Volume carrier to add to smpl								1.0358	ml
Volume carrier to add to vol A									ml
Volume carrier to add to vol. B									ml
	Tare between mass measurements								
Mass 100 ml volumetric	67.6888	67.0051	68.8731	67.7434	67.3558	67.4178	66.1256	66.3039	66.9239 g
100ml volumetric+sample+2%HCl	168.7731	168.0311	169.7857	168.6779	168.4420	168.5324	167.0750	167.2346	166.9875 g
Mass 5 ml smpl pipetted to vol A	5.0094	5.0353	5.0025	5.1115	5.0869	5.0043	5.0435	5.0682	5.0000 g
Bring up to 10 ml by 2%HCl	10.0320	10.1283	10.0308	10.0178	10.0305	10.0162	10.0629	10.0066	
Mass 10 ml Sample to Vial B	10.0494	10.0096	10.0499	10.0217	10.0144	10.0146	10.0724	10.0217	
Final Mass of 100 ml vol and smpl	153.7011	152.9602	154.7216	153.5333	153.3306	153.5042	151.9491	152.1384	1.0100 g
Mass AI carrier to remaining (row 18)									1.0100 g
Unaccounted mass									0.0100 g

3 Get digestion vessel and cover ready, Do not wipe now.

4 Transfer the 90 ml sample back into vessel

5 Bring contents of volumetrics A and B to 10 ml

6 Transfer contents volumetrics to ICP vials with same number

GY July 16, 2003 update

This worksheet outlines the steps for the Cation Column Chemistry

Chemist: ^{GY/JG}

Date: ^{mm/dd/yy}

Print this page

- ₁ Dissolve in 5 ml conc. HCl and evaporate to dryness at 125°C
- ₂ Redissolve in 2.5 ml 1N HCl and 2.5 ml 0.5 N HCl
- ₃ Transfer to centrifuge tube, rinse with 1 ml 0.5N, and centrifuge

Column ID	1	2	3	4	5	6	7	8	examples
CNEF ID	1601	1602	1603	1604	1605	1606	1589	1623	105
Vessel	B9	B10	B11	B12	B13	B14	B15	B16	
Sample ID	GC-04-LF-404.30p	GC-04-LF-404.60p	GC-04-LF-404.100p	GC-04-LF-404.140p	GC-04-LF-404.180p	GC-04-LF-404.220p	BPK-04-C2	Blank	WY-96-001

- ₄ Pipette all of the sample into designated conditioned cation column
- ₅ Discard the eluant. Add 220 ml 0.5 N HCL (bottle C6)
- ₆ Collect eluant as Cation Supernate, add 200 ml 0.5 N HCl (bottle C7)
- ₇ Collect eluant as Be-Sample into vessels.
- ₈ Add 30 ml 1N HCl (bottle8)
- ₉ Save this as Be-sample as well.
- ₁₀ Add 100 ml 4.5 N HCl, save as Al sample.

₁₃ **CONDITION CATION COLUMN**

- (bottle C1) 100 ml 9N HCl
- (bottle C2) 50 ml 4.5 N HCl
- (bottle C3) 50 ml 1 N HCl
- (bottle C4) 50 ml water
- (bottle C5) 100 ml 0.5 N HCl

WS9_Be Sample Chemistry

This worksheet outlines the steps to prepare the BeO sample

Chemist: ^{GY}

Date: ^{form: mm/dd/yy}

Print this page

- ₁ Evaporate Be Sample from column in wiped digestion vessels at 125°C
- ₂ Add 2-5 ml 20% perchloric and evaporate at 200°C
- ₃ Again, add 2-5 ml 20% perchloric and evaporate at 200°C
- ₄ Dissolve sample in 10 ml of 0.5 N HCl (optima grade)
- ₅ Transfer to 15 ml centrifuge tube
- ₆ Centrifuge and decant into clean centrifuge tube
- ₇ Heat centrifuge tubes in water bath at 60°C
- ₈ Precipitate Be(OH)₂ using Matheson ultimate grade ammonia gas
Gently bubble NH₃ with clean pipet tip on hose
for ca.15 bubbles, or ca. 8-12 sec until ppt forms
Optimum pH=9.2; 1N HCl may be added
- ₉ Centrifuge 15 min., decant (save and redo ₈ if pH of liquid is < 8)
- ₁₀ Wash with water, vortex, centrifuge for 10 min, and decant
- ₁₁ Record mass quartz vials, label, and place them in furnace holder

CNEF ID	1601	1602	1603	1604	1605	1606	1589	1623	105
Sample ID	GC-04-LF-404.30p	GC-04-LF-404.60p	GC-04-LF-404.100p	GC-04-LF-404.140p	GC-04-LF-404.180p	GC-04-LF-404.220p	BPK-04-C2	Blank	WY-96-001
Vessel	B9	B10	B11	B12	B13	B14	B15	B16	
Mass Qtz Vial	2.4836	2.5207	2.5147	2.5537	2.5549	2.4373	2.619	2.4714	2.1400 g
Mass Vial+Spl	2.4842	2.5215	2.5155	2.5544	2.5557	2.4382	2.6196	2.4718	2.1410 g
Mass Spl	0.0006	0.0008	0.0008	0.0007	0.0008	0.0009	0.0006	0.0004	1 mg

- ₁₂ Add 1 small drop of water with micropipet, slurry precipitate
- ₁₃ Transfer sample into quartz vial, cover with alumina vial
- ₁₄ Heat in oven at 120°C for 2-3 hours
- ₁₅ Let cool and scrape sample down from walls of quartz tube
- ₁₈ Place in furnace. Convert to BeO in furnace at 850°C for minimum 1 hr
- ₁₉ Determine mass of vial + sample

A.2. Supplemental Information for Hidy et al.: Climatically-driven Variation in Sediment Flux from Interior Texas Established with Cosmogenic ^{10}Be and ^{26}Al

A.2.1. TCN Sample Collection and Preparation

Samples of ~2 kg of medium to coarse sand were collected from point bar facies within active or abandoned channel-belt packages on the coastal plain. For all samples, this sediment fraction had a fairly homogeneous mineral composition that was dominantly quartz (>90%) with the remaining component made up primarily of feldspars and micas. These were then washed and sieved to extract the 355-500 μm grain size fractions. If samples were mass deficient in this range, or if duplicates were desired, alternate ranges were utilized in the following order: 250-355 μm , 150-250 μm , then 500-850 μm (note: only two samples were processed outside the 250-500 μm range, and in each case they were duplicates). Chemical preparation was performed at the Dalhousie Geochronology Centre, whose laboratory manual is available online at <http://cnf.earthsciences.dal.ca>. Quartz purification included, in the following order: magnetic separation, treatment with aqua regia (3:1 of $\text{HCl}:\text{HNO}_3$), HF etching, and multiple cycles of dilute HF ultrasonication (after Kohl and Nishiizumi, 1992). These procedures purified the samples to ~99% quartz, dissolved aggregate grains and weak silicates, and removed any atmospheric ^{10}Be adsorbed to the grain surfaces. The samples were then digested in a $\text{HF}-\text{HClO}_4$ mixture and the Be^{+2} and Al^{+2} cations extracted via ion chromatography. After precipitating the cations, the samples were oxidized to produce a small amount of beryllium and aluminum oxide powders. Be and Al oxides were mixed 1:1 with niobium and silver (by volume), respectively, and sent to the Center for Accelerator Mass Spectrometry at Lawrence Livermore National Laboratory (CAMS-

LLNL) for AMS analysis. Standards at CAMS-LLNL used for Be and Al measurements were 07KNSTD3110 with a ratio of 2850×10^{-15} (Nishiizumi et al., 2007), and KNSTD10650 with a ratio of 10650×10^{-15} (Nishiizumi, 2004), respectively. Process blanks for Be and Al were analyzed and used to subtract any background concentration. A summary of chemical data is shown in Table A.2.1.

Table A.2.1. Chemical data and AMS results

CNEF ID	Site # (river)	Target surface	Depth ¹ (cm)	Thick. (cm)	Grain size (µm)	Qtz. mass (g)	¹⁰ Be/ ⁹ Be ² (x 10 ⁻¹³)	²⁶ Al/ ²⁷ Al (x 10 ⁻¹³)	[¹⁰ Be] (atoms g ⁻¹)	1σ error ³	[²⁶ Al] (atoms g ⁻¹)	1σ error ⁴
1975	2 (Col)	Beaumont (L)	995	4.0	355 - 500	119.9969	17.398		294207	3.06%		
1976 [†]	3 (Col)	Lissie	303	5.0	355 - 500	94.7074	11.018		236242	3.30%		
1977 [†]	3 (Col)	Lissie	333	6.0	355 - 500	95.7291	10.363		220287	3.07%		
1978 [†]	3 (Col)	Lissie	367	5.0	355 - 500	78.0629	7.680		207915	3.07%		
1979 [†]	3 (Col)	Lissie	387	5.0	355 - 500	77.8248	8.045		198211	3.35%		
1980 [†]	3 (Col)	Lissie	418	4.0	355 - 500	72.6366	6.527		184723	3.08%		
1981	4 (Col)	Lissie	509	5.0	355 - 500	123.2440	11.623		191952	3.06%		
1932 [‡]							0.084					
2125 [†]	10 (Tri)	H. Dew eyville	148	4.0	250 - 355	120.0081	7.890		98745	4.44%		
2126 [†]	10 (Tri)	H. Dew eyville	179	5.0	250 - 355	120.0025	8.201		103587	3.94%		
2128 [†]	10 (Tri)	H. Dew eyville	261	5.0	250 - 355	119.9997	7.584		97029	3.76%		
2129 [†]	10 (Tri)	H. Dew eyville	301	6.0	250 - 355	120.0005	7.574		94658	4.48%		
2130 [†]	10 (Tri)	H. Dew eyville	341	6.0	250 - 355	120.0003	7.942		101081	3.86%		
2131 [†]	10 (Tri)	H. Dew eyville	388	5.0	250 - 355	120.0217	7.725	3.541	98886	5.23%	724402	6.12%
2080 [†]							0.122	0.010				
2132	11 (Tri)	M. Dew w yville (L)	512	6.0	150 - 250	120.0365	6.540	3.203	84112	4.67%	445876	6.02%
2133	11 (Tri)	M. Dew w yville (L)	482	5.0	150 - 250	120.6702	6.973		88793	3.14%		
2134	11 (Tri)	M. Dew w yville (U)	383	5.0	150 - 250	120.7315	5.738		74632	5.17%		
2135	11 (Tri)	M. Dew w yville (U)	351	6.0	250 - 355	120.1937	5.850		72786	6.05%		
2081 [†]							0.088	0.010				
2139	7 (Col)	Beaumont (U)	691	5.0	250 - 355	100.0752	18.097		280300	2.68%		
2140	7 (Col)	Beaumont (U)	732	5.0	250 - 355	100.0115	19.811		298079	3.33%		
2141	7 (Col)	Beaumont (U)	937	7.0	355 - 500	100.0388	13.762	7.252	216766	2.68%	1214987	6.87%
2142	8 (Col)	modern pre-dam	427	8.0	355 - 500	90.1047	13.464	7.989	223303	2.71%	1388435	6.02%
2143	12 (Tri)	modern pre-dam	550	10.0	250 - 355	100.3179	5.728	2.693	83873	3.12%	513463	7.77%
2144	8 (Col)	modern pre-dam	427	8.0	355 - 500	92.1266	13.046		220090	3.05%		
2145	12 (Tri)	modern pre-dam	550	10.0	250 - 355	100.5119	5.336		79991	2.70%		
2084 [†]							0.127	0.101				
2070	5 (Col)	CBA-1	550	20.0	355 - 500	149.1788	26.021	7.999	257180	3.37%	1266392	5.92%
2072	1 (Bra)	modern post-dam	30	10.0	355 - 500	150.0114	21.565	6.091	214702	2.93%	1167776	6.02%
2254 [†]	13 (Tri)	Lissie	408	6.0	250 - 355	149.9414	10.814	3.410	106314	2.80%	561269	7.13%
2255 [†]	13 (Tri)	Lissie	543	7.0	250 - 355	150.2143	10.381	3.439	104073	2.92%	540383	6.17%
2256 [†]	13 (Tri)	Lissie	713	10.0	355 - 500	150.7835	9.134	2.668	94214	2.61%	370723	6.36%
2257	13 (Tri)	Willis/Flemming	2674	10.0	150 - 355	150.0817	1.271	0.373	11777	3.36%	49552	20.51%
2258	13 (Tri)	Willis/Flemming	2674	10.0	150 - 250	137.3109	1.254	0.299	12197	3.31%	48303	26.46%
2163 [†]							0.094	0.034				
2315	3 (Col)	Lissie	418	4.0	500 - 850	82.0009	8.121	5.004	140361	2.54%	711905	5.93%
2316	14 (Tri)	L. Dew eyville	1020	5.0	355 - 500	100.1201	6.535	3.205	95034	2.97%	477658	6.15%
2317	15 (Tri)	L. Dew eyville	615	6.0	355 - 500	100.0063	6.999	3.151	101215	2.79%	517008	6.44%
2318	9 (Col)	Dew eyville	575	10.0	355 - 500	100.0472	14.375	8.296	220080	2.46%	1167347	5.91%
2319	7 (Col)	Beaumont (U)	815	6.0	250 - 355	100.8627	18.411	9.409	272026	2.46%	1567494	5.62%
2320	7 (Col)	Beaumont (U)	937	7.0	250 - 355	100.0430	19.156	8.941	286584	2.46%	1383557	6.51%
2071	6 (Col)	modern post-dam	20	10.0	355 - 500	100.1685	17.301	7.354	252415	3.28%	1489576	6.72%
2167 [†]							0.192	0.016				

¹ All depths are measured from top of sample swath to the surface of the outcrop

² All ratios were corrected for boron and measured with standard 07KNSTD3110 except for samples 1975-1981, which were measured with standard KNSTD3110 and then renormalized to 07KNSTD3110 (Nishiizumi et al. 2007)

³ Includes AMS measurement error, blank correction error, and an additional 2% error in sample preparation and analysis

⁴ Includes AMS measurement error, blank correction error, and an additional 5% error in sample preparation, analysis, and ICP measurement of native

† Process blank are listed beneath each relevant batch of samples

‡ Sample is part of a depth profile

A.2.2. ^{10}Be Catchment-wide Denudation Rates

Directly measured (for modern rates) or modeled (for paleo-rates) concentrations of ^{10}Be in fluvial sediment can be used to infer average rates of denudation over catchment areas sourcing the sediment (Brown et al., 1995; Bierman and Steig, 1996; Granger et al., 1996; Von Blanckenburg, 2005). Because in situ ^{10}Be is dominantly produced near the Earth's surface (uppermost 3-4 m), the amount accrued in material eroded from a particular catchment surface depends on its average residence time through that shallow depth zone, which is related to rate of surface denudation. Since material deposited by a stream is a collection of material eroding from the entire catchment, its ^{10}Be signature is thus controlled by the average denudation rate of the catchment area. Catchment-wide denudation rates are given by Lal (1991):

$$\varepsilon = (P_0/N - \lambda_{\text{Be}}) \cdot \Lambda/\rho, \quad (3)$$

where ε is the catchment-wide denudation rate (cm a^{-1}), P_0 is the average surface production rate of ^{10}Be over the entire catchment ($\text{atoms g}^{-1} \text{a}^{-1}$), N is the depositional ^{10}Be concentration (atoms g^{-1}), λ_{Be} is the decay constant for ^{10}Be ($4.997 \times 10^{-7} \text{a}^{-1}$) (Chmeleff et al., 2010; Korschinek et al., 2010), Λ is the effective attenuation length of the cosmic flux near the Earth's surface (160cm g^{-2} for mid-latitudes), and ρ is the mean density of the eroding material (2.65g cm^{-3} for quartz). This denudation rate can be converted to a sediment flux by multiplying equation (3) by the density of the eroding material and the catchment area A (km^2):

$$Q_s = A\Lambda(P_0/N - \lambda_{\text{Be}}) \cdot 10^5, \quad (4)$$

where Q_s is in units of MT a^{-1} .

Application of this technique involves several assumptions. 1) Catchment surfaces erode primarily by surface erosion and not via mass wasting that would incorporate buried material. This assumption may be invalid for catchments with high relief or in tectonically active or glaciated regions. These attributes were specifically avoided for the catchments in this study. However, lateral erosion of cut banks, which becomes increasingly significant on coastal plains, may produce a similar effect by recycling stored sediment into the active stream (see A.2.2.3.). 2) The sampled material statistically represents the catchment area. This requires that the sampled lithology and grain size (in our case, medium- to coarse-grained quartz) is distributed uniformly throughout the catchment, so that the spatially-averaged catchment-wide surface production rate (P_0) is relevant to the sample (see A.2.2.1.). 3) Timescales of temporary sediment storage and transport are short compared to the interval of time averaged in the catchment-wide denudation rate. Equation (3) produces erosion rate estimates averaged over T_{av} (a) such that:

$$T_{av} = \Lambda / \rho \varepsilon . \quad (5)$$

For the catchments in this study, T_{av} ranges from ~20-40 ka which is assumed to be sufficiently longer than mean up-catchment residence times due to the high water discharges. Within and basin-ward of the stream hinge zones (inner coastal plain), however, these rivers incise into Plio-Pleistocene sediments. Buried sediments of this age may not have equilibrated their ^{10}Be concentrations to long-term surface denudation rates and potentially contain an inherited ^{10}Be signature with a complex exposure and burial history (and we can use this to our advantage; see section A.2.2.3.). 4) Temporal changes in catchment characteristics such as total area, lithology type and abundance, relief, and

mean elevation are negligible over T_{av} and over the entire span for which paleodenudation rates are calculated. Long-term catchment stability (Reeves, 1976; Winker, 1979; Galloway et al., 2011) and the lack of active tectonics support our assumption that these characteristics have been static for the studied catchments at the timescales of interest.

A.2.2.1. Calculating Catchment-wide Production Rates (P_0)

Catchment-wide average production rates were calculated uniquely for each site based on the hypsometry and surficial geology of the upstream drainage area (Table A.2.2). This was done by: 1) obtaining a flow network from a digital elevation model (DEM; USGS NED 1/3 arc second) to define the catchment area above each sample, 2) using a digitized surficial geology map to remove areas in the catchment where medium- to coarse-grained quartz is unlikely to originate (e.g. areas mapped as carbonates, siltstones, and mudstones), and 3) calculating the surface production rate from the DEM at each remaining pixel in the catchment, and averaging the values (Fig. A.2.1). Nucleogenic and muogenic surface production rates were calculated with the scaling schemes described in A.2.3. In a precursory calculation, internal topographic shielding was also considered; however, due to the low internal relief in these catchments this had <1% effect on the calculated rate and was ignored for the final calculation. Differences between the mean production rates calculated over the entire catchment and those calculated from quartz-containing areas in the catchment are minimal (~5-6% in the Colorado River catchment; ~1.5% in the Trinity River catchment) implying the quartz distribution is approximately homogeneous with respect to catchment hypsometry. Furthermore, catchment-wide production rates calculated for sites within the same

catchment are approximately constant (all within 1%) since the vast majority of contributing drainage area for these catchments is upstream from the sampled region.

Site ¹	location data				total catchment area		quartz-containing areas		Δ area ² (%)	Δ prod rate ³ (%)
	Latitude (deg)	Longitude (deg)	Elevation (m)	Catchment	Above site (km ²)	¹⁰ Be prod. rate (atoms g ⁻¹ a ⁻¹)	Above site (km ²)	¹⁰ Be prod. rate (atoms g ⁻¹ a ⁻¹)		
1	29.675	-96.026	20	Brazos	115636	6.85	81673	7.27	29.37	6.20
2	28.930	-96.013	12	Colorado	110091	7.41	67534	7.78	38.66	5.06
3	29.584	-96.473	63	Colorado	108569	7.45	66426	7.84	38.82	5.23
4	29.589	-96.480	66	Colorado	108567	7.45	66424	7.84	38.82	5.23
5	29.611	-96.451	44	Colorado	108547	7.45	66406	7.84	38.82	5.23
6	29.617	-96.418	46	Colorado	108542	7.45	66401	7.84	38.82	5.24
7	29.274	-96.096	27	Colorado	109326	7.43	67007	7.81	38.71	5.13
8	29.731	-96.539	55	Colorado	107367	7.48	65520	7.88	38.98	5.38
9	29.313	-96.143	22	Colorado	109285	7.43	66983	7.81	38.71	5.12
10	30.055	-94.819	10	Trinity	45339	4.92	28509	4.85	37.12	1.49
11	30.106	-94.815	9	Trinity	45321	4.92	28493	4.85	37.13	1.49
12	30.272	-94.819	8	Trinity	44697	4.93	27968	4.86	37.43	1.45
13	30.538	-94.830	46	Trinity	43854	4.94	27246	4.87	37.87	1.39
14	30.588	-95.033	24	Trinity	42984	4.95	26580	4.88	38.16	1.37
15	30.113	-94.815	8	Trinity	45292	4.92	28465	4.85	37.15	1.48

1 See Chapter 3

2 Represents area difference between total catchment and mapped catchment areas likely to contain quartz upstream from each sampling site

3 Represents difference in basin-averaged production rate between total catchment and mapped catchment areas likely to contain quartz upstream from

Table A.2.2. Site and up-catchment data

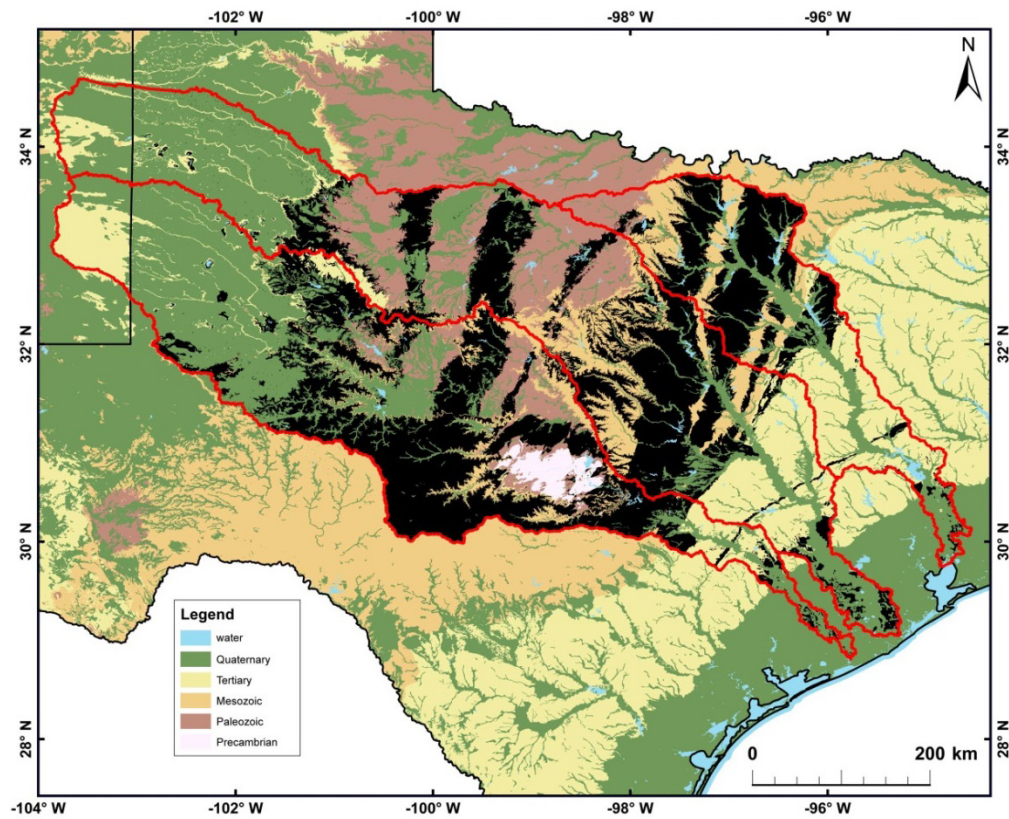


Figure A.2.1. General geologic map of Texas with Colorado, Brazos, and Trinity (left to right) catchments outlined in red. Blackened regions indicate areas inferred to contribute no medium- to coarse-grained quartz to stream bed load.

A.2.2.2. Obtaining Depositional ^{10}Be (N) and ^{26}Al

For modern sediment samples, ^{10}Be and ^{26}Al measurements are interpreted directly as depositional values. For samples taken in older sediment, the measured concentrations include an in situ component that accrued after deposition. Since TCN production rates are strongly depth-dependent, we constructed depth histories of each sample to calculate the in situ component. For all non-modern samples, this required: 1) discretizing the overlying stratigraphy into rapidly-emplaced packages, 2) applying independent chronology in each discrete package to obtain time intervals over which the sample resided at different depths, 3) summing the decay-corrected concentrations for all time intervals using Equation 1 of Hidy et al. (2010) and subtracting this quantity from the measured concentrations, and 4) correcting the remaining concentrations for decay over a time equal to the sum of all time intervals (total time since deposition). Thicknesses for each deposit were based on observed paleosols between channel-belt sections, and deposition of each package is assumed instantaneous. Surface erosion between depositional events is considered negligible as all sample sites were collected on the relatively stable coastal plain. In all cases, the stratigraphy overlying and containing each sample could be modeled by up to three depositional events.

Measurements from duplicate samples were combined unless 1) the samples were of different grain sizes, or 2) ^{26}Al was measured in some, but not all of the duplicates. Depositional concentrations for samples of different grain sizes are not combined because of their potential to represent slightly different source areas in the upstream catchment, and thus slightly different average denudation rates. Several studies have documented a discernable inversely proportional relationship of grain size to depositional TCN

concentration (Brown et al., 1998; Matmon et al., 2003; Belmont et al., 2007; Wittmann et al., 2011a; Codilean et al., 2012; Aguilar et al., 2013). Duplicate samples for which the same isotopes were not measured were not combined in order to remove bias in calculating depositional $^{26}\text{Al}/^{10}\text{Be}$ values.

A.2.2.3. Sediment Recycling with ^{26}Al and ^{10}Be

In the Trinity catchment, mass calculations of sediment excavation on the outer coastal plain during valley formation over the last interglacial period suggest that excavated stored sediment could vary between 12-34% of the total bedload as sea level falls (Garvin, 2008). In order to assess whether there is a potential coastal plain mixing effect on our TCN measurements, a pair of samples in the Low Deweyville unit within the Trinity catchment (representing low-stand sea level during the last glacial maximum) were collected, one near the hinge zone and another 105 km downstream on the distal coastal plain. If these samples yield similar depositional ^{10}Be and ^{26}Al concentrations, then we can assume that sediment recycling from the coastal plain has a negligible effect on our measurements of up-catchment average denudation rates as suggested by Wittmann and Von Blanckenburg (2009) and Wittmann et al. (2009); if the concentrations are significantly different, then this experiment can help quantify this recycling effect.

Near the surface, ^{26}Al and ^{10}Be are produced at a constant ratio (~ 6.75), and over time their expected ratio and concentrations from material derived solely from vertical surficial erosion are predicted to plot within the “erosion banana” on a burial plot (Fig. A.2.2). However, if TCN production is shut off or greatly diminished during temporary sediment storage, then the ratio will deviate from the expected value as the two isotopes

decay; this deviance can be quantified as an apparent burial age for the sediment (Granger and Muzikar, 2001). Realistically, a discernible deviation in the $^{26}\text{Al}/^{10}\text{Be}$ isotopic pair requires a minimum burial duration of ~ 0.2 Ma; furthermore, because any recycled stored sediment with a lowered $^{26}\text{Al}/^{10}\text{Be}$ would be mixed with surficially eroded sediment from up-catchment sources at the expected $^{26}\text{Al}/^{10}\text{Be}$, any detected deviation in the measured $^{26}\text{Al}/^{10}\text{Be}$ would indicate recycling of sediment stored for durations much greater than 0.2 Ma. If the source of the stored sediment can be constrained, and its average $^{26}\text{Al}/^{10}\text{Be}$ can be assumed, then relative amounts of sediment from storage and from surficial hinterland erosion could be determined using the binary mixing algorithm (Wittmann et al., 2011b)

$$\frac{Al_d}{Be_d} = \frac{Al_{nb} \cdot (1 - f_b) + Al_b \cdot f_b}{Be_{nb} \cdot (1 - f_b) + Be_b \cdot f_b}, \quad (6)$$

where the subscripts d , nb , and b describe isotopic concentrations (atoms $\text{g}^{-1} \text{a}^{-1}$) that are depositional, from sources that were not buried (i.e., up-catchment), and from sources that experienced burial, respectively, and f_b is the fraction of total sediment from a significantly buried source. In order to remove the buried component from our depositional ^{10}Be concentrations (Be_d), we solve for Be_{nb} using

$$\frac{Al_{nb}}{Be_{nb}} = 6.75, \quad (7)$$

$$\frac{Al_b}{Be_b} = R_b, \quad \text{and} \quad (8)$$

$$f_b = \frac{6.75 - \frac{Al_d}{Be_d}}{6.75} \quad (9)$$

where up-catchment $^{26}\text{Al}/^{10}\text{Be}$ is assumed to be at the production ratio (based on the high catchment-wide denudation rates observed for these systems), the buried sediment has some average ratio R_b (estimated value of 3 for this work based on measurements of pre-Lissie sediment; see Table A.2.1), and the buried fraction is weighted by the difference between the depositional ratio and the production ratio. Finally, we assume the average buried ^{10}Be concentration is

$$Be_b = Be_{av} \cdot \exp(-\lambda_{Be} \cdot t) \quad (10)$$

where Be_{av} is estimated as the average depositional ^{10}Be observed in each catchment (atoms $\text{g}^{-1} \text{a}^{-1}$), and t is the time (a) taken for $^{26}\text{Al}/^{10}\text{Be}$ to decrease from the production ratio to R_b , which is calculated from Equation 6 of Granger and Muzikar (2001). Although this assumes that the depositional concentrations in the storage are similar to those during the Late Pleistocene (only true if denudation rates, on average, were similar for that period), the calculated correction is insensitive to the value for Be_{av} chosen due to the long time taken for the production ratio to decay to 3 (~ 2.4 Ma). Finally, the flux of mass derived from buried sources can be estimated by substituting N in Equation 4 with the value for Be_{nb} calculated from equations 6-10, and multiplying the resulting flux by the factor

$$\frac{f_b}{(1 - f_b)} \quad (11)$$

It should be noted, however, that equation 11 estimates the instantaneous storage flux at time of sample deposition (i.e. the relative amount of stored sediment in the acquired sample). It does *not* represent the time-averaged flux calculated from the up-catchment denudation rate. Thus, it likely not appropriate to add the storage flux signal to that of the up-catchment flux in order to obtain a total sediment flux.

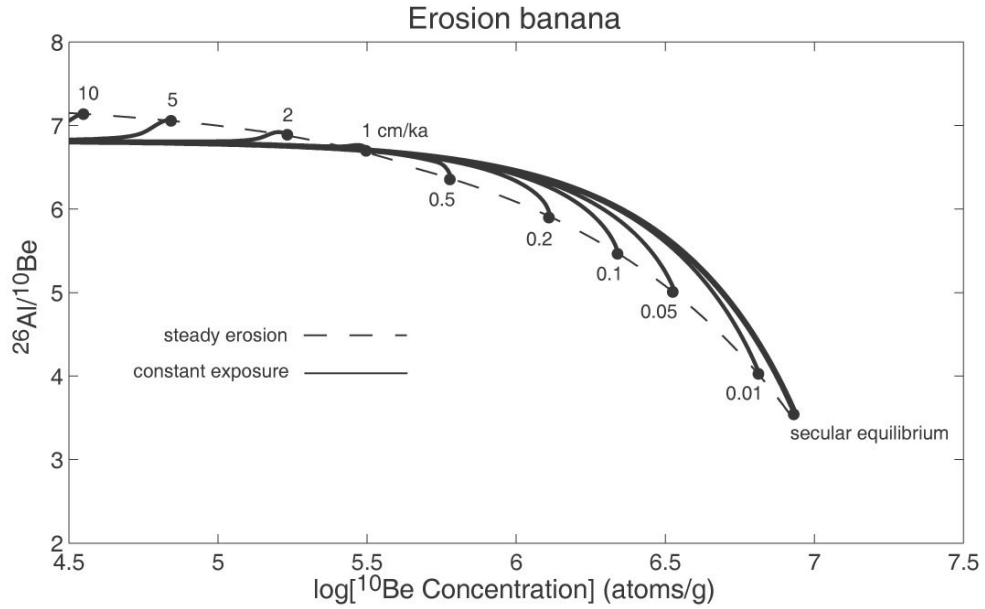


Figure A.2.2. This is an example of a surface erosion “banana” showing equilibrium values for $^{26}\text{Al}/^{10}\text{Be}$ at different erosion rates. For catchment-wide erosion rates $>1 \text{ cm ka}^{-1}$ (pertinent to this study) the equilibrium $^{26}\text{Al}/^{10}\text{Be}$ does not fall below, and is approximately equal to, the spallogenic production production ratio (~ 6.75). Faster erosion rates produce higher equilibrium ratios due to the increased importance of muogenic production with depth. Samples that represent catchments only eroding vertically, with instantaneous transport downstream, should plot somewhere along one of the curves in the erosion banana. If samples plot below the banana, this implies the sediment has experienced burial en route to its current emplacement.

A.2.3. ^{10}Be Depth Profiles

Depth profiles of ^{10}Be through a column of sediment can be used to model exposure age, surficial erosion (or aggradation) rate, and depositional (inherited) ^{10}Be concentration of a given sediment package (Anderson et al., 1996); several sedimentological conditions, however, need be met for a depth profile to produce a viable age. The sampled zone of the sediment package must 1) have been deposited relatively quickly, thus limiting exposure to cosmic flux during accumulation, 2) have been vertically well-mixed at time of deposition, so the ^{10}Be concentration over the sampled depth was approximately constant at $t=0$, 3) not be vertically mixed since deposition, and 4) underlie a surface that can be approximated with a continuous steady-state erosion or aggradation rate. In the depositional environment of the Texas coastal plain, all of these conditions can be met by careful sampling and a combination of sedimentological and geomorphic constraints. Restricting profile sampling to preserved lateral accretion sets of point-bar facies—which emplace rapidly and are likely to be well-mixed—and avoiding vertically accreted overbank and abandoned channel-fill sediment accommodates the first three requirements. The assumption of continuous, steady-state erosion or aggradation is more difficult to justify since flood deposits accrete from gradually higher flood stages in a nonlinear relationship with time. However, if the depositional age of the sediment is much greater than the total accretion time of the overbank, then the flood plain accumulation phase can be considered negligible. Choosing locations with a smooth surface morphology and spatially consistent soil thickness reduces the likelihood that episodic erosion has occurred subsequently.

Additionally, for a depth profile to produce a unique solution for both age and surface erosion rate, the sampled depth range must adequately characterize ^{10}Be production from both the muogenic and nucleogenic production pathways (Braucher et al., 2009). This requires multiple samples both from the near surface zone where nucleogenic production dominates ($\sim 0 - 800 \text{ g cm}^{-2}$, or $\sim 0 - 4 \text{ m}$ unconsolidated material) and at a mass-depth where muogenic production dominates ($>800 \text{ g cm}^{-2}$). Unfortunately, sedimentological requirements and sampling logistics make it difficult to sample a continuous 4 m deposit on the Texas coastal plain since 1) fluvial channel-belt sand packages generally fine upward, implying incomplete mixing over the entire depth range, 2) quartz clasts in the uppermost $\sim 2 \text{ m}$ are often too fine-grained ($< 150 \mu\text{m}$) to survive the TCN chemical preparation procedure, 3) post-depositional vertical mixing via bioturbation is ubiquitous in the uppermost $\sim 1 \text{ m}$ on the coastal plain, and 4) most of the exposed sections of older sediment are restricted to cut-banks along the active stream, limiting viable sampling sites and restricting maximum sampling depth to above stream level. Where these incomplete depth profiles are the only option, additional constraints must be imposed on either age or erosion rate in order to resolve the other parameters (Hidy et al., 2010).

The ^{10}Be profiles in this work are modeled using the Matlab™ Monte Carlo-based depth profile simulator (version 1.2) of Hidly et al. (2010). Nucleogenic ^{10}Be production rates are based on the Stone (2000) after Lal (1991) scaling scheme with a reference production rate of $4.76 \text{ atoms g}^{-1} \text{ a}^{-1}$ (Stone (2000) recalibrated according to Nishiizumi et al. (2007)). Each profile is modeled with a mid-latitude neutron attenuation length of 160 g cm^{-2} (Gosse and Phillips, 2001). We reduced the muon production rates to half the

built-in theoretical values of Heisinger et al. (2002a; 2002b). This modification was implemented because a growing body of evidence suggests that the Heisinger et al. rates significantly overestimate deep muon production (Braucher et al., 2003; Balco et al., 2005; Braucher et al., 2011; Hidy et al., 2013). Furthermore, the values adopted here are supported by preliminary data from the Beacon Heights bedrock core in Antarctica that indicate Heisinger et al. (2002a; 2002b) systematically overestimate muon production by a factor of ~ 2 (pers. comm. J. Stone). Input for the ^{10}Be profiles analyzed with the Hidy et al. (2010) model along with details outlining the rationale for imposed parameter constraints are given in the following sections; model output is presented in Table A.2.3. For the depth profiles, each simulation was run until 100,000 theoretical profiles were found within a 95% confidence window based on a reduced χ^2 statistic. Bayesian probability density functions (PDFs) and cumulative distribution functions (CDFs) for parameter solutions were constructed from all simulated profiles, including ones rejected by the χ^2 cutoff, and are therefore continuous between the boundaries of the simulated parameter spaces.

Table A.2.3. Model output for depth profiles

Statistic	Age (ka)	¹⁰ Be inheritance (10 ⁴ atoms g ⁻¹)	Erosion rate (cm ka ⁻¹)
<i>Colorado profile (site 4)</i>			
mean	580	18.7	0.00
median	590	18.7	0.00
mode	550	18.9	0.00
χ ² optimum	560	18.4	0.00
χ ² ≤ 95% maximum	880	21.3	0.00
χ ² ≤ 95% minimum	320	16.1	0.00
Bayesian optimum	570	18.8	0.00
Bayesian 2σ upper	870	20.0	0.00
Bayesian 2σ lower	330	17.0	0.00
<i>Trinity profile (site 13)</i>			
mean	530	10.2	0.60
median	520	10.2	0.58
mode	390	10.2	0.48
χ ² optimum	590	10.2	0.59
χ ² ≤ 95% maximum	890	11.6	1.1
χ ² ≤ 95% minimum	280	9.40	0.34
Bayesian optimum	470	10.2	0.50
Bayesian 2σ upper	940	10.8	1.9
Bayesian 2σ lower	140	9.59	0.28

A.2.3.1. Lissie Surface, Colorado River (site 4)

The 5-sample depth profile acquired at this location was collected from an active gravel mine away ~2 km from the modern stream channel. Because of a lack of preserved sedimentary structures, fine grain size, and well-developed soil in the uppermost ~3 m, samples were collected at regular intervals over a depth range of 303-418 cm. The terrace surface here is broadly flat and undissected within a >100 m radius of the site, indicating little surface erosion has occurred following abandonment by the Colorado River. No absolute chronology existed at this site prior to this work, with only a ballpark figure from its association with other Lissie sediment whose general age is described in *Chapter 3*. Thus, in the model for this site we assume negligible erosion and stochastically sample the inheritance and age parameters over arbitrarily large ranges. (Note: there is some confusion in the published literature as to whether this particular site consists of Lissie or Beaumont sediment. Several published maps indicate a remnant island of Lissie deposits at this location (Doering, 1935; Winker, 1979; Blum and Valastro, 1994); however, the most up-to-date geologic quadrangle available from the BEG marks our site as Bay City fill of the Beaumont Formation (Proctor Jr et al., 1974). This island of Lissie material was likely lost somewhere in the compilation of the more regional BEG maps.)

A.2.3.2. Lissie Surface, Trinity River (site 13)

Here, a 3-sample profile was collected along the Trinity River from an active cut bank. Samples were collected between depths of 408-713 cm; none were collected shallower than ~400 cm since grain sizes were prohibitively small. The sampled section exhibited intact sedimentary structures throughout the exposed cut bank and was capped by a moderately-developed ~1.5 m thick soil. The surface above this section was

moderately vegetated with deep-rooted deciduous trees that penetrated the entire ~8 m section; however, care was taken during sampling to avoid roots, and the quality of sediment structure preservation in their vicinity indicated negligible bioturbation. The terrace surface here gently sloped from a side-drainage parallel to the main stem Trinity River to an intact and flat pad approximately 25 m landward from the sampled cut bank. Projections indicated that ~3 m of surface material was removed since original emplacement. Thus, for the depth profile model at this site we stochastically sampled the inheritance, age, and erosion rate parameters over arbitrarily large ranges, and constrained the net erosion to 2.5 -3.5 m.

A.2.4. OSL Chronology

A singular sample collected for Optically Stimulated Luminescence was acquired within the sampled range of the ^{10}Be depth profile collected at site 13. Here, a sample collected at ~4.9 m depth was sent to the Utah State University Luminescence Lab where 25 aliquots from the sample were analyzed using the single-aliquot regenerative-dose procedure of Murray and Wintle (2000). The equivalent dose was calculated to 186 ± 41 Gy; the equivalent ambient dose rate for the sample was 0.36 ± 0.06 Gy ka^{-1} with a cosmogenic component calculated to be ~ 0.11 Gy ka^{-1} after Prescott and Hutton (1994), and yielded an age of 520 ± 150 ka. Because the sample equivalent dose was very close to saturation, this value is considered a minimum age.

A.2.5. Matlab Codes for Computing Depositional Concentrations

Listed below are Matlab scripts to calculate depositional concentrations of ^{10}Be and ^{26}Al from their measured values and step-wise depth history for a particular location. The primary input function is *calculate_init_conc.m*, and internally calls three additional scripts that were created or modified for this work and are listed below. The muon production rate function, *depos_muonproduction.m*, is modified after (Balco et al., 2008), and based on half the Heisinger et al. (2002a; 2002b) production rates.

Codes used to calculate depositional concentrations:

- 1) *calculate_init_conc.m* (primary) ✓
- 2) *depositional_concs.m* ✓
- 3) *depos_stone2000.m* ✓
- 4) *depos_muonproduction.m* ✓

A.2.5.1. *calculate_init_conc.m*

```
function out = calculate_init_conc(datafile, muontype)

data = load(datafile);

CNEF = data(:,1);
lat = data(:,2);
elev = data(:,3)*1000;
depth1 = data(:,4);
depth2 = data(:,5);
depth3 = data(:,6);
thick = data(:,7);
age1 = data(:,8)*1000;
age1err = data(:,9);
sig1 = data(:,10);
age2 = data(:,11)*1000;
age2err = data(:,12);
sig2 = data(:,13);
age3 = data(:,14)*1000;
age3err = data(:,15);
sig3 = data(:,16);
meas_conc = data(:,17);
meas_conc_1serr = data(:,18);
datatype = data(:,19);
density = data(:,20);

erate = 0.000; %cm/a

for k = 1:length(CNEF);

    %calculate production at duration of lowest depth
    prod1 = zeros(length(CNEF),1);
    delprod1 = zeros(length(CNEF),1);

    if isnan(depth2(k)) == 1
        prod1(k) =
depositional_concs(lat(k),elev(k),density(k),depth1(k),thick(k),erate,age1(k),datatype(k),muontype);
        delprod1(k) =
depositional_concs(lat(k),elev(k),density(k),depth1(k),thick(k),erate,age1(k).*age1err(k)./sig1(k),datatype(k),muontype);

    else
        prod1(k) =
depositional_concs(lat(k),elev(k),density(k),depth1(k),thick(k),erate,age1(k) - age2(k),datatype(k),muontype);
        delprod1(k) =
depositional_concs(lat(k),elev(k),density(k),depth1(k),thick(k),erate,((age1(k).*age1err(k)./sig1(k))^2+(age2(k).*age2err(k)./sig2(k))^2)^0.5,datatype(k),muontype);
```

```

end

%calculate production at duration of depth2
prod2 = zeros(length(CNEF),1);
delprod2 = zeros(length(CNEF),1);

if isnan(age2(k)) == 1
    prod2(k) = 0;
    delprod2(k) = 0;

else if isnan(depth3(k)) == 1
    prod2(k) =
depositional_concs(lat(k),elev(k),density(k),depth2(k),thick(k),0,age2(k)
),datatype(k),muontype);
    delprod2(k) =
depositional_concs(lat(k),elev(k),density(k),depth2(k),thick(k),0,age2(k)
).*age2err(k)./sig2(k),datatype(k),muontype);

else
    prod2(k) =
depositional_concs(lat(k),elev(k),density(k),depth2(k),thick(k),0,age2(k)
) - age3(k),datatype(k),muontype);
    delprod2(k) =
depositional_concs(lat(k),elev(k),density(k),depth2(k),thick(k),0,((age2
(k).*age2err(k)./sig2(k))^2+(age3(k).*age3err(k)./sig3(k))^2)^0.5,dataty
pe(k),muontype);

end
end

%calculate production at final depth3
prod3 = zeros(length(CNEF),1);
delprod3 = zeros(length(CNEF),1);

if isnan(age3(k)) == 1
    prod3(k) = 0;
    delprod3(k) = 0;

else
    prod3(k) =
depositional_concs(lat(k),elev(k),density(k),depth3(k),thick(k),0,age3(k)
),datatype(k),muontype);
    delprod3(k) =
depositional_concs(lat(k),elev(k),density(k),depth3(k),thick(k),0,age3(k)
).*age3err(k)./sig3(k),datatype(k),muontype);

end

%subtract cumulative production from measured
prod_sub = zeros(length(CNEF),1);
delprod_sub = zeros(length(CNEF),1);

```

```

    prod_sub(k) = meas_conc(k) - prod1(k) - prod2(k) - prod3(k);
    delprod_sub(k) = ((meas_conc_1serr(k).*meas_conc(k))^2 +
delprod1(k)^2 + delprod2(k)^2 + delprod3(k)^2)^0.5;

    %calculate decay term
    decay_term = zeros(length(CNEF),1);
    deldecay_term = zeros(length(CNEF),1);

    if datatype(k) == 1 %for Be
        decay = log(2)/1378000;
    else if datatype(k) == 2 %for Al
        decay = log(2)/720000;
    end
    end

    decay_term(k) = exp(-decay*age1(k));
    deldecay_term(k) = decay_term(k) - exp(-decay*(age1(k) +
age1(k).*age1err(k)./sig1(k)));

    %calculate inherited value with error

    inherited(k) = prod_sub(k)./exp(-decay*age1(k));
    inherited_err(k) = ((delprod_sub(k)./prod_sub(k))^2 +
(deldecay_term(k)./decay_term(k))^2)^0.5;

end

format longG

out = [CNEF meas_conc inherited' (inherited_err.*inherited)'];

end

```

A.2.5.2. depositional_concs.m

```

function out =
depositional_concs(lat,elev,dens,depth,thick,e_rate,time,datatype,muonty
pe)

%decay constants (1/s)

if datatype == 1 %for Be
    decay = log(2)/1378000;
else if datatype ==2 %for Al
    decay = log(2)/720000;
end
end
end

```

```

%neutron attenuation length (g/cm^2)

neutron_atten = 160;

%spallogenic production (atoms/g/a)

refspalprod = 4.76;
ratio_init = 6.75;

%at site

if datatype == 1 %for Be
    spallprodrate = depos_stone2000(lat, elev).*refspalprod;
else if datatype == 2 %for Al
    spallprodrate =
depos_stone2000(lat,elev).*refspalprod*ratio_init;
    end
end

%muogenic production at current sample depth from (Heisinger 2002), Stone
pers. comm.,
%and none (atoms/g/a)

if muontype == 0 %no muons
    muonprod = 0;
else if muontype == 1 %Use pers. comm. from Stone
    if datatype == 1
        muonprod = depos_muonproduction(depth.*dens,elev,1)/2;
    else if datatype == 2
        muonprod = depos_muonproduction(depth.*dens,elev,0)/2;
    end
    end
else if muontype == 2 %Use Heisinger otherwise
    if datatype == 1
        muonprod = depos_muonproduction(depth.*dens,elev,1);
    else if datatype == 2
        muonprod = depos_muonproduction(depth.*dens,elev,0);
    end
    end
end
end

%build production equation
%=====
===
%=====
===

%general erosion and density corrected lambda term to simplify
production
%equation

function lambda_gen = lambda(erosion_rate)

```

```

        lambda_gen = decay + (erosion_rate.*dens)./(neutron_atten);
    end

%general exponential term for spallogenic concentration buildup

    function buildup_exp = buildup(dpth,erosion_rate)
        buildup_exp = (spallprodrate*exp((-
dpth.*dens)/neutron_atten))./...
            (lambda(erosion_rate)).*...
            (1-exp(-lambda(erosion_rate).*time));
    end

%generic exponential term for depth-integrated spallogenic concentration
buildup; this
%is needed since we have sampled over depth

    function buildup_exp_int = buildup_int(dpth,erosion_rate)
        buildup_exp_int = (spallprodrate.*neutron_atten./dens.*exp((-
dpth.*dens)/neutron_atten))./...
            (lambda(erosion_rate)).*...
            (exp(-lambda(erosion_rate).*time)-1);
    end

out = (buildup_int(depth+thick,e_rate) -
buildup_int(depth,e_rate))/thick + muonprod/decay*(1-exp(-decay*time));

end

```

A.2.5.3. depos_stone2000.m

```

function scal = depos_stone2000(lat, elev)

press = 1013.25*exp((-0.03417/0.0065)*(log(288.15)-log(288.15-
0.0065*elev)));
if size(lat,2) > 1
    error('Input lat must be a column vector.')
end
if ~isequal(size(lat), size(press))
    error('Inputs lat and press must have the same size.')
end
npress = numel(press);
lat = abs(lat);
lat(lat>60) = 60;

stonecoeff = [31.8518    34.3699    40.3153    42.0983    56.7733
69.0720    71.8733
    250.3193    258.4759    308.9894    512.6857    649.1343    832.4566
863.1927
    -0.083393    -0.089807    -0.106248    -0.120551    -0.160859    -0.199252    -
0.207069

```

```

    7.4260e-5  7.9457e-5  9.4508e-5  1.1752e-4  1.5463e-4  1.9391e-4
2.0127e-4
    -2.2397e-8 -2.3697e-8 -2.8234e-8 -3.8809e-8 -5.0330e-8 -6.3653e-8 -
6.6043e-8];

latgrid = 0:10:60;
nlatgrid = numel(latgrid);

scalgrid = nan(npress, nlatgrid);
for k = 1:nlatgrid
    scalgrid(:,k) = stonecoeff(1,k) + stonecoeff(2,k)*exp(press/-150) +
stonecoeff(3,k)*press + stonecoeff(4,k)*(press.^2) +
stonecoeff(5,k)*(press.^3);
end

scal = nan(npress,1);
for k = 1:npress
    scal(k) = interp1(latgrid, scalgrid(k,:), lat(k));
end

```

A.2.5.4. depos_muonproduction.m

```

function [total fastmuons negmuons] =
depos_muonproduction(massdepth,elev,isotope)

%convert elevation to atmospheric pressure

h = 1013.25*exp((-0.03417/0.0065)*(log(288.15)-log(288.15-
0.0065*elev)));

%remember depth is in mass depth here

z = massdepth;

%The following is modified from P_mu_total.m of Balco 2006 code:

% remember what direction the z vector came in

in_size = size(z);

% standardize direction

if size(z,1) > 1
    z = z';
end

% figure the atmospheric depth in g/cm2

H = (1013.25 - h).*1.019716;

```



```

% find the vertical flux at SLHL

a = 258.5*(100.^2.66);
b = 75*(100.^1.66);

phi_vert_slhl = (a./((z+21000).*((z+1000).^1.66) + b)).*exp(-5.5e-6 .*
z);

% The above expression is only good to 2e5 g/cm2. We don't ever consider
production
% below that depth. The full-depth scheme appears in the comments below.
% ----- begin full-depth flux equations -----
%phiz_1 = (a./((z+21000).*((z+1000).^1.66) + b)).*exp(-5.5e-6 .* z);
%phiz_2 = 1.82e-6.*((121100./z).^2).*exp(-z./121100) + 2.84e-13;
%out(find(z<200000)) = phiz_1(find(z<200000));
%out(find(z>=200000)) = phiz_2(find(z>=200000));
% ----- end full-depth flux equations -----

% find the stopping rate of vertical muons at SLHL
% this is done in a subfunction Rv0, because it gets integrated later.

R_vert_slhl = Rv0(z);

% find the stopping rate of vertical muons at site

R_vert_site = R_vert_slhl.*exp(H./LZ(z));

% find the flux of vertical muons at site
phi_vert_site = nan(1,length(z));
for a = 1:length(z);
    % integrate
    % ends at 200,001 g/cm2 to avoid being asked for an zero
    % range of integration --
    % get integration tolerance -- want relative tolerance around
    % 1 part in 10^4.
    tol = phi_vert_slhl(a) * 1e-4;
    [temp,fcnt] = quad(@ (x) Rv0(x).*exp(H./LZ(x)),z(a),(2e5+1),tol);
    % second variable assignment here to preserve fcnt if needed
    phi_vert_site(a) = temp;
end;

% invariant flux at 2e5 g/cm2 depth - constant of integration
% calculated using commented-out formula above
phi_200k = (a./((2e5+21000).*((2e5+1000).^1.66) + b)).*exp(-5.5e-6 .*
2e5);
phi_vert_site = phi_vert_site + phi_200k;

% find the total flux of muons at site

% angular distribution exponent
nofz = 3.21 - 0.297.*log((z+H)./100 + 42) + 1.21e-5.*(z+H);
% derivative of same
dndz = (-0.297./100)./((z+H)./100 + 42) + 1.21e-5;

```

```

phi_temp = phi_vert_site .* 2 .* pi ./ (nofz+1);

% that was in muons/cm2/s
% convert to muons/cm2/yr

phi = phi_temp*60*60*24*365;

% find the total stopping rate of muons at site

R_temp = (2.*pi./(nofz+1)).*R_vert_site ...
    - phi_vert_site.*(-2.*pi.*((nofz+1).^(-2))).*dndz;

% that was in total muons/g/s
% convert to negative muons/g/yr

R = R_temp*0.44*60*60*24*365;

% Now calculate the production rates.

% Depth-dependent parts of the fast muon reaction cross-section

Beta = 0.846 - 0.015 .* log((z./100)+1) + 0.003139 .*
(log((z./100)+1).^2);
Ebar = 7.6 + 321.7.*(1 - exp(-8.059e-6.*z)) + 50.7.*(1-exp(-5.05e-
7.*z));

aalpha = 0.75;
if isotope == 1 % Be10
    % internally defined constants
    sigma0 = (0.094e-27/1.096)./(190.^aalpha);
    % fast muon production
    fastmuons = phi.*Beta.*(Ebar.^aalpha).*sigma0.*2.006e22;
    % negative muon capture
    negmuons = R.*(0.704*0.1828*0.0043)/1.096;
else % Al26
    % internally defined constants
    sigma0 = (1.41e-27)./(190.^aalpha);
    % fast muon production
    fastmuons = phi.*Beta.*(Ebar.^aalpha).*sigma0.*1.003e22;
    % negative muon capture
    negmuons = R.*(0.296*0.6559*0.022);
end

% total

total = fastmuons + negmuons;

% -----
---
```

```

function out = Rv0(z)

% this subfunction returns the stopping rate of vertically traveling
muons
% as a function of depth z at sea level and high latitude.

a = exp(-5.5e-6.*z);
b = z + 21000;
c = (z + 1000).^1.66 + 1.567e5;
dadz = -5.5e-6 .* exp(-5.5e-6.*z);
dbdz = 1;
dcdz = 1.66.*(z + 1000).^0.66;

out = -5.401e7 .* (b.*c.*dadz - a.*(c.*dbdz + b.*dcdz))./(b.^2 .* c.^2);

% full depth calculation appears in comments below
%R_1 = -5.401e7 .* (b.*c.*dadz - a.*(c.*dbdz + b.*dcdz))./(b.^2 .*
c.^2);
%f = (121100./z).^2;
%g = exp(-z./121100);
%dfdZ = (-2.*(121100.^2))./(z.^3);
%dgdz = -exp(-z./121100)./121100;
%R_2 = -1.82e-6.*(g.*dfdZ + f.*dgdz);
%out(find(z<200000)) = R_1(find(z<200000));
%out(find(z>=200000)) = R_2(find(z>=200000));

% -----
---

function out = LZ(z)

% this subfunction returns the effective atmospheric attenuation length
for
% muons of range Z

% define range/momentum relation
% table for muons in standard rock in Groom and others 2001

data = [4.704e1 8.516e-1
5.616e1 1.542e0
6.802e1 2.866e0
8.509e1 5.698e0
1.003e2 9.145e0
1.527e2 2.676e1
1.764e2 3.696e1
2.218e2 5.879e1
2.868e2 9.332e1
3.917e2 1.524e2
4.945e2 2.115e2
8.995e2 4.418e2
1.101e3 5.534e2
1.502e3 7.712e2
2.103e3 1.088e3
3.104e3 1.599e3

```

```

4.104e3 2.095e3
8.105e3 3.998e3
1.011e4 4.920e3
1.411e4 6.724e3
2.011e4 9.360e3
3.011e4 1.362e4
4.011e4 1.776e4
8.011e4 3.343e4
1.001e5 4.084e4
1.401e5 5.495e4
2.001e5 7.459e4
3.001e5 1.040e5
4.001e5 1.302e5
8.001e5 2.129e5];

% ignore ranges bigger than 2e5 g/cm2
% 1.000e6 2.453e5
% 1.4e6 2.990e5
% 2.0e6 3.616e5
% 3.0e6 4.384e5
% 4.0e6 4.957e5
% 8.0e6 6.400e5
% 1.0e7 6.877e5
% 1.4e7 7.603e5
% 2.0e7 8.379e5
% 3.0e7 9.264e5
% 4.0e7 9.894e5
% 8.0e7 1.141e6
% 1.0e8 1.189e6];

% units are range in g cm-2 (column 2)
% momentum in MeV/c (column 1)

% deal with zero situation

z(z < 1) = 1;

% obtain momenta
% use log-linear interpolation

P_MeVc = exp(interp1q(log(data(:,2)),log(data(:,1)),log(z')));

% obtain attenuation lengths

out = 263 + 150 .* (P_MeVc./1000);

% -----
---
```

A.2.6. Input and Output for Depositional Concentration Calculations

CNEF ID	Matlab™ Input															Matlab™ Output					
	Lat. (deg)	Elev. (km)	D1 ¹ (cm)	D2 ¹ (cm)	D3 ¹ (cm)	Thick (cm)	T1 ² (ka)	T1err (dec)	σ	T2 ² (ka)	T2err (dec)	σ	T3 ² (ka)	T3err (dec)	σ	[TCN] (atoms/g)	[TCN] 1σ err (dec)	Type ³	Density (g cm ⁻³)	Dep. [TCN] (atoms/g)	Dep. [TCN] 1σ err (atoms/g)
1975	28.930	0.012	220	620	995	4	155	0.097	1	118	0.068	1	10	0.100	1	251007	0.0306	1	1.8	261714	8795
1975	28.930	0.012	220	620	995	4	155	-0.097	1	118	-0.068	1	10	-0.100	1	251007	0.0306	1	1.8	261714	-8798
1981	29.589	0.066	509	nan	nan	5	560	0.339	1	nan	nan	nan	nan	nan	nan	163424	0.0306	1	1.8	173827	23390
1981	29.589	0.066	509	nan	nan	5	560	-0.232	1	nan	nan	nan	nan	nan	nan	163424	0.0306	1	1.8	173827	-17902
2070	29.611	0.044	475	550	nan	20	8.5	0.412	1	2	0.100	1	nan	nan	nan	257180	0.0337	1	1.8	257695	8720
2070	29.611	0.044	475	550	nan	20	8.5	-0.412	1	2	-0.100	1	nan	nan	nan	257180	0.0337	1	1.8	257695	-8720
2070	29.611	0.044	475	550	nan	20	8.5	0.412	1	2	0.100	1	nan	nan	nan	1266392	0.0592	2	1.8	1272101	75687
2070	29.611	0.044	475	550	nan	20	8.5	-0.412	1	2	-0.100	1	nan	nan	nan	1266392	0.0592	2	1.8	1272101	-75687
2071	29.617	0.046	20	nan	nan	10	0.01	0.100	1	nan	nan	nan	nan	nan	nan	252415	0.0328	1	1.8	252385	8281
2071	29.617	0.046	20	nan	nan	10	0.01	-0.100	1	nan	nan	nan	nan	nan	nan	252415	0.0328	1	1.8	252385	-8281
2071	29.617	0.046	20	nan	nan	10	0.01	0.100	1	nan	nan	nan	nan	nan	nan	1489576	0.0672	2	1.8	1489375	100146
2071	29.617	0.046	20	nan	nan	10	0.01	-0.100	1	nan	nan	nan	nan	nan	nan	1489576	0.0672	2	1.8	1489375	-100146
2072	29.675	0.020	30	nan	nan	10	0.1	0.050	1	nan	nan	nan	nan	nan	nan	214702	0.0293	1	1.8	214434	6296
2072	29.675	0.020	30	nan	nan	10	0.1	-0.050	1	nan	nan	nan	nan	nan	nan	214702	0.0293	1	1.8	214434	-6296
2072	29.675	0.020	30	nan	nan	10	0.1	0.050	1	nan	nan	nan	nan	nan	nan	1167776	0.0602	2	1.8	1165995	70341
2072	29.675	0.020	30	nan	nan	10	0.1	-0.050	1	nan	nan	nan	nan	nan	nan	1167776	0.0602	2	1.8	1165995	-70341
2131	30.055	0.010	388	nan	nan	5	33	0.061	1	nan	nan	nan	nan	nan	nan	98886	0.0523	1	1.8	96917	5266
2131	30.055	0.010	388	nan	nan	5	33	-0.061	1	nan	nan	nan	nan	nan	nan	98886	0.0523	1	1.8	96917	-5266
2131	30.055	0.010	388	nan	nan	5	33	0.061	1	nan	nan	nan	nan	nan	nan	724402	0.0612	2	1.8	719966	45790
2131	30.055	0.010	388	nan	nan	5	33	-0.061	1	nan	nan	nan	nan	nan	nan	724402	0.0612	2	1.8	719966	-45791
2132	30.106	0.009	512	nan	nan	6	29	0.193	1	nan	nan	nan	nan	nan	nan	84112	0.0467	1	1.8	83465	4007
2132	30.106	0.009	512	nan	nan	6	29	-0.193	1	nan	nan	nan	nan	nan	nan	84112	0.0467	1	1.8	83465	-4007
2132	30.106	0.009	512	nan	nan	6	29	0.193	1	nan	nan	nan	nan	nan	nan	445876	0.0602	2	1.8	443281	27879
2132	30.106	0.009	512	nan	nan	6	29	-0.193	1	nan	nan	nan	nan	nan	nan	445876	0.0602	2	1.8	443281	-27882
2133	30.106	0.009	482	nan	nan	5	29	0.193	1	nan	nan	nan	nan	nan	nan	88793	0.0314	1	1.8	88022	2866
2133	30.106	0.009	482	nan	nan	5	29	-0.193	1	nan	nan	nan	nan	nan	nan	88793	0.0314	1	1.8	88022	-2866
2134	30.106	0.009	383	nan	nan	5	25	0.193	1	nan	nan	nan	nan	nan	nan	74632	0.0517	1	1.8	72757	3946
2134	30.106	0.009	383	nan	nan	5	25	-0.193	1	nan	nan	nan	nan	nan	nan	74632	0.0517	1	1.8	72757	-3946
2135	30.106	0.009	351	nan	nan	6	25	0.193	1	nan	nan	nan	nan	nan	nan	72786	0.0605	1	1.8	70277	4513
2135	30.106	0.009	351	nan	nan	6	25	-0.193	1	nan	nan	nan	nan	nan	nan	72786	0.0605	1	1.8	70277	-4513
2139	29.274	0.027	691	nan	nan	5	119	0.080	1	nan	nan	nan	nan	nan	nan	280300	0.0268	1	1.8	292020	8122
2139	29.274	0.027	691	nan	nan	5	119	-0.080	1	nan	nan	nan	nan	nan	nan	280300	0.0268	1	1.8	292020	-8124
2140	29.274	0.027	732	nan	nan	5	119	0.080	1	nan	nan	nan	nan	nan	nan	298079	0.0333	1	1.8	311178	10650
2140	29.274	0.027	732	nan	nan	5	119	-0.080	1	nan	nan	nan	nan	nan	nan	298079	0.0333	1	1.8	311178	-10651
2141	29.274	0.027	937	nan	nan	7	119	0.080	1	nan	nan	nan	nan	nan	nan	216766	0.0268	1	1.8	225846	6280
2141	29.274	0.027	937	nan	nan	7	119	-0.080	1	nan	nan	nan	nan	nan	nan	216766	0.0268	1	1.8	225846	-6281
2141	29.274	0.027	937	nan	nan	7	119	0.080	1	nan	nan	nan	nan	nan	nan	1214987	0.0687	2	1.8	1325805	94448
2141	29.274	0.027	937	nan	nan	7	119	-0.080	1	nan	nan	nan	nan	nan	nan	1214987	0.0687	2	1.8	1325805	-94463
2142	29.731	0.055	427	nan	nan	8	0.1	0.100	1	nan	nan	nan	nan	nan	nan	223303	0.0271	1	1.8	223305	6057
2142	29.731	0.055	427	nan	nan	8	0.1	-0.100	1	nan	nan	nan	nan	nan	nan	223303	0.0271	1	1.8	223305	-6057
2142	29.731	0.055	427	nan	nan	8	0.1	0.100	1	nan	nan	nan	nan	nan	nan	1388435	0.0602	2	1.8	1388499	83646
2142	29.731	0.055	427	nan	nan	8	0.1	-0.100	1	nan	nan	nan	nan	nan	nan	1388435	0.0602	2	1.8	1388499	-83646
2143	30.272	0.008	550	nan	nan	10	0.1	0.100	1	nan	nan	nan	nan	nan	nan	83873	0.0312	1	1.8	83871	2617
2143	30.272	0.008	550	nan	nan	10	0.1	-0.100	1	nan	nan	nan	nan	nan	nan	83873	0.0312	1	1.8	83871	-2617
2143	30.272	0.008	550	nan	nan	10	0.1	0.100	1	nan	nan	nan	nan	nan	nan	513463	0.0777	2	1.8	513465	39885
2143	30.272	0.008	550	nan	nan	10	0.1	-0.100	1	nan	nan	nan	nan	nan	nan	513463	0.0777	2	1.8	513465	-39885
2144	29.731	0.055	427	nan	nan	8	0.1	0.100	1	nan	nan	nan	nan	nan	nan	220090	0.0305	1	1.8	220092	6704

1 Sample depths corresponding to respective times (T1 - T3) for incremental deposition episodes

2 Depositional ages of incremental deposits above and containing sample

3 1 = ¹⁰Be sample; 2 = ²⁶Al sample

CNEF ID	Matlab™ Input															Matlab™ Output					
	Lat. (deg)	Elev. (km)	D1 ¹ (cm)	D2 ¹ (cm)	D3 ¹ (cm)	Thick (cm)	T1 ² (ka)	T1err (dec)	σ	T2 ² (ka)	T2err (dec)	σ	T3 ² (ka)	T3err (dec)	σ	[TCN] (atoms/g)	[TCN] 1σ err (dec)	Type ³	Density (g cm ⁻³)	Dep. [TCN] (atoms/g)	Dep. [TCN] 1σ err (atoms/g)
2144	29.731	0.055	427	nan	nan	8	0.1	-0.100	1	nan	nan	nan	nan	nan	nan	220090	0.0305	1	1.8	220092	-6704
2145	30.272	0.008	550	nan	nan	10	0.1	0.100	1	nan	nan	nan	nan	nan	nan	79991	0.0270	1	1.8	79989	2156
2145	30.272	0.008	550	nan	nan	10	0.1	-0.100	1	nan	nan	nan	nan	nan	nan	79991	0.0270	1	1.8	79989	-2156
2254	30.538	0.046	408	nan	nan	6	590	0.186	1	nan	nan	nan	nan	nan	nan	106314	0.0280	1	1.8	95133	14204
2254	30.538	0.046	408	nan	nan	6	590	-0.525	1	nan	nan	nan	nan	nan	nan	106314	0.0280	1	1.8	95133	-90430
2254	30.538	0.046	408	nan	nan	6	590	0.186	1	nan	nan	nan	nan	nan	nan	561269	0.0713	2	1.8	538436	154482
2254	30.538	0.046	408	nan	nan	6	590	-0.525	1	nan	nan	nan	nan	nan	nan	561269	0.0713	2	1.8	538436	-941756
2255	30.538	0.046	543	nan	nan	7	590	0.186	1	nan	nan	nan	nan	nan	nan	104073	0.0292	1	1.8	103384	10756
2255	30.538	0.046	543	nan	nan	7	590	-0.525	1	nan	nan	nan	nan	nan	nan	104073	0.0292	1	1.8	103384	-40738
2255	30.538	0.046	543	nan	nan	7	590	0.186	1	nan	nan	nan	nan	nan	nan	540383	0.0617	2	1.8	602782	120531
2255	30.538	0.046	543	nan	nan	7	590	-0.525	1	nan	nan	nan	nan	nan	nan	540383	0.0617	2	1.8	602782	-458007
2256	30.538	0.046	713	nan	nan	10	590	0.186	1	nan	nan	nan	nan	nan	nan	94214	0.0261	1	1.8	96998	8843
2256	30.538	0.046	713	nan	nan	10	590	-0.525	1	nan	nan	nan	nan	nan	nan	94214	0.0261	1	1.8	96998	-27128
2256	30.538	0.046	713	nan	nan	10	590	0.186	1	nan	nan	nan	nan	nan	nan	370723	0.0636	2	1.8	368069	87138
2256	30.538	0.046	713	nan	nan	10	590	-0.525	1	nan	nan	nan	nan	nan	nan	370723	0.0636	2	1.8	368069	-281531
2257	30.538	0.046	2674	nan	nan	10	590	0.186	1	nan	nan	nan	nan	nan	nan	13086	0.0336	1	1.8	10352	5107
2257	30.538	0.046	2674	nan	nan	10	590	-0.525	1	nan	nan	nan	nan	nan	nan	13086	0.0336	1	1.8	10352	-4859
2257	30.538	0.046	2674	nan	nan	10	590	0.186	1	nan	nan	nan	nan	nan	nan	49552	0.2051	2	1.8	17812	23516
2257	30.538	0.046	2674	nan	nan	10	590	-0.525	1	nan	nan	nan	nan	nan	nan	49552	0.2051	2	1.8	17812	-31772
2258	30.538	0.046	2674	nan	nan	10	590	0.186	1	nan	nan	nan	nan	nan	nan	13555	0.0331	1	1.8	10989	5408
2258	30.538	0.046	2674	nan	nan	10	590	-0.525	1	nan	nan	nan	nan	nan	nan	13555	0.0331	1	1.8	10989	-5064
2258	30.538	0.046	2674	nan	nan	10	590	0.186	1	nan	nan	nan	nan	nan	nan	48303	0.2646	2	1.8	15574	26602
2258	30.538	0.046	2674	nan	nan	10	590	-0.525	1	nan	nan	nan	nan	nan	nan	48303	0.2646	2	1.8	15574	-34277
2315	29.584	0.063	448	nan	nan	4	560	0.339	1	nan	nan	nan	nan	nan	nan	140361	0.0254	1	1.8	132562	23716
2315	29.584	0.063	448	nan	nan	4	560	-0.232	1	nan	nan	nan	nan	nan	nan	140361	0.0254	1	1.8	132562	-17868
2315	29.584	0.063	448	nan	nan	4	560	0.339	1	nan	nan	nan	nan	nan	nan	711905	0.0593	2	1.8	740108	240167
2315	29.584	0.063	448	nan	nan	4	560	-0.232	1	nan	nan	nan	nan	nan	nan	711905	0.0593	2	1.8	740108	-196458
2316	30.588	0.024	560	1020	nan	5	20	0.050	1	2	1.000	1	nan	nan	nan	95034	0.0297	1	1.8	94895	2853
2316	30.588	0.024	560	1020	nan	5	20	-0.050	1	2	-1.000	1	nan	nan	nan	95034	0.0297	1	1.8	94895	-2853
2316	30.588	0.024	560	1020	nan	5	20	0.050	1	2	1.000	1	nan	nan	nan	477658	0.0615	2	1.8	477045	29998
2316	30.588	0.024	560	1020	nan	5	20	-0.050	1	2	-1.000	1	nan	nan	nan	477658	0.0615	2	1.8	477045	-29998
2317	30.113	0.008	301	615	nan	6	20	0.050	1	2	1.000	1	nan	nan	nan	101215	0.0279	1	1.8	98591	2887
2317	30.113	0.008	301	615	nan	6	20	-0.050	1	2	-1.000	1	nan	nan	nan	101215	0.0279	1	1.8	98591	-2887
2317	30.113	0.008	301	615	nan	6	20	0.050	1	2	1.000	1	nan	nan	nan	517008	0.0644	2	1.8	500270	34086
2317	30.113	0.008	301	615	nan	6	20	-0.050	1	2	-1.000	1	nan	nan	nan	517008	0.0644	2	1.8	500270	-34086
2318	29.313	0.022	325	575	nan	10	35	0.050	1	5	0.100	1	nan	nan	nan	220080	0.0246	1	1.8	219341	5495
2318	29.313	0.022	325	575	nan	10	35	-0.050	1	5	-0.100	1	nan	nan	nan	220080	0.0246	1	1.8	219341	-5495
2318	29.313	0.022	325	575	nan	10	35	0.050	1	5	0.100	1	nan	nan	nan	1167347	0.0591	2	1.8	1169369	70670
2318	29.313	0.022	325	575	nan	10	35	-0.050	1	5	-0.100	1	nan	nan	nan	1167347	0.0591	2	1.8	1169369	-70670
2319	29.274	0.027	815	nan	nan	6	119	0.100	1	nan	nan	nan	nan	nan	nan	272026	0.0246	1	1.8	283982	7325
2319	29.274	0.027	815	nan	nan	6	119	-0.100	1	nan	nan	nan	nan	nan	nan	272026	0.0246	1	1.8	283982	-7327
2319	29.274	0.027	815	nan	nan	6	119	0.100	1	nan	nan	nan	nan	nan	nan	1567494	0.0562	2	1.8	1716587	100792
2319	29.274	0.027	815	nan	nan	6	119	-0.100	1	nan	nan	nan	nan	nan	nan	1567494	0.0562	2	1.8	1716587	-100838
2320	29.274	0.027	937	nan	nan	7	119	0.100	1	nan	nan	nan	nan	nan	nan	286584	0.0246	1	1.8	299970	7714
2320	29.274	0.027	937	nan	nan	7	119	-0.100	1	nan	nan	nan	nan	nan	nan	286584	0.0246	1	1.8	299970	-7716
2320	29.274	0.027	937	nan	nan	7	119	0.100	1	nan	nan	nan	nan	nan	nan	1383557	0.0651	2	1.8	1514836	102547
2320	29.274	0.027	937	nan	nan	7	119	-0.100	1	nan	nan	nan	nan	nan	nan	1383557	0.0651	2	1.8	1514836	-102583

1 Sample depths corresponding to respective times (T1 - T3) for incremental deposition episodes

2 Depositional ages of incremental deposits above and containing sample

3 1 = ¹⁰Be sample; 2 = ²⁶Al sample

A.2.7. Matlab Codes for Calculating ^{10}Be Catchment-wide Production Rate

Listed below are the Matlab scripts created to calculate a ^{10}Be catchment-wide production rate from a DEM. These scripts do not include the effects of internal topographic shielding, which may be significant in smaller, high-relief catchments. Because the codes for calculating muogenic and spallogenic ^{10}Be production are the same as those listed in A.2.6., they are not restated here. However, these codes are labeled with the prefix 'Basin' rather than 'depos' when they are called internally by the primary input function, *Basin_production.m*. This function utilizes five additional scripts that were not standard Matlab functions, or were created or modified for this work (listed below). The muon production rate function, *Basin_muonproduction.m*, is modified after (Balco et al., 2008), and based on half the Heisinger et al. (2002a; 2002b) production rates. A function to graphically display the progress of the catchment-wide production rate calculation, *progressbar.m*, was obtained from the Matlab Central File Exchange at <http://www.mathworks.com/matlabcentral/fileexchange/6922-progressbar>; the code for this function is not reproduced here.

Codes used to calculate depositional concentrations:

- 1) *Basin_production.m* (primary) ✓
- 2) *getlatelev.m* ✓
- 3) *readgisdata.m* ✓
- 4) *Basin_stone2000.m* (see A.2.6.)
- 5) *Basin_muonproduction.m* (see A.2.6.)
- 6) *Progressbar.m* (see Matlab Central File Exchange)

A.2.7.1. Basin_production.m

```
function out = Basin_production(fname)

%This function calculates a basin-wide average production rate. No
%shielding is included in the calculation. For catchments where internal
%topographic shielding is significant, this script will yield an
%over-estimate of the basin-wide average production rate.
%
%out = Basin_production(fname)
%fname = an ASCII file of a DEM exported from ArcMap using the 'raster
to
%ASCII' tool. The ASCII file should retain its header. The production
%rate is calculated for all values that are > 0. Thus, null values in
this
%file should be either negative, or zero to avoid calculating regions
%outside your catchment.
% - A. Hidy

d = readgisdata(fname);

latelev = getlatelev(d);

histresolution = 100;

[N,X] = hist(latelev(:,2),histresolution);

muonrate = zeros(histresolution,1);

for i = 1:histresolution
    muonrate(i,1) = Basin_muonproduction(0,X(1,i));
end

binvalue = N';

meanmuonrate = sum(muonrate(:,1).*binvalue(:,1))/size(latelev,1);

refprod = 4.76;

spallrate = zeros(size(latelev,1),1);

for i = 1:size(latelev,1)
    spallrate(i,1) = Basin_stone2000(latelev(i,1),latelev(i,2));
    stopBar = progressbar(i/size(latelev,1),0);
    if (stopBar)
        break; end
end

out = mean(spallrate)*refprod + meanmuonrate;
```


A.2.7.2. getlatelev.m

```
function out = getlatelev(data)

ind = find(data.data > 0);
latind = mod(ind-1,size(data.data,1))+1;

out = nan(length(ind), 2);
out(:,2) = data.data(ind);

latvec = linspace(data.yllcorner+(data.nrows-1)*data.cellsize,
data.yllcorner, data.nrows);
out(:,1) = latvec(latind);
```

A.2.7.3. readgisdata.m

```
function d = readgisdata(fname)

d = importdata(fname, ' ', 6);

for k = 1:numel(d.textdata)
    tmp = regexp(d.textdata{k}, '(\w+)\s+([0-9.-]+)', 'tokens');
    d.(tmp{1}{1}) = str2double(tmp{1}{2});
end
```


WS5_ICP Aliquot and Al spiking

This worksheet outlines the steps for collecting ICP aliquots and adding Al carrier.

Chemist: AH

Date: 02/12/07

- 1 Label one 10 ml volumetric flasks per sample (16)
- 2 Label one ICP vial with CNEF ID per sample (16)

	B32	B31	B29	B25	B17	B99	B27	B20	examples
CNEF ID	1975	1976	1977	1978	1979	1980	1981	1932	105
Sample ID	TX-06-COL-BEA-01	TX-06-COL-LIS-02	TX-06-COL-LIS-03	TX-06-COL-LIS-04	TX-06-COL-LIS-05	TX-06-COL-LIS-06	TX-06-COL-LIS-07	Blank Wk20070127	WY-96-001
Al carrier ID	4	4	4	4	4	4	4	4	ALI-carrier
Quant-EM est. Al in qtz	50	50	50	50	50	50	50	50	ppm
Volume carrier to add to smpl	0.8012	0.8037	0.8013	0.8009	0.8016	0.8056	0.8017	0.8016	ml
Volume carrier to add to vol A									ml
Volume carrier to add to vol B									ml
Tare between mass measurements									
Mass 100 ml volumetric	65.2033	66.7037	66.4906	68.8726	67.7437	67.3556	67.7301	67.0046	66.9239 g
100ml volumetric+sample+2%HCl	166.1732	167.5190	167.2272	169.6588	168.5492	168.1584	168.7082	167.8426	166.9875 g
Mass 10 ml smple pipetted to vol A	9.7684	10.0030	10.0090	10.0080	10.0012	10.0075	10.0074	10.0026	5.0000 g
100ml-10ml mass	156.3974	157.5120	157.2130	159.6465	158.5427	158.1462	158.6966	157.8353	
100-10 mass + Carrier	157.1986	158.3157	158.0143	160.4474	159.3443	158.9518	159.4983	158.6369	
Mass 5 ml Sample to Vial B	5.0575	5.0066	5.0226	5.0203	5.0046	5.0023	4.9997	5.0143	
Bring up to 10 ml by 2%HCl	10.0285	10.0302	10.0534	10.0280	10.0050	10.0441	10.0089	10.0288	
Final Mass of 100 ml vol and smpl	152.1287	153.2993	152.9804	155.4214	154.3350	153.9441	154.4923	153.6141	1.0100 g
Mass Al carrier to remaining (row 18)									1.0100 g
Unaccounted mass									0.0100 g

- 3 Get digestion vessel and cover ready, Do not wipe now.
- 4 Transfer the 90 ml sample back into vessel
- 5 Bring contents of volumetrics A and B to 10 ml
- 6 Transfer contents volumetrics to ICP vials with same number

GY July 16, 2003 update

GY May 11, 2005 updated, Take 2 Aliquots one sample. 10ml and 5 ml –then bring up to 10ml

GY Feb 2007: Take 2 Aliquots, First one, 10ml without Al carrier, to vial A. Then add ~1.0ml Al carrier to

the rest of ..about 90g, shake, take second aliquot 5ml to vial B, bring up to 10ml by 2%HCl.

WS7_Controlled Precipitate

This worksheet outlines the steps for the controlled precipitation chemistry

Chemist: ^{AH}

Date: ^{form: MM/DD/YY}

Print this page

- ₁ Evaporate "anion" elute to dryness at 125°C
- ₂ Dissolve in 10 ml of a 1:1 solution of 0.5N HCl and 2% NH₄Cl
- ₃ Transfer to 15 ml centrifuge, centrifuge for 10 minutes
- ₄ Decant into clean test tube, heat in water bath at 60°C
- ₅ Add drops of 1:1 NH₄OH:H₂O to pH=9.2 (5 drops first then single)
- ₆ Centrifuge for 15 minutes
- ₇ Check pH of liquid, if less than pH=7, redo step ₅
- ₈ Decant, save with Anion Supernate
- ₉ Wash with deionized water, vortex, centrifuge, decant
- ₁₀ Wash with deionized water, vortex, centrifuge, decant
- ₁₁ Wash with deionized water, vortex, centrifuge, decant

CNEF ID	1975	1976	1977	1978	1979	1980	1981	1932
Vessel	B32	B31	B29	B25	B17	B99	B27	B20
Sample ID	X-06-COL-BEA-0	X-06-COL-LIS-02	X-06-COL-LIS-03	X-06-COL-LIS-04	X-06-COL-LIS-05	X-06-COL-LIS-06	X-06-COL-LIS-07	Blank Wk20070127
Approx. vol. Ptte								

Comments

WS8_Cation Column Chemistry

This worksheet outlines the steps for the Cation Column Chemistry

Chemist: ^{GY/JG}

Date: ^{mm/dd/yy}

[Print this page](#)

- ₁ Dissolve in 5 ml conc. HCl and evaporate to dryness at 125°C
- ₂ Redissolve in 2.5 ml 1N HCl and 2.5 ml 0.5 N HCl
- ₃ Transfer to centrifuge tube, rinse with 1 ml 0.5N, and centrifuge

Column ID	1	2	3	4	5	6	7	8	examples
Vessel	B32	B31	B29	B25	B17	B99	B27	B20	
CNEF ID	1975	1976	1977	1978	1979	1980	1981	1932	105
Sample ID	X-06-COL-BEA-0	X-06-COL-LIS-02	X-06-COL-LIS-03	X-06-COL-LIS-04	X-06-COL-LIS-05	X-06-COL-LIS-06	X-06-COL-LIS-07	Bank Wk2007012	WY-96-001

- ₄ Pipette all of the sample into designated conditioned cation column
- ₅ Discard the eluant. Add 220 ml 0.5 N HCL (bottle C6)
- ₆ Collect eluant as Cation Supernate, add 200 ml 0.5 N HCl (bottle C7)
- ₇ Collect eluant as Be-Sample into vessels.
- ₈ Add 30 ml 1N HCl (bottle8)
- ₉ Save this as Be-sample as well.
- ₁₀ Add 100 ml 4.5 N HCl, save as Al sample.
- ₁₁
- ₁₂
- ₁₃ **CONDITION CATION COLUMN**

- (bottle C1) 100 ml 9N HCl
- (bottle C2) 50 ml 4.5 N HCl
- (bottle C3) 50 ml 1 N HCl
- (bottle C4) 50 ml water
- (bottle C5) 100 ml 0.5 N HCl

WS9_Be Sample Chemistry

This worksheet outlines the steps to prepare the BeO sample

Chemist: ^{AH}

Date: ^{form: mm/dd/yy}

Print this page

- ₁ Evaporate Be Sample from column in wiped digestion vessels at 125°C
- ₂ Add 2-5 ml 20% perchloric and evaporate at 200°C
- ₃ Again, add 2-5 ml 20% perchloric and evaporate at 200°C
- ₄ Dissolve sample in 10 ml of 0.5 N HCl (optima grade)
- ₅ Transfer to 15 ml centrifuge tube
- ₆ Centrifuge and decant into clean centrifuge tube
- ₇ Heat centrifuge tubes in water bath at 60°C
- ₈ Precipitate Be(OH)₂ using Matheson ultimate grade ammonia gas
Gently bubble NH₃ with clean pipet tip on hose
for ca.15 bubbles, or ca. 8-12 sec until ppt forms
Optimum pH=9.2; 1N HCl may be added
- ₉ Centrifuge 15 min., decant (save and redo ₈ if pH of liquid is < 8)
- ₁₀ Wash with water, vortex, centrifuge for 10 min, and decant
- ₁₁ Record mass quartz vials, label, and place them in furnace holder

CNEF ID	1975	1976	1977	1978	1979	1980	1981	1932	<small>105</small>
Vessel	B32	B31	B29	B25	B17	B99	B27	B20	
Sample ID	X-06-COL-BEA-0	X-06-COL-LIS-0	X-06-COL-LIS-0	X-06-COL-LIS-0	X-06-COL-LIS-0	X-06-COL-LIS-0	X-06-COL-LIS-0	ank Wk2007012	<small>WY-96-001</small>
Mass Qtz Vial	2.4753	2.4343	2.4961	2.4536	2.5174	2.5048	2.4699	2.314	<small>2.1400 g</small>
Mass Vial+Spl	2.476	2.4352	2.4968	2.4541	2.5178	2.5055	2.4701	2.3144	<small>2.1410 g</small>
Mass Spl	0.0007	0.0009	0.0007	0.0005	0.0004	0.0007	0.0002	0.0004	<small>1 mg</small>

- ₁₂ Add 1 small drop of water with micropipet, slurry precipitate
- ₁₃ Transfer sample into quartz vial, cover with alumina vial
- ₁₄ Heat in oven at 120°C for 2-3 hours
- ₁₅ Let cool and scrape sample down from walls of quartz tube
- ₁₈ Place in furnace. Convert to BeO in furnace at 850°C for minimum 1 hr
- ₁₉ Determine mass of vial + sample

WS10_AI Sample Chemistry

This worksheet outlines the steps to prepare the Al oxide sample

Chemist:

Date:

[Print this page](#)

- 1 Evaporate Al Sample from column in wiped teflon vessel at 125°C
- 2 Dissolve sample in 10 ml of 0.5 N HCl (optima grade)
- 3 Transfer to 15 ml centrifuge tube
- 4 Centrifuge and decant into clean centrifuge tube
- 5 Heat centrifuge tubes in water bath at 60°C
- 6 Precipitate Al(OH)₃ using 50% NH₃OH (drops: 25, 5, 5, 3, 2...)
Optimum pH=6.3; 1N HCl may be added
- 7 Centrifuge 15 min., decant (save and redo 6 if pH of liquid is < 8)
- 8 Wash with water, vortex, centrifuge for 10 min, and decant
- 9 Record mass quartz vials, label, and place them in furnace holder

CNEF ID	1975	1976	1977	1978	1979	1980	1981	1932	
Sample ID	X-06-COL-BEA-0	X-06-COL-LIS-02	X-06-COL-LIS-03	X-06-COL-LIS-04	X-06-COL-LIS-05	X-06-COL-LIS-06	X-06-COL-LIS-07	Blank Wk20070127	105
Mass Qtz Vial	2.4574	2.5043	2.4637	2.5275	2.5418	2.4731	2.5162	2.5348	WY-96-001
Mass Vial+Spl	2.4738	2.5145	2.4762	2.5395	2.5532	2.4833	2.531	2.5356	2.1400 g
Mass Spl	0.0164	0.0102	0.0125	0.012	0.0114	0.0102	0.0148	0.0008	2.1410 g
									1 mg

- 10 Add 1 small drop of water with micropipet, slurry precipitate
- 11 Transfer sample into quartz vial, cover with alumina vial
- 12 Heat in oven at 120°C for 2-3 hours
- 13 Let cool and scrape sample down from walls of quartz tube
- 14 Convert to Al₂O₃ in furnace at 950°C for minimum of 1 hr
- 15 Determine mass of vial + sample

WS5_ICP Aliquot and Al spiking

This worksheet outlines the steps for collecting ICP aliquots and adding Al carrier.

Chemist: ^{AH}

Date: ^{form: 02/17/01}

- 1 Label one 10 ml volumetric flasks per sample (16)
- 2 Label one ICP vial with CNEF ID per sample (16)

	A1/B9	A2/B10	A3/B11	A4/B12	A5/B13	A6/B14	A7/B15	B99	examples
CNEF ID	2125	2126	2127	2128	2129	2130	2131	2080	105
Sample ID	07-TRI-DEWH-13	07-TRI-DEWH-14	07-TRI-DEWH-15	07-TRI-DEWH-16	07-TRI-DEWH-17	07-TRI-DEWH-18	07-TRI-DEWH-19	blank for 2008011	WY-96-001
Al carrier ID									ALI-carrier
Quant-EM est. Al in qtz									ppm
Volume carrier to add to smpl									ml
Volume carrier to add to vol A									ml
Volume carrier to add to vol. B									ml
Tare between mass measurements									
Mass 100 ml volumetric	67.1822	67.7947	66.9346	68.8736	65.2044	67.1377	67.7320	67.0059	66.9239 g
100ml volumetric+sample+2%HCl	168.1191	168.6739	167.8336	170.3888	166.1870	167.9573	168.7183	167.8155	166.9875 g
Mass 10 ml smple pipetted to vol A	10.0042	10.0026	10.0017	10.0149	10.0138	10.0018	10.0018	10.0056	10.0000 g
Mass 5 ml Sample to Vial B	5.0001	5.0047	5.0023	5.0009	5.0093	5.0085	5.0099	5.0118	5.0000g
Bring up to 10 ml by 2%HCl	10.0057	10.0069	10.0084	10.0055	10.0089	10.0082	10.0343	9.9960	10.0000g
Final Mass of 100 ml vol and smple	153.1143	153.5634	152.8193	155.3743	151.1574	152.9325	153.7004	152.7916	150.0100 g
Mass Al carrier to remaining (row 18)									1.0100 g
Unaccounted mass	0.0005	0.1032	0.0103	0.0013	0.0065	0.0145	0.0062	0.0065	0.0100 g

- 3 Get digestion vessel and cover ready, Do not wipe now.
- 4 Transfer the 90 ml sample back into vessel
- 5 Bring contents of volumetrics A and B to 10 ml
- 6 Transfer contents volumetrics to ICP vials with same number

GY July 16, 2003 update

GY May 11, 2005 updated, Take 2 Aliquots one sample. 10ml and 5 ml –then bring up to 10ml

GY Feb 2007: Take 2 Aliquots, First one, 10ml without Al carrier, to vial A. Then add ~1.0ml Al carrier to

the rest of ..about 90g, shake, take second aliquot 5ml to vial B, bring up to 10ml by 2%HCl.

WS6_Anion Column Chemistry

This worksheet outlines the steps for the Anion Column Chemistry (2ml size small column)

Chemist: AH

Date: 07/02/08

If we don't need any AI-26 data, we could skip Step WS5.

- ₁ Evaporate 20 ml to dryness at 100-120°C (will take at least 3 hrs)
- ₂ Dissolve in 10 ml 9N HCl (let stand for several hours)
- ₃ Transfer to 15 ml centrifuge tubes, rinse digestion vessels with 9N HCl to bring volume in tube to 10 ml
- ₄ Centrifuge at 1500 rpm or higher for minimum of 10 minutes
- ₅ Allow any 9 N HCl in columns to drain out; discard

Column ID	A	B	C	D	E	F	G	H	
Vessel	A1/B9	A2/B10	A3/B11	A4/B12	A5/B13	A6/B14	A7/B15	B99	AnionColumnID
CNEF ID	2125	2126	2127	2128	2129	2130	2131	2080	105
Sample ID	07-TRI-DEWH-13	07-TRI-DEWH-14	07-TRI-DEWH-15	07-TRI-DEWH-16	07-TRI-DEWH-17	07-TRI-DEWH-18	07-TRI-DEWH-19	blank for 2008011	WY-96-001

- ₆ With stopcock closed, pipet sample (avoid residue) onto 2ml size columns.
- ₇ Collect sample in same 300 ml teflon vessel.
- ₈ Elute with 10 ml 9 N HCl, and collect that, close stopcock
- ₉ 5 ml 4.5 N HCl, collect Anion Supernate in labeled 10 ml bottle
- ₁₀ 10 ml 1 N HCl, collect Anion Supernate
- ₁₁ 50 ml deionized water. Discard.
- ₁₂ **CONDITION ANION COLUMN**

(bottle A1) 10 ml 1N HCl, discard
 (bottle A2) 10 ml 4.5 N HCl, discard
 (bottle A3) 10 ml 9 N HCl, discard, but retain acid approx. 2 mm above resin

Comments

WS8_Cation Column Chemistry

This worksheet outlines the steps for the Cation Column Chemistry

Chemist: ^{GY/JG}

Date: ^{mm/dd/yy}

Print this page

- ₁ Dissolve in 5 ml conc. HCl and evaporate to dryness at 125°C
- ₂ Redissolve in 2.5 ml 1N HCl and 2.5 ml 0.5 N HCl
- ₃ Transfer to centrifuge tube, rinse with 1 ml 0.5N, and centrifuge

Column ID	1	2	3	4	5	6	7	8	examples
Vessel	A1/B9	A2/B10	A3/B11	A4/B12	A5/B13	A6/B14	A7/B15	B99	
CNEF ID	2125	2126	2127	2128	2129	2130	2131	2080	105
Sample ID	07-TRI-DEWH-13	07-TRI-DEWH-14	07-TRI-DEWH-15	07-TRI-DEWH-16	07-TRI-DEWH-17	07-TRI-DEWH-18	07-TRI-DEWH-19	Blank for 2008011	WY-96-001

- ₄ Pipette all of the sample into designated conditioned cation column
- ₅ Discard the eluant. Add 220 ml 0.5 N HCL (bottle C6)
- ₆ Collect eluant as Cation Supernate, add 200 ml 0.5 N HCl (bottle C7)
- ₇ Collect eluant as Be-Sample into vessels.
- ₈ Add 30 ml 1N HCl (bottle8)
- ₉ Save this as Be-sample as well.
- ₁₀ Add 100 ml 4.5 N HCl, save as Al sample.
- ₁₁
- ₁₂
- ₁₃ **CONDITION CATION COLUMN**

- (bottle C1) 100 ml 9N HCl
- (bottle C2) 50 ml 4.5 N HCl
- (bottle C3) 50 ml 1 N HCl
- (bottle C4) 50 ml water
- (bottle C5) 100 ml 0.5 N HCl

WS10_AI Sample Chemistry

This worksheet outlines the steps to prepare the Al oxide sample

Chemist: ^{AH}

Date: ^{form: mm/dd/yy}

[Print this page](#)

- ₁ Evaporate Al Sample from column in wiped teflon vessel at 125°C
- ₂ Dissolve sample in 10 ml of 0.5 N HCl (optima grade)
- ₃ Transfer to 15 ml centrifuge tube
- ₄ Centrifuge and decant into clean centrifuge tube
- ₅ Heat centrifuge tubes in water bath at 60°C
- ₆ Precipitate Al(OH)₃ using 50% NH₃OH (drops: 25, 5, 5, 3, 2...)
Optimum pH=6.3; 1N HCl may be added
- ₇ Centrifuge 15 min., decant (save and redo ₆ if pH of liquid is < 8)
- ₈ Wash with water, vortex, centrifuge for 10 min, and decant
- ₉ Record mass quartz vials, label, and place them in furnace holder

CNEF ID	2125	2126	2127	2128	2129	2130	2131	2080	
Sample ID	07-TRI-DEWH-13	07-TRI-DEWH-14	07-TRI-DEWH-15	07-TRI-DEWH-16	07-TRI-DEWH-17	07-TRI-DEWH-18	07-TRI-DEWH-19	blank for 20080114	105 WY-96-001
Mass Qtz Vial	2.5397	2.4853	2.5083	2.5466	2.5184	2.5725	2.5833	2.5248	2.1400 g
Mass Vial+Spl	2.5508	2.4923	2.5119	2.5562	2.5350	2.5803	2.5975	2.5259	2.1410 g
Mass Spl	0.0111	0.0070	0.0036	0.0096	0.0166	0.0078	0.0142	0.0011	1 mg

- ₁₀ Add 1 small drop of water with micropipet, slurry precipitate
- ₁₁ Transfer sample into quartz vial, cover with alumina vial
- ₁₂ Heat in oven at 120°C for 2-3 hours
- ₁₃ Let cool and scrape sample down from walls of quartz tube
- ₁₄ Convert to Al₂O₃ in furnace at 950°C for minimum of 1 hr
- ₁₅ Determine mass of vial + sample

A.2.8.3. Sample IDs 2132-2136 and blank 2081

WS4_QtzDissolution

This worksheet outlines the steps for dissolving quartz and adding Be carrier.

Chemist: AH

Date: 01/19/08

	1	2	3	4	5	6	7	8	
CNEF ID	2132	2133	2134	2135	2136	2081			examples
Sample ID	<small>07-TRI-DEWM-08</small>	<small>07-TRI-DEWM-09</small>	<small>07-TRI-DEWM-10</small>	<small>07-TRI-DEWM-11</small>	<small>07-TRI-DEWM-12</small>	<small>blank for 20080119</small>			105
500 ml vessel ID	A23/B17	A14/B31	A24/B18	A13/B16	A19/B24	A20/B25			WY-96-001
Beryl Carrier ID	bottle 3	bottle 3	bottle 3	bottle 3	bottle 3	bottle 3			AA
Al Carrier ID	al carrier 4	al carrier 4	al carrier 4	al carrier 4	al carrier 4	al carrier 4			BeI-Carrier
	<small>(tare balance after each measurement)</small>								
Mass 300 ml vessel	17.6027	17.5756	17.2323	17.6957	17.6003	17.0815			148.7188 g
Mass 40g quartz	120.0365	120.6702	120.7315	120.1937	121.8874				20.0000 g
Mass Be carrier	0.2391	0.2378	0.2437	0.2320	0.2387	0.2341			1.0147 g
Mass Al Carrier	1.1032	1.1080	1.1135	1.1057	1.1111	2.5093			

SAVE AS: C:/Chemistry/CHEM_WK YYMMDD .xls then PRINT

- 1 Add 20 ml conc. HF and 2 ml HClO₄ per 5 g of quartz
- 2 Add 5 ml Aqua Regia
- 3 Heat at 100-125° C until quartz dissolves, add HF if needed
- 4 Raise to 200° C and evaporate to dryness
- 5 Add 5 ml HClO₄ and evaporate to dryness
- 6 Add 8 to 10 ml conc. HNO₃, swirl, and evaporate to dryness
- 7 Dissolved dried sample in 20 ml of 2% HCl

Comments

Initially dissolved in 500 ml teflon beakers; will transfer later into 300 ml containers.									

WS5_ICP Aliquot and AI spiking

This worksheet outlines the steps for collecting ICP aliquots and adding AI carrier.

Chemist: AH

Date: 02/05/08

- 1 Label one 10 ml volumetric flasks per sample (16)
- 2 Label one ICP vial with CNEF ID per sample (16)

	A23/B17	A14/B31	A24/B18	A13/B16	A19/B24	A20/B25	0	0	examples
CNEF ID	2132	2133	2134	2135	2136	2081	0.00	0.00	105
Sample ID	07-TRI-DEWM-08	07-TRI-DEWM-09	07-TRI-DEWM-10	07-TRI-DEWM-11	07-TRI-DEWM-12	blank for 20080119	0	0	WY-96-001
AI carrier ID	al carrier 4	al carrier 4	al carrier 4	al carrier 4	al carrier 4	al carrier 4			ALI-carrier
Quant-EM est. AI in qtz	50	50	50	50	50	50			ppm
Volume carrier to add to smpl									ml
Volume carrier to add to vol A									ml
Volume carrier to add to vol. B									ml
Tare between mass measurements									
Mass 100 ml volumetric	66.7043	66.5905	67.7459	66.4911	66.3039	67.4192			66.9239 g
100ml volumetric+sample+2%HCl	167.5152	167.5699	168.7729	167.4883	167.1195	168.3975			166.9875 g
Mass 10 ml smple pipetted to vol A	10.0084	10.0062	10.0191	10.0039	10.0004	10.0119			10.0000 g
Mass 5 ml Sample to Vial B	5.0148	5.0348	5.0105	5.0086	5.0039	5.0125			5.0000g
Bring up to 10 ml by 2%HCl	10.0080	10.0059	10.0075	10.0021	10.0012	10.0009			10.0000g
Final Mass of 100 ml vol and smple	152.4878	152.5232	153.7707	152.4638	152.2010	153.3688			150.0100 g
Mass AI carrier to remaining (row 18)									1.0100 g
Unaccounted mass	0.0042	0.0057	0.0274	0.0120	0.0858	0.0043			0.0100 g

- 3 Get digestion vessel and cover ready, Do not wipe now.
- 4 Transfer the 90 ml sample back into vessel
- 5 Bring contents of volumetrics A and B to 10 ml
- 6 Transfer contents volumetrics to ICP vials with same number

GY July 16, 2003 update

GY May 11, 2005 updated, Take 2 Aliquots one sample. 10ml and 5 ml –then bring up to 10ml

GY Feb 2007: Take 2 Aliquots, First one, 10ml without AI carrier, to vial A. Then add ~1.0ml AI carrier to

the rest of ..about 90g, shake, take second aliquot 5ml to vial B, bring up to 10ml by 2%HCl.

WS8_Cation Column Chemistry

This worksheet outlines the steps for the Cation Column Chemistry

Chemist: ^{GY/JG}

Date: ^{mm/dd/yy}

Print this page

- ₁ Dissolve in 5 ml conc. HCl and evaporate to dryness at 125°C
- ₂ Redissolve in 2.5 ml 1N HCl and 2.5 ml 0.5 N HCl
- ₃ Transfer to centrifuge tube, rinse with 1 ml 0.5N, and centrifuge

Column ID	1	2	3	4	5	6	7	8	examples
Vessel	A23/B17	A14/B31	A24/B18	A13/B16	A19/B24	A20/B25	0	0	
CNEF ID	2132	2133	2134	2135	2136	2081	0	0	105
Sample ID	07-TRI-DEWM-08	07-TRI-DEWM-09	07-TRI-DEWM-10	07-TRI-DEWM-11	07-TRI-DEWM-12	blank for 20080119	0	0	WY-96-001

- ₄ Pipette all of the sample into designated conditioned cation column
- ₅ Discard the eluant. Add 220 ml 0.5 N HCL (bottle C6)
- ₆ Collect eluant as Cation Supernate, add 200 ml 0.5 N HCl (bottle C7)
- ₇ Collect eluant as Be-Sample into vessels.
- ₈ Add 30 ml 1N HCl (bottle8)
- ₉ Save this as Be-sample as well.
- ₁₀ Add 100 ml 4.5 N HCl, save as Al sample.
- ₁₁
- ₁₂
- ₁₃ **CONDITION CATION COLUMN**

- (bottle C1) 100 ml 9N HCl
- (bottle C2) 50 ml 4.5 N HCl
- (bottle C3) 50 ml 1 N HCl
- (bottle C4) 50 ml water
- (bottle C5) 100 ml 0.5 N HCl

WS9_Be Sample Chemistry

This worksheet outlines the steps to prepare the BeO sample

Chemist: ^{AH}

Date: ^{form: mm/dd/yy}

Print this page

- ₁ Evaporate Be Sample from column in wiped digestion vessels at 125°C
- ₂ Add 2-5 ml 20% perchloric and evaporate at 200°C
- ₃ Again, add 2-5 ml 20% perchloric and evaporate at 200°C
- ₄ Dissolve sample in 10 ml of 0.5 N HCl (optima grade)
- ₅ Transfer to 15 ml centrifuge tube
- ₆ Centrifuge and decant into clean centrifuge tube
- ₇ Heat centrifuge tubes in water bath at 60°C
- ₈ Precipitate Be(OH)₂ using Matheson ultimate grade ammonia gas
Gently bubble NH₃ with clean pipet tip on hose
for ca.15 bubbles, or ca. 8-12 sec until ppt forms
Optimum pH=9.2; 1N HCl may be added
- ₉ Centrifuge 15 min., decant (save and redo ₈ if pH of liquid is < 8)
- ₁₀ Wash with water, vortex, centrifuge for 10 min, and decant
- ₁₁ Record mass quartz vials, label, and place them in furnace holder

CNEF ID	2132	2133	2134	2135	2136	2081	0	0	105
Vessel	A23/B17	A14/B31	A24/B18	A13/B16	A19/B24	A20/B25	0	0	
Sample ID	07-TRI-DEWM-08	07-TRI-DEWM-09	07-TRI-DEWM-10	07-TRI-DEWM-11	07-TRI-DEWM-12	blank for 20080119	0	0	WY-96-001
Mass Qtz Vial	2.1881	2.2043	2.2273	2.2052	2.1813	2.0969			2.1400 g
Mass Vial+Spl	2.1904	2.2065	2.23	2.208	2.1836	2.0978			2.1410 g
Mass Spl	0.0023	0.0022	0.0027	0.0028	0.0023	0.0009	0	0	1 mg

- ₁₂ Add 1 small drop of water with micropipet, slurry precipitate
- ₁₃ Transfer sample into quartz vial, cover with alumina vial
- ₁₄ Heat in oven at 120°C for 2-3 hours
- ₁₅ Let cool and scrape sample down from walls of quartz tube
- ₁₈ Place in furnace. Convert to BeO in furnace at 850°C for minimum 1 hr
- ₁₉ Determine mass of vial + sample

This worksheet outlines the steps to prepare the Al oxide sample

Chemist: ^{AH}

Date: ^{form: mm/dd/yy}

Print this page

- ₁ Evaporate Al Sample from column in wiped teflon vessel at 125°C
- ₂ Dissolve sample in 10 ml of 0.5 N HCl (optima grade)
- ₃ Transfer to 15 ml centrifuge tube
- ₄ Centrifuge and decant into clean centrifuge tube
- ₅ Heat centrifuge tubes in water bath at 60°C
- ₆ Precipitate Al(OH)₃ using 50% NH₃OH (drops: 25, 5, 5, 3, 2...)

Optimum pH=6.3; 1N HCl may be added

- ₇ Centrifuge 15 min., decant (save and redo ₆ if pH of liquid is < 8)
- ₈ Wash with water, vortex, centrifuge for 10 min, and decant
- ₉ Record mass quartz vials, label, and place them in furnace holder

CNEF ID	2132	2133	2134	2135	2136	2081	0	0	105
Sample ID	TRI-DEWM	TRI-DEWM	TRI-DEWM	TRI-DEWM	TRI-DEWM	TRI-DEWM	0	0	WY-96-001
Mass Qtz Vial	2.5958	2.5386	2.4470	2.5152	2.5795	2.5074			2.1400 g
Mass Vial+Spl	2.6113	2.5565	2.4717	2.5414	2.6038	2.5112			2.1410 g
Mass Spl	0.0155	0.0179	0.0247	0.0262	0.0243	0.0038	0	0	1 mg

- ₁₀ Add 1 small drop of water with micropipet, slurry precipitate
- ₁₁ Transfer sample into quartz vial, cover with alumina vial
- ₁₂ Heat in oven at 120°C for 2-3 hours
- ₁₃ Let cool and scrape sample down from walls of quartz tube
- ₁₄ Convert to Al₂O₃ in furnace at 950°C for minimum of 1 hr
- ₁₅ Determine mass of vial + sample

A.2.8.4. Sample IDs 2139-2145 and blank 2084

WS4_QtzDissolution

This worksheet outlines the steps for dissolving quartz and adding Be carrier.

Chemist: AH

form: mm/dd/yy

Date: 06/07/08

	1	2	3	4	5	6	7	8	
CNEF ID	2139	2140	2141	2142	2143	2144	2145	2084	examples 105
Sample ID	<small>TX-08-COL-BEA-01</small>	<small>TX-08-COL-BEA-02</small>	<small>TX-08-COL-BEA-05</small>	<small>TX-08-COL-CBA3-801</small>	<small>TX-08-TRI-CBA3-802</small>	<small>TX-08-COL-CBA3-801</small>	<small>TX-08-TRI-CBA3-802</small>	blank	WY-96-001
1000 ml vessel ID	E1	E2	E3	E4	E5	E6	E7	E8	AA
Beryl Carrier ID	Bottle 2	Bottle 2	Bottle 2	Bottle 2	Bottle 2	Bottle 2	Bottle 2	Bottle 2	BeI-Carrier
Al Carrier ID	ICP-013-5	ICP-013-5	ICP-013-5	ICP-013-5	ICP-013-5	ICP-013-5	ICP-013-5	ICP-013-5	
	(tare balance after each measurement)								
Mass 300 ml vessel	17.2243	17.6122	17.6877	17.0863	17.0784	17.5749	17.0806	2.7107	148.7188 g
Mass 100g quartz	100.0752	100.0115	100.0388	90.1047	100.3179	92.1266	100.5119	NA	20.0000 g
Mass Be carrier	0.2385	0.2314	0.2430	0.2305	0.2295	0.2398	0.2358	0.2395	1.0147 g
Mass Al Carrier	1.0018	1.0094	1.0011	1.0503	1.0100	1.0070	0.9978	2.5381	

SAVE AS:

C:/Chemistry/CHEM_WK YMMDD .xls

then PRINT

- 1 Add 20 ml conc. HF and 2 ml HClO₄ per 5 g of quartz
- 2 Add 5 ml Aqua Regia
- 3 Heat at 100-125° C until quartz dissolves, add HF if needed
- 4 Raise to 200° C and evaporate to dryness
- 5 Add 5 ml HClO₄ and evaporate to dryness
- 6 Add 8 to 10 ml conc. HNO₃, swirl, and evaporate to dryness
- 7 Dissolved dried sample in 20 ml of 2% HCl

Comments

added:									
300 mL HF									
50 mL Aqua Regia									
50 mL HNO ₃									
10 mL HClO ₄									
put on hot plate at 125 C									

WS5_ICP Aliquot and AI spiking

This worksheet outlines the steps for collecting ICP aliquots and adding AI carrier.

Chemist: ^{AH}

Date: ^{form: 02/17/01}

- 1 Label one 10 ml volumetric flasks per sample (16)
- 2 Label one ICP vial with CNEF ID per sample (16)

	E1	E2	E3	E4	E5	E6	E7	E8	examples
CNEF ID	2139	2140	2141	2142	2143	2144	2145	2084	105
Sample ID	X-08-COL-BEA-01	X-08-COL-BEA-02	X-08-COL-BEA-05	X-08-COL-CBA3-80	X-08-TRI-CBA3-80	X-08-COL-CBA3-80	X-08-TRI-CBA3-80	blank	WY-96-001
AI carrier ID	ICP-013-5	ICP-013-5	ICP-013-5	ICP-013-5	ICP-013-5	ICP-013-5	ICP-013-5	ICP-013-5	ALI-carrier
Quant-EM est. AI in qtz	50	50	50	50	50	50	50	50	ppm
Volume carrier to add to smpl									ml
Volume carrier to add to vol A									ml
Volume carrier to add to vol. B									ml
Tare between mass measurements									
Mass 100 ml volumetric	66.9341	67.0047	67.4182	66.5899	67.7313	67.1395	66.4964	67.3712	66.9239 g
100ml volumetric+sample+2%HCl	166.8980	167.0294	167.3988	166.5889	167.7028	167.1484	166.5643	167.3870	166.9875 g
Mass 10 ml smple pipetted to vol A	10.0047	10.0477	10.0005	10.2110	10.0299	10.0709	10.0182	10.0225	10.0000 g
Mass 5 ml Sample to Vial B									5.0000g
Bring up to 10 ml by 2%HCl									10.0000g
Final Mass of 100 ml vol and smple	156.8784	156.9667	157.3819	156.3641	157.6595	157.0554	156.5421	157.3485	150.0100 g
Mass AI carrier to remaining (row 18)									1.0100 g
Unaccounted mass	0.0149	0.0150	0.0164	0.0138	0.0134	0.0221	0.0040	0.0160	0.0100 g

- 3 Get digestion vessel and cover ready, Do not wipe now.
- 4 Transfer the 90 ml sample back into vessel
- 5 Bring contents of volumetrics A and B to 10 ml
- 6 Transfer contents volumetrics to ICP vials with same number

GY July 16, 2003 update

GY May 11, 2005 updated, Take 2 Aliquots one sample. 10ml and 5 ml –then bring up to 10ml

GY Feb 2007: Take 2 Aliquots, First one, 10ml without AI carrier, to vial A. Then add ~1.0ml AI carrier to

the rest of ..about 90g, shake, take second aliquot 5ml to vial B, bring up to 10ml by 2%HCl.

WS6_Anion Column Chemistry

This worksheet outlines the steps for the Anion Column Chemistry

Chemist: ^{AH} AH

Date: ^{form: MM/DD/YY} 12/07/08

Print this page

- ₁ Evaporate 80 ml to dryness at 100-120°C (will take at least 3 hrs)
- ₂ Dissolve in 10 ml 9N HCl (let stand for several hours)
- ₃ Transfer to 15 ml centrifuge tubes, rinse digestion vessels with 9N HCl to bring volume in tube to 10 ml
- ₄ Centrifuge at 1500 rpm or higher for minimum of 10 minutes
- ₅ Allow any 9 N HCl in columns to drain out; discard

Column ID	A	B	C	D	E	F	G	H
Vessel	E1	E2	E3	E4	E5	E6	E7	E8
CNEF ID	2139	2140	2141	2142	2143	2144	2145	2084
Sample ID	K-08-COL-BEA-0	K-08-COL-BEA-0	K-08-COL-BEA-0	08-COL-CBA3-8	08-TRI-CBA3-8	08-COL-CBA3-8	08-TRI-CBA3-8	blank

- ₆ With stopcock closed, pipet sample (avoid residue) onto columns.
- ₇ Collect sample in same (wiped) 120 ml teflon vessel
- ₈ Elute with 30 ml 9 N HCl, and collect that, close stopcock
- ₉ 5 ml 4.5 N HCl, collect Anion Supernate in labeled 100 ml bottle
- ₁₀ 100 ml 1 N HCl, collect Anion Supernate
- ₁₁ 50 ml deionized water. Discard.
- ₁₂ **CONDITION ANION COLUMN**

(bottle A1) 50 ml 1N HCl, discard
 (bottle A2) 50 ml 4.5 N HCl, discard
 (bottle A3) 100 ml 9 N HCl, discard, but retain acid approx. 2 mm above resin

Comments

WS7_Controlled Precipitate

This worksheet outlines the steps for the controlled precipitation chemistry

Chemist: ^{AH}

Date: ^{form: MM/DD/YY}

[Print this page](#)

- ₁ Evaporate "anion" elute to dryness at 125°C
- ₂ Dissolve in 10 ml of a 1:1 solution of 0.5N HCl and 2% NH₄Cl
- ₃ Transfer to 15 ml centrifuge, centrifuge for 10 minutes
- ₄ Decant into clean test tube, heat in water bath at 60°C
- ₅ Add drops of 1:1 NH₄OH:H₂O to pH=9.2 (5 drops first then single)
- ₆ Centrifuge for 15 minutes
- ₇ Check pH of liquid, if less than pH=7, redo step ₅
- ₈ Decant, save with Anion Supernate
- ₉ Wash with deionized water, vortex, centrifuge, decant
- ₁₀ Wash with deionized water, vortex, centrifuge, decant
- ₁₁ Wash with deionized water, vortex, centrifuge, decant

CNEF ID	2139	2140	2141	2142	2143	2144	2145	2084
Vessel	E1	E2	E3	E4	E5	E6	E7	E8
Sample ID	X-08-COL-BEA-01	X-08-COL-BEA-02	X-08-COL-BEA-03	08-COL-CBA3-80	08-TRI-CBA3-80	08-COL-CBA3-80	08-TRI-CBA3-80	blank
Approx. vol. Ptte	2	1.5	1.5	1.5	1.5	1	1.5	0.3

Comments

WS8_Cation Column Chemistry

This worksheet outlines the steps for the Cation Column Chemistry

Chemist: ^{GY/JG}

Date: ^{mm/dd/yy}

Print this page

- ₁ Dissolve in 5 ml conc. HCl and evaporate to dryness at 125°C
- ₂ Redissolve in 2.5 ml 1N HCl and 2.5 ml 0.5 N HCl
- ₃ Transfer to centrifuge tube, rinse with 1 ml 0.5N, and centrifuge

Column ID	1	2	3	4	5	6	7	8	examples
Vessel	E1	E2	E3	E4	E5	E6	E7	E8	
CNEF ID	2139	2140	2141	2142	2143	2144	2145	2084	105
Sample ID	X-08-COL-BEA-0	X-08-COL-BEA-02	X-08-COL-BEA-04	X-08-COL-CBA3-80	X-08-TRI-CBA3-80	X-08-COL-CBA3-80	X-08-TRI-CBA3-80	blank	WY-96-001

- ₄ **Pipette all of the sample into designated conditioned cation column, 17ml**
- ₅ Discard the eluant. Add 285 ml 0.5 N HCL (Bottle C6)
- ₆ **Drain the column, discard the first 300ml of eluant**
- ₇ Add 60ml of 0.5N HCl, (Bottle 7), Collect eluant as Cation Supernate
- ₈ Add 65ml of 0.5N HCl, (Bottle 8), Save it as Be-Sample
- ₉ Add 120 ml 1N HCl (bottle9)
- ₁₀ Save this as Be-sample as well.
- ₁₁ Add 80 ml 4.5 N HCl (bottle 10) , save the eluant as Al sample.

₁₂

₁₃ **CONDITION CATION COLUMN**

- (bottle C1) 100 ml 9N HCl
- (bottle C2) 50 ml 4.5 N HCl
- (bottle C3) 50 ml 1 N HCl
- (bottle C4) 50 ml water
- (bottle C5) 100 ml 0.5 N HCl

* 17 ml Column

WS9_Be Sample Chemistry

This worksheet outlines the steps to prepare the BeO sample

Chemist: ^{AH}

Date: ^{form: mm/dd/yy}

Print this page

- ₁ Evaporate Be Sample from column in wiped digestion vessels at 125°C
- ₂ Add 2-5 ml 20% perchloric and evaporate at 200°C
- ₃ Again, add 2-5 ml 20% perchloric and evaporate at 200°C
- ₄ Dissolve sample in 10 ml of 0.5 N HCl (optima grade)
- ₅ Transfer to 15 ml centrifuge tube
- ₆ Centrifuge and decant into clean centrifuge tube
- ₇ Heat centrifuge tubes in water bath at 60°C
- ₈ Precipitate Be(OH)₂ using Matheson ultimate grade ammonia gas
Gently bubble NH₃ with clean pipet tip on hose
for ca.15 bubbles, or ca. 8-12 sec until ppt forms
Optimum pH=9.2; 1N HCl may be added
- ₉ Centrifuge 15 min., decant (save and redo ₈ if pH of liquid is < 8)
- ₁₀ Wash with water, vortex, centrifuge for 10 min, and decant
- ₁₁ Record mass quartz vials, label, and place them in furnace holder

CNEF ID	2139	2140	2141	2142	2143	2144	2145	2084	
Vessel	E1	E2	E3	E4	E5	E6	E7	E8	105
Sample ID	08-COL-BEA-0	08-COL-BEA-0	08-COL-BEA-0	08-COL-CBA3-8	08-TRI-CBA3-80	08-COL-CBA3-8	08-TRI-CBA3-80	blank	WY-96-001
Mass Qtz Vial	2.4963	2.5419	2.5008	2.4393	2.3806	2.5105	2.6231	2.4175	2.1400 g
Mass Vial+Spl	2.4973	2.5428	2.5016	2.4404	2.3813	2.5116	2.6237	2.418	2.1410 g
Mass Spl	0.0010	0.0009	0.0008	0.0011	0.0007	0.0011	0.0006	0.0005	1 mg

- ₁₂ Add 1 small drop of water with micropipet, slurry precipitate
- ₁₃ Transfer sample into quartz vial, cover with alumina vial
- ₁₄ Heat in oven at 120°C for 2-3 hours
- ₁₅ Let cool and scrape sample down from walls of quartz tube
- ₁₈ Place in furnace. Convert to BeO in furnace at 850°C for minimum 1 hr
- ₁₉ Determine mass of vial + sample

WS10_AI Sample Chemistry

This worksheet outlines the steps to prepare the Al oxide sample

Chemist: ^{AH}

Date: ^{form: mm/dd/yy}

[Print this page](#)

- 1 Evaporate Al Sample from column in wiped teflon vessel at 125°C
- 2 Dissolve sample in 10 ml of 0.5 N HCl (optima grade)
- 3 Transfer to 15 ml centrifuge tube
- 4 Centrifuge and decant into clean centrifuge tube
- 5 Heat centrifuge tubes in water bath at 60°C
- 6 Precipitate Al(OH)₃ using 50% NH₃OH (drops: 25, 5, 5, 3, 2...)
Optimum pH=6.3; 1N HCl may be added
- 7 Centrifuge 15 min., decant (save and redo 6 if pH of liquid is < 8)
- 8 Wash with water, vortex, centrifuge for 10 min, and decant
- 9 Record mass quartz vials, label, and place them in furnace holder

CNEF ID	2139	2140	2141	2142	2143	2144	2145	2084	
Sample ID	08-COL-BEA-0	08-COL-BEA-02	08-COL-BEA-05	08-COL-CBA3-84	08-TRI-CBA3-80	08-COL-CBA3-80	08-TRI-CBA3-80	blank	105 WY-96-001
Mass Qtz Vial	2.4876	2.5669	2.5126	2.4903	2.5057	2.4537	2.5457	2.5148	2.1400 g
Mass Vial+Spl	2.5026	2.5804		2.5022	2.5205		2.5617	2.5183	2.1410 g
Mass Spl	0.015	0.0135	-2.5126	0.0119	0.0148	-2.4537	0.016	0.0035	1 mg

- 10 Add 1 small drop of water with micropipet, slurry precipitate
- 11 Transfer sample into quartz vial, cover with alumina vial
- 12 Heat in oven at 120°C for 2-3 hours
- 13 Let cool and scrape sample down from walls of quartz tube
- 14 Convert to Al₂O₃ in furnace at 950°C for minimum of 1 hr
- 15 Determine mass of vial + sample

A.2.8.5. Sample IDs 2070, 2072, 2255-2258 and blank 2163

WS4_QtzDissolution

This worksheet outlines the steps for dissolving quartz and adding Be carrier.

Chemist: JG/GY
AH

Date: form:mm/dd/yy
11/26/08

	1	2	3	4	5	6	7	8	examples
CNEF ID	2070	2072	2254	2255	2256	2257	2258	2163	105
Sample ID	<small>Colorado/Altair/CBA1</small>	<small>Brazos/Wallis/Bar</small>	<small>8-TX-TRI-WILLIS-803</small>	<small>8-TX-TRI-WILLIS-803</small>	<small>8-TX-TRI-WILLIS-803</small>	<small>8-TX-TRI-WILLIS-803</small>	<small>8-TX-TRI-WILLIS-803</small>	blank	WY-96-001
1 L vessel ID	E1/B1	E2/B4	E3/B19	E4/B23	E5/B26	E6/B28	E7/B29	E8/B32	AA
Beryl Carrier ID	Bottle 2	Bottle 2	Bottle 2	Bottle 2	Bottle 2	Bottle 2	Bottle 2	Bottle 2	Bel-Carrier
Al Carrier ID	NA	NA	NA	NA	NA	NA	NA	ICP-013-5	
	(tare balance after each measurement)								
Mass vessel	18.0485	18.1135	18.0434	18.1013	18.0540	18.1400	18.1130	18.0412	148.7188 g
Mass 40g quartz	149.1788	150.0114	149.9414	150.2143	150.7835	150.0817	137.3109	0.0000	20.0000 g
Mass Be carrier	0.2261	0.2292	0.2272	0.2322	0.2401	0.2294	0.2205	0.2472	1.0147 g
Mass Al Carrier	0.0000	0.0000	0.0000	0.0000	0.0000	0.0000	0.0000	2.9131	

SAVE AS: C:/Chemistry/CHEM_WK YYMMDD .xls then PRINT

- ₁ Add 20 ml conc. HF and 2 ml HClO₄ per 5 g of quartz
- ₂ Add 5 ml Aqua Regia
- ₃ Heat at 100-125° C until quartz dissolves, add HF if needed
- ₄ Raise to 200° C and evaporate to dryness
- ₅ Add 5 ml HClO₄ and evaporate to dryness
- ₆ Add 8 to 10 ml conc. HNO₃, swirl, and evaporate to dryness
- ₇ Dissolved dried sample in 20 ml of 2% HCl

Comments

total acid added for digestion:								
600 mL HF								
50 mL Aqua Regia								
20 mL HNO ₃								
10 mL HClO ₄								

WS5_ICP Aliquot and AI spiking

This worksheet outlines the steps for collecting ICP aliquots and adding AI carrier.

Chemist: ^{AH}

Date: ^{form: 02/17/01}

- 1 Label one 10 ml volumetric flasks per sample (16)
- 2 Label one ICP vial with CNEF ID per sample (16)

	E1/B1	E2/B4	E3/B19	E4/B23	E5/B26	E6/B28	E7/B29	E8/B32	examples
CNEF ID	2070	2072	2254	2255	2256	2257	2258	2163	105
Sample ID	Florida/Altair/CBA1	Brazos/Wallis/Bar	TX-TRI-WILLIS-80	TX-TRI-WILLIS-80	TX-TRI-WILLIS-80	TX-TRI-WILLIS-80	TX-TRI-WILLIS-80	blank	WY-96-001
AI carrier ID	na	na	na	na	na	na	na	ICP-013-5	ALI-carrier
Quant-EM est. AI in qtz	22	25	16	17	16	19	22	na	ppm
Volume carrier to add to smpl									ml
Volume carrier to add to vol A									ml
Volume carrier to add to vol. B									ml
Tare between mass measurements									
Mass 100 ml volumetric	67.7448	67.7321	66.3068	67.1411	67.1829	65.2052	68.8735	66.7049	66.9239 g
100ml volumetric+sample+2%HNO3	101.1606	101.3164	101.0296	101.1921	101.2202	101.3011	101.1575	101.1800	166.9875 g
Mass 10 ml smple pipetted to vol A	10.1099	10.1217	10.1136	10.1395	10.1118	10.1371	10.1383	10.0787	10.0000 g
Final Mass of 100 ml vol and smple	158.7835		157.2144	158.1880	158.2802	156.3601	159.8831	157.7858	150.0100 g
Unaccounted mass	0.0120		0.0084	0.0057	0.0111	0.0091	0.0096	0.0204	0.0100 g

- 3 Get digestion vessel and cover ready, Do not wipe now.
- 4 Transfer the 90 ml sample back into vessel
- 5 Bring contents of volumetrics A and B to 10 ml
- 6 Transfer contents volumetrics to ICP vials with same number

GY July 16, 2003 update
 GY May 11, 2005 updated, Take 2 Aliquots one sample. 10ml and 5 ml –then bring up to 10ml
 AH Dec 08, 2008: using HNO3 instead of HCl as requested by ICP in Bedford

WS6_Anion Column Chemistry

This worksheet outlines the steps for the Anion Column Chemistry (2ml size small column)

Chemist: AH

Date: 09/12/08

If we don't need any AI-26 data, we could skip Step WS5.

- ₁ Evaporate 20 ml to dryness at 100-120°C (will take at least 3 hrs)
- ₂ Dissolve in 10 ml 9N HCl (let stand for several hours)
- ₃ Transfer to 15 ml centrifuge tubes, rinse digestion vessels with 9N HCl to bring volume in tube to 10 ml
- ₄ Centrifuge at 1500 rpm or higher for minimum of 10 minutes
- ₅ Allow any 9 N HCl in columns to drain out; discard

Column ID	A	B	C	D	E	F	G	H	AnionColumnID
Vessel	E1/B1	E2/B4	E3/B19	E4/B23	E5/B26	E6/B28	E7/B29	E8/B32	
CNEF ID	2070	2072	2254	2255	2256	2257	2258	2163	105
Sample ID	lorado/Altair/CBA	Brazos/Wallis/Bar	TX-TRI-WILLIS-8	TX-TRI-WILLIS-8	TX-TRI-WILLIS-8	TX-TRI-WILLIS-8	TX-TRI-WILLIS-8	blank	WY-96-001

- ₆ With stopcock closed, pipet sample (avoid residue) onto 2ml size columns.
- ₇ Collect sample in same 300 ml teflon vessel.
- ₈ Elute with 10 ml 9 N HCl, and collect that, close stopcock
- ₉ 5 ml 4.5 N HCl, collect Anion Supernate in labeled 100 ml bottle
- ₁₀ 10 ml 1 N HCl, collect Anion Supernate
- ₁₁ 50 ml deionized water. Discard.
- ₁₂ **CONDITION ANION COLUMN**

(bottle A1) 10 ml 1N HCl, discard
 (bottle A2) 10 ml 4.5 N HCl, discard
 (bottle A3) 10 ml 9 N HCl, discard, but retain acid approx. 2 mm above resin

Comments

WS7_Controlled Precipitate

This worksheet outlines the steps for the controlled precipitation chemistry

Chemist: ^{AH}

Date: ^{form: MM/DD/YY}

[Print this page](#)

- ₁ Evaporate "anion" elute to dryness at 125°C
- ₂ Dissolve in 10 ml of a 1:1 solution of 0.5N HCl and 2% NH₄Cl
- ₃ Transfer to 15 ml centrifuge, centrifuge for 10 minutes
- ₄ Decant into clean test tube, heat in water bath at 60°C
- ₅ Add drops of 1:1 NH₄OH:H₂O to pH=9.2 (5 drops first then single)
- ₆ Centrifuge for 15 minutes
- ₇ Check pH of liquid, if less than pH=7, redo step ₅
- ₈ Decant, save with Anion Supernate
- ₉ Wash with deionized water, vortex, centrifuge, decant
- ₁₀ Wash with deionized water, vortex, centrifuge, decant
- ₁₁ Wash with deionized water, vortex, centrifuge, decant

CNEF ID	2070	2072	2254	2255	2256	2257	2258	2163
Vessel	E1/B1	E2/B4	E3/B19	E4/B23	E5/B26	E6/B28	E7/B29	E8/B32
Sample ID	Colorado/Altair/CBA	Brazos/Wallis/Bar	TX-TRI-WILLIS-8	TX-TRI-WILLIS-8	TX-TRI-WILLIS-8	TX-TRI-WILLIS-8	TX-TRI-WILLIS-8	blank
Approx. vol. Ptte (mL)	2	2	2	2	1.5	1.5	1.5	0.3

Comments

2256 precipitated ~0.1 mL in water bath								

WS8_Cation Column Chemistry

This worksheet outlines the steps for the Cation Column Chemistry

Chemist: ^{GY/JG}

Date: ^{mm/dd/yy}

[Print this page](#)

- ₁ Dissolve in 5 ml conc. HCl and evaporate to dryness at 125°C
- ₂ Redissolve in 2.5 ml 1N HCl and 2.5 ml 0.5 N HCl
- ₃ Transfer to centrifuge tube, rinse with 1 ml 0.5N, and centrifuge

Column ID	1	2	3	4	5	6	7	8	examples
Vessel	E1/B1	E2/B4	E3/B19	E4/B23	E5/B26	E6/B28	E7/B29	E8/B32	
CNEF ID	2070	2072	2254	2255	2256	2257	2258	2163	105
Sample ID	lorado/Altair/CBA	Brazos/Wallis/Bar	TX-TRI-WILLIS-8	TX-TRI-WILLIS-8	TX-TRI-WILLIS-8	TX-TRI-WILLIS-8	TX-TRI-WILLIS-8	blank	WY-96-001

- ₄ **Pipette all of the sample into designated conditioned cation column, 17ml**
- ₅ Discard the eluant. Add 285 ml 0.5 N HCL (Bottle C6)
- ₆ **Drain the column, discard the first 300ml of eluant**
- ₇ Add 60ml of 0.5N HCl, (Bottle 7), Collect eluant as Cation Supernate
- ₈ Add 65ml of 0.5N HCl, (Bottle 8), Save it as Be-Sample
- ₉ Add 120 ml 1N HCl (bottle9)
- ₁₀ Save this as Be-sample as well.
- ₁₁ Add 80 ml 4.5 N HCl (bottle 10) , save the eluant as Al sample.

₁₂

₁₃ **CONDITION CATION COLUMN**

- (bottle C1) 100 ml 9N HCl
- (bottle C2) 50 ml 4.5 N HCl
- (bottle C3) 50 ml 1 N HCl
- (bottle C4) 50 ml water
- (bottle C5) 100 ml 0.5 N HCl

* 17 ml Column

WS9_Be Sample Chemistry

This worksheet outlines the steps to prepare the BeO sample

Chemist: ^{AH} AH

Date: ^{form: mm/dd/yy} 12/16/2008

Print this page

- ₁ Evaporate Be Sample from column in wiped digestion vessels at 125°C
- ₂ Add 2-5 ml 20% perchloric and evaporate at 200°C
- ₃ Again, add 2-5 ml 20% perchloric and evaporate at 200°C
- ₄ Dissolve sample in 10 ml of 0.5 N HCl (optima grade)
- ₅ Transfer to 15 ml centrifuge tube
- ₆ Centrifuge and decant into clean centrifuge tube
- ₇ Heat centrifuge tubes in water bath at 60°C
- ₈ Precipitate Be(OH)₂ using Matheson ultimate grade ammonia gas
Gently bubble NH₃ with clean pipet tip on hose
for ca.15 bubbles, or ca. 8-12 sec until ppt forms
Optimum pH=9.2; 1N HCl may be added
- ₉ Centrifuge 15 min., decant (save and redo ₈ if pH of liquid is < 8)
- ₁₀ Wash with water, vortex, centrifuge for 10 min, and decant
- ₁₁ Record mass quartz vials, label, and place them in furnace holder

CNEF ID	2070	2072	2254	2255	2256	2257	2258	2163	105
Vessel	E1/B1	E2/B4	E3/B19	E4/B23	E5/B26	E6/B28	E7/B29	E8/B32	
Sample ID	orado/Altair/CBA	razos/Wallis/Ba	X-TRI-WILLIS-8	X-TRI-WILLIS-8	X-TRI-WILLIS-8	X-TRI-WILLIS-8	X-TRI-WILLIS-8	blank	WY-96-001
Mass Qtz Vial	2.3046	2.4978	2.2745	2.2850	2.3642	2.3579	2.2832	2.3270	2.1400 g
Mass Vial+Spl	2.3077	2.5005	2.2762	2.2873	2.3650	2.3594	2.2851	2.3277	2.1410 g
Mass Spl	0.0031	0.0027	0.0017	0.0023	0.0008	0.0015	0.0019	0.0007	1 mg

- ₁₂ Add 1 small drop of water with micropipet, slurry precipitate
- ₁₃ Transfer sample into quartz vial, cover with alumina vial
- ₁₄ Heat in oven at 120°C for 2-3 hours
- ₁₅ Let cool and scrape sample down from walls of quartz tube
- ₁₈ Place in furnace. Convert to BeO in furnace at 850°C for minimum 1 hr
- ₁₉ Determine mass of vial + sample

WS10_AI Sample Chemistry

This worksheet outlines the steps to prepare the Al oxide sample

Chemist: ^{AH}

Date: ^{form: mm/dd/yy}

Print this page

- ₁ Evaporate Al Sample from column in wiped teflon vessel at 125°C
- ₂ Dissolve sample in 10 ml of 0.5 N HCl (optima grade)
- ₃ Transfer to 15 ml centrifuge tube
- ₄ Centrifuge and decant into clean centrifuge tube
- ₅ Heat centrifuge tubes in water bath at 60°C
- ₆ Precipitate Al(OH)₃ using 50% NH₃OH (drops: 25, 5, 5, 3, 2...)
Optimum pH=6.3; 1N HCl may be added
- ₇ Centrifuge 15 min., decant (save and redo ₆ if pH of liquid is < 8)
- ₈ Wash with water, vortex, centrifuge for 10 min, and decant
- ₉ Record mass quartz vials, label, and place them in furnace holder

CNEF ID	2070	2072	2254	2255	2256	2257	2258	2163	105
Sample ID	lorado/Altair/CBA	Brazos/Wallis/Bar	TX-TRI-WILLIS-8	TX-TRI-WILLIS-8	TX-TRI-WILLIS-8	TX-TRI-WILLIS-8	TX-TRI-WILLIS-8	blank	WY-96-001
Mass Qtz Vial	2.4535	2.4741	2.5403	2.5171	2.4155	2.5046	2.5194	2.5387	2.1400 g
Mass Vial+Spl									2.1410 g
Mass Spl	-2.4535	-2.4741	-2.5403	-2.5171	-2.4155	-2.5046	-2.5194	-2.5387	1 mg

- ₁₀ Add 1 small drop of water with micropipet, slurry precipitate
- ₁₁ Transfer sample into quartz vial, cover with alumina vial
- ₁₂ Heat in oven at 120°C for 2-3 hours
- ₁₃ Let cool and scrape sample down from walls of quartz tube
- ₁₄ Convert to Al₂O₃ in furnace at 950°C for minimum of 1 hr
- ₁₅ Determine mass of vial + sample

A.2.8.6. Sample IDs 2071, 2315-2320 and blank 2167

WS4_QtzDissolution

This worksheet outlines the steps for dissolving quartz and adding Be carrier.

Chemist: AH JG/GY Date: 03/12/09 form:mm/dd/yy

	1	2	3	4	5	6	7	8	
CNEF ID	2071	2315	2316	2317	2318	2319	2320	2167	examples 105
Sample ID	Col-Altair-Bar	TX-06-COL-LIS-06	TX-08-TRI-DEWL-80	07-TX-TRI-DEWL-01	Rust ELA	TX-08-COL-BEA-04	TX-08-COL-BEA-05	blank	WY-96-001
1000 ml vessel ID	E1	E2	E3	E4	E5	E6	E7	E8	AA
Beryl Carrier ID	Bottle 2	Bottle 2	Bottle 2	Bottle 2	Bottle 2	Bottle 2	Bottle 2	Bottle 2	Bel-Carrier
Al Carrier ID	ICP-013-5	ICP-013-5	ICP-013-5	ICP-013-5	ICP-013-5	ICP-013-5	ICP-013-5	ICP-013-5	
<small>(tare balance after each measurement)</small>									
f transfer vessel (g)	17.5746	17.6775	17.6071	17.6848	17.2180	17.6841	17.0788	17.5637	148.7188 g
Mass 100g quartz	100.1685	82.0009	100.1201	100.0063	100.0472	100.8627	100.0430	NA	20.0000 g
Mass Be carrier	0.2258	0.2218	0.2292	0.2272	0.2372	0.2301	0.2310	0.2456	1.0147 g
Mass Al Carrier	1.5656	1.8572	1.5699	1.5559	1.6023	1.5514	1.5750	2.9705	

SAVE AS: C:/Chemistry/CHEM_WK YYMMDD .xls then PRINT

- ₁ Add 20 ml conc. HF and 2 ml HClO₄ per 5 g of quartz
- ₂ Add 5 ml Aqua Regia
- ₃ Heat at 100-125° C until quartz dissolves, add HF if needed
- ₄ Raise to 200° C and evaporate to dryness
- ₅ Add 5 ml HClO₄ and evaporate to dryness
- ₆ Add 8 to 10 ml conc. HNO₃, swirl, and evaporate to dryness
- ₇ Dissolved dried sample in 20 ml of 2% HCl

Comments

for digestion:									
added:		added:							
350 mL HF		50 mL HF							
50 mL Aqua Regia		20 mL HNO3							
10 mL HClO4									
* added 20 mL HNO3 for step #6 for larger mass									

WS5_ICP Aliquot and Al spiking

This worksheet outlines the steps for collecting ICP aliquots and adding Al carrier.

Chemist: ^{AH}

Date: ^{form: 02/17/01}

- 1 Label one 100 ml volumetric flasks per sample (16)
- 2 Label one ICP vial with CNEF ID per sample (16)

	E1	E2	E3	E4	E5	E6	E7	E8	examples
CNEF ID	2071	2315	2316	2317	2318	2319	2320	2167	105
Sample ID	Col-Altair-Bar	TX-06-COL-LIS-06	X-08-TRI-DEWL-807-TX-TRI-DEWL-0		Rust ELA	TX-08-COL-BEA-04	X-08-COL-BEA-05	blank	WY-96-001
Al carrier ID	ICP-013-5	ICP-013-5	ICP-013-5	ICP-013-5	ICP-013-5	ICP-013-5	ICP-013-5	ICP-013-5	ALI-carrier
Quant-EM est. Al in qtz	28	23	25	27	24	22	22	NA	ppm
Volume carrier to add to smpl									ml
Volume carrier to add to vol A									ml
Volume carrier to add to vol. B									ml
Tare between mass measurements									
Mass 100 ml volumetric sample+2%HCl	67.7453	65.2039	67.7312	67.1385	66.3066	67.0055	66.7049	67.1824	66.9239 g
Mass 1 ml smple pipetted to vol A	1.0115	1.0133	1.0216	1.0189	1.0140	1.0038	1.0077	1.0262	10.0000 g
Mass 5 ml Sample to Vial B									5.0000g
Bring up to 10 ml by 2%HCl									10.0000g
Final Mass of 100 ml vol and smple	167.4346	164.9991	167.4290	166.6085	165.9700	166.5187	166.5137	166.8457	150.0100 g
Mass Al carrier to remaining (row 18)									1.0100 g
Unaccounted mass	0.0012	0.0036	0.0064	0.0147	0.0028	0.0025	0.0131	0.0014	0.0100 g

- 3 Get digestion vessel and cover ready, Do not wipe now.
- 4 Transfer the 90 ml sample back into vessel
- 5 Bring contents of volumetrics A and B to 10 ml
- 6 Transfer contents volumetrics to ICP vials with same number

Used 1 mL aliquot for high mass samples (ICP detection limit) AH

WS7_Controlled Precipitate

This worksheet outlines the steps for the controlled precipitation chemistry

Chemist: ^{AH}

Date: ^{form: MM/DD/YY}

[Print this page](#)

- ₁ Evaporate "anion" elute to dryness at 125°C
- ₂ Dissolve in 10 ml of a 1:1 solution of 0.5N HCl and 2% NH₄Cl
- ₃ Transfer to 15 ml centrifuge, centrifuge for 10 minutes
- ₄ Decant into clean test tube, heat in water bath at 60°C
- ₅ Add drops of 1:1 NH₄OH:H₂O to pH=9.2 (5 drops first then single)
- ₆ Centrifuge for 15 minutes
- ₇ Check pH of liquid, if less than pH=7, redo step ₅
- ₈ Decant, save with Anion Supernate
- ₉ Wash with deionized water, vortex, centrifuge, decant
- ₁₀ Wash with deionized water, vortex, centrifuge, decant
- ₁₁ Wash with deionized water, vortex, centrifuge, decant

CNEF ID	2071	2315	2316	2317	2318	2319	2320	2167
Vessel	E1	E2	E3	E4	E5	E6	E7	E8
Sample ID	Col-Altair-Bar	X-06-COL-LIS-06-08-TRI-DEWL-87	X-07-TX-TRI-DEWL-0	Rust ELA	X-08-COL-BEA-04	X-08-COL-BEA-05	blank	
Approx. vol. Ptte	1.5	1	1.6	1.5	1.2	1.5	1.5	0.2

Comments

WS8_Cation Column Chemistry

This worksheet outlines the steps for the Cation Column Chemistry

Chemist: ^{GY/JG}

Date: ^{mm/dd/yy}

[Print this page](#)

- ₁ Dissolve in 5 ml conc. HCl and evaporate to dryness at 125°C
- ₂ Redissolve in 2.5 ml 1N HCl and 2.5 ml 0.5 N HCl
- ₃ Transfer to centrifuge tube, rinse with 1 ml 0.5N, and centrifuge

Column ID	1	2	3	4	5	6	7	8	examples
Vessel	E1	E2	E3	E4	E5	E6	E7	E8	
CNEF ID	2071	2315	2316	2317	2318	2319	2320	2167	105
Sample ID	Col-Altair-Bar	X-06-COL-LIS-06	08-TRI-DEWL-8	07-TX-TRI-DEWL-0	Rust ELA	X-08-COL-BEA-04	X-08-COL-BEA-05	blank	WY-96-001

- ₄ **Pipette all of the sample into designated conditioned cation column, 17ml**
- ₅ Discard the eluant. Add 285 ml 0.5 N HCL (Bottle C6)
- ₆ **Drain the column, discard the first 300ml of eluant**
- ₇ Add 60ml of 0.5N HCl, (Bottle 7), Collect eluant as Cation Supernate
- ₈ Add 65ml of 0.5N HCl, (Bottle 8), Save it as Be-Sample
- ₉ Add 120 ml 1N HCl (bottle9)
- ₁₀ Save this as Be-sample as well.
- ₁₁ Add 80 ml 4.5 N HCl (bottle 10) , save the eluant as Al sample.

₁₂

₁₃ **CONDITION CATION COLUMN**

- (bottle C1) 100 ml 9N HCl
- (bottle C2) 50 ml 4.5 N HCl
- (bottle C3) 50 ml 1 N HCl
- (bottle C4) 50 ml water
- (bottle C5) 100 ml 0.5 N HCl

* 17 ml Column

Chemist: ^{AH}

Date: ^{form: mm/dd/yy}

Print this page

- ₁ Evaporate Be Sample from column in wiped digestion vessels at 125°C
- ₂ Add 2-5 ml 20% perchloric and evaporate at 200°C
- ₃ Again, add 2-5 ml 20% perchloric and evaporate at 200°C
- ₄ Dissolve sample in 10 ml of 0.5 N HCl (optima grade)
- ₅ Transfer to 15 ml centrifuge tube
- ₆ Centrifuge and decant into clean centrifuge tube
- ₇ Heat centrifuge tubes in water bath at 60°C
- ₈ Precipitate Be(OH)₂ using Matheson ultimate grade ammonia gas
Gently bubble NH₃ with clean pipet tip on hose
for ca.15 bubbles, or ca. 8-12 sec until ppt forms
Optimum pH=9.2; 1N HCl may be added
- ₉ Centrifuge 15 min., decant (save and redo ₈ if pH of liquid is < 8)
- ₁₀ Wash with water, vortex, centrifuge for 10 min, and decant
- ₁₁ Record mass quartz vials, label, and place them in furnace holder

CNEF ID	2071	2315	2316	2317	2318	2319	2320	2167	105
Vessel	E1	E2	E3	E4	E5	E6	E7	E8	
Sample ID	Col-Altair-Bar	X-06-COL-LIS-06	08-TRI-DEWL-8	TX-TRI-DEWL-0	Rust ELA	X-08-COL-BEA-0	X-08-COL-BEA-0	blank	WY-96-001
Mass Qtz Vial	2.5209	2.6095	2.5881	2.4709	2.4934	2.5806	2.5092	2.5731	2.1400 g
Mass Vial+Spl	2.5219	2.6103	2.5892	2.4723	2.4941	2.5821	2.5099	2.5733	2.1410 g
Mass Spl	0.0010	0.0008	0.0011	0.0014	0.0007	0.0015	0.0007	0.0002	1 mg

- ₁₂ Add 1 small drop of water with micropipet, slurry precipitate
- ₁₃ Transfer sample into quartz vial, cover with alumina vial
- ₁₄ Heat in oven at 120°C for 2-3 hours
- ₁₅ Let cool and scrape sample down from walls of quartz tube
- ₁₈ Place in furnace. Convert to BeO in furnace at 850°C for minimum 1 hr
- ₁₉ Determine mass of vial + sample

WS10_AI Sample Chemistry

This worksheet outlines the steps to prepare the Al oxide sample

Chemist:

Date:

[Print this page](#)

- 1 Evaporate Al Sample from column in wiped teflon vessel at 125°C
- 2 Dissolve sample in 10 ml of 0.5 N HCl (optima grade)
- 3 Transfer to 15 ml centrifuge tube
- 4 Centrifuge and decant into clean centrifuge tube
- 5 Heat centrifuge tubes in water bath at 60°C
- 6 Precipitate Al(OH)₃ using 50% NH₃OH (drops: 25, 5, 5, 3, 2...)
Optimum pH=6.3; 1N HCl may be added
- 7 Centrifuge 15 min., decant (save and redo 6 if pH of liquid is < 8)
- 8 Wash with water, vortex, centrifuge for 10 min, and decant
- 9 Record mass quartz vials, label, and place them in furnace holder

CNEF ID	2071	2315	2316	2317	2318	2319	2320	2167	
Sample ID	Col-Altair-Bar	X-06-COL-LIS-06	08-TRI-DEWL-8	TX-TRI-DEWL-0	Rust ELA	X-08-COL-BEA-04	X-08-COL-BEA-04	blank	105
Mass Qtz Vial	2.4922	2.5653	2.5862	2.4736	2.5993	2.6281	2.5214	2.5974	WY-96-001
Mass Vial+Spl	2.5092	2.5759	2.6016	2.4887	2.6125	2.642	2.5352	2.6011	2.1400 g
Mass Spl	0.017	0.0106	0.0154	0.0151	0.0132	0.0139	0.0138	0.0037	2.1410 g
									1 mg

- 10 Add 1 small drop of water with micropipet, slurry precipitate
- 11 Transfer sample into quartz vial, cover with alumina vial
- 12 Heat in oven at 120°C for 2-3 hours
- 13 Let cool and scrape sample down from walls of quartz tube
- 14 Convert to Al₂O₃ in furnace at 950°C for minimum of 1 hr
- 15 Determine mass of vial + sample

A.2.9. References for A.2.

- Aguilar, G., Carretier, S., Regard, V., Vassallo, R., Riquelme, R., and Martinod, J., 2013, Grain size-dependent ^{10}Be concentrations in alluvial stream sediment of the Huasco Valley, a semi-arid Andes region: Quaternary Geochronology.
- Anderson, R. S., Repka, J. L., and Dick, G. S., 1996, Explicit treatment of inheritance in dating depositional surfaces using in situ ^{10}Be and ^{26}Al : *Geology*, v. 24, no. 1, p. 47.
- Balco, G., Stone, J. O. H., and Mason, J. A., 2005, Numerical ages for Plio-Pleistocene glacial sediment sequences by $^{26}\text{Al}/^{10}\text{Be}$ dating of quartz in buried paleosols: *Earth and Planetary Science Letters*, v. 232, no. 1, p. 179-191.
- Belmont, P., Pazzaglia, F., and Gosse, J., 2007, Cosmogenic ^{10}Be as a tracer for hillslope and channel sediment dynamics in the Clearwater River, western Washington State: *Earth and Planetary Science Letters*, v. 264, no. 1, p. 123-135.
- Bierman, P., and Steig, E. J., 1996, Estimating rates of denudation using cosmogenic isotope abundances in sediment: *Earth Surface Processes and Landforms*, v. 21, no. 2, p. 125-139.
- Blum, M. D., and Valastro, S. J., 1994, Late Quaternary sedimentation, lower Colorado River, Gulf Coastal Plain of Texas: *Geological Society of America Bulletin*, v. 106, no. 8, p. 1002-1016.
- Braucher, R., Brown, E., Bourles, D., and Colin, F., 2003, In situ produced ^{10}Be measurements at great depths: implications for production rates by fast muons: *Earth and Planetary Science Letters*, v. 211, no. 3, p. 251-258.

- Braucher, R., Del Castillo, P., Siame, L., Hidy, A., and Bourlès, D., 2009, Determination of both exposure time and denudation rate from an in situ-produced ^{10}Be depth profile: A mathematical proof of uniqueness. Model sensitivity and applications to natural cases: *Quaternary Geochronology*, v. 4, no. 1, p. 56-67.
- Braucher, R., Merchel, S., Borgomano, J., and Bourlès, D., 2011, Production of cosmogenic radionuclides at great depth: A multi element approach: *Earth and Planetary Science Letters*, v. 309, no. 1-2, p. 1-9.
- Brown, E. T., Stallard, R. F., Larsen, M. C., Bourlès, D. L., Raisbeck, G. M., and Yiou, F., 1998, Determination of predevelopment denudation rates of an agricultural watershed (Cayaguás River, Puerto Rico) using in-situ-produced ^{10}Be in river-borne quartz: *Earth and Planetary Science Letters*, v. 160, no. 3, p. 723-728.
- Brown, E. T., Stallard, R. F., Larsen, M. C., Raisbeck, G. M., and Yiou, F., 1995, Denudation rates determined from the accumulation of in situ-produced ^{10}Be in the Luquillo Experimental Forest, Puerto Rico: *Earth and Planetary Science Letters*, v. 129, no. 1-4, p. 193-202.
- Chmeleff, J., von Blanckenburg, F., Kossert, K., and Jakob, D., 2010, Determination of the ^{10}Be half-life by multicollector ICP-MS and liquid scintillation counting: *Nuclear Instruments and Methods in Physics Research Section B: Beam Interactions with Materials and Atoms*, v. 268, no. 2, p. 192-199.
- Codilean, A. T., Fenton, C. R., Fabel, D., Bishop, P., and Xu, S., 2012, Discordance between cosmogenic nuclide concentrations in amalgamated sands and individual fluvial pebbles in an arid zone catchment: *Quaternary Geochronology*.

- Doering, J., 1935, Post-Fleming surface formations of coastal southeast Texas and south Louisiana: *Assoc. Petroleum Geologists Bull*, v. 19, no. 5, p. 651-688.
- Galloway, W. E., Whiteaker, T. L., and Ganey-Curry, P., 2011, History of Cenozoic North American drainage basin evolution, sediment yield, and accumulation in the Gulf of Mexico basin: *Geosphere*, v. 7, no. 4, p. 938.
- Garvin, M. G., 2008, Late Quaternary Geochronologic, Stratigraphic, and Sedimentologic Framework of the Trinity River Incised Valley: East Texas Coast [Masters: Louisiana State University].
- Gosse, J. C., and Phillips, F. M., 2001, Terrestrial in situ cosmogenic nuclides: theory and application: *Quaternary Science Reviews*, v. 20, no. 14, p. 1475-1560.
- Granger, D., and Muzikar, P., 2001, Dating sediment burial with in situ-produced cosmogenic nuclides: theory, techniques, and limitations: *Earth and Planetary Science Letters*, v. 188, no. 1-2, p. 269-281.
- Granger, D. E., Kirchner, J. W., and Finkel, R., 1996, Spatially averaged long-term erosion rates measured from in situ-produced cosmogenic nuclides in alluvial sediment: *Journal of Geology*, v. 104, no. 3, p. 249-257.
- Heisinger, B., Lal, D., Jull, A., Kubik, P., Ivy-Ochs, S., Knie, K., and Nolte, E., 2002a, Production of selected cosmogenic radionuclides by muons: 2. Capture of negative muons: *Earth and Planetary Science Letters*, v. 200, no. 3-4, p. 357-369.
- Heisinger, B., Lal, D., Jull, A., Kubik, P., Ivy-Ochs, S., Neumaier, S., Knie, K., Lazarev, V., and Nolte, E., 2002b, Production of selected cosmogenic radionuclides by muons: 1. Fast muons: *Earth and Planetary Science Letters*, v. 200, no. 3-4, p. 345-355.

- Hidy, A. J., Gosse, J. C., Froese, D. G., Bond, J. D., and Rood, D. H., 2013, A latest Pliocene age for the earliest and most extensive Cordilleran Ice Sheet in northwestern Canada: *Quaternary Science Reviews*, v. 61, p. 77-84.
- Hidy, A. J., Gosse, J. C., Pederson, J. L., Mattern, J. P., and Finkel, R. C., 2010, A geologically constrained Monte Carlo approach to modeling exposure ages from profiles of cosmogenic nuclides: An example from Lees Ferry, Arizona: *Geochem. Geophys. Geosyst.*, v. 11, p. Q0AA10.
- Kohl, C., and Nishiizumi, K., 1992, Chemical isolation of quartz for measurement of in-situ-produced cosmogenic nuclides: *Geochimica Et Cosmochimica Acta*, v. 56, no. 9, p. 3583-3587.
- Korschinek, G., Bergmaier, A., Faestermann, T., Gerstmann, U., Knie, K., Rugel, G., Wallner, A., Dillmann, I., Dollinger, G., and Von Gostomski, C. L., 2010, A new value for the half-life of ^{10}Be by Heavy-Ion Elastic Recoil Detection and liquid scintillation counting: *Nuclear Instruments and Methods in Physics Research Section B: Beam Interactions with Materials and Atoms*, v. 268, no. 2, p. 187-191.
- Lal, D., 1991, Cosmic ray labeling of erosion surfaces: in situ nuclide production rates and erosion models: *Earth and Planetary Science Letters*, v. 104, no. 2-4, p. 424-439.
- Matmon, A., Bierman, P., Larsen, J., Southworth, S., Pavich, M., Finkel, R., and Caffee, M., 2003, Erosion of an ancient mountain range, the Great Smoky Mountains, North Carolina and Tennessee: *American Journal of Science*, v. 303, no. 9, p. 817-855.

- Murray, A. S., and Wintle, A. G., 2000, Luminescence dating of quartz using an improved single-aliquot regenerative-dose protocol: *Radiation measurements*, v. 32, no. 1, p. 57-73.
- Nishiizumi, K., 2004, Preparation of ^{26}Al AMS standards: *Nuclear Instruments and Methods in Physics Research Section B: Beam Interactions with Materials and Atoms*, v. 223, p. 388-392.
- Nishiizumi, K., Imamura, M., Caffee, M. W., Southon, J. R., Finkel, R. C., and McAninch, J., 2007, Absolute calibration of ^{10}Be AMS standards: *Nuclear Instruments and Methods in Physics Research Section B: Beam Interactions with Materials and Atoms*, v. 258, no. 2, p. 403-413.
- Prescott, J., and Hutton, J., 1994, Cosmic ray contributions to dose rates for luminescence and ESR dating: large depths and long-term time variations: *Radiation measurements*, v. 23, no. 2, p. 497-500.
- Proctor Jr, C., Brown, T., Waechter, N., Aronow, S., and Barnes, V., 1974, Seguin sheet: The University of Texas at Austin: Bureau of Economic Geology, *Geologic Atlas of Texas*, scale, v. 1, no. 250,000.
- Reeves Jr, C., 1976, Quaternary stratigraphy and geologic history of southern High Plains, Texas and New Mexico: *Quaternary stratigraphy of North America: Stroudsburg, Pa., Dowden, Hutchinson and Ross*, p. 213-223.
- Stone, J. O., 2000, Air pressure and cosmogenic isotope production: *Journal of Geophysical Research*, v. 105, no. B10, p. 23753-23723,23759.

- Von Blanckenburg, F., 2005, The control mechanisms of erosion and weathering at basin scale from cosmogenic nuclides in river sediment: *Earth and Planetary Science Letters*, v. 237, no. 3, p. 462-479.
- Winker, C. D., 1979, Late Pleistocene fluvial-deltaic deposition, Texas coastal plain and shelf.
- Wittmann, H., and Von Blanckenburg, F., 2009, Cosmogenic nuclide budgeting of floodplain sediment transfer: *Geomorphology*, v. 109, no. 3, p. 246-256.
- Wittmann, H., Von Blanckenburg, F., Guyot, J. L., Maurice, L., and Kubik, P., 2009, From source to sink: Preserving the cosmogenic ^{10}Be -derived denudation rate signal of the Bolivian Andes in sediment of the Beni and Mamoré foreland basins: *Earth and Planetary Science Letters*, v. 288, no. 3, p. 463-474.
- Wittmann, H., von Blanckenburg, F., Maurice, L., Guyot, J. L., Filizola, N., and Kubik, P. W., 2011a, Sediment production and delivery in the Amazon River basin quantified by in situ-produced cosmogenic nuclides and recent river loads: *Geological Society of America Bulletin*, v. 123, no. 5-6, p. 934-950.
- Wittmann, H., von Blanckenburg, F., Maurice, L., Guyot, J. L., and Kubik, P. W., 2011b, Recycling of Amazon floodplain sediment quantified by cosmogenic Al-26 and Be-10: *Geology*, v. 39, no. 5, p. 467-470.

A.3. Supplemental Information for Hidy et al. (2013): A latest Pliocene Age for the Earliest and Most Extensive Cordilleran Ice Sheet in Northwestern Canada

A.3.1. Matlab Codes for Calculating Burial Ages

Listed below are Matlab scripts written to calculate burial ages using measured concentrations of ^{10}Be and ^{26}Al . The code has a primary input function *burial_ages.m* and internally calls six specialized scripts that are not standard Matlab functions. Three of these functions were created in this work, the others are 1) an optimization algorithm, *fminlbgf.m*, obtained from the Matlab Central File Exchange at <http://www.mathworks.com/matlabcentral/fileexchange/23245-fminlbfgs-fast-limited-memory-optimizer>, 2) a function to determine and plot the error ellipses on a burial plot, *ellipse.m*, obtained from the CRONUS online calculator (Balco et al., 2008), and 3) a function that calculates muon production at depth based on half the Heisinger et al. (2002a; 2002b) production rates, *Burial_muonproduction.m*, modified from the CRONUS online calculator. Codes documented in this appendix are noted with a checkmark below. Codes not included are *fminlbgf.m* and *ellipse.m* since these were not modified for this work.

Codes used to calculate burial ages:

- 1) *burial_ages.m* (primary) ✓
- 2) *burialage.m* ✓
- 3) *Burial_stone2000.m* ✓
- 4) *Burial_muonproduction.m* ✓
- 5) *Burialplot.m* ✓
- 6) *fminlbgf.m* (see Matlab Central File Exchange)
- 7) *ellipse.m* (see Balco et al., 2008)

A.3.3.1. burial_ages.m

```
function out = burial_ages(data, muontype, sigma)

%obtain ages for each sample

datafile = load(data);
rows = length(datafile(:,1));

solution_vec = zeros(rows,3);

burialplot(data, muontype, 1, sigma)

for k = 1:rows
    vect = burialage(data,muontype,k);
    solution_vec(k,1) = vect(1);
    solution_vec(k,2) = vect(2);
    solution_vec(k,3) = vect(3);
end

out = solution_vec;

end
```

A.3.3.2. burialage.m

```
function out = burialage(data, muontype, sample)

%This function determines the exposure age/burial age pair that best
fits
%concentrations of Be-10 and Al-26 given a simple surface buildup and
%burial history. Muon production is included for both the buildup period
%and the burial period.
%
%
%INPUTS:
%data = name of ascii file with four columns of data (e.g. 'data.txt'):
%  column 1 is the depth of burial for each sample; (cm)
%  column 2 is the average density of material above each sample;
(g/cc)
%  column 3 is the decimal latitude of each sample (used in buildup
model for production)
%  column 4 is the elevation of each sample site; (m)
%  column 5 is measured [10Be]; (atoms/g)
%  column 6 is the 1 sigma error in [10Be]; (atoms/g)
%  column 7 is measured [26Al]; (atoms/g)
%  column 8 is the 1 sigma error in [26Al]; (atoms/g)
%
%muontype = deep muon scheme to use; surface buildup model always uses
Heisinger
```

```

%(2002), but this parameter refers to the scheme used after burial. If =
0, there is no
%deep muon production; if = 1, half of Heisinger (2002) is used at depth
%(estimate from J. Stone, pers. comm.); if = 2, full Heisinger (2002) is
%used at depth
%
%sample = the row number of the sample you wish to analyze from your
data
%file
%
%OUTPUTS:
%The function outputs a 3 element row matrix consisting of 1) the best
%estimate for pre-burial exposure age (Ma), 2) the best estimate for
burial
%age (Ma), and 3) the residual of the fit to the concentration data
%(should be close to zero).
%
%A. Hidy
%%%%%%%%%%%%%%%%%%%%%%%%%%%%%%%%%%%%%%%%%%%%%%%%%%%%%%%%%%%%%%%%%%%%%%%%
%%
%%%%%%%%%%%%%%%%%%%%%%%%%%%%%%%%%%%%%%%%%%%%%%%%%%%%%%%%%%%%%%%%%%%%%%%%
%%

%load data

burial_data = load(data);

depths = burial_data(:,1);
densities = burial_data(:,2);
lats = burial_data(:,3);
elevs = burial_data(:,4);
Be_concs = burial_data(:,5);
Al_concs = burial_data(:,7);

%decay constants (1/s)

Be10_lambda = log(2)/1378000;
Al26_lambda = log(2)/720000;

%neutron attenuation length (g/cm^2)

neutron_atten = 160;

%spallogenic production (atoms/g/a)

refspalprod = 4.76;
ratio_init = 6.75;

%at site
Be10_spalprodrate = Burial_stone2000(lats(sample),
elevs(sample))*refspalprod;
Al26_spalprodrate = Be10_spalprodrate*ratio_init;

```

```

%rock density used for buildup (g/cc)

r_density = 2.65;

%mean, basin-wide average production rate (atoms/g/a)

be_mean_prod = 11.2; %should include both muons and spallation

%muogenic production at current sample depth from (Heisinger 2002), Stone
pers. comm.,
%and none (atoms/g/a)

if muontype == 0 %no muons
    Be10_muonprodrate = 0;
    Al26_muonprodrate = 0;
else if muontype == 1 %Use pers. comm. from Stone
    Be10_muonprodrate =
Burial_muonproduction(depths(sample)*densities(sample),elevs(sample),1)/
2;
    Al26_muonprodrate =
Burial_muonproduction(depths(sample)*densities(sample),elevs(sample),0)/
2;
    else if muontype == 2 %Use Heisinger otherwise
        Be10_muonprodrate =
Burial_muonproduction(depths(sample)*densities(sample),elevs(sample),1);
        Al26_muonprodrate =
Burial_muonproduction(depths(sample)*densities(sample),elevs(sample),0);
    end
end
end

%simple buildup model with no erosion

%buildup due to exposure at bedrock surfaces (use mean catchment value;
%assumes no inheritance

function Be10_conc_buildup = Be10_buildup(t_exposure)
    Be10spall_buildup = (Be10_spalprodrate/Be10_lambda)*(1-exp(-
Be10_lambda*t_exposure));
    Be10muon_buildup =
(Burial_muonproduction(0,elevs(sample),1)/Be10_lambda)*(1-exp(-
Be10_lambda*t_exposure));
    Be10_conc_buildup = Be10spall_buildup + Be10muon_buildup;

    %use this for basin wide option
    %Be10_conc_buildup = (be_mean_prod/Be10_lambda)*(1-exp(-
Be10_lambda*t_exposure));
end

% option for modeling assuming a depositional ratio other than
simple
% buildup model; to use, uncomment this function and comment the
active
% Al26_buildup function
%
```

```

%     function Al26_conc_buildup = Al26_buildup(t_exposure)
%         Al26_conc_buildup = Be10_buildup(t_exposure)*(6.2);
%     end

function Al26_conc_buildup = Al26_buildup(t_exposure)
    Al26spall_buildup = (Al26_spalprodrate/Al26_lambda)*(1-exp(-
Al26_lambda*t_exposure));
    Al26muon_buildup =
(Burial_muonproduction(0,elevs(sample),0)/Al26_lambda)*(1-exp(-
Al26_lambda*t_exposure));
    Al26_conc_buildup = Al26spall_buildup + Al26muon_buildup;

    %use this for basin wide option
    %Al26_conc_buildup = (be_mean_prod*ratio_init/Al26_lambda)*(1-
exp(-Al26_lambda*t_exposure));
end

%burial production; assume buildup is inheritance

function Be10_conc_burial = Be10_burial(t_exposure, t_burial)
    Be10spall_burial = (Be10_spalprodrate/Be10_lambda)*exp(-
depths(sample)*densities(sample)/neutron_atten)*(1-exp(-
Be10_lambda*t_burial));
    Be10muon_burial = (Be10_muonprodrate/Be10_lambda)*(1-exp(-
Be10_lambda*t_burial));
    Be10inheritance = Be10_buildup(t_exposure)*exp(-
Be10_lambda*t_burial);
    Be10_conc_burial = Be10spall_burial + Be10muon_burial +
Be10inheritance;
end

function Al26_conc_burial = Al26_burial(t_exposure, t_burial)
    Al26spall_burial = (Al26_spalprodrate/Al26_lambda)*exp(-
depths(sample)*densities(sample)/neutron_atten)*(1-exp(-
Al26_lambda*t_burial));
    Al26muon_burial = (Al26_muonprodrate/Al26_lambda)*(1-exp(-
Al26_lambda*t_burial));
    Al26inheritance = Al26_buildup(t_exposure)*exp(-
Al26_lambda*t_burial);
    Al26_conc_burial = Al26spall_burial + Al26muon_burial +
Al26inheritance;
end

%simple buildup model with erosion

%new lambda term spallation

function Be10lambda = Be10_elambda(erate)

    Be10lambda = Be10_lambda + erate*r_density/neutron_atten;
end

function Al26lambda = Al26_elambda(erate)

```

```

    Al26lambda = Al26_lambda + erate*r_density/neutron_atten;
end

%need effective lambda for muons; dominated by spall, so use rough
%estimate of 1500

function Be10lambdamu = Be10_elambdamu(erate)

    Be10lambdamu = Be10_lambda + erate*r_density/1500;
end

function Al26lambdamu = Al26_elambdamu(erate)

    Al26lambdamu = Al26_lambda + erate*r_density/1500;
end

%      %buildup due to exposure at surface; assumes no inheritance
%
%      function eBe10_conc_buildup = eBe10_buildup(t_exposure, erate)
%          Be10spall_buildup =
%          (Be10_spalprodrate/Be10_elambda(erate))*(1-exp(-
%          Be10_elambda(erate)*t_exposure));
%          Be10muon_buildup =
%          (Burial_muonproduction(0,elevs(sample),1)/Be10_elambdamu(erate))*(1-
%          exp(-Be10_elambdamu(erate)*t_exposure));
%          eBe10_conc_buildup = Be10spall_buildup + Be10muon_buildup;
%      end
%
%      function eAl26_conc_buildup = eAl26_buildup(t_exposure, erate)
%          Al26spall_buildup =
%          (Al26_spalprodrate/Al26_elambda(erate))*(1-exp(-
%          Al26_elambda(erate)*t_exposure));
%          Al26muon_buildup =
%          (Burial_muonproduction(0,elevs(sample),0)/Al26_elambdamu(erate))*(1-
%          exp(-Al26_elambdamu(erate)*t_exposure));
%          eAl26_conc_buildup = Al26spall_buildup + Al26muon_buildup;
%      end

%analytical solution

%deviation equation: goal is to find exposure/burial pair that best fits
%the data

function Z = del_init(x)
    Z = abs(Al26_burial(x(1),x(2)) - Al_concs(sample)) +
abs(Be10_burial(x(1),x(2)) - Be_concs(sample));
end

%parameters for optimization algorithm

n = 50; %grid size
grid_burs = linspace(1000,10000000,n); %burial age range
grid_exps = linspace(1000,1000000,n); %exposure age range

```

```

options = struct('GoalsExactAchieve',0, 'MaxIter', 500, 'MaxFunEvals',
1000);

%calculation of best fit using grid approach

counter = 0;
while counter < 1
    kexp = randi(numel(grid_burs),1);
    kbur = randi(numel(grid_burs),1);
    [X fval] = fminlbfgs(@del_init,[grid_exps(kexp), grid_burs(kbur)],
options);
    if fval >= 1
        continue
    else
        counter = counter + 1;
    end
    solution = [X(1)/1e6 X(2)/1e6 fval];
end
format long
out = solution;

end

```

A.3.3.3. Burial_stone2000.m

```

function scal = Burial_stone2000(lat, elev)

press = 1013.25*exp((-0.03417/0.0065)*(log(288.15)-log(288.15-
0.0065*elev)));
if size(lat,2) > 1
    error('Input lat must be a column vector.')
end
if ~isequal(size(lat), size(press))
    error('Inputs lat and press must have the same size.')
end
npress = numel(press);
lat = abs(lat);
lat(lat>60) = 60;

stonecoeff = [31.8518    34.3699    40.3153    42.0983    56.7733
69.0720    71.8733
    250.3193    258.4759    308.9894    512.6857    649.1343    832.4566
863.1927
    -0.083393    -0.089807    -0.106248    -0.120551    -0.160859    -0.199252 -
0.207069
    7.4260e-5    7.9457e-5    9.4508e-5    1.1752e-4    1.5463e-4    1.9391e-4
2.0127e-4
    -2.2397e-8    -2.3697e-8    -2.8234e-8    -3.8809e-8    -5.0330e-8    -6.3653e-8 -
6.6043e-8];

```



```

latgrid = 0:10:60;
nlatgrid = numel(latgrid);

scalgrid = nan(npres, nlatgrid);
for k = 1:nlatgrid
    scalgrid(:,k) = stonecoeff(1,k) + stonecoeff(2,k)*exp(press/-150) +
stonecoeff(3,k)*press + stonecoeff(4,k)*(press.^2) +
stonecoeff(5,k)*(press.^3);
end

scal = nan(npres,1);
for k = 1:npres
    scal(k) = interp1(latgrid, scalgrid(k,:), lat(k));
end

```

A.3.3.4. Burial_muonproduction.m

```

function [total fastmuons negmuons] =
Burial_muonproduction(massdepth,elev,isotope)

%convert elevation to atmospheric pressure

h = 1013.25*exp((-0.03417/0.0065)*(log(288.15)-log(288.15-
0.0065*elev)));

%remember depth is in mass depth here

z = massdepth;

%The following is modified from P_mu_total.m of Balco 2006 code:

% remember what direction the z vector came in

in_size = size(z);

% standardize direction

if size(z,1) > 1
    z = z';
end

% figure the atmospheric depth in g/cm2

H = (1013.25 - h).*1.019716;

% find the vertical flux at SLHL

a = 258.5*(100.^2.66);
b = 75*(100.^1.66);

```

```

phi_vert_slhl = (a./((z+21000).*((z+1000).^1.66) + b)).*exp(-5.5e-6 .*
z);

% The above expression is only good to 2e5 g/cm2. We don't ever consider
production
% below that depth. The full-depth scheme appears in the comments below.
% ----- begin full-depth flux equations -----
%phiz_1 = (a./((z+21000).*((z+1000).^1.66) + b)).*exp(-5.5e-6 .* z);
%phiz_2 = 1.82e-6.*((121100./z).^2).*exp(-z./121100) + 2.84e-13;
%out(find(z<200000)) = phiz_1(find(z<200000));
%out(find(z>=200000)) = phiz_2(find(z>=200000));
% ----- end full-depth flux equations -----

% find the stopping rate of vertical muons at SLHL
% this is done in a subfunction Rv0, because it gets integrated later.

R_vert_slhl = Rv0(z);

% find the stopping rate of vertical muons at site

R_vert_site = R_vert_slhl.*exp(H./LZ(z));

% find the flux of vertical muons at site
phi_vert_site = nan(1,length(z));
for a = 1:length(z);
    % integrate
    % ends at 200,001 g/cm2 to avoid being asked for an zero
    % range of integration --
    % get integration tolerance -- want relative tolerance around
    % 1 part in 10^4.
    tol = phi_vert_slhl(a) * 1e-4;
    [temp,fcnt] = quad(@ (x) Rv0(x).*exp(H./LZ(x)),z(a),(2e5+1),tol);
    % second variable assignment here to preserve fcnt if needed
    phi_vert_site(a) = temp;
end;

% invariant flux at 2e5 g/cm2 depth - constant of integration
% calculated using commented-out formula above
phi_200k = (a./((2e5+21000).*((2e5+1000).^1.66) + b)).*exp(-5.5e-6 .*
2e5);
phi_vert_site = phi_vert_site + phi_200k;

% find the total flux of muons at site

% angular distribution exponent
nofz = 3.21 - 0.297.*log((z+H)./100 + 42) + 1.21e-5.*(z+H);
% derivative of same
dndz = (-0.297./100)./((z+H)./100 + 42) + 1.21e-5;

phi_temp = phi_vert_site .* 2 .* pi ./ (nofz+1);

% that was in muons/cm2/s
% convert to muons/cm2/yr

```

```

phi = phi_temp*60*60*24*365;

% find the total stopping rate of muons at site

R_temp = (2.*pi./(nofz+1)).*R_vert_site ...
- phi_vert_site.*(-2.*pi.*((nofz+1).^(-2))).*dndz;

% that was in total muons/g/s
% convert to negative muons/g/yr

R = R_temp*0.44*60*60*24*365;

% Now calculate the production rates.

% Depth-dependent parts of the fast muon reaction cross-section

Beta = 0.846 - 0.015 .* log((z./100)+1) + 0.003139 .*
(log((z./100)+1).^2);
Ebar = 7.6 + 321.7.*(1 - exp(-8.059e-6.*z)) + 50.7.*(1-exp(-5.05e-
7.*z));

aalpha = 0.75;
if isotope == 1 % Be10
    % internally defined constants
    sigma0 = (0.094e-27/1.096)./(190.^aalpha);
    %sigma0 = 0.79e-30;
    % fast muon production
    fastmuons = phi.*Beta.*(Ebar.^aalpha).*sigma0.*2.006e22;
    %negative muon capture
    negmuons = R.*(0.704*0.1828*0.0043)/1.096;
    %negmuons = R.*(0.704*0.1828*0.0012);
else % Al26
    % internally defined constants
    sigma0 = (1.41e-27)./(190.^aalpha);
    %sigma0 = 13.6e-30;
    % fast muon production
    fastmuons = phi.*Beta.*(Ebar.^aalpha).*sigma0.*1.003e22;
    %negative muon capture
    negmuons = R.*(0.296*0.6559*0.022);
    %negmuons = R.*(0.296*0.6559*0.0084);
end

% total

total = fastmuons + negmuons;

% -----
---
```

```

function out = Rv0(z)

% this subfunction returns the stopping rate of vertically traveling
muons
% as a function of depth z at sea level and high latitude.

a = exp(-5.5e-6.*z);
b = z + 21000;
c = (z + 1000).^1.66 + 1.567e5;
dadz = -5.5e-6 .* exp(-5.5e-6.*z);
dbdz = 1;
dcdz = 1.66.*(z + 1000).^0.66;

out = -5.401e7 .* (b.*c.*dadz - a.*(c.*dbdz + b.*dcdz))./(b.^2 .* c.^2);

% full depth calculation appears in comments below
%R_1 = -5.401e7 .* (b.*c.*dadz - a.*(c.*dbdz + b.*dcdz))./(b.^2 .*
c.^2);
%f = (121100./z).^2;
%g = exp(-z./121100);
%dfdZ = (-2.*(121100.^2))./(z.^3);
%dgdz = -exp(-z./121100)./121100;
%R_2 = -1.82e-6.*(g.*dfdZ + f.*dgdz);
%out(find(z<200000)) = R_1(find(z<200000));
%out(find(z>=200000)) = R_2(find(z>=200000));

% -----
---

function out = LZ(z)

% this subfunction returns the effective atmospheric attenuation length
for
% muons of range Z

% define range/momentum relation
% table for muons in standard rock in Groom and others 2001

data = [4.704e1 8.516e-1
5.616e1 1.542e0
6.802e1 2.866e0
8.509e1 5.698e0
1.003e2 9.145e0
1.527e2 2.676e1
1.764e2 3.696e1
2.218e2 5.879e1
2.868e2 9.332e1
3.917e2 1.524e2
4.945e2 2.115e2
8.995e2 4.418e2
1.101e3 5.534e2
1.502e3 7.712e2
2.103e3 1.088e3
3.104e3 1.599e3

```

```

4.104e3 2.095e3
8.105e3 3.998e3
1.011e4 4.920e3
1.411e4 6.724e3
2.011e4 9.360e3
3.011e4 1.362e4
4.011e4 1.776e4
8.011e4 3.343e4
1.001e5 4.084e4
1.401e5 5.495e4
2.001e5 7.459e4
3.001e5 1.040e5
4.001e5 1.302e5
8.001e5 2.129e5];

% ignore ranges bigger than 2e5 g/cm2
% 1.000e6 2.453e5
% 1.4e6 2.990e5
% 2.0e6 3.616e5
% 3.0e6 4.384e5
% 4.0e6 4.957e5
% 8.0e6 6.400e5
% 1.0e7 6.877e5
% 1.4e7 7.603e5
% 2.0e7 8.379e5
% 3.0e7 9.264e5
% 4.0e7 9.894e5
% 8.0e7 1.141e6
% 1.0e8 1.189e6];

% units are range in g cm-2 (column 2)
% momentum in MeV/c (column 1)

% deal with zero situation

z(z < 1) = 1;

% obtain momenta
% use log-linear interpolation

P_MeVc = exp(interp1q(log(data(:,2)),log(data(:,1)),log(z')));

% obtain attenuation lengths

out = 263 + 150 .* (P_MeVc./1000);

A.3.3.5. burialplot.m

function out = burialplot(data, muontype, sample, sigma, plotbanana)

%This function creates a blue whale (muon inclusive) burial plot for a

```

```

%sample-specific location and depth assuming a simple surface buildup
and
%burial history.
%
%INPUTS:
%data = name of ascii file with four columns of data (e.g. 'data.txt'):
%  column 1 is the depth of burial for each sample; (cm)
%  column 2 is the average density of material above each sample;
(g/cc)
%  column 3 is the decimal latitude of each sample (used in buildup
model for production)
%  column 4 is the elevation of each sample site; (m)
%  column 5 is measured [10Be]; (atoms/g)
%  column 6 is the 1 sigma error in [10Be]; (atoms/g)
%  column 7 is measured [26Al]; (atoms/g)
%  column 8 is the 1 sigma error in [26Al]; (atoms/g)
%
%muontype = deep muon scheme to use; surface buildup model uses
Heisinger
%(2002), but this refers to the scheme used at depth. If = 0, there is
no
%deep muon production; if = 1 half of Heisinger (2002) is used at depth
%(estimate from J. Stone, pers. comm.); if = 2 full Heisinger (2002) is
%used at depth.
%
%sample = the row number of the sample you wish to plot; all samples
will
%plot regardless, however, because of muon production, the plot is
structurally
%different at different depths and will therefore only be accurate for
the
%sample specified here unless 1) all sample depths are identical or 2)
muon
%production is not included (muontype = 0)
%
%sigma = specifies the sigma confidence for the error ellipse
%
%plotbanana = if true, will also plot the banana window
%
%
%A. Hidy
%%%%%%%%%%%%%%%%%%%%%%%%%%%%%%%%%%%%%%%%%%%%%%%%%%%%%%%%%%%%%%%%%%%%%%%%
%%
%%%%%%%%%%%%%%%%%%%%%%%%%%%%%%%%%%%%%%%%%%%%%%%%%%%%%%%%%%%%%%%%%%%%%%%%
%%

%load data

burial_data = load(data);

depths = burial_data(:,1);
densities = burial_data(:,2);
lats = burial_data(:,3);
elevs = burial_data(:,4);
Be_concs = burial_data(:,5);
Be_errs = burial_data(:,6);

```

```

Al_concs = burial_data(:,7);
Al_errs = burial_data(:,8);
ratios = Al_concs./Be_concs;

%decay constants (1/s)

Be10_lambda = log(2)/1378000;
Al26_lambda = log(2)/720000;

%neutron attenuation length (g/cm^2)

neutron_atten = 160;

%spallogenic production (atoms/g/a)

refspalprod = 4.76;
ratio_init = 6.75;

%at site
Be10_spalprodrate = Burial_stone2000(lats(sample),
elevs(sample))*refspalprod;
Al26_spalprodrate = Be10_spalprodrate*ratio_init;

%rock density used for buildup (g/cc)

r_density = 2.65;

%muogenic production at sample depth from (Heisinger 2002), Stone pers.
comm.,
%and none (atoms/g/a)

if muontype == 0 %Use pers. comm. from Stone
    Be10_muonprodrate = 0;
    Al26_muonprodrate = 0;
else if muontype == 1 %no muons
    Be10_muonprodrate =
Burial_muonproduction(depths(sample)*densities(sample),elevs(sample),1)/
2;
    Al26_muonprodrate =
Burial_muonproduction(depths(sample)*densities(sample),elevs(sample),0)/
2;
    else if muontype == 2 %Use Heisinger otherwise
        Be10_muonprodrate =
Burial_muonproduction(depths(sample)*densities(sample),elevs(sample),1);
        Al26_muonprodrate =
Burial_muonproduction(depths(sample)*densities(sample),elevs(sample),0);
    end
end
end

%simple buildup model with no erosion

```

```

%buildup due to exposure at surface; assumes no inheritance

function Be10_conc_buildup = Be10_buildup(t_exposure)
    Be10spall_buildup = (Be10_spalprodrate/Be10_lambda)*(1-exp(-
Be10_lambda*t_exposure));
    Be10muon_buildup =
(Burial_muonproduction(0,elevs(sample),1)/Be10_lambda)*(1-exp(-
Be10_lambda*t_exposure));
    Be10_conc_buildup = Be10spall_buildup + Be10muon_buildup;
end

function Al26_conc_buildup = Al26_buildup(t_exposure)
    Al26spall_buildup = (Al26_spalprodrate/Al26_lambda)*(1-exp(-
Al26_lambda*t_exposure));
    Al26muon_buildup =
(Burial_muonproduction(0,elevs(sample),0)/Al26_lambda)*(1-exp(-
Al26_lambda*t_exposure));
    Al26_conc_buildup = Al26spall_buildup + Al26muon_buildup;
end

%burial production; assume buildup is inheritance

function Be10_conc_burial = Be10_burial(t_exposure, t_burial)
    Be10spall_burial = (Be10_spalprodrate/Be10_lambda)*exp(-
depths(sample)*densities(sample)/neutron_atten)*(1-exp(-
Be10_lambda*t_burial));
    Be10muon_burial = (Be10_muonprodrate/Be10_lambda)*(1-exp(-
Be10_lambda*t_burial));
    Be10inheritance = Be10_buildup(t_exposure)*exp(-
Be10_lambda*t_burial);
    Be10_conc_burial = Be10spall_burial + Be10muon_burial +
Be10inheritance;
end

function Al26_conc_burial = Al26_burial(t_exposure, t_burial)
    Al26spall_burial = (Al26_spalprodrate/Al26_lambda)*exp(-
depths(sample)*densities(sample)/neutron_atten)*(1-exp(-
Al26_lambda*t_burial));
    Al26muon_burial = (Al26_muonprodrate/Al26_lambda)*(1-exp(-
Al26_lambda*t_burial));
    Al26inheritance = Al26_buildup(t_exposure)*exp(-
Al26_lambda*t_burial);
    Al26_conc_burial = Al26spall_burial + Al26muon_burial +
Al26inheritance;
end

%simple buildup model with erosion

%new lambda term spallation

function Be10lambda = Be10_elambda(erate)

    Be10lambda = Be10_lambda + erate*r_density/neutron_atten;
end

```



```

function Al26lambda = Al26_elambda(erate)

    Al26lambda = Al26_lambda + erate*r_density/neutron_atten;
end

%need effective lambda for muons; dominated by spall, so use rough
%estimate of 1500

function Be10lambdamu = Be10_elambdamu(erate)

    Be10lambdamu = Be10_lambda + erate*r_density/1500;
end

function Al26lambdamu = Al26_elambdamu(erate)

    Al26lambdamu = Al26_lambda + erate*r_density/1500;
end

%buildup due to exposure at surface; assumes no inheritance

function eBe10_conc_buildup = eBe10_buildup(t_exposure, erate)
    Be10spall_buildup = (Be10_spalprodrate/Be10_elambda(erate))*(1-
exp(-Be10_elambda(erate)*t_exposure));
    Be10muon_buildup =
(Burial_muonproduction(0,elevs(sample),1)/Be10_elambdamu(erate))*(1-
exp(-Be10_elambdamu(erate)*t_exposure));
    eBe10_conc_buildup = Be10spall_buildup + Be10muon_buildup;
end

function eAl26_conc_buildup = eAl26_buildup(t_exposure, erate)
    Al26spall_buildup = (Al26_spalprodrate/Al26_elambda(erate))*(1-
exp(-Al26_elambda(erate).*t_exposure));
    Al26muon_buildup =
(Burial_muonproduction(0,elevs(sample),0)/Al26_elambdamu(erate))*(1-
exp(-Al26_elambdamu(erate).*t_exposure));
    eAl26_conc_buildup = Al26spall_buildup + Al26muon_buildup;
end

%define axis for plot

plot_axis = [4 7.5 0 7.2];

%Define locations of contours on burial plot, un years
n1 = [200000 500000 1000000 2000000 2800000 4000000 8000000]; %burial
contours
n2 = [3000 10000 30000 100000 300000 1000000]; %exposure contours
%erosion rate contours, cm/year
%n3 = [0.001 0.0001 0.0005 0.00001];
n3 = 0.00001:0.00002:0.001;

figure %no erosion contours for this burial plot

```

```

hold on
axis(plot_axis);
for k = 1:numel(Be_concs)
    ellipse(Be_concs(k),Be_errs(k),Al_concs(k),Al_errs(k),sigma);
end
texp = 1:100:10000000;
tbur = 1:100:10000000;
xlabel('log[10Be Concentration] (atoms/g)');
ylabel('26Al/10Be');
title('Burial Plot for 26Al and 10Be');

for k = 1:numel(n1)
plot(log10(Be10_burial(texp,n1(k))),Al26_burial(texp,n1(k))./Be10_burial
(texp,n1(k)),'b-');
end

for k = 1:numel(n2)
plot(log10(Be10_burial(n2(k),tbur)),Al26_burial(n2(k),tbur)./Be10_burial
(n2(k),tbur),'k--');
end

plot(log10(Be_concs),ratios,'k. ');
plot(log10(Be10_burial(texp,0)),Al26_burial(texp,0)./Be10_burial(texp,0)
,'r-','linewidth',2);
plot(log10(Be10_burial(100000000,tbur)),Al26_burial(100000000,tbur)./Be1
0_burial(100000000,tbur),'k-','linewidth',2);

if margin < 5
    return
end

for k = 1:numel(n3)
    plot(log10(eBe10_buildup(texp,n3(k))),
eAl26_buildup(texp,n3(k))./eBe10_buildup(texp,n3(k)),'g');

plot(log10(Be10_burial(texp,0)),Al26_burial(texp,0)./Be10_burial(texp,0)
,'r-','linewidth',2);
end

end

```


WS5B_ICP Aliquot and Al spiking

This worksheet outlines the steps for collecting ICP aliquots and adding Al carrier.

Updated Sept. 1, 2009

Chemist: ^{AH} AH

Date: ^{form: 02/17/01} 02/09/09

- 1 Label one 100 ml volumetric flasks per sample
- 2 Label one ICP vial with CNEF ID per sample

Vessel ID	E1/B7	A1/B13	E2/B14	A2/B19	E3/B20	E4/B21	A3/B22	E5/B24	examples
CNEF ID	2333	2335	2336	2337	2338	2339	2340	2341	105
Sample ID	YUK-09-LWC-001	YUK-09-LWC-003	YUK-09-LWC-004	YUK-09-LWC-005	YUK-09-UWC-006	YUK-09-UWC-007	YUK-09-UWC-008	YUK-09-UWC-009	WY-96-001
Al carrier ID	ICP-013-5	ICP-013-5	ICP-013-5	ICP-013-5	ICP-013-5	ICP-013-5	ICP-013-5	ICP-013-5	ALI-carrier
Quant-EM est. Al in qtz	5	5	10	10	8	8	9	8	ppm
Mass 100 ml volumetric	67.1804	66.9344	67.7946	67.7433	67.1366	66.7119	66.4907	67.0048	66.9239 g
100ml vol+sample+2%HCl	167.5102	167.7182	168.6285	168.4909	167.9077	167.4000	167.0985	167.4102	166.9239 g
Mass 5 ml vol A	4.9952	4.9982	4.9992	4.9993	5.0059	5.0220	5.0119	5.1010	5.0000g
Al Carrier Added	1.5697	2.2590	0.1003	1.3492	1.2072	0.9118	2.0290	1.0151	1.000g
Mass 5 ml Vol B	5.0051	5.0384	4.9972	5.0006	5.0022	5.0049	5.0045	5.0229	5.0000g
Final Mass	159.0389	159.9099	158.7123	159.8214	159.0917	158.2609	159.0995	158.2905	159.000g
	0.0407	0.0307	0.0201	0.0188	0.0151	0.0240	0.0116	0.0109	0.0100g
Mass A, dried, with HNO3									
Mass B, Dried, with HNO3									0.0100 g

- 3 Get digestion vessel and cover ready, Do not wipe now.
- 4 Transfer the 90 ml sample back into vessel
- 5
- 6 Transfer contents volumetrics to ICP vials with same number

WS8_Cation Column Chemistry

This worksheet outlines the steps for the Cation Column Chemistry

Chemist: ^{GY/JG}

Date: ^{mm/dd/yy}

[Print this page](#)

- ₁ Dissolve in 5 ml conc. HCl and evaporate to dryness at 125°C
- ₂ Redissolve in 2.5 ml 1N HCl and 2.5 ml 0.5 N HCl
- ₃ Transfer to centrifuge tube, rinse with 1 ml 0.5N, and centrifuge

Column ID	1	2	3	4	5	6	7	8	examples
Vessel	E1/B7	A1/B13	E2/B14	A2/B19	E3/B20	E4/B21	A3/B22	E5/B24	
CNEF ID	2333	2335	2336	2337	2338	2339	2340	2341	105
Sample ID	YUK-09-LWC-001	YUK-09-LWC-003	YUK-09-LWC-004	YUK-09-LWC-005	YUK-09-UWC-006	YUK-09-UWC-007	YUK-09-UWC-008	YUK-09-UWC-009	WY-96-001

- ₄ **Pipette all of the sample into designated conditioned cation column, 17ml**
- ₅ Discard the eluant. Add 285 ml 0.5 N HCL (Bottle C6)
- ₆ **Drain the column, discard the first 300ml of eluant**
- ₇ Add 60ml of 0.5N HCl, (Bottle 7), Collect eluant as Cation Supernate
- ₈ Add 65ml of 0.5N HCl, (Bottle 8), Save it as Be-Sample
- ₉ Add 120 ml 1N HCl (bottle9)
- ₁₀ Save this as Be-sample as well.
- ₁₁ Add 80 ml 4.5 N HCl (bottle 10) , save the eluant as Al sample.

₁₂

₁₃ **CONDITION CATION COLUMN**

- (bottle C1) 100 ml 9N HCl
- (bottle C2) 50 ml 4.5 N HCl
- (bottle C3) 50 ml 1 N HCl
- (bottle C4) 50 ml water
- (bottle C5) 100 ml 0.5 N HCl

* 17 ml Column

WS9_Be Sample Chemistry

This worksheet outlines the steps to prepare the BeO sample

Chemist: ^{AH}

Date: ^{form: mm/dd/yy}

Print this page

- ₁ Evaporate Be Sample from column in wiped digestion vessels at 125°C
- ₂ Add 2-5 ml 20% perchloric and evaporate at 200°C
- ₃ Again, add 2-5 ml 20% perchloric and evaporate at 200°C
- ₄ Dissolve sample in 10 ml of 0.5 N HCl (optima grade)
- ₅ Transfer to 15 ml centrifuge tube
- ₆ Centrifuge and decant into clean centrifuge tube
- ₇ Heat centrifuge tubes in water bath at 60°C
- ₈ Precipitate Be(OH)₂ using Matheson ultimate grade ammonia gas
Gently bubble NH₃ with clean pipet tip on hose
for ca.15 bubbles, or ca. 8-12 sec until ppt forms
Optimum pH=9.2; 1N HCl may be added
- ₉ Centrifuge 15 min., decant (save and redo ₈ if pH of liquid is < 8)
- ₁₀ Wash with water, vortex, centrifuge for 10 min, and decant
- ₁₁ Record mass quartz vials, label, and place them in furnace holder

CNEF ID	2333	2335	2336	2337	2338	2339	2340	2341	¹⁰⁵
Vessel	E1/B7	A1/B13	E2/B14	A2/B19	E3/B20	E4/B21	A3/B22	E5/B24	
Sample ID	YUK-09-LWC-001	YUK-09-LWC-003	YUK-09-LWC-004	YUK-09-LWC-005	YUK-09-UWC-006	YUK-09-UWC-007	YUK-09-UWC-008	YUK-09-UWC-009	WY-96-001
Mass Qtz Vial	2.5749	2.5781	2.3654	2.5774	2.4870	2.5438	2.5092	2.6171	2.1400 g
Mass Vial+Spl	2.5752	2.5783	2.3656	2.5778	2.4880	2.5451	2.5097	2.6181	2.1410 g
Mass Spl	0.0003	0.0002	0.0002	0.0004	0.0010	0.0013	0.0005	0.0010	1 mg

- ₁₂ Add 1 small drop of water with micropipet, slurry precipitate
- ₁₃ Transfer sample into quartz vial, cover with alumina vial
- ₁₄ Heat in oven at 120°C for 2-3 hours
- ₁₅ Let cool and scrape sample down from walls of quartz tube
- ₁₈ Place in furnace. Convert to BeO in furnace at 850°C for minimum 1 hr
- ₁₉ Determine mass of vial + sample

WS10_AI Sample Chemistry

This worksheet outlines the steps to prepare the Al oxide sample

Chemist: ^{AH}

Date: ^{form: mm/dd/yy}

[Print this page](#)

- ₁ Evaporate Al Sample from column in wiped teflon vessel at 125°C
- ₂ Dissolve sample in 10 ml of 0.5 N HCl (optima grade)
- ₃ Transfer to 15 ml centrifuge tube
- ₄ Centrifuge and decant into clean centrifuge tube
- ₅ Heat centrifuge tubes in water bath at 60°C
- ₆ Precipitate Al(OH)₃ using 50% NH₃OH (drops: 25, 5, 5, 3, 2...)
Optimum pH=6.3; 1N HCl may be added
- ₇ Centrifuge 15 min., decant (save and redo ₆ if pH of liquid is < 8)
- ₈ Wash with water, vortex, centrifuge for 10 min, and decant
- ₉ Record mass quartz vials, label, and place them in furnace holder

CNEF ID	2333	2335	2336	2337	2338	2339	2340	2341	
Sample ID	YUK-09-LWC-001	YUK-09-LWC-003	YUK-09-LWC-004	YUK-09-LWC-005	YUK-09-UWC-006	YUK-09-UWC-007	YUK-09-UWC-008	YUK-09-UWC-009	105
Mass Qtz Vial	2.5538	2.5248	2.5651	2.5719	2.5131	2.5653	2.7043	2.6185	WY-96-001
Mass Vial+Spl	2.5770	2.5349	2.5755	2.5802	2.5250	2.5742	2.7115	2.6299	2.1400 g
Mass Spl	0.0232	0.0101	0.0104	0.0083	0.0119	0.0089	0.0072	0.0114	2.1410 g
									1 mg

- ₁₀ Add 1 small drop of water with micropipet, slurry precipitate
- ₁₁ Transfer sample into quartz vial, cover with alumina vial
- ₁₂ Heat in oven at 120°C for 2-3 hours
- ₁₃ Let cool and scrape sample down from walls of quartz tube
- ₁₄ Convert to Al₂O₃ in furnace at 950°C for minimum of 1 hr
- ₁₅ Determine mass of vial + sample

WS5B_ICP Aliquot and Al spiking

This worksheet outlines the steps for collecting ICP aliquots and adding Al carrier.

Updated Sept. 1, 2009

Chemist: ^{AH}

Date: ^{form: 02/17/01}

- 1 Label one 100 ml volumetric flasks per sample
- 2 Label one ICP vial with CNEF ID per sample

Vessel ID	A5/B25	E6/B28	A6/B29	B11	B12	0	0	0	examples
CNEF ID	2342	2343	2357	2309	2310	0.00	0.00	0.00	105
Sample ID	YUK-09-UWC-010	YUK-09-KG-011	YUK-09-HOL-025	Be blank	Be/Al blank	0	0	0	WY-96-001
Al carrier ID	ICP-013-5	ICP-013-5	ICP-013-5	ICP-013-5	ICP-013-5				ALI-carrier
Quant-EM est. Al in qtz	5	75	5	NA	NA				ppm
Mass 100 ml volumetric	67.3492	66.3021	65.2044	66.5905	67.7317				66.9239 g
100ml vol+sample+2%HCl	167.7316	166.9048	165.7134	167.2395	168.4180				166.9239 g
Mass 5 ml vol A	5.0092	5.0047	5.0012	4.9849	5.0389				5.0000g
Al Carrier Added	2.0681	0.0000	2.4091	0.0000	2.9725				1.000g
Mass 5 ml Vol B	5.0109	0.0000	5.0368	0.0000	5.0141				5.0000g
Final Mass	159.7619	161.8934	158.0737	162.2490	161.3273				159.000g
	0.0177	0.0067	0.0108	0.0056	0.0102				0.0100g
Mass A, dried, with HNO3									
Mass B, Dried, with HNO3									0.0100 g

- 3 Get digestion vessel and cover ready, Do not wipe now.
- 4 Transfer the 90 ml sample back into vessel
- 5
- 6 Transfer contents volumetrics to ICP vials with same number

WS8_Cation Column Chemistry

This worksheet outlines the steps for the Cation Column Chemistry

Chemist: ^{GY/JG}

Date: ^{mm/dd/yy}

[Print this page](#)

- ₁ Dissolve in 5 ml conc. HCl and evaporate to dryness at 125°C
- ₂ Redissolve in 2.5 ml 1N HCl and 2.5 ml 0.5 N HCl
- ₃ Transfer to centrifuge tube, rinse with 1 ml 0.5N, and centrifuge

Column ID	1	2	3	4	5	6	7	8	examples
Vessel	A5/B25	E6/B28	A6/B29	B11	B12	0	0	0	
CNEF ID	2342	2343	2357	2309	2310	0	0	0	105
Sample ID	YUK-09-UWC-010	YUK-09-KG-011	YUK-09-HOL-025	Be blank	Be/Al blank	0	0	0	WY-96-001

- ₄ **Pipette all of the sample into designated conditioned cation column, 17ml**
- ₅ Discard the eluant. Add 285 ml 0.5 N HCL (Bottle C6)
- ₆ **Drain the column, discard the first 300ml of eluant**
- ₇ Add 60ml of 0.5N HCl, (Bottle 7), Collect eluant as Cation Supernate
- ₈ Add 65ml of 0.5N HCl, (Bottle 8), Save it as Be-Sample
- ₉ Add 120 ml 1N HCl (bottle9)
- ₁₀ Save this as Be-sample as well.
- ₁₁ Add 80 ml 4.5 N HCl (bottle 10) , save the eluant as Al sample.

₁₂

₁₃ **CONDITION CATION COLUMN**

- (bottle C1) 100 ml 9N HCl
- (bottle C2) 50 ml 4.5 N HCl
- (bottle C3) 50 ml 1 N HCl
- (bottle C4) 50 ml water
- (bottle C5) 100 ml 0.5 N HCl

* 17 ml Column

WS9_Be Sample Chemistry

This worksheet outlines the steps to prepare the BeO sample

Chemist: ^{AH}

Date: ^{form: mm/dd/yy}

Print this page

- ₁ Evaporate Be Sample from column in wiped digestion vessels at 125°C
- ₂ Add 2-5 ml 20% perchloric and evaporate at 200°C
- ₃ Again, add 2-5 ml 20% perchloric and evaporate at 200°C
- ₄ Dissolve sample in 10 ml of 0.5 N HCl (optima grade)
- ₅ Transfer to 15 ml centrifuge tube
- ₆ Centrifuge and decant into clean centrifuge tube
- ₇ Heat centrifuge tubes in water bath at 60°C
- ₈ Precipitate Be(OH)₂ using Matheson ultimate grade ammonia gas
Gently bubble NH₃ with clean pipet tip on hose
for ca.15 bubbles, or ca. 8-12 sec until ppt forms
Optimum pH=9.2; 1N HCl may be added
- ₉ Centrifuge 15 min., decant (save and redo ₈ if pH of liquid is < 8)
- ₁₀ Wash with water, vortex, centrifuge for 10 min, and decant
- ₁₁ Record mass quartz vials, label, and place them in furnace holder

CNEF ID	2342	2343	2357	2309	2310	0	0	0	<small>105</small>
Vessel	A5/B25	E6/B28	A6/B29	B11	B12	0	0	0	
Sample ID	<small>YUK-09-UWC-010</small>	<small>YUK-09-KG-011</small>	<small>YUK-09-HOL-025</small>	Be blank	Be/Al blank	0	0	0	<small>WY-96-001</small>
Mass Qtz Vial	2.5301	2.3540	2.3539	2.5178	2.5987				<small>2.1400 g</small>
Mass Vial+Spl	2.5308	2.3542	2.3552	2.5179	2.5991				<small>2.1410 g</small>
Mass Spl	0.0007	0.0002	0.0013	0.0001	0.0004	0.0000	0.0000	0.0000	<small>1 mg</small>

- ₁₂ Add 1 small drop of water with micropipet, slurry precipitate
- ₁₃ Transfer sample into quartz vial, cover with alumina vial
- ₁₄ Heat in oven at 120°C for 2-3 hours
- ₁₅ Let cool and scrape sample down from walls of quartz tube
- ₁₈ Place in furnace. Convert to BeO in furnace at 850°C for minimum 1 hr
- ₁₉ Determine mass of vial + sample

WS10_AI Sample Chemistry

This worksheet outlines the steps to prepare the Al oxide sample

Chemist: ^{AH}

Date: ^{form: mm/dd/yy}

[Print this page](#)

- 1 Evaporate Al Sample from column in wiped teflon vessel at 125°C
- 2 Dissolve sample in 10 ml of 0.5 N HCl (optima grade)
- 3 Transfer to 15 ml centrifuge tube
- 4 Centrifuge and decant into clean centrifuge tube
- 5 Heat centrifuge tubes in water bath at 60°C
- 6 Precipitate Al(OH)₃ using 50% NH₃OH (drops: 25, 5, 5, 3, 2...)
Optimum pH=6.3; 1N HCl may be added
- 7 Centrifuge 15 min., decant (save and redo 6 if pH of liquid is < 8)
- 8 Wash with water, vortex, centrifuge for 10 min, and decant
- 9 Record mass quartz vials, label, and place them in furnace holder

CNEF ID	2342	2343	2357	2309	2310	2343+	0	0	105
Sample ID	YUK-09-UWC-010	YUK-09-KG-011	YUK-09-HOL-025	Be blank	Be/Al blank	YUK-09-KG-011	0	0	WY-96-001
Mass Qtz Vial	2.5114	2.5989	2.5540		2.6105	2.5983			2.1400 g
Mass Vial+Spl	2.5223	2.6249	2.5622		2.6128	2.6087			2.1410 g
Mass Spl	0.0109	0.0260	0.0082	0.0000	0.0023	0.0104	0.0000	0.0000	1 mg

- 10 Add 1 small drop of water with micropipet, slurry precipitate
- 11 Transfer sample into quartz vial, cover with alumina vial
- 12 Heat in oven at 120°C for 2-3 hours
- 13 Let cool and scrape sample down from walls of quartz tube
- 14 Convert to Al₂O₃ in furnace at 950°C for minimum of 1 hr
- 15 Determine mass of vial + sample

A.4. License Agreement for Manuscript ‘A Geologically Constrained Monte Carlo Approach to Modeling Exposure Ages from Profiles of Cosmogenic Nuclides: An Example from Lees Ferry, Arizona’, Published in Geochemistry, Geophysics, Geosystems

Dear Alan:

RE: Hidy, A. J., J. C. Gosse, J. L. Pederson, J. P. Mattern, and R. C. Finkel (2010), A geologically constrained Monte Carlo approach to modeling exposure ages from profiles of cosmogenic nuclides: An example from Lees Ferry, Arizona, *Geochem. Geophys. Geosyst.*, 11, Q0AA10, doi:10.1029/2010GC003084.

Thank you for your request. John Wiley & Sons, Inc. has no objections to your proposed reuse of this material.

Permission is hereby granted for the use requested subject to the usual acknowledgements (title, volume number, issue number, year, page numbers. Copyright [year and owner]. And the statement “This material is reproduced with permission of John Wiley & Sons, Inc.”). Any third party material is expressly excluded from this permission. If any of the material you wish to use appears within our work with credit to another source, authorization from that source must be obtained.

This permission does not include the right to grant others permission to photocopy or otherwise reproduce this material except for accessible versions made by non-profit organizations serving the blind, visually impaired and other persons with print disabilities.

Best wishes,

Paulette Goldweber

Associate Manager/Permissions-Global Rights

Professional Development

Wiley

111 River Street, 4-02

Hoboken, NJ 07030-5774

U.S.

www.wiley.com

T [+1 201-748-8765](tel:+12017488765)

F [+1 201-748-6008](tel:+12017486008)

pgoldweb@wiley.com

PermissionsUS@wiley.com

A.5. License Agreement for Manuscript ‘A Latest Pliocene Age for the Earliest and Most Extensive Cordilleran Ice Sheet in Northwestern Canada’, Published in Quaternary Science Reviews

**ELSEVIER LICENSE
TERMS AND CONDITIONS**

Mar 21, 2013

This is a License Agreement between Alan J Hidy ("You") and Elsevier ("Elsevier") provided by Copyright Clearance Center ("CCC"). The license consists of your order details, the terms and conditions provided by Elsevier, and the payment terms and conditions.

All payments must be made in full to CCC. For payment instructions, please see information listed at the bottom of this form.

Supplier

Elsevier Limited
The Boulevard, Langford Lane
Kidlington, Oxford, OX5 1GB, UK

Registered Company Number

1982084

Customer name

Alan J Hidy

Customer address

1459 Oxford St.

Halifax, NS B3H 4R2

License number

3112540472741

License date

Mar 19, 2013

Licensed content publisher

Elsevier

Licensed content publication

Quaternary Science Reviews

Licensed content title

A latest Pliocene age for the earliest and most extensive Cordilleran Ice Sheet in northwestern Canada

Licensed content author

Alan J. Hidy, John C. Gosse, Duane G. Froese, Jeffrey D. Bond, Dylan H. Rood

Licensed content date

1 February 2013

Licensed content volume number

61

Licensed content issue number

Number of pages

8

Start Page

77

End Page

84

Type of Use

reuse in a thesis/dissertation

Portion

full article

Format

both print and electronic

Are you the author of this Elsevier article?

Yes

Will you be translating?

No

Order reference number

Title of your thesis/dissertation

Cosmogenic nuclide quantification of paleo-fluvial sedimentation rates in response to climate change

Expected completion date

Apr 2013

Estimated size (number of pages)

250

Elsevier VAT number

GB 494 6272 12

Permissions price

0.00 USD

VAT/Local Sales Tax

0.0 USD / 0.0 GBP

Total

0.00 USD

Terms and Conditions

INTRODUCTION

1. The publisher for this copyrighted material is Elsevier. By clicking "accept" in connection with completing this licensing transaction, you agree that the following terms and conditions apply to this transaction (along with the Billing and Payment terms and conditions established by Copyright Clearance Center, Inc. ("CCC"), at the time that you opened your Rightslink account and that are available at any time at <http://myaccount.copyright.com>).

GENERAL TERMS

2. Elsevier hereby grants you permission to reproduce the aforementioned material subject to the terms and conditions indicated.

3. Acknowledgement: If any part of the material to be used (for example, figures) has appeared in our publication with credit or acknowledgement to another source, permission must also be sought from that source. If such permission is not obtained then that material may not be included in your publication/copies. Suitable acknowledgement to the source must be made, either as a footnote or in a reference list at the end of your publication, as follows:

“Reprinted from Publication title, Vol /edition number, Author(s), Title of article / title of chapter, Pages No., Copyright (Year), with permission from Elsevier [OR APPLICABLE SOCIETY COPYRIGHT OWNER].” Also Lancet special credit - “Reprinted from The Lancet, Vol. number, Author(s), Title of article, Pages No., Copyright (Year), with permission from Elsevier.”

4. Reproduction of this material is confined to the purpose and/or media for which permission is hereby given.

5. Altering/Modifying Material: Not Permitted. However figures and illustrations may be altered/adapted minimally to serve your work. Any other abbreviations, additions, deletions and/or any other alterations shall be made only with prior written authorization of Elsevier Ltd. (Please contact Elsevier at permissions@elsevier.com)

6. If the permission fee for the requested use of our material is waived in this instance, please be advised that your future requests for Elsevier materials may attract a fee.

7. Reservation of Rights: Publisher reserves all rights not specifically granted in the combination of (i) the license details provided by you and accepted in the course of this licensing transaction, (ii) these terms and conditions and (iii) CCC's Billing and Payment terms and conditions.

8. License Contingent Upon Payment: While you may exercise the rights licensed immediately upon issuance of the license at the end of the licensing process for the transaction, provided that you have disclosed complete and accurate details of your proposed use, no license is finally effective unless and until full payment is received from you (either by publisher or by CCC) as provided in CCC's Billing and Payment terms and conditions. If full payment is not received on a timely basis, then any license preliminarily granted shall be deemed automatically revoked and shall be void as if never granted. Further, in the event that you breach any of these terms and conditions or any of CCC's Billing and Payment terms and conditions, the license is automatically revoked and shall be void as if never granted. Use of materials as described in a revoked license, as well as any use of the materials beyond the scope of an unrevoked license, may

constitute copyright infringement and publisher reserves the right to take any and all action to protect its copyright in the materials.

9. Warranties: Publisher makes no representations or warranties with respect to the licensed material.

10. Indemnity: You hereby indemnify and agree to hold harmless publisher and CCC, and their respective officers, directors, employees and agents, from and against any and all claims arising out of your use of the licensed material other than as specifically authorized pursuant to this license.

11. No Transfer of License: This license is personal to you and may not be sublicensed, assigned, or transferred by you to any other person without publisher's written permission.

12. No Amendment Except in Writing: This license may not be amended except in a writing signed by both parties (or, in the case of publisher, by CCC on publisher's behalf).

13. Objection to Contrary Terms: Publisher hereby objects to any terms contained in any purchase order, acknowledgment, check endorsement or other writing prepared by you, which terms are inconsistent with these terms and conditions or CCC's Billing and Payment terms and conditions. These terms and conditions, together with CCC's Billing and Payment terms and conditions (which are incorporated herein), comprise the entire agreement between you and publisher (and CCC) concerning this licensing transaction. In the event of any conflict between your obligations established by these terms and conditions and those established by CCC's Billing and Payment terms and conditions, these terms and conditions shall control.

14. Revocation: Elsevier or Copyright Clearance Center may deny the permissions described in this License at their sole discretion, for any reason or no reason, with a full refund payable to you. Notice of such denial will be made using the contact information provided by you. Failure to receive such notice will not alter or invalidate the denial. In no event will Elsevier or Copyright Clearance Center be responsible or liable for any costs, expenses or damage incurred by you as a result of a denial of your permission request, other than a refund of the amount(s) paid by you to Elsevier and/or Copyright Clearance Center for denied permissions.

LIMITED LICENSE

The following terms and conditions apply only to specific license types:

15. **Translation:** This permission is granted for non-exclusive world **English** rights only unless your license was granted for translation rights. If you licensed translation rights you may only translate this content into the languages you requested. A professional translator must perform all translations and reproduce the content word for word

preserving the integrity of the article. If this license is to re-use 1 or 2 figures then permission is granted for non-exclusive world rights in all languages.

16. **Website:** The following terms and conditions apply to electronic reserve and author websites:

Electronic reserve: If licensed material is to be posted to website, the web site is to be password-protected and made available only to bona fide students registered on a relevant course if:

This license was made in connection with a course,

This permission is granted for 1 year only. You may obtain a license for future website posting,

All content posted to the web site must maintain the copyright information line on the bottom of each image,

A hyper-text must be included to the Homepage of the journal from which you are licensing at <http://www.sciencedirect.com/science/journal/xxxxx> or the Elsevier homepage for books at <http://www.elsevier.com> , and

Central Storage: This license does not include permission for a scanned version of the material to be stored in a central repository such as that provided by Heron/XanEdu.

17. **Author website** for journals with the following additional clauses:

All content posted to the web site must maintain the copyright information line on the bottom of each image, and the permission granted is limited to the personal version of your paper. You are not allowed to download and post the published electronic version of your article (whether PDF or HTML, proof or final version), nor may you scan the printed edition to create an electronic version. A hyper-text must be included to the Homepage of the journal from which you are licensing

at <http://www.sciencedirect.com/science/journal/xxxxx> . As part of our normal production process, you will receive an e-mail notice when your article appears on Elsevier's online service ScienceDirect (www.sciencedirect.com). That e-mail will include the article's Digital Object Identifier (DOI). This number provides the electronic link to the published article and should be included in the posting of your personal version. We ask that you wait until you receive this e-mail and have the DOI to do any posting.

Central Storage: This license does not include permission for a scanned version of the material to be stored in a central repository such as that provided by Heron/XanEdu.

18. **Author website** for books with the following additional clauses:

Authors are permitted to place a brief summary of their work online only.

A hyper-text must be included to the Elsevier homepage at <http://www.elsevier.com> . All content posted to the web site must maintain the copyright information line on the bottom of each image. You are not allowed to download and post the published electronic version of your chapter, nor may you scan the printed edition to create an electronic version.

Central Storage: This license does not include permission for a scanned version of the material to be stored in a central repository such as that provided by Heron/XanEdu.

19. **Website** (regular and for author): A hyper-text must be included to the Homepage of the journal from which you are licensing at <http://www.sciencedirect.com/science/journal/xxxxx>. or for books to the Elsevier homepage at <http://www.elsevier.com>

20. **Thesis/Dissertation**: If your license is for use in a thesis/dissertation your thesis may be submitted to your institution in either print or electronic form. Should your thesis be published commercially, please reapply for permission. These requirements include permission for the Library and Archives of Canada to supply single copies, on demand, of the complete thesis and include permission for UMI to supply single copies, on demand, of the complete thesis. Should your thesis be published commercially, please reapply for permission.

21. **Other Conditions**:

v1.6

If you would like to pay for this license now, please remit this license along with your payment made payable to "COPYRIGHT CLEARANCE CENTER" otherwise you will be invoiced within 48 hours of the license date. Payment should be in the form of a check or money order referencing your account number and this invoice number RLNK500980646.

Once you receive your invoice for this order, you may pay your invoice by credit card. Please follow instructions provided at that time.

**Make Payment To:
Copyright Clearance Center
Dept 001
P.O. Box 843006
Boston, MA 02284-3006**

For suggestions or comments regarding this order, contact RightsLink Customer Support: customercare@copyright.com or +1-877-622-5543 (toll free in the US) or +1-978-646-2777.

Gratis licenses (referencing \$0 in the Total field) are free. Please retain this printable license for your reference. No payment is required.
